# The Flow Behaviour of Non~Newtonian Sludges

Stephen Nicholas Little

A thesis submitted in partial fulfilment of the requirements for a

Doctor of Philosophy



Centre for Numerical Modelling and Process Analysis
University of Greenwich, London

in collaboration with

Water Research Centre, Swindon, Wilts

February 1998

To my parents

# Summary

A large body of data is analysed of the flow of concentrated sewage sludge through straight pipes. Mathematical models are obtained of the laminar and turbulent flow of each main category of sewage sludge. The sludges are modelled as time-independent, non-Newtonian relations between shear stress, rate of shearing strain, and solids concentration. Due to the inhomogeneity of sewage sludge, error analysis becomes pivotal to the data analysis, and options are examined for reducing the error of each model with one or more user-fitted parameters.

Parameter estimation is discussed for viscous, time-independent, non-Newtonian, laminar and turbulent flow models. Due to extensive requirements of the data analysis, the parameter estimation methods are robust, and generally suitable for any shear flow relation. The difficulties of estimating parameters of shear flow models from pipe flow data are addressed.

Numerical algorithms are presented for modelling the flow of time-independent, non-Newtonian, viscous fluids through a straight pipe. Laminar, critical and turbulent flow algorithms are developed to offer predictions such as pressure gradient, mean cross-sectional velocity, and the velocity distribution. To handle the requirements of the data analysis, the algorithms impose few restrictions on the type of shear flow relation, the flow velocity, and the pipe diameter. Suitable pipe flow equations are chosen, and are manipulated mathematically into forms that would yield robust and efficient schemes. The appropriate use of numerical methods for the algorithms is investigated.

Mathematical models of sludge are for use by the sewage industry to give an idea of the flow behaviour of sludges for any relevant application. The parameter estimation techniques and pipe flow algorithms are not constrained to any particular pipe, fluid or flow conditions, so they would be useful for any relevant application.

# Acknowledgements

I would like to thank my academic supervisors Dr. D. Edwards and Prof. K. Pericleous for their considerable help and guidance throughout the research. Gratitude also extends to my industrial supervisor Dr. J. Dudley for his support with the industrial requirements of the research.

I would like to thank my original academic supervisors Dr. C. Richards and Dr. S. Salvini for launching the project; my original industrial supervisor Dr. G. Hoyland has also been of great help. Appreciation extends to the Science and Engineering Research Council and the Water Research Centre for financially supporting the project.

# Contents

# 1 Introduction

## 1.1 Sewage Sludge

Sewage originates from domestic waste, industrial waste and storm water (see Figure 1-1). *Domestic waste* is produced by every household where each person per day typically discards several hundred litres of dirty water, several hundred grams of human effluent, and some fibrous material. Human effluent, which has an insignificant regional variation, typically accounts for about half of the solids content of a sludge; the rest is mostly accounted for by *industrial waste*, which varies considerably with region and time. Examples of industrial waste include coal dust, wood or paper fibre, clay, grease and oil. *Storm water*, which varies greatly with both time and season, may or may not have its own disposal system. A trait of storm water is the considerable amount of dirt, grit and pebbles that it washes into the system. Finally, climate and climatic history affect the biochemical makeup and flow rate of sewage flowing through a sewer.

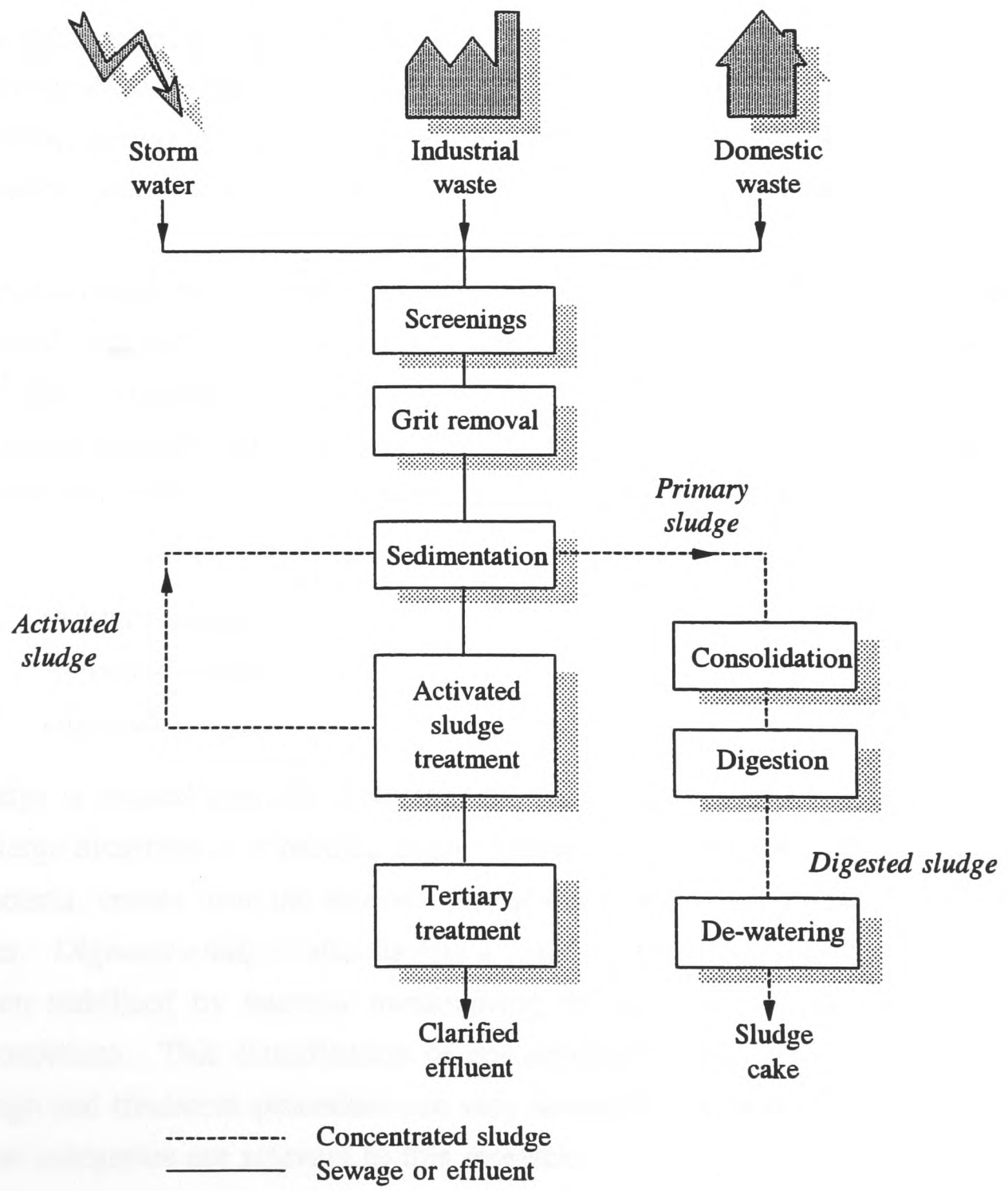


**Figure 1-1** Sewage treatment

Sewage enters a sewage plant (or sewerage) as a very dilute mixture of human, industrial and natural waste. A preliminary treatment involves removing most of the water content to yield a much thicker, more concentrated sludge. There is an important distinction between raw sewage that flows through the sewers, and the concentrated sewage that is handled and treated at a sewage plant. Raw sewage is essentially dirty water that flows through a sewer with considerable volumetric throughput, though not usually at full capacity; this is a major industry that has received extensive research [1]. Concentrated sewage, on the other hand, is the largely dewatered product of raw sewage, and is transported within the plant through pipelines running at full capacity with a considerable reduction in volumetric throughput. Since concentrated sewage is a far less major part of the industry than raw sewage, considerably less research has gone into it. This research focuses only on concentrated sewage sludge so only the full pipe situation applies.

Once raw sewage reaches a plant, treatment can vary considerably from one region to another. There are, of course, common principles such as the dewatering and disposal of the effluent, but there is much variation in the way these things are achieved. One factor is the expense and availability of land. Where land is expensive—such as London—much of the treatment is done underground; where land is cheap—normally in rural country—treatment can be carried out in large pools. Any further reference to sewage in this report will mean the concentrated sewage that is handled and transported at a sewerage.

The *preliminary treatment* of sewage sludge involves the removal of large objects, grit, and fibrous materials using bar screens and grit settling tanks. This safeguards against pump damage and pipe blockage, thus prolonging the operating life of the equipment. The remaining process involves removing the solids from the water, and includes handling sewage sludges of about five percent solids by mass. Broadly speaking, these sludges fall into three categories:

(i) Primary sludge,
(ii) Activated sludge,
(iii) Digested sludge.

*Primary sludge* is created from the first stage of sedimentation and is comprised of organic matter of a large distribution of particle sizes. *Activated sludge*, which contains much living and dead bacteria, comes from the second stage of treatment, and has a small distribution of particle sizes. *Digested sludge*—also having a small particle size distribution—is a sludge that has been stabilised by bacteria metabolising the organic material under aerobic or anaerobic conditions. This classification of concentrated sludges is a broad generalisation as plant design and treatment procedure can vary so much from one region to another. All three of these categories are relevant to this research.

Sewage sludge consists of solid particles suspended in a liquid medium which is mostly water. Babbitt and Caldwell [2] identified many factors that affect the flow of sludge, such as solids concentration, particle size distribution, nature of liquid medium, temperature, degree of agitation and gas content. The one factor that considerably affects sludge flow is the concentration of solids present [3, 4] which can vary between about three to fifteen percent by mass. The particles have a size distribution that reduces with each stage of treatment. Primary sludge contains particles up to a centimetre in diameter, and for activated and digested sludges, the particles having been reduced to less than a millimetre (the difference between a relish and a ketchup provides a suitable analogy).

Sewage plants operate using positive displacement pumps where a sludge throughput is specified; smaller plants might run on peristaltic pumps like those used in kidney machines, and larger plants might run on piston pumps. These positive displacement pumps cause pulsating flow that is necessarily damped to reduce equipment wear. Due to the amount of grit and fibrous material in the system, impeller-style pumps are never installed. Sewage can be pumped at distances of anything from a metre or less to a kilometre or more in a pipe that can vary from one to several centimetres in diameter. The shorter distances might occur within a plant building and the longer distances occur between buildings sometimes separated by some distance—even roads. Pipelines are kept straight wherever possible, though pipe bends and other fittings are certainly used. Choosing the size of pump to fit an application can be a tortuous task. There have been occasions when a particular pump size was estimated to be easily powerful enough to transport a particular sludge, yet when installed, was not even able to overcome the yield resistance of the fluid. In such cases, the expense of dismantling the pump and installing a different one has been incurred; on occasion, even a second attempt has failed. On the other hand, if an oversized pump had been fitted, then unnecessary expense would have been wasted on outlay and running costs.

The reason for the difficulties of modelling sewage sludge lie in the extreme complexity of its flow behaviour and the extreme variation of its constituents. There is an informal edict in the industry that every sample of sewage examined is different, even from the same batch. Some sludges with a low moisture content can be quite liquid while others with an even higher content may essentially act as a solid mass [5]. If a sludge is left undisturbed for several days it often has an initial resistance to flow, and gauging this resistance becomes an important criterion when installing a pump. Once this initial resistance is overcome, the sludge will flow more readily (much like the behaviour of a ketchup) until at high shear, the viscosity of water is approached. Sewage will recover this initial viscosity in a time-dependent process that varies from being almost instantaneous to several days. From the discussion given so far, it is clear that the flow behaviour of concentrated sewage sludge is extremely complex.

A fluid with a constant viscosity over the applicable range is known as a *Newtonian* fluid. But a fluid (such as concentrated sewage sludge) whose laminar flow viscosity is related to shear or time is known as a *non-Newtonian* fluid. Like a Newtonian fluid, a non-Newtonian fluid can exhibit *laminar* (or streamline) flow at low shear, and *turbulent* (or chaotic) flow at higher shear. There is a transitional region for which the flow is neither laminar nor fully-developed turbulent. The concept of *critical* flow is useful where the fluid flows at the upper bound of laminar flow. The ideal rate at which to pump sewage is often at its critical rate since its apparent laminar flow viscosity is at its minimum, and since energy loss due to turbulent flow is non-existent. However, it is unlikely that the critical conditions of the sewage would just happen to occur within the operating limits of the pump.

Sewage sludge is usually characterised by the two parameter Bingham model or the three parameter general Bingham model [6]. Both of these models have one parameter to describe an initial resistance to shear, and the latter model has a further parameter to describe the decrease (or increase) of viscosity under increasing shear. In 1939, Babbitt and Caldwell [2] showed that sewage sludge could be described by the Bingham model, and other researchers [3, 4] have since followed suit. In 1970, Cheng [7] reported that the Warren Spring Laboratories had been using the general Bingham model to characterise sludge, and Frost [8] followed suit. For a general Bingham fluid, Heywood [9] offers an extensive summary of pipeline design procedures.

There are many practical problems with measuring the viscometric properties of a concentrated sewage sludge. Due to the lumpiness and handling difficulties of sludge (particularly primary), conventional viscometers such as capillary, concentric cylinder, or cone-and-plate are impractical to use. Therefore tubes and pipes are often used where the diameter is appreciably bigger than the particle sizes of the sludge. (Note that there is no formal distinction between capillaries, tubes and pipes, so the terms are used here to give an idea of their scale.)

Many engineering tasks in a sewage plant require on-the-job predictions such as those used for pump installation. Design procedures are often conducted with a limited amount of information. The sludge type is always known and the mass solids concentration is easy to obtain, but the viscometric properties of a sludge are often guesswork. Sometimes a simple on-site test is possible—such as pumping the sludge through an installed pipeline at a given flow rate to obtain one or perhaps two measurements—but any detailed analysis is usually impractical.

One of the reasons for the failure of a design procedure such as pump installation results from rough predictions without knowledge of their accuracy. For an on-site design procedure, any guide for making a prediction could be valuable however rough that guide

may be. For instance, if only the sludge type and the solids concentration are known about a sludge, then a very rough prediction with a large associated error could be invaluable. With each successive piece of information—such as a pressure drop reading at a given flow rate—it should possible to reduce the error of a prediction. Rheological modelling of sewage sludge with its corresponding error analysis shall be a topic of this research.

## 1.2 Background

This research has been conducted in collaboration with the Water Research Centre (WRC) at Swindon, UK. The formal objectives arose from informal discussions with a senior engineer at WRC. Before these formal objectives are presented, some of the informal background will be discussed to clarify their purpose. The literature reveals a surprising lack of basic rheological data on sewage sludge, and in England alone has been largely restricted to investigations by Johnson *et al*[10], Binnie and partners[11], and to some extent Hayes *et al*[12]. The data of Johnson involves the laminar, transitional and turbulent flow of sewage sludge through straight pipes. Frost analysed some of the data, and as a result, produced a widely used report[8] on the flow of sewage sludge through straight pipes. The report is based on an engineering approach for pipeline predictions using graphical methods and tables. Some of the data used in this research are the same as those used by Frost.

In the longer term, WRC were interested in modelling the flow of sewage sludge in geometries more complex than straight pipes, such as pipe bends, pipe fittings, and sewage stirring tanks. Such modelling requires two- or three-dimensional flow fields with laminar or turbulent flow regimes (or often a mixture of the two). At that time, there was (and still is) a growing interest and accessibility of computational fluid dynamics (CFD) codes such as Phoenics[13] (based on the Simplest algorithm of Patankar and Spalding[14, 15]). Simplest numerically solves the Navier-Stokes equations[16] over a domain that has been divided up into control volumes (à la finite volumes from which the Navier-Stokes equations are derived). All variables are treated on a local basis where scalar quantities (such as density and viscosity) reside within the control volume, and the velocity vectors reside on the boundaries of the control volume. The Phoenics code allows for the rheological model and any of the property variables of the fluid to be defined on a volume-by-volume basis within program subroutines of the code. The time-independent, viscous flow of sewage sludge in complex geometries using CFD codes requires rheological models of sewage sludge, and this is one of the main objectives of this research. WRC have since commissioned the sewage stirring tank to be modelled[17] using the Phoenics code. Further examples of CFD used for industrial and environmental modelling of non-Newtonian fluid flows are given by Pericleous and Patel[18]. The latest advances in finite element and finite volume methods of non-Newtonian flows has been the subject of a recent workshop[19].

Shear flow relations were required for modelling the laminar and turbulent flow of sewage sludge for many suitable geometrical configurations. The widely used Metzner-Reed [20] friction plot would have been inappropriate in this case as it is only relevant for pipe flow geometries. Similarly, the Dodge-Metzner relation [21] between friction factor and Reynolds number for turbulent flow would have been equally restrictive. Nevertheless, it was noted that since the data were of pipe flow, friction plots could be created and compared with frictional versions of the rheological models. Furthermore, it was stressed that generality took priority over accuracy, so a few all-encompassing, powerful models with realistic (albeit large) standard errors were required. It was then decided that each model would have an associated standard error which would decrease as more information about the sludge became available. Such models are not only useful for larger modelling applications, but also on-the-job calculations discussed in the previous section.

It was decided that the flow behaviour of sewage sludge could be modelled using the extensive tube and pipe flow data. However, it was clear that before any serious analysis could proceed, the laminar, transitional and turbulent flow of a non-Newtonian fluid through straight tubes and pipes had to be modelled. This objective was to be considered a by-product of the data analysis, though one to be taken seriously so that it could, for instance, be easily extended to include fixtures and fittings. Furthermore, the data discussed at the beginning of this section are all based on pipes with smooth walls, so pipe roughness was to be of cursory interest.

It was decided that the modelling should focus on the relationship between pressure per unit length of pipe and mean cross-sectional velocity of the fluid, as this was essentially how the WRC data were measured. (Sewage is transported using peristaltic pumps, which means that pressure gradient is the unknown quantity. However mean cross-sectional velocity predictions are often needed too.) With this simple model, a prediction can be made for any angle of pipe by introducing a simple extra term to account for the effect of gravity [22]. Furthermore, it is assumed that the flow is axially symmetric—an assumption that is particularly questionable with horizontal flow. This is unfortunate as horizontal flow is far more common than vertical flow in the slurry industry as a whole. Vertical flows occur in well drilling (particularly for oil) where the gravitational effect often dominates the pressure gradient, especially when the solids density is significantly different from that of the liquid medium [23].

Even though the body of data is large, it is restricted in many respects. Modelling assumptions had to be made particularly about the nature of the fluid and the way it flowed through the pipes. The assumptions were that sewage sludge is pseudo-homogeneous (ie smooth—a crude assumption, particularly for primary sludge) and time-independent—ie its apparent viscosity does not change with time. The question arose as to whether any serious

models could be formulated from such crude assumptions. However, it was made clear that, for process design purposes, conservative estimates of a sludge were required; for instance, the predictions had to be of a sludge at its least agitated where its apparent viscosity would be at its greatest.

In question of the pseudohomogeneous assumption, it is known that the average concentration of solids decrease close to the pipe wall, partly because of the finite sizes of the particles and partly because the solid particles tend to migrate radially inwards when the fluid flows. These effects are often misleadingly termed as 'wall slippage' as they can be realistically modelled as a discontinuity of the rate of shear at the pipe wall. During a WRC meeting, it was pointed out that the data were inadequate to model wall slippage, but a no-slip assumption would anyhow be less significant than the time-independent assumption. However, if significant wall slippage was to be ignored, then tubes with narrower diameters would show a reduced apparent viscosity of the sludge, and low predictions of the pressure gradient would generally result.

For straight pipe flow modelling to commence, it became clear that models of the viscous flow of time-independent pseudohomogeneous suspensions were required. For the laminar flow model, a relation between shear stress and rate of shearing strain, either of the explicit form $\tau = g(\dot{\gamma})$ or of the implicit form $G(\dot{\gamma}, \tau) = 0$ was considered appropriate [24]. There is a choice between many such relations ranging from well-established empirical models to more recent models with a theoretical basis to them. There has never been a clear-cut choice between them, and even if there ever was, something better could always come along.

To resolve the problem of the bewildering choice of rheological models, a novel suggestion was put forward: to allow the end-user of the algorithm to define the shear flow relation, such as through a program subroutine. Some shear flow relations have already been resolved for pipe flow geometry (see, for instance, Chapter 5 of Grovier and Aziz [24]), and these formulae can usually be evaluated directly or using a simple iterative procedure. With a user-definable relation, it became clear that more elaborate numerical methods would be required, though not nearly as complex as those normally used for computational fluid dynamics.

Nothing concrete was decided about the critical and turbulent flow models to use. These models are often based on the laminar shear flow relation (to be defined by the end-user), so a similar approach with the numerical methods was deemed necessary. It was suggested that well-established models based on the fewest possible assumptions should be considered. For turbulent flow, Prandtl-style shear flow models [25] were noted as being of particular interest since they contained a quadratic shear rate term (ie $\tau = \tau_L + \rho l^2 \dot{\gamma}^2$ where $\tau_L$ is the laminar shear stress), and could be treated like an extended version of a laminar flow model.

An obvious contender was the non-Newtonian turbulent flow model proposed by Hanks [26] as it was based on few underlying assumptions. In fact, turbulent flow models such as this are often much purer in form than friction factor relations, such as the well known non-Newtonian turbulence model proposed by Torrance [27]. This is based on the same mixing length model as Hanks but makes several simplifying assumptions when integrating the velocity profile.

Current literature tends to suggest that numerical procedures are used for complex pipe flow situations rather than the relatively simple ones of this research. For instance, lagrangian numerical simulation [28] has been used to model the conveying of dry solids through a pipe where the flow is necessarily pulsating. Transient flow of liquid through a pipe has been modelled using the method of characteristics [29] where the continuity and momentum partial differential equations reduce to ordinary differential equations along characteristic lines. Direct numerical simulation [30, 31] has been used to examine fully-developed turbulent flow of a fluid through a pipe using finite volume techniques.

In terms of unsettled solids, there is much in the literature about hindered settling; an excellent review of the subject is given by Khan and Richardson [32]. In comparison, there is little about hindered settling in a non-Newtonian medium, but recent work includes that of Chhabra *et al* [33]. In turbulent flow, the solids do not always settle because they are held in suspension by eddy diffusivity [34]. This effect has recently been modelled using lagrangian statistics [35] to describe the concentration profile of the suspension. There is precious little in the literature about the effects of solid suspensions on the rheology of a fluid, and these effects are of fundamental importance to this work. A brief summary of slurry pipe flow for both coarse and fine particles was recently offered by Bouzaïene and Hassani [36]. Einstein [37] derived a theoretical relation between solids concentration and Newtonian viscosity of a non-interacting particle suspension. Thomas treated the interaction of particles [38] and the extension to non-Newtonian fluids [39] in an empirical way. A plot of particular rheological parameters against solids concentration can be useful. For several different sewage sludge types, such plots are offered by Dick and Ewing [40], Mulbarger *et al* [3] and Carthew *et al* [4]. Frost [8] presented his relations in tabular form.

For this research, it was clear that the rheological models would need to be a function of solids concentration $\Phi$, so that the laminar flow relation would take a form such as $\tau = g(\dot{\gamma}; \Phi)$, and the turbulent flow relation would take a form such as $\tau = \tau_L + \rho l^2(\Phi)\dot{\gamma}^2$. These relations, to be derived from the pipe flow data, were to be ultimately used to model more complicated flow fields of sewage sludge. These fields are of no explicit interest to this work, needless to say that any of the pipe flow assumptions would need to hold on a local basis of these more complex geometries (for instance, they would have to hold within a control volume). These assumptions would require the flow to be steady, viscous, and

pseudohomogeneous on a local basis. The assumption that body forces (such as gravity) have a negligible effect on the pseudohomogeneity of the fluid would have to be adhered to. Furthermore, the rate of shear for any part of a geometry would have to lie within the range determined from the pipe flow data, and separate ranges would apply to the laminar and turbulent flow regimes.

## 1.3 Objectives and Assumptions

The background to the formal objectives was discussed in the previous subsection. The three main objectives are now given as follows:

(a) To design and implement numerical algorithms for modelling the flow of a non-Newtonian fluid through a straight pipe. The assumptions are:

- The pipe is straight, smooth and running at full capacity.
- The fluid is viscous, pseudohomogeneous and time-independent.
- The flow fields may be laminar, transitional or turbulent.
- There may be slippage of fluid at the pipe wall.

The algorithms must depend on a relation between shear stress and rate of shearing strain to characterise the fluid, but must not be limited to an actual choice of function. Therefore, the shear flow function may either be of the explicit form $\tau = g(\dot{\gamma})$, or of the implicit form $G(\dot{\gamma}, \tau) = 0$, and would be specified by the end-user. The algorithms are to solve for any pipe diameter and appropriate choice of shear flow function, offering predictions such as mean cross-sectional velocity, pressure gradient and radial velocity distribution (as a set of points). The algorithms must also extend to critical flow predictions such as the critical velocity and critical pressure gradient. The limitations of each algorithm must be specified.

The algorithms will <u>not</u> allow for time-dependent, inhomogeneous fluids (although wall slippage is strictly an inhomogeneous effect), and pipe roughness (usually affecting turbulent flow).

(b) To analyse a large body of concentrated sewage sludge data from several different regions in the south of England. The data are of the flow at full capacity of primary, activated and digested sludges through straight, smooth pipes (sometimes of varying diameter), where the flow regimes include laminar, transitional and turbulent. Analysis is required to:

- use the algorithms and assumptions of part (a) to analyse the data;
- identify and implement the necessary statistical tools to perform the data analysis;

- statistically determine the most suitable models (such as rheological models) of the data, and examine their suitability and limitations both analytically and graphically;
- compare the results with those of other researchers in the field, exploiting in particular the widely used friction plots for straight pipe flow.

(c) To derive generalised rheological models that account for factors such as sludge type and solids concentration. The laminar flow model is to take a form such as $\tau = g(\dot{\gamma}; \Phi)$ where $\Phi$ is solids concentration, and a turbulent flow relation is to take a form such as $\tau = \tau_L + \rho\, l^2(\Phi)\dot{\gamma}^2$. The objectives of this task are to

- use graphical and statistical methods to derive each generalised model;
- estimate the standard error on each of the models derived;
- identify user-fitting parameters that would reduce the standard error of the generalised models;
- define the applicable range of each model.

## 1.4 Presentation of Thesis

The body of the thesis is conceptually divided into three main parts: review, mathematical modelling and data analysis. The review is covered by the first four chapters, placing the problem in context with other work, introducing the data to be analysed, and discussing some pipe flow models. The development of the numerical algorithms is discussed in Chapters 5 and 6, and is original work. Relevant mathematical equations are rearranged and numerical methods are tested for their suitability. These algorithms are not presented in a computer-oriented way, so any software discussion or computer terminology will be dealt with in the appendices. The analysis of data is presented in Chapters 7 and 8, and is also original work; this is the statistical part of the thesis that ties in with the work of the preceding Chapters. Chapter 9 concludes the thesis.

# 2 Rheological Considerations

## 2.1 General Classification

Rheology is the study of the deformation of fluids, where a fluid may be viewed as a substance that exhibits continuous deformation for some range of shearing stresses. Fluid deformation is best perceived by its behaviour between two parallel plates separated by a distance $\Delta y$ (see Figure 2-1). The lower plate is stationary, and the upper plate moves at a uniform speed $\Delta u$ through the action of a force $F$. Under steady conditions where the flow is laminar (or streamline), the force $F$ per unit area $A$ of the plate is related to the velocity gradient by

$$\frac{F}{A} = g\left(\frac{\Delta u}{\Delta y}\right), \tag{2.1}$$

where $g$ is some function. For the expression to be valid for any geometry, the velocity gradient is defined on a local basis. *Shear stress* is defined to be the force per unit area,

$$\tau = F/A, \tag{2.2}$$

and the velocity gradient is the *rate of shearing strain*,

$$\frac{du}{dy} = \frac{d}{dt}\left[\frac{dx}{dy}\right]. \tag{2.3}$$

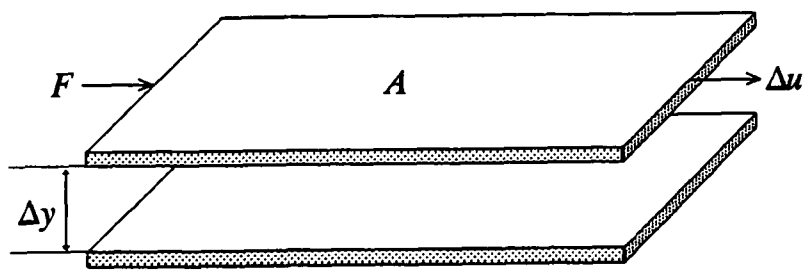


**Figure 2-1** The deformation of a fluid between parallel plates separated by distance $\Delta y$. The top plate area $A$ moves at speed $\Delta u$ under an applied force $F$.

Since shear strain is often denoted by $\gamma$, and the rate of shearing strain by $\dot{\gamma}$, this equation can be equivalently expressed as

$$\dot{\gamma} = \frac{d}{dt}\gamma. \tag{2.4}$$

For a time-independent, non-Newtonian, viscous fluid, Equation (2.1) is therefore generalised as

$$\tau = g(\dot{\gamma}), \tag{2.5}$$

and shall be referred to as the laminar *shear flow function*. Sometimes, this function is modelled as a two-variable function of the form

$$G(\dot{\gamma}, \tau) = 0. \tag{2.6}$$

For a *Newtonian* fluid, shear stress is a linear relation of rate of shearing strain (or shear rate),

$$\tau = \mu\dot{\gamma}, \tag{2.7}$$

where the constant of proportionality $\mu$ is known as the *viscosity* of the fluid. This model—which was first proposed by Newton—is shown in Figure 2-2. Whereas this relation is defined by the single parameter $\mu$, a time-independent non-Newtonian viscous fluid requires at least two parameters.

It is possible to sub-divide time-independent non-Newtonian viscous fluids into those that exhibit a yield resistance to shearing, and those that do not. For the former category, a yield stress is to be overcome if the fluid is to flow. The *Bingham plastic* fluid has the simplest relationship of this category; it is a linear relation between shear stress and rate of shear defined as

$$\tau = \tau_y + \eta\dot{\gamma}, \tag{2.8}$$

where $\tau_y$ is the *yield stress* and $\eta$ is the known as the *coefficient of rigidity*. For a zero yield stress, it is clear that the Bingham plastic model becomes Newtonian and $\eta$ becomes the Newtonian viscosity.

A fluid that has no yield stress, but whose gradient of the shear flow function decreases with increasing shear rate until a limiting slope is reached, is known as a *pseudoplastic* fluid. The *power law* model is widely used to describe the flow behaviour of these fluids, and has the relation

$$\tau = K\dot{\gamma}^n, \qquad n < 1, \tag{2.9}$$

where $K$ and $n$ are known as the *consistency coefficient* and *consistency index* respectively. The popularity of this model has been sustained by the convenience with which $K$ and $n$ can be estimated from a log-log plot of shear flow data. In practice, the power law model fits soundly to the curved part of a pseudoplastic relationship, and although it does not model the limiting viscosity (the limiting viscosity of a sludge is roughly that of the liquid medium), these conditions are not often attained in reality. For $n = 1$, the power law model becomes Newtonian where $K$ corresponds to the Newtonian viscosity. The departure of $n$ from unity is therefore an indication of the departure of the fluid from being Newtonian. The power law model is widely renowned for describing pseudoplastic fluids with remarkable accuracy. However, the model is empirical, and as such fails to model pseudoplastics under very low or very high shear. The viscosity can be defined as the gradient of the shear flow function. For low shear or high shear, the viscosity of a pseudoplastic is constant and can therefore be regarded as Newtonian. At low shear, this viscosity is generally very high though finite, but the power law models this as infinite. For suspensions under high shear, the viscosity roughly tends to that of the liquid medium, and for sewage this is mostly water. It is

intuitively clear that the viscosity of a suspension could never be less than that of the liquid medium, but the power law model describes a vanishingly small viscosity. Nevertheless, the accuracy of the model is guaranteed for all but the most extreme of applications.

A fluid that has no yield stress, but whose gradient of the shear flow function increases with increasing shear rate, is known as *dilatant* fluid. A dilatant fluid can be represented with a power law model where $n > 1$. These fluids are rarely encountered in practice.

A *yield pseudoplastic* fluid has both a yield stress and a decreasing gradient of the shear flow function for increasing shear rate; it is a hybrid of the Bingham and pseudoplastic fluids. This is often represented by the *general Bingham* model[6], which is given as

$$\tau = \tau_y + K\dot{\gamma}^n. \tag{2.10}$$

The general Bingham model is, in fact, much less frequently used than both the power law and Bingham models since two parameters are often enough to model a fluid. Nevertheless, some complex mixtures require a three parameter model. The general Bingham model describes yield pseudoplastic fluids with good accuracy, but fails for very high shear. Defining the viscosity as the gradient of the shear flow function, the viscosity of a yield pseudoplastic is constant for high shear, and can therefore be regarded as Newtonian. But much like the power law model, the general Bingham model erroneously describes a vanishingly small viscosity under high shear.

Figure 2-2 portrays the shear flow curves for time-independent, non-Newtonian, viscous fluids. Regarding these rheological models, whereas viscosity $\mu$, coefficient of rigidity $\eta$, and yield stress $\tau_y$ can be regarded as properties of their respective fluids, consistency coefficient $K$, and consistency index $n$ are truly empirical parameters. There are some shear flow models of pseudoplastic fluids that have a theoretical basis to them that can be regarded as *semi-empirical.* One such model is the Eyring-Prandtl equation[41, 42] based on the kinetic

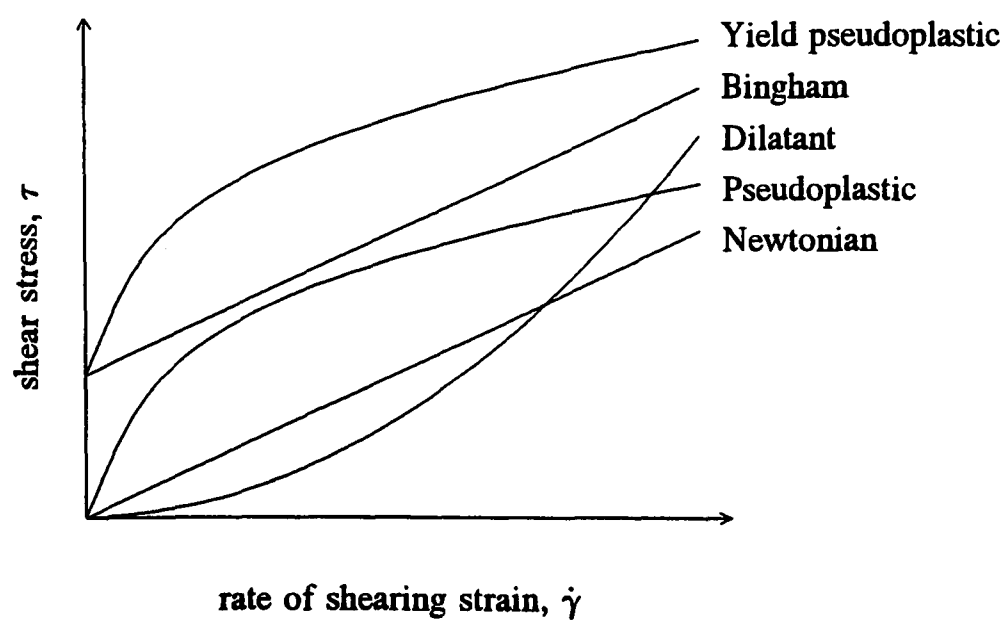


**Figure 2-2** Shear flow diagrams of some time-independent non-Newtonian fluids.

theory of liquids, which is given as

$$\tau = A \sinh^{-1}\left[\frac{\dot{\gamma}}{B}\right], \tag{2.11}$$

where $A$ and $B$ are coefficients characteristic of the fluid. Another well-known model founded on theory is the Carreau model [43] given by

$$\tau = \mu_0 \dot{\gamma}\left[1 + (\lambda\dot{\gamma})^2\right]^{\frac{m-1}{2}}. \tag{2.12}$$

This equation has a viscosity $\mu_0$ for low shear rates, which is a measured quantity rather than a fitted quantity. $\lambda$ is a characteristic time and $m$ is a measure of the rate of change of viscosity with shear rate in the shear thinning region. It is interesting to note that Equations (2.11) and (2.12) are completely different in form—Equation (2.11) is an inverse hyperbolic sine model and Equation (2.12) is a power law model—yet both equations are based on theory to model pseudoplastic fluids. Both equations were derived from the macroscopic considerations of molecules, but each using different underlying assumptions.

The Meter model [44] is an example of an implicit shear flow function for modelling pseudoplastics. It is a versatile four-parameter equation given by

$$\frac{\tau}{\dot{\gamma}} = \mu_\infty + \frac{\mu_0 - \mu_\infty}{1 + \left(\frac{\tau}{\tau_m}\right)^{a-1}}. \tag{2.13}$$

Unlike the power law model, it describes constant viscosities for both very low and very high shear—$\mu_0$ and $\mu_\infty$ respectively. These are measured quantities rather than fitted quantities. $\tau_m$ is the shear stress for which the viscosity is $\frac{1}{2}(\mu_0 + \mu_\infty)$.

So far, only time-independent fluids have been discussed where the fluid response is rapid enough to be considered as instantaneous. However, a fluid that exhibits changes in its rheology over time is a time-dependent fluid. For a *thixotropic* fluid, the 'viscosity' decreases under shear stress followed by a gradual recovery when the stress is removed. None-the-less, the time-dependency of a fluid is a matter of subjectivity as a pseudoplastic fluid could be considered as thixotropic with a very rapid recovery time. Taking the other extreme, recovery may be slow enough to consider the changes in the fluid as irreversible. For a *rheopectic* fluid, the 'viscosity' increases under shear stress followed by a gradual decline when the stress is removed. These fluids are relatively rare. Figure 2-3 offers a general classification of the fluids discussed so far.

A crude explanation of the flow behaviour of pseudohomogeneous fluids is obtained by considering the interaction of the solid particles in suspension [45]. The solid particles form a three-dimensional, solid elastic network (see Figure 2-4) that can withstand shearing

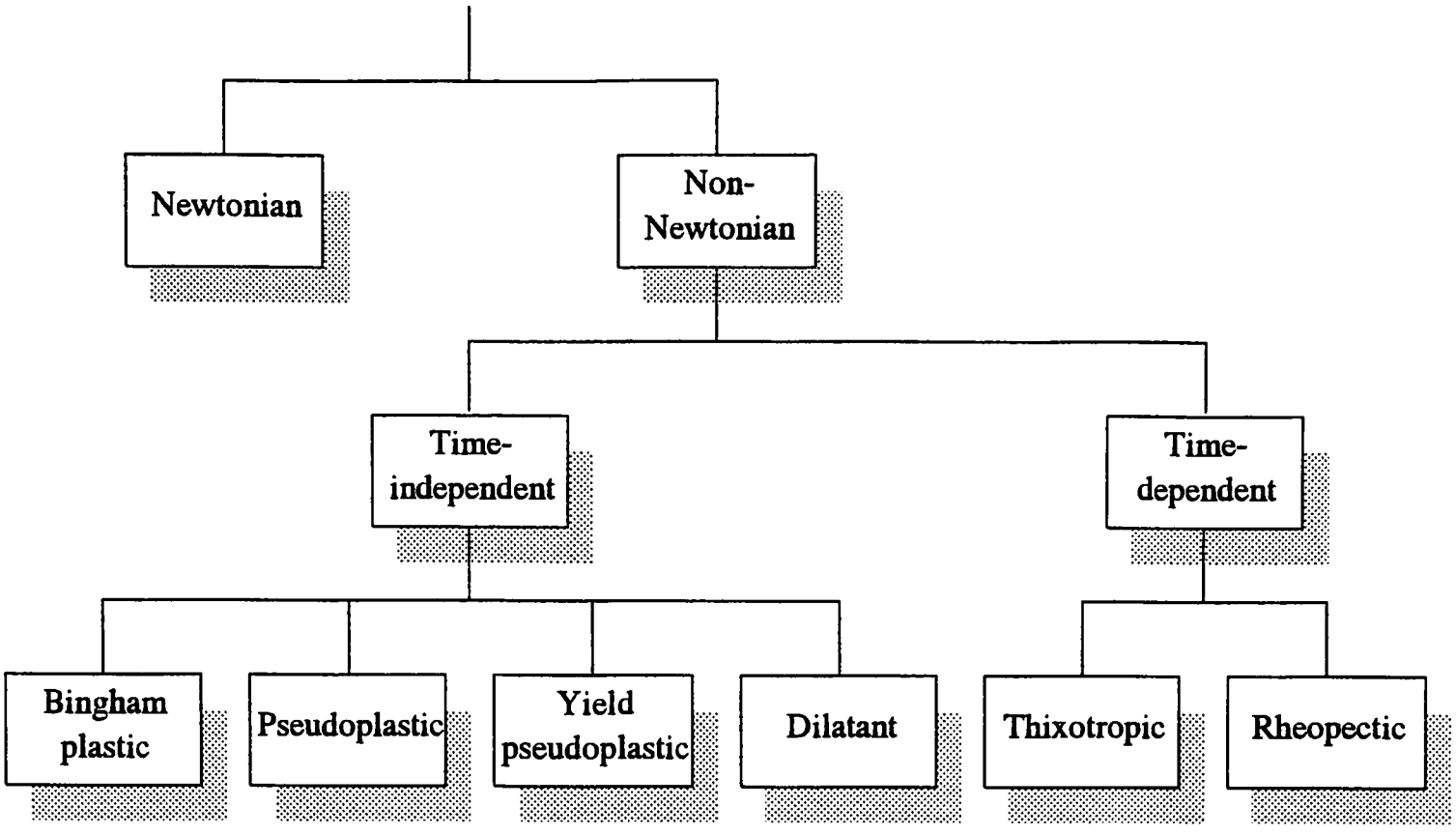


**Figure 2-3** Classification of pseudohomogeneous viscous fluids

stresses below the yield stress. Once the yield resistance to shearing is overcome, the particle network breaks up into particle agglomerates, which continue to break up at higher shear rates. The solid particles reassemble into a network, which can happen very rapidly (milliseconds) for a 'time-independent' fluid, or very slowly (days) in the case of a thixotropic fluid.

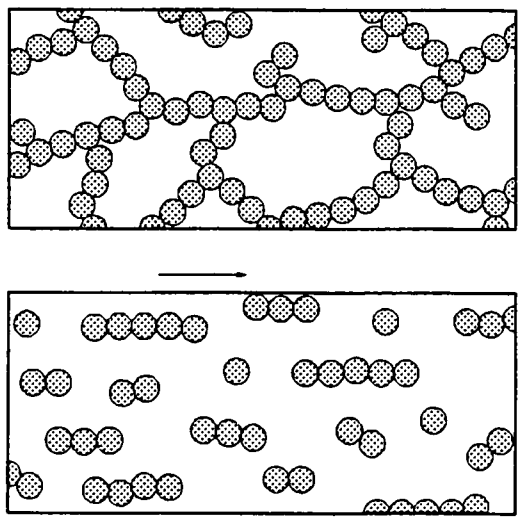

**Figure 2-4** The breakdown of a complex fluid under shear. The solid particles form a structure within the liquid medium that decays under shear stress.

Although viscosity is strictly the concept of a Newtonian fluid, there have been many definitions of a generalised viscosity for non-Newtonian fluids. An intuitive definition of viscosity is the gradient of the shear function given as

$$\mu = \frac{d\tau}{d\dot{\gamma}}. \tag{2.14}$$

Since this is difficult to work with mathematically, an apparent viscosity is a widely used alternative,

$$\mu_a = \frac{\tau}{\dot{\gamma}}. \tag{2.15}$$

The viscosity of a pseudoplastic fluid is constant for very low and very high shear, so Equations (2.14) and (2.15) are identical at these limits. It is much easier to picture a viscometric relationship than a shear flow relationship, but viscosity has no meaning for a Bingham plastic where the fluid is solid below a certain yield stress. For these fluids, shear stress is related to the *rate* of shearing strain for the fluid regions, and to shear strain for the solid regions. The former can be modelled by Equation (2.5), and the latter can be modelled by a function of the form

$$\tau = h(\gamma), \tag{2.16}$$

where $\gamma$ without the dot is strain rather than strain rate. Although the concept of viscosity is difficult to apply to Bingham fluids, this is not the case with pseudoplastic fluids. For instance, the Carreau equation (2.12) is often expressed as the apparent viscosity

$$\mu_a = \mu_0\left[1 + (\lambda\dot{\gamma})^2\right]^{\frac{m-1}{2}}.$$

## 2.2 Reynolds Stress

For steady turbulent flow, the instantaneous velocity at a point is not constant as for laminar flow, but fluctuates randomly about a mean value. For $x$-directional flow, but conveniently considering the fluctuations in two-dimensions, the instantaneous velocities in the $x$- and $y$-directions are respectively given by

$$\begin{aligned} u &= \bar{u} + u', \\ v &= v', \end{aligned} \tag{2.17}$$

where $\bar{u}$ is the mean velocity, and $u'$ and $v'$ are the fluctuating components. Placing Equations (2.17) into the time-averaged momentum equation yields the turbulent stress term

$$\tau_T = \rho\overline{u'v'}, \tag{2.18}$$

known as the *Reynolds stress*.

*Prandtl's mixing length* theory [25] is one of the simplest for estimating the Reynolds stress. The theory is based on the assumption that a fluid element, displaced in the transverse direction due to turbulent motion, transfers its $x$-momentum to the new location. The transverse displacement is known as the mixing length. Prandtl assumed that the standard deviations of the $x$- and $y$-direction velocity fluctuations are equal to the product of a mixing length and a velocity gradient, ie

$$\sqrt{\overline{u'^2}} = \sqrt{\overline{v'^2}} = l\frac{du}{dy}. \tag{2.19}$$

From Equation (2.18), this then gives the Reynolds stress as

$$\tau_T = \rho l^2 \left[ \frac{du}{dy} \right]^2. \tag{2.20}$$

Since the mixing length varies with distance from the wall, a simple assumption is a linear variation, ie

$$l = \kappa y, \tag{2.21}$$

where $\kappa$ is a universal constant taken to be 0.36. Van Driest[46] extended the model to include a wall damping factor, giving

$$l = \kappa y(1 - e^{-y/A}), \tag{2.22}$$

where $A$ is constant. Experimentally, damping has been found to be a function of the Reynolds number, so Gill and Scher[47] refined the mixing length model to give

$$l = \kappa y(1 - e^{-\phi \frac{y}{Y}}), \tag{2.23}$$

where

$$\phi = \frac{\mathrm{Re}^* - a}{b},$$

and

$$\mathrm{Re}^* = \frac{\rho U^* Y}{\mu}.$$

$Y$ is the maximum value of $y$, and $U^*$ is a friction velocity given as $\sqrt{(\tau_w/\rho)}$. The constant $a$—the critical value of $\mathrm{Re}^*$—was taken to be 60, and constant $b$ was determined experimentally to be 22.

Now total stress is just the sum of the laminar (or viscous) stress and the Reynolds stress, and is given by

$$\tau = \tau_L + \tau_T. \tag{2.24}$$

If $\mathrm{Re}^*$ is little larger than its critical value $a$, then the viscous stress term dominates Equation (2.24), whereas if $\mathrm{Re}^*$ is much larger than $a$, then the Reynolds stress dominates Equation (2.24). The mixing length model defined by Equation (2.23) is therefore valid for laminar-turbulent transitional flow and fully-developed turbulent flow. In Chapter 4, the discussion will be extended to time-independent, non-Newtonian, viscous flow through a pipe, which will be especially relevant to our application.

## 2.3 Solids Concentration Relations

In general, shear stress is related to rate of shear and other properties of a liquid suspension such as solids concentration, particle size distribution, and particle shape etc. Although

considerable effort has been spent in looking for an exact relationship between these variables [24], due to the inherent complexities of the system, there has been very little progress in establishing one. The differences between Equations (2.11) and (2.12) are therefore due to the particular assumptions on which each model is based.

The laminar flow viscosity of a suspension of rigid spheres was the subject of a theoretical analysis of Einstein [37], who derived the equation

$$\mu_m = \mu_l(1 + 2.5\,\Phi), \tag{2.25}$$

where $\mu_m$ is the viscosity of the mixture, $\mu_l$ is the viscosity of the liquid, and $\Phi$ is the volume fraction of solids. The equation—which was derived on the assumption that there were no particle interactions—is accurate for suspensions of less than about two percent by volume. A more complex empirical relation derived by Thomas [38] is

$$\mu_m = \mu_l(1 + 2.5\,\Phi + 10.05\,\Phi^2 + 0.00273\,e^{16.6\,\Phi}), \tag{2.26}$$

and agrees with data for suspensions of up to twenty percent by volume. The main drawback of the two models is that they do not account for particle agglomeration and are therefore only relevant for Newtonian fluids.

For a Bingham fluid, Thomas [39] obtained relations that may be applied to a broad range of materials. These are given as

$$\tau_y = k_1\Phi^3, \tag{2.27}$$

and

$$\eta = \mu_l e^{k_2\Phi}. \tag{2.28}$$

These relations are valid for suspensions of up to twenty three percent by volume. Relationships between volume fraction of solids and rheological parameters are often expressed graphically rather than functionally. For an activated sewage sludge, Dick and Ewing [40] offer a plot of yield stress against solids concentration from three different sewage plants, each crudely exhibiting a different linear relation on a log-linear scale, thus suggesting an exponential relationship between yield stress and solids concentration. For primary, secondary and digested sludges, Mulbarger *et al* [3] offer plots of yield stress and coefficient of rigidity against solids concentration on a log-linear scale. There is an immense amount of scatter, particularly for yield stress, making it difficult to establish any specific relation between each parameter and solids concentration. Carthew *et al* [4] extended the plots of Mulbarger with there own data. On these log-linear plots of yield stress and coefficient of rigidity, the correlations that are almost linear, suggesting exponential relations between these parameters with solids concentration. A main objective of this research is to examine the behaviour of rheological parameters with solids concentration. Firstly, however, an introduction of the data to be analysed is the subject of the next chapter.

# 3 The Data

This chapter briefly introduces an extensive body of sewage sludge flow data on which this research is primarily centred. The objectives are not to present all of the data, but a selection of it that includes a sample of typical data, an illustration of time-dependency, a sample of unusual data, evidence of wall slippage, and the effect of solids concentration. The data [10] were compiled from viscometric measurements of concentrated sewage sludge originating from several different regions of England (mainly the south), and with varying solids concentration. The data were recorded at the Warren Spring Laboratories for the Water Research Centre during October 1978 to May 1980. The measurements are of two types: full-scale pipeline that includes the entire laminar, transitional and turbulent flow regimes, and tube viscometry, that generally includes the laminar flow regime only. For a pipe flow test, the sewage was pumped from a tank, through a straight smooth pipe, into a sump, and sometimes recirculated back to the tank. The tube viscometric measurements were generally recorded before, during and after each pump-pipe trial. The pipe was of length 21 m and diameter 104.3 mm from which pressure gradient readings of known flow rate were taken along a 9 m section. The tube was usually of 26.65 mm diameter.

## 3.1 Data Sample

A fairly typical set of data is illustrated by Figures 3-1 and 3-2 and is of a digested sludge from Perry Oaks. The second figure is of four pipe flow tests where the sludge is recirculated from the sump back to the tank in each case. The first of the figures shows the three tube flow tests recorded before, during, and after the pump-pipe trial respectively. As noted in the introduction to this chapter, whereas the tube flow measurements only generally include the laminar flow regime, the pipe flow measurements include the laminar, transitional and turbulent flow regimes.

Sewage sludge can be lumpy and difficult to manage, so this is why tubes and pipes have been effectively used as viscometers. Consequently, the tube flow data are given as pseudo-shear flow data—namely wall stress $\tau_R$ versus pseudo-shear rate $8U/D$. For a Newtonian fluid, the pseudo-shear flow relationship is, in fact, the same as the true shear flow relationship (this will be further discussed in Chapter 4). For a non-Newtonian fluid, although the pseudo-shear flow relationship is not the same as the true shear flow relationship, it can, none-the-less, be regarded as comparable. For instance, Figure 3-1 shows that the viscosity of the sludge decreases with increasing shear (pseudoplasticity), and that there is a yield stress to the sludge which is given at the intersection of the curve with the wall stress axis.

Pipe flow data are given as hydraulic gradient $i$ versus mean cross-sectional velocity $U$ measurements. The more familiar friction plots are used in this report where the coefficient

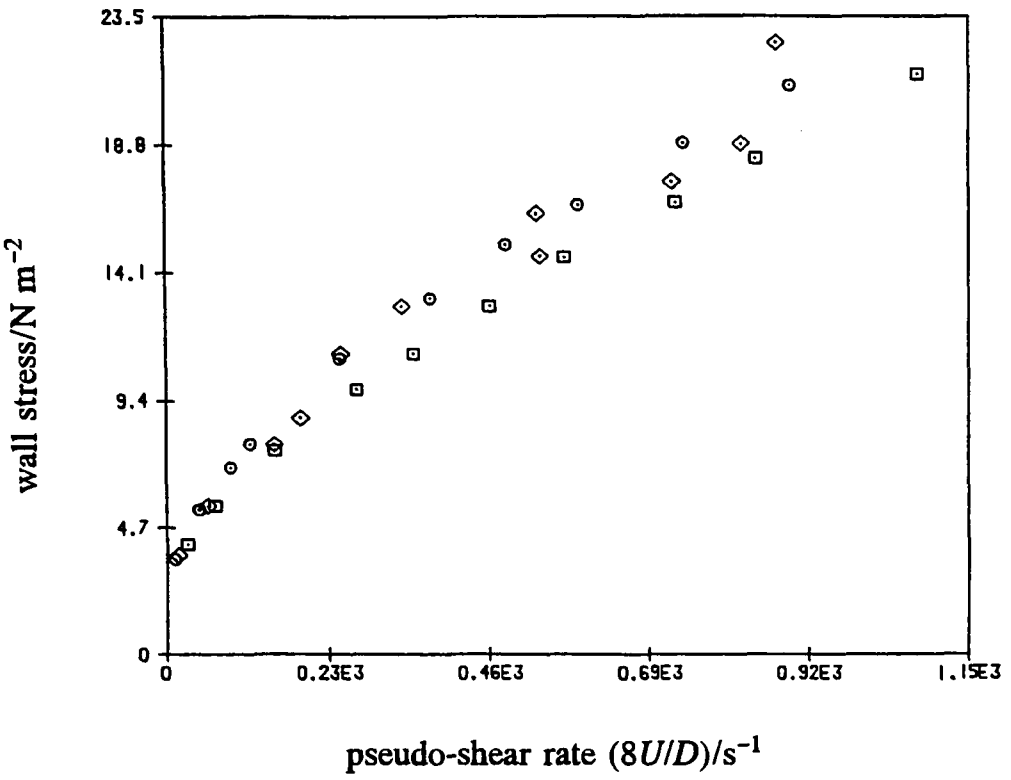


tube flow test:
- ⊙ before pumping
- ◇ during pumping
- ⊡ after pumping

**Figure 3-1** Tube flow tests of a digested sludge from Perry Oaks taken before, during and after the pump-pipe trials.

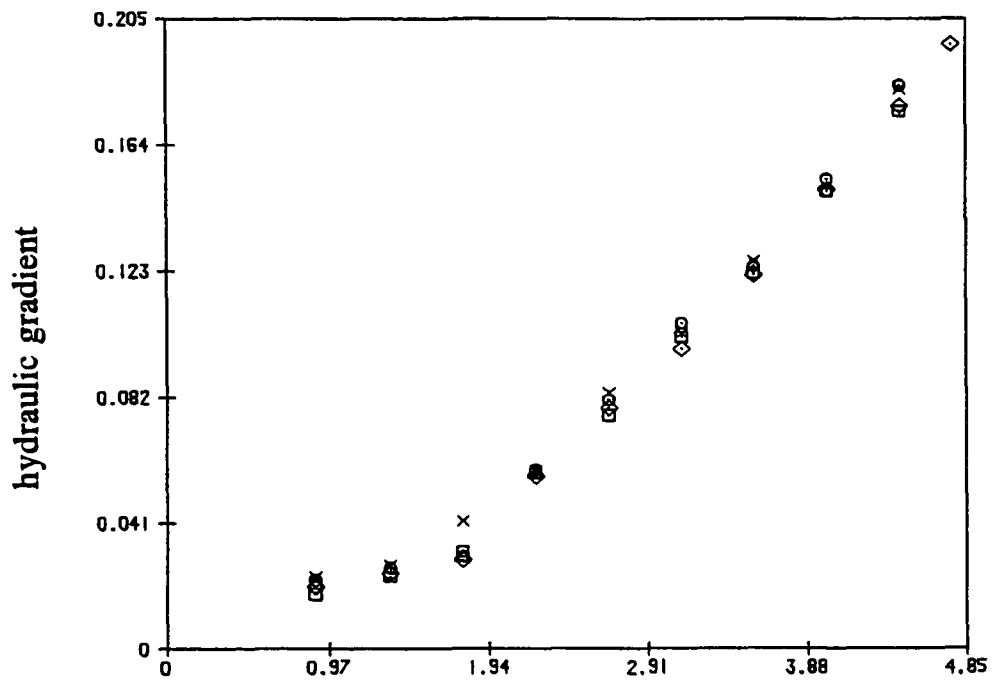


pipe flow test:
- × 1
- ⊙ 2
- ◇ 3
- ⊡ 4

**Figure 3-2** Four pipe flow tests of the sludge sample of Figure 3-1. Notice the 'smooth' transition from laminar to turbulent flow of the first test.

of friction is given by

$$f = \frac{gDi}{2U^2},$$

where $g$ is the acceleration due to gravity. For pipe flow data such as Figure 3-2, the critical point is sometimes conspicuous as it is the point where the gradient changes discontinuously. However, looking at the first pipe flow result in isolation, there is a smooth transition from laminar to turbulent flow making a qualitative assessment of the critical point difficult. Most other sludge tests from this data body admit this smooth transitional region.

## 3.2 Sludge Categories

Figures 3-1 and 3-2 showed the data of just one set out of a total of nearly one hundred sets. This gives some idea of the enormity of the data body, and may give the impression that it

is very extensive. However, the possible sources of sewage sludge variation are themselves numerous. The three main variants of a sewage sludge that were included in the measurements are: region (town and county of origin), sludge type (primary, activated or digested), and solids concentration by mass. These three variants are all likely to affect the flow behaviour of a sludge. Summaries of these are as follows:

1. **Region** Regional variation arises from industrial content and sewage plant design. Industrial content, hence regional variation, can vary considerably with time.

2. **Sludge type** *Primary sludge* is raw untreated sludge; *activated sludge* is sludge that has been broken down by bacteria in large open pools; *digested sludge* is sludge that has undergone decomposition in large tanks.

3. **Solids concentration by mass** This varies with a maximum of twelve percent. Solids concentration was artificially varied by successively diluting the sludge with water in the test laboratory.

Table 3-1 lists the three variants—region, sludge type and solids concentration—for each batch of sludge tested. Also included is the total pseudo-shear rate $8U/D$ range over which the measurements were made. Note that, although there is a total of 96 data sets, there is only one batch of activated sludge and the other batches came from a limited number of regions. Although Figures 3-1 and 3-2 portray a typical data set, it would be misleading to suggest that all of the data sets contain the same type and number of tests. Some of the other data include variations such as sludge density, pipe diameter, and time dependency.

**Table 3-1** Short summary of the Water Research Centre data

| Region | Sludge type | No of Sets | Solids range | $(8U/D)/s^{-1}$ |
|---|---|---|---|---|
| Bedlow | Primary | 1 | 3.0% | 71.3 - 382 |
| Rye Meads | Primary | 1 | 4.1% | 17.3 - 587 |
| Mansfield | Primary | 1 | 7.6% | 80.9 - 959 |
| Southend | Primary | 1 | 6.9% | 163.5 - 1523 |
| Southend | Primary | 7 | 3.5 - 8.9% | 20.5 - 1476 |
| Ipswich | Primary | 7 | 2.6 - 6.4% | 5.9 - 959 |
| Maple Lodge | Activated | 10 | 1.3 - 6.4% | 2.3 - 1339 |
| Letchworth | Digested | 8 | 1.8 - 5.8% | 4.4 - 2278 |
| Perry Oaks | Digested | 2 | 5.2 - 6.5% | 1.0 - 1943 |
| Perry Oaks | Digested | 7 | 4.5 - 6.5% | 2.0 - 859 |
| Perry Oaks | Digested | 51 | 3.7 - 12.0% | 1.3 - 2474 |
| | Total | 96 | | |

## 3.3 Data Entry

The data were supplied from the Water Research Centre in text form rather than in computer compatible media. There was no access to a text scanner, though even if there had been, the

text was so small and illegible that a scanner was unlikely to have been helpful. All the text therefore had to be entered manually on to a PC. The data were structured into a format that enabled it to be accessed directly from computer files. This was to enable the data to be graphically displayed or plotted, and subsequently analysed. A file structure was constructed to cater for each and every type of test, and considering the diversity of the data, this was not a simple problem.

## 3.4 Time Dependency

The data of the laboratory report contain much evidence that sewage sludge is thixotropic. Figure 3-3 shows the 'gelling' effect of a digested sludge from Perry Oaks that has been tested over a several day period. Notice that the apparent viscosity of the sludge increases as time progresses. The effect is not very pronounced, but the viscosity increase is more notable at first, reaching a limiting viscosity with time.

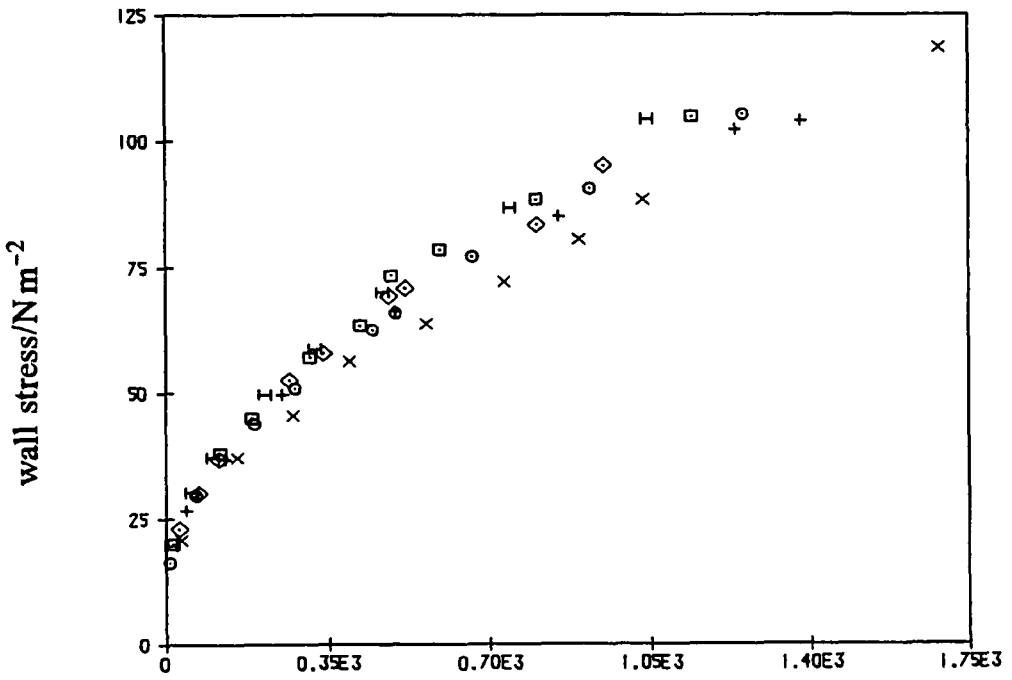


**Figure 3-3** Digested sludge from Perry Oaks tested on the day indicated.

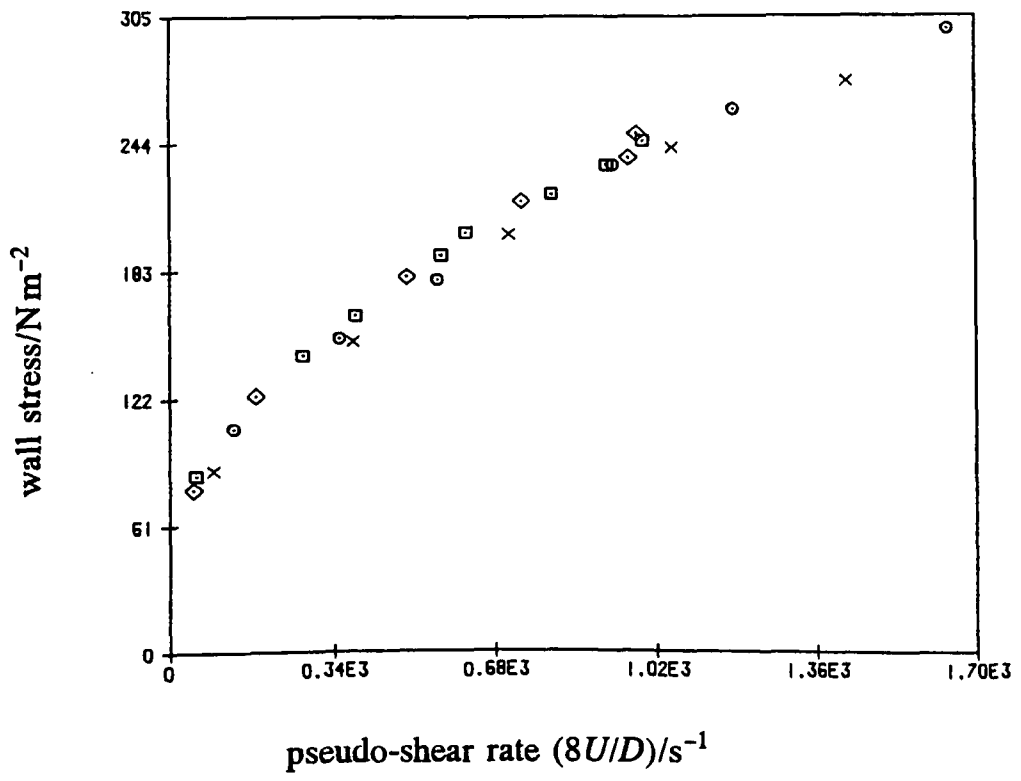


**Figure 3-4** Digested sludge from Perry Oaks left standing for indicated time period.

Figure 3-4 is another such plot tested over a similar time span, though measured in hours. In this case the effect is less pronounced but still observable. The reason for the difference between the figures is not clear as both sludge samples are from the same batch. However, the first sample has a concentration of 12 percent solids by weight and the second sample has been diluted to 8.6 percent. It would be reasonable to suggest that the thicker sludge is more thixotropic than the thinner sludge, but the sample history would have to be considered also.

Figures 3-5 and 3-6 are tube flow measurements of a Perry Oaks digested sludge with a mass solids content of 6.5 percent. Both figures are measurements of the same batch of sludge but recorded on different days. The first figure shows that there is a radical difference in

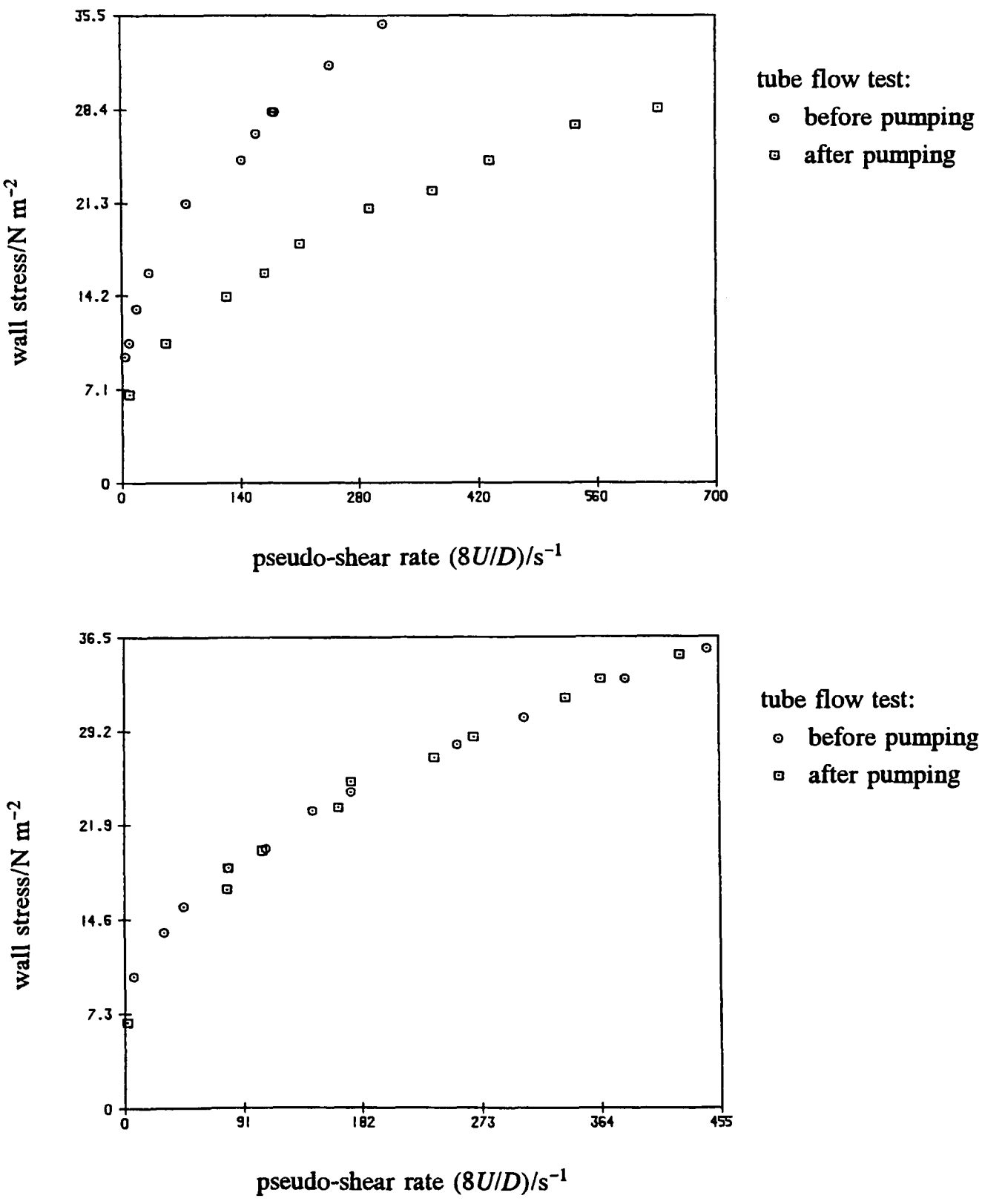


**Figures 3-5 and 3-6** Tube flow data of a digested sludge from Perry Oaks recorded on different days. The first figure shows that there is a radical difference of viscosity as a result of pumping; the second figure shows the difference to be negligible.

the apparent viscosity of the sludge before and after the pump-pipe trial, but the second figure shows that there is virtually no change in viscosity as a result of pumping. Again, there is no way of quantifying these effects for the data; there is no way of knowing the exact shear history of any particular sludge batch, or for that matter, any particular volume of sludge. It would be consistent with the laboratory record to suggest that, whereas the first test was conducted on undisturbed sludge, the second test was conducted on agitated sludge. There is one effect that is invariably consistent with all data: a sludge before pumping is *never* more viscous during pumping, and similarly, a sludge during pumping is *never* more viscous after pumping.

Now referring to Figures 3-7 and 3-8. These are plots of some tube flow data from a Southend primary sludge, and are rather unusual. Considering the first of the figures, there is a gradient change consistent with a regime change from laminar to turbulent flow. Although this change was questioned on the merit of a single outlying point of datum, the

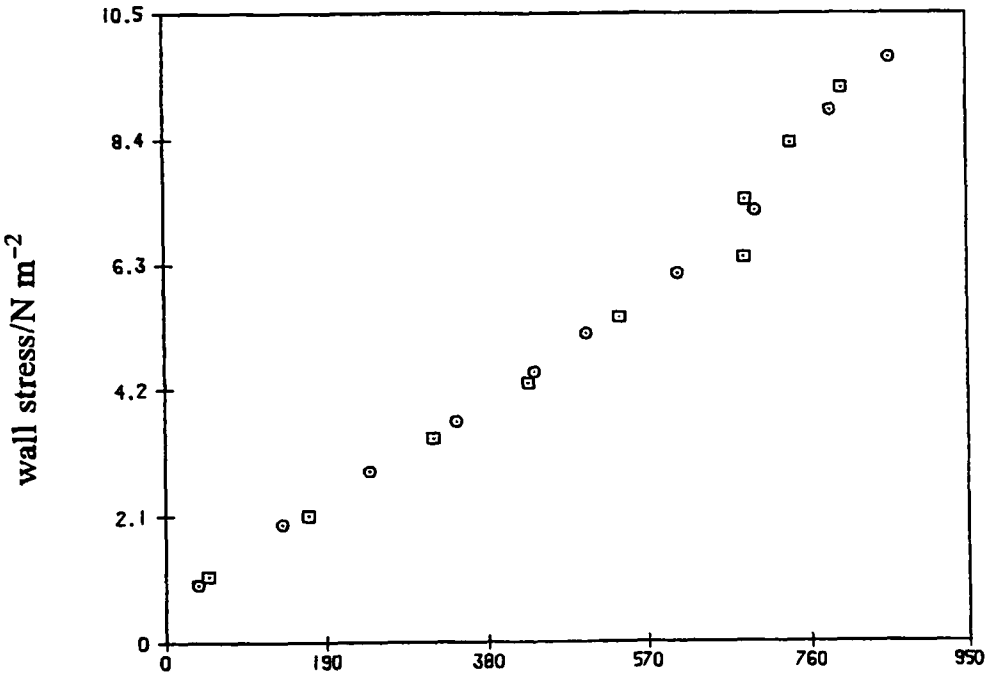


**Figure 3-7** Although tube flow data in general are laminar, there are some non-laminar measurements in these data of a primary sludge from southend.

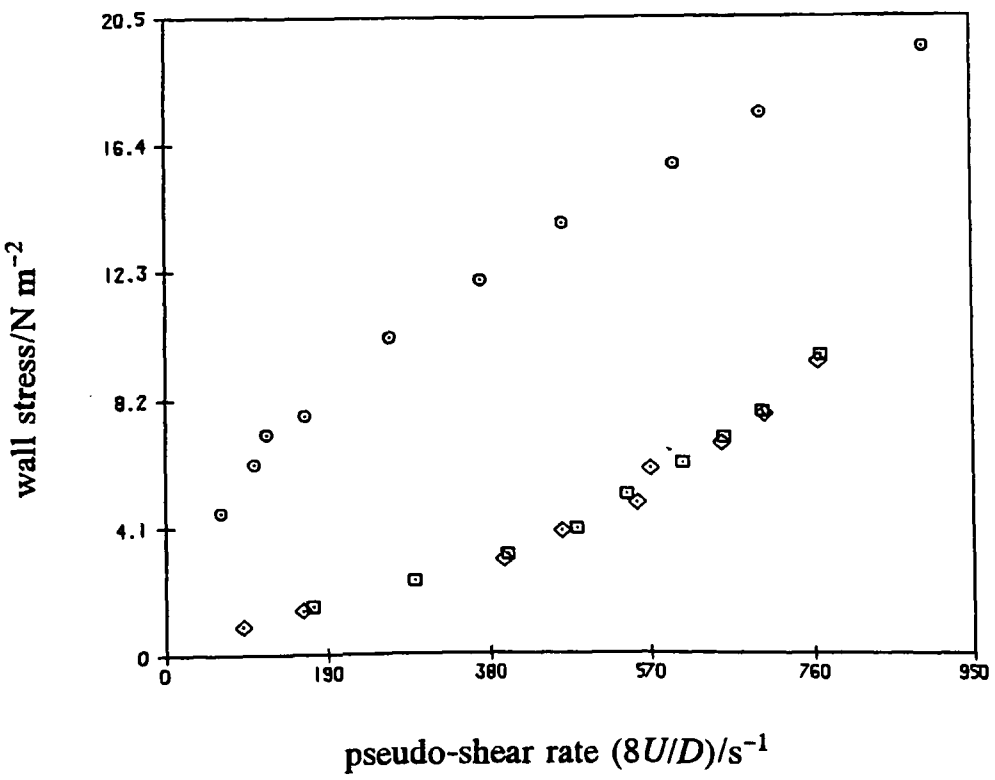


**Figure 3-8** Tube flow data of a primary sludge from Southend appear to be all laminar before the pump-pipe trials, but not all laminar during and after the pump-pipe trials.

outlying point does however mark the beginning of a gradient increase in the plot. To accept the gradient increase as part of the laminar flow regime would be to accept that the sludge had shear thickening properties (thicker at higher shear rates). Since none of the data of the laboratory report support this conjecture, the gradient increase must be due to a change of flow regime.

Figure 3-8—the second of the figures—is a particularly interesting example. The tube flow measurements were taken, as usual, before, during and after pumping and, as usual, on the same day. Whereas the test taken before pumping shows an expected decrease in gradient, the tests taken during and after pumping show a marked increase in the gradient. As with the previous figure, a gradient increase can only be due to a laminar to turbulent change of flow regime. This explanation is validated by noting that tube flow data includes the laminar flow range; if this had been the case before pumping, then the same range used during and after pumping would result in a laminar-turbulent change of flow regime. Figure 3-8 clearly shows that the sludge experienced shear thinning, generally becoming much thinner during and after pumping, which resulted in an early onset of the laminar-turbulent change of regime. The only alternative explanation is that the fluid transformed from a shear thinning fluid before pumping to a shear thickening fluid during and after pumping; a scenario that is totally implausible.

Although it may seem like trivial observations are being made about the data, a main objective is to obtain laminar flow models from laminar flow data only. Not to recognise any turbulent flow data would result in erroneous laminar flow functions being modelled on it. Since there are vast amounts of data, another main objective is to automatically produce shear flow function parameters from the raw data with the aid of a computer program. This is regarded as a potential blind procedure that requires careful overseeing.

## 3.5 Evidence of Wall Slippage

Wall slippage occurs when there is a finite velocity of fluid at a wall. A formal treatment of this effect will be given in the next chapter, but for the moment, it is adequate to say that pipe wall slip is a function of both wall stress and pipe diameter. Such an effect can be identified by plotting the pseudo-shear flow data at each diameter; if the curves coincide then there would be no wall slippage, but if the curves are different, wall slippage would be present. Very few tests were conducted on pipe diameter variation and all of them used digested sludge only. The one result of any real significance is shown by Figure 3-9 of a digested sludge from Perry Oaks at 8.8 percent concentration by mass. The tests are plotted in the order they were conducted but notice that the same pipe diameter is used in two of the tests. A close examination of these limited data shows that there is a consistent correlation between pipe diameter and apparent viscosity—the larger the diameter the greater the

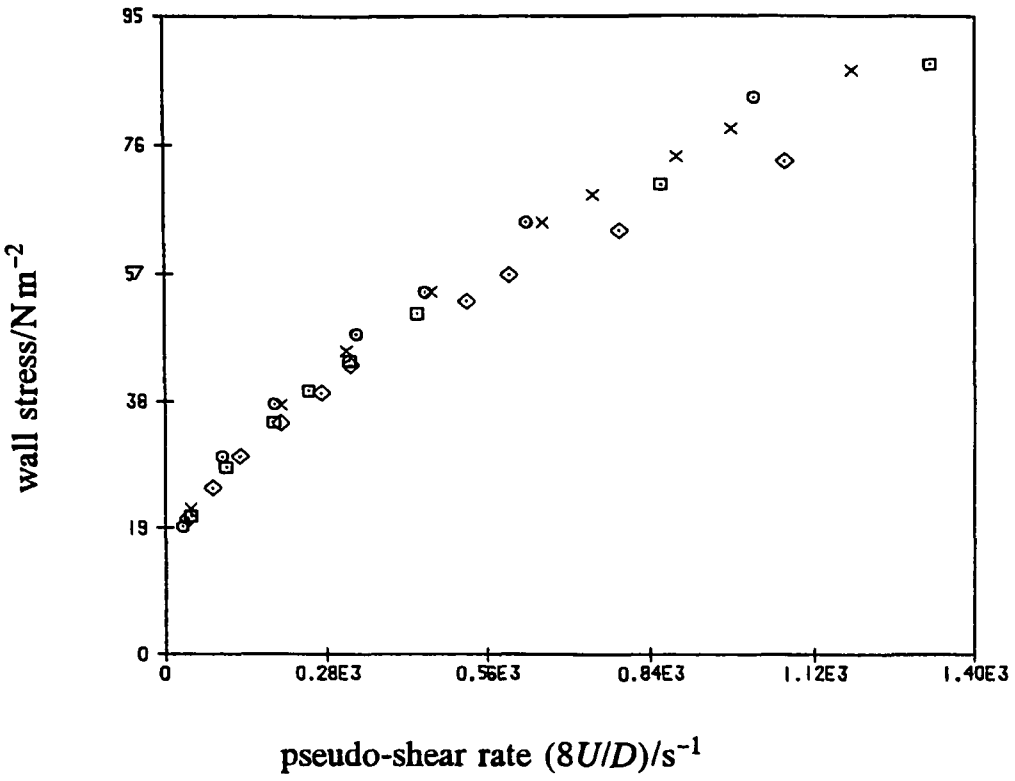


**Figure 3-9** Variation of pipe diameter on a digested sludge from Perry Oaks.

viscosity. The figure also shows that there is a difference, though lesser in extent, between the two tests of the same diameter. From this plot it can be concluded that wall slippage occurs. Unfortunately, it is not possible to gauge the effect of different sludge types at different solids concentrations, all of which are likely to have an effect. Wall slippage can also be examined by comparing the tube flow data with the pipe flow data since the diameters of these tests are considerably different. Unfortunately, besides there being only two diameters to compare, much of the pipe flow data are non-laminar. Nevertheless, wall slippage should affect the accuracy of a scale-up prediction, and such an appraisal will be given in Chapter 7.

## 3.6 Solids Concentration

Overleaf, Figures 3-10, 3-11 and 3-12 show the variation of solids concentration by mass for tube flow measurements of primary, activated and digested sludges respectively. For consistency, all the tube flow measurements have been chosen before pumping, and for each sludge type, the data are from the same batch, but successively diluted over a period of several days. It can clearly be seen that solids concentration has a dramatic effect on the viscosity of a sludge; an increase in sludge concentration radically increases the overall sludge viscosity. It can also be observed that the effect is non-linear; the rate of increase of viscosity increases with solids concentration. Other effects such as shear thinning would also be present, though even in the most extreme case (see Figure 3-5) it can be seen that shear thinning is still a relatively minor effect. It must therefore be concluded that a sewage sludge model should account for the effects of solids concentration—the subject of Chapter 8. Firstly though, the necessary algorithms for modelling pipe flow are addressed in the next chapter.

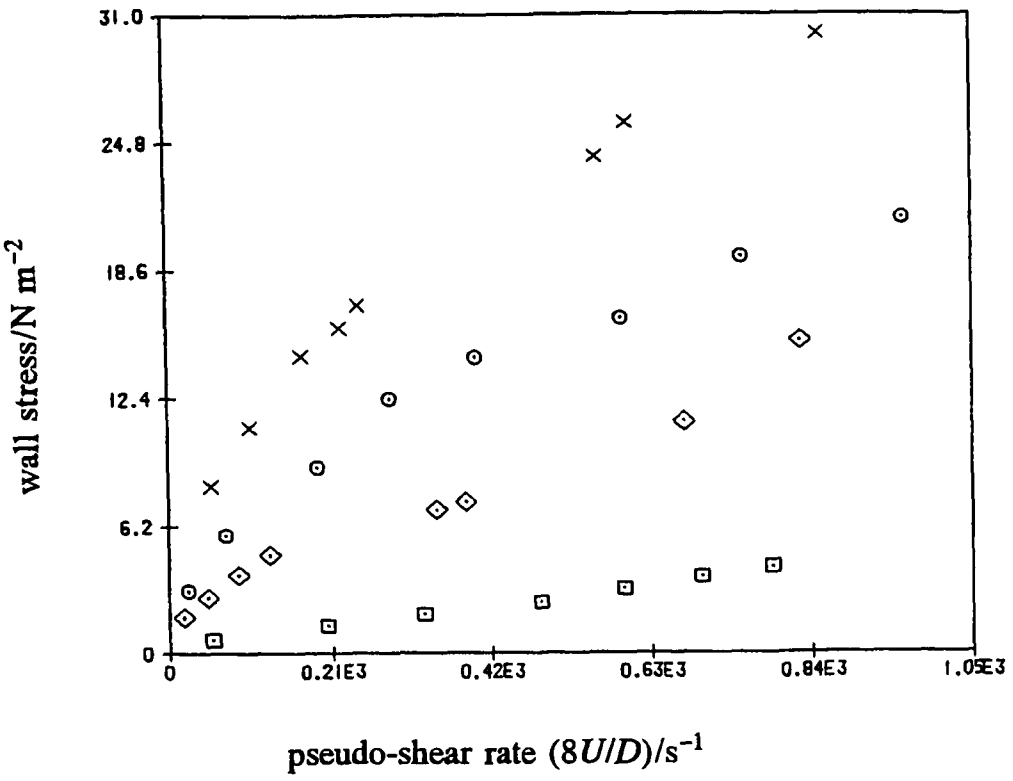


solids concentration:
- × 6.44%
- ⊙ 5.55%
- ◇ 4.81%
- ⊡ 2.77%

**Figure 3-10** Variation of viscosity with solids concentration by mass for a primary sludge from Ipswich.

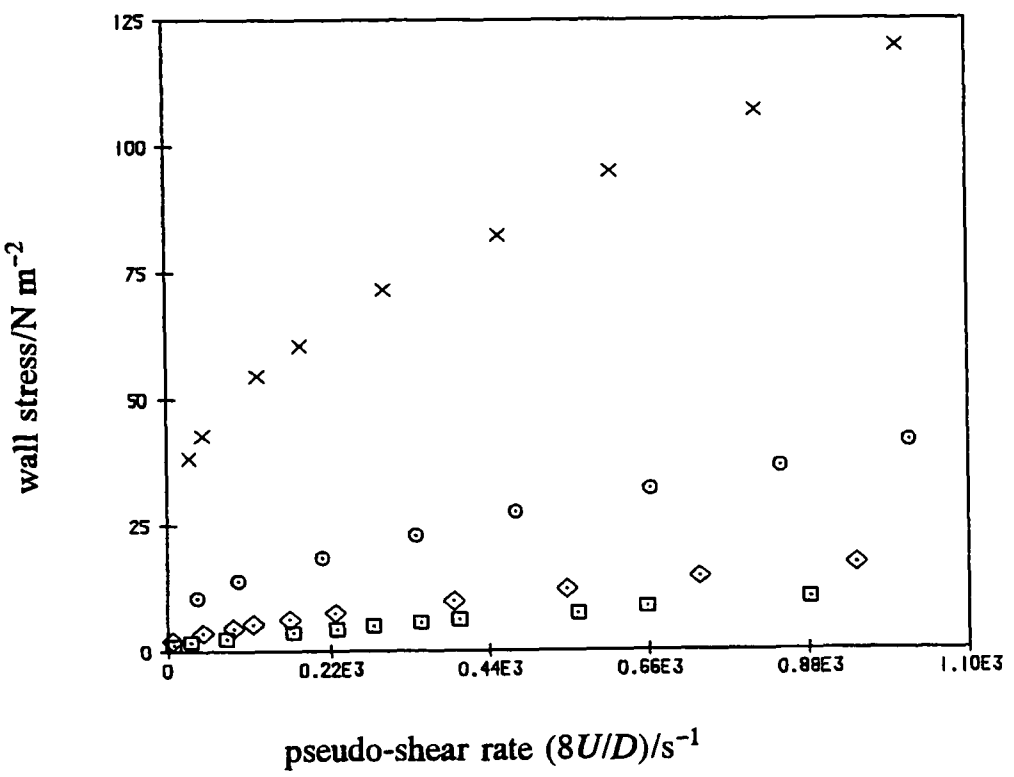


solids concentration:
- × 4.56%
- ⊙ 3.50%
- ◇ 2.62%
- ⊡ 2.19%

**Figure 3-11** Variation of viscosity with solids concentration by mass for an activated sludge from Maple Lodge.

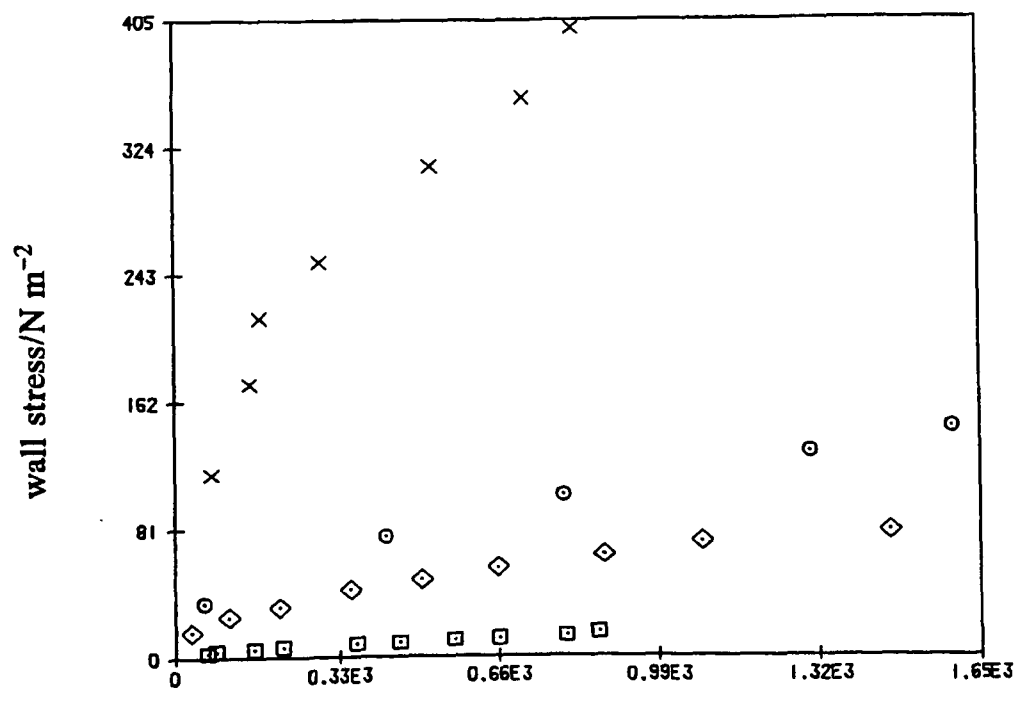


solids concentration:
- × 12.00%
- ⊙ 10.00%
- ◇ 7.86%
- ⊡ 4.27%

**Figure 3-12** Variation of viscosity with solids concentration by mass for a digested sludge from Perry Oaks respectively.

# 4 Pipe Flow Equations

In the previous chapter, it was remarked that sewage sludge is lumpy and difficult to manage, so the viscometry was conducted by the sewage industry using pipes and tubes. As a result, the flow behaviour of sewage sludge has to be deduced from pipe flow data. This chapter reviews mathematical models of the flow of time-independent, non-Newtonian, viscous fluids through a straight pipe where laminar, critical and turbulent flow regimes are considered in turn. The fluid will primarily be regarded as pseudohomogeneous, but in the final section, wall slippage will be considered. The equations of particular relevance are given in borders, and the other equations either highlight the development of the material, or provide useful analytical solutions to which numerical approximations can be compared later.

## 4.1 Governing Equations

Consider the flow of fluid through a straight pipe as illustrated by Figure 4-1.

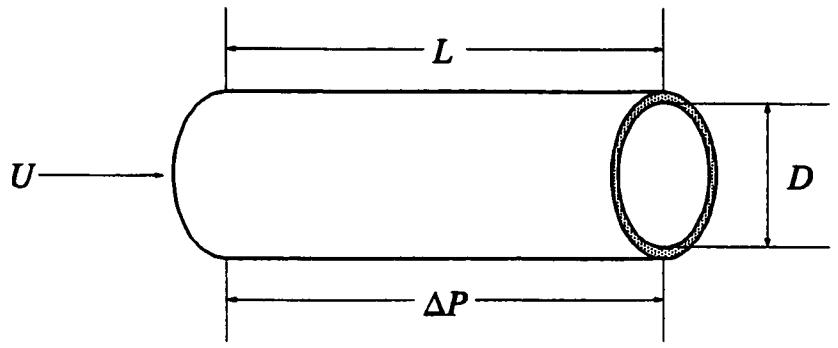


**Figure 4-1** Pipe and flow parameters.

For fully-developed flow, it may be assumed that the radial and angular velocity components are zero, and that the only stress component acts in the axial direction on a surface normal to the radial direction. With these assumptions in mind, the equations of motion[48] are given by

$$\begin{aligned} r\text{-equation:}\ & \frac{\partial P}{\partial r} = 0, \\ \theta\text{-equation:}\ & \frac{1}{r}\frac{\partial P}{\partial \theta} = 0, \\ z\text{-equation:}\ & \frac{\partial P}{\partial z} = \frac{1}{r}\frac{\mathrm{d}}{\mathrm{d}r}(r\tau). \end{aligned} \tag{4.1}$$

Without loss of generality, $P$ may include a gravity term where, for instance, the pipe flow is non-horizontal. The first two expressions show that $P = P(z)$ only, and therefore

$$\frac{\mathrm{d}P}{\mathrm{d}z} = \frac{\Delta P}{L}. \tag{4.2}$$

Using the initial condition $\tau = 0$ at $r = 0$, the third expression integrates to give

$$\tau = \frac{r}{2}\frac{\Delta P}{L}. \tag{4.3}$$

At $r = R$, this gives the following relationship between wall stress and pressure gradient:

$$\tau_R = \frac{R}{2}\frac{\Delta P}{L}. \tag{4.4}$$

The above equation pair can be combined to give a linear relationship between shear stress and radial distance, which is

$$\frac{\tau}{\tau_R} = \frac{r}{R}. \tag{4.5}$$

Since Equations (4.1) are in terms of shear stress, the equations so far make no assumptions about the rheology of the fluid being used. These equations are valid for any fluid, and will often be referred to in the following discussion of laminar, critical and turbulent flow.

### 4.1.1 Dimensionless Forms

Flow equations can be expressed as relationships between dimensionless groups [49] that are especially useful for defining graphical or empirical relationships of a flow situation. Since the objectives of this research are to use well-heeled numerical methods to model the flow equations, these dimensionless groups are less useful. In other words, rather than depend on graphical relations between dimensionless groups, the emphasis will be on providing PC based computer algorithms to perform the calculations. However, dimensionless groups are more than just a convenient way of expressing flow relations as they can, for instance, be used to identify the critical point that divides the laminar flow regime from the transitional/ turbulent flow regime. In this subsection, three widely used dimensionless groups will be introduced: the Fanning friction factor, the Reynolds number and the Hedström number. The latter two groups were originally derived for specific fluid types, but extension to other fluids will be discussed later on in this chapter.

The Fanning friction factor is a dimensionless group defined as the following ratio between frictional forces to inertial forces:

$$f = \frac{\tau_R}{\frac{\rho U^2}{2}}. \tag{4.6}$$

Notice that this ratio is indicative of the relative importance of the wall stress with respect to the kinetic energy per unit volume of fluid.

The Reynolds number for a Newtonian fluid is defined as the dimensionless group

$$\mathrm{Re} = \frac{\rho UD}{\mu}, \tag{4.7}$$

and is a measure of the ratio of inertial forces, $\rho U^2/D$, to viscous forces, $\mu U/D^2$. In 1883, Reynolds conducted some classical experiments of Newtonian fluid flow through pipes, and

showed that fluid flow may either exhibit laminar or turbulent motion. For low Reynolds numbers of less than about 2 100, the viscous forces dominate the inertial forces, and laminar (or streamlined) flow prevails. However, for high Reynolds numbers greater than about 4 000, the inertial forces dominate the viscous forces and, as reviewed in Section 2.2, turbulent flow prevails. For intermediate Reynolds numbers, fluid flows in a transitional state between laminar and turbulent flow.

The Hedström number[50] is a group that accounts for the yield stress of a fluid. For Bingham fluids, $\tau = \tau_y + \eta\dot{\gamma}$, Hedström used dimensional analysis[49] to show that the friction factor has the functional form

$$f = \phi\left(\frac{\rho D^2 \tau_y}{\eta^2}, \frac{\rho VD}{\eta}\right), \tag{4.8}$$

where the first of these groups is known as the Hedström number, He. The second of these groups has the form of a Reynolds number, and can be considered as a Reynolds number for Bingham fluids.

## 4.2 Laminar Flow Equations

For steady flow through a pipe, the volumetric flow rate is

$$\pi R^2 U = 2\pi \int_{r_y}^{R} r u(r) \mathrm{d}r + \pi r_y^2 u(r_y), \tag{4.9}$$

where $U$ is the mean cross-sectional velocity, $r$ is the radial distance, $u(r)$ is the velocity at $r$, and $r_y$ is the radius of the plug core. The two parts of the right-hand side of the equation define the fluid and solid regions of the flow respectively. In practice, a relation between pressure per unit length of pipe, $\Delta P/L$, and mean cross-sectional velocity, $U$, is required. However, the relation between the pipe wall stress, $\tau_R$, and a *pseudo-shear rate* defined as

$$\Gamma = \frac{8U}{D}, \tag{4.10}$$

is equivalent, but much more convenient to work with.

Integrating Equation (4.9), combining it with Equations (4.5) and (4.10), and using $-\mathrm{d}u/\mathrm{d}r = \dot{\gamma}$, yields

$$\boxed{\Gamma = \frac{4}{\tau_R^3} \int_{\tau_y}^{\tau_R} \tau^2 \dot{\gamma} d\tau.} \tag{4.11}$$

The rate of shear term, $\dot{\gamma}$, can be eliminated from this equation with a relevant rheological equation, such as one of the equations (2.7) to (2.13). This gives a relation—known as the *pseudo-shear flow function*—between the pipe wall stress and the pseudo-shear rate. The pseudo-shear flow function is a pipe flow equivalent of the true shear flow function; the former models the viscosity within a pipe and the latter models the viscosity between parallel plates.

For the Newtonian case, using Equation (2.7) to eliminating $\dot{\gamma}$ from Equation (4.11) gives the Hagen-Poiseuille equation,

$$\tau_R = \mu\Gamma. \tag{4.12}$$

Via Equations (4.4) and (4.10), this establishes a relation between pressure gradient and mean cross-sectional velocity. It is no coincidence that this equation has the same form as the corresponding shear flow function $\tau = \mu\dot{\gamma}$ as it is from this equation that $\Gamma$ is normally defined. It therefore follows that $\Gamma = \dot{\gamma}_R$ for Newtonian fluids, though this is not generally true for other fluids.

Using Equations (4.6) and (4.7), a well-known relationship between $f$ and Re is revealed by Equation (4.12), and is given by

$$f = \frac{16}{\mathrm{Re}}. \tag{4.13}$$

This is significant as it defines a theoretical relation between $f$ and Re for the laminar flow of a Newtonian fluid through a straight pipe. This has been the impetus for obtaining semi-empirical relations between $f$ and Re for turbulent flow, and some of these relations will be discussed in Section 4.4.

For the Bingham case, using Equation (2.8) to eliminate $\dot{\gamma}$ from Equation (4.11) gives the Buckingham [51] equation,

$$\Gamma = \frac{\tau_R}{\eta}\left[1 - \frac{4}{3}\left[\frac{\tau_y}{\tau_R}\right] + \frac{1}{3}\left[\frac{\tau_y}{\tau_R}\right]^4\right]. \tag{4.14}$$

It is apparent that, via Equations (4.10) and (4.4), this equation can be used to directly evaluate the mean cross-sectional velocity for a given pressure gradient. For the inverse problem where $U$ is known and $\Delta P/L$ is required, an iterative scheme is needed. However, if the ratio $\tau_y/\tau_R$ is small, the quartic term can be neglected to give the explicit approximation

$$\tau_R = \frac{4}{3}\tau_y + \eta\Gamma. \tag{4.15}$$

The yield stress of this equation is $(4/3)\tau_y$ which is a contradiction in terms since it should be $\tau_y$. None-the-less, Equation (4.15) is a good approximation of Equation (4.14) for higher

values of $\Gamma$. Equation (4.15) is also often expressed as the following dynamic head loss per unit length of pipe,

$$\frac{H}{L} = 32\left[\frac{\tau_y}{6\rho g D} + \frac{\eta}{\rho g D^2}\right]. \tag{4.16}$$

For the power law case, combining Equations (2.9) and (4.11) yields

$$\tau_R = K\left[\frac{3n + 1}{4n}\right]^n \Gamma^n. \tag{4.17}$$

The functional form of this equation is similar to Equation (2.9), which is convenient as the consistency coefficient $K$ and consistency index $n$ can be estimated from this equation using a log-log plot of the pipe flow data.

For the general Bingham case, combining Equations (2.10) and (4.11) gives

$$\Gamma = \frac{4n}{3n+1}\left[\frac{\tau_R - \tau_y}{K}\right]^{\frac{1}{n}}\left\{1 - \frac{1}{2n+1}\frac{\tau_y}{\tau_R}\left[1 + \frac{2n}{n+1}\frac{\tau_y}{\tau_R}\left[1 + n\frac{\tau_y}{\tau_R}\right]\right]\right\}. \tag{4.18}$$

For $n = 1$, this equation reduces to the Buckingham equation and, like the Buckingham equation, the mean cross-sectional velocity can be estimated directly for a given pressure gradient, but the inverse procedure would require an iterative scheme. There is also an approximation to Equation (4.18) analogous to Equation (4.15) for the Buckingham equation. This is given as

$$\tau_R = \left[\frac{3n + 1}{2n + 1}\right]\tau_y + K\left[\frac{3n + 1}{4n}\right]^n \Gamma^n, \tag{4.19}$$

and can be evaluated directly for $\Delta P/L$. Likewise, although the yield stress is incorrectly given as $\tau_y(3n + 1)/(2n + 1)$, this equation is suitable for higher values of pseudo-shear rate.

For the Meter model, Equations (2.13) and (4.11) give

$$\Gamma = \frac{\tau_R}{\mu_0}\left\{\left[1 + \frac{4}{a+3}\left[\frac{\tau_R}{\tau_m}\right]^{a-1}\right] - \left[\frac{\mu_\infty}{\mu_0}\right]\left[\frac{\tau_R}{\tau_m}\right]^{a-1}\left[\frac{4}{a+3} + \frac{2}{a+1}\left[\frac{\tau_R}{\tau_m}\right]^{a-1}\right]\right\} + O\left[\left[\frac{\mu_\infty}{\mu_0}\right]^2\right]. \tag{4.20}$$

The $O$ term is usually very small, and neglected to yield a good first order approximation.

For any pseudoplastic fluid, Equation (4.11) can be differentiated with respect to $\tau_R$ and rearranged to give the Mooney-Rabinowitsch [52, 53] equation,

$$\dot{\gamma}_R = \left[\frac{3n' + 1}{4n'}\right]\Gamma, \tag{4.21}$$

where

$$n' = \frac{d\ln\tau_R}{d\ln\Gamma}.$$

This equation gives a relation between the wall shear rate and the pseudo-shear rate where $n'$ is the slope of the log-log pseudo-shear flow function. Thus from a practical viewpoint, values of $n'$ can be estimated from a log-log plot of the pipe flow data, and used to estimate corresponding values of $\dot{\gamma}_R$. Metzner and Reed [20] carried the approach further by writing

$$\tau_R = K'\Gamma^{n'}. \tag{4.22}$$

Taking $n' = n$ and $K' = K[(3n + 1)/4n]^n$, this equation reduces to Equation (4.17).

## 4.2.1 Velocity Distribution

In this subsection, the velocity distribution $u(r)$—the distribution of axial direction velocity against radial distance—is considered. The rate of shearing strain, defined to be positive, is $\dot{\gamma} = -du/dr$. Assuming the no-slip condition $u(R) = 0$, this integrates to give

$$u(r) = \int_r^R \dot{\gamma}\,dr. \tag{4.23}$$

Considering the linear relation between $\tau$ and $r$ defined by Equation (4.5), $\dot{\gamma}$ can be eliminated from this equation using a rheological equation such as one of the equations (2.7) to (2.13).

For the Newtonian case, substituting Equations (2.7) and (4.5) into (4.23) gives the velocity distribution

$$u(r) = 2U\left[1 - \left[\frac{r}{R}\right]^2\right], \tag{4.24}$$

where $U$ is the mean cross-sectional velocity. $u$ clearly has a parabolic profile as illustrated by Figure 4-2.

For the Bingham case, an unsheared solid plug core is retained at the centre of the pipe surrounded by a region of sheared fluid. Now the radius of the plug core is given from Equation (4.5) as

$$r_y = R\frac{\tau_y}{\tau_R}, \tag{4.25}$$

where $\tau_y$ is the yield stress. For the sheared part of the velocity distribution where $r > r_y$, combining Equation (4.23) with (2.8) and (4.5) gives

$$u(r) = \frac{R\tau_R}{2\eta}\left[1 - \left[\frac{r}{R}\right]^2\right] - \frac{R\tau_y}{\eta}\left[1 - \left[\frac{r}{R}\right]\right]. \tag{4.26}$$

Substituting Equation (4.25) into this equation gives the velocity of the plug core,

$$u(r_y) = \frac{R\tau_R}{2\eta}\left[1 - \frac{r_y}{R}\right]^2. \tag{4.27}$$

The velocity profile is shown on Figure 4-2 where the flat part of the profile represents the solid plug core and the curved part of the profile represents the sheared fluid. Equation (4.25) implies that the plug core diminishes in size at higher shear without ever completely disappearing.

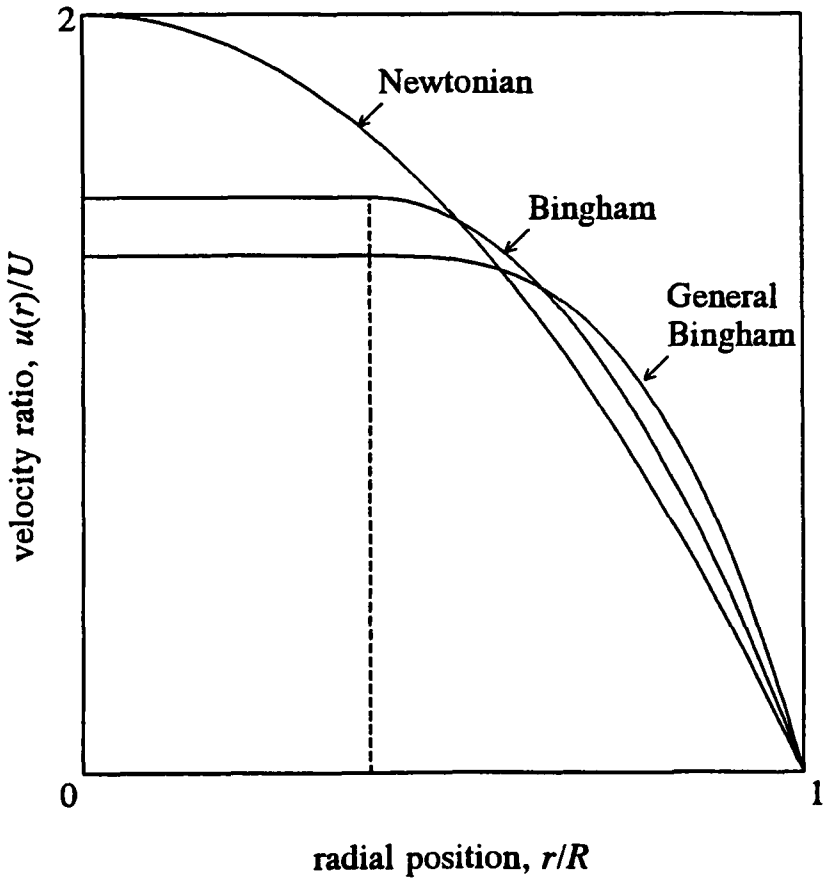


**Figure 4-2** Some laminar flow velocity profiles of non-Newtonian fluids. The dashed lines mark the solid core boundaries of Bingham and general Bingham fluids.

For the power law case, placing Equations (2.9) and (4.5) into (4.23) gives the velocity distribution

$$u(r) = U\left[\frac{3n + 1}{n + 1}\right]\left[1 - \left[\frac{r}{R}\right]^{\frac{n+1}{n}}\right], \tag{4.28}$$

where $U$ is the mean cross-sectional velocity.

Figure 4-3 illustrates the effect of $n$ on the profile. For $n = 1$, the profile is the parabola defined by a Newtonian fluid. For $n < 1$, the profile becomes flatter than a parabola, until $n$ approaches zero where plug flow results. For $n > 1$, the profile becomes sharper than a parabola, until $n$ approaches infinity where a triangular profile results.

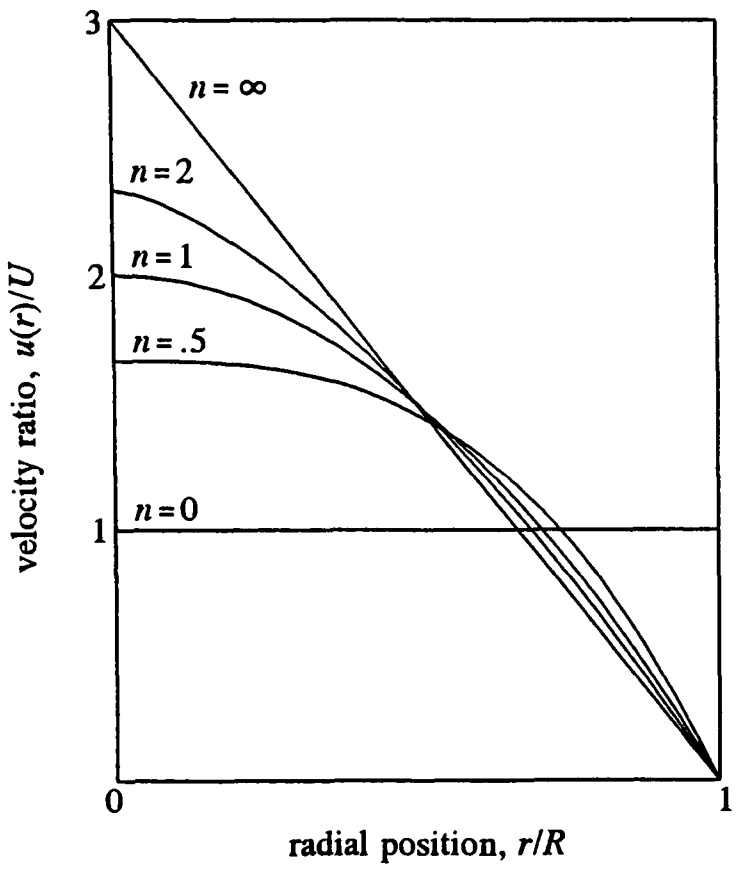


**Figure 4-3** Some laminar flow velocity profiles of power law fluids.

For the general Bingham case, substituting Equations (2.10) and (4.5) into (4.23) gives the velocity distribution

$$u(r) = R\frac{n}{n+1}\left[\frac{\tau_R}{K}\right]^{\frac{1}{n}}\left[\left[1-\frac{r_y}{R}\right]^{\frac{n+1}{n}} - \left[\frac{r}{R}-\frac{r_y}{R}\right]^{\frac{n+1}{n}}\right], \tag{4.29}$$

where $r_y$ is the radius of the plug core. The velocity of the plug core is obtained from this equation at $r = r_y$, whereupon the second term disappears. The velocity profile (see Figure 4-2) has the combined features of the Bingham and power law profiles: a flat region that represents the plug core, and a curved region that represents the sheared fluid surrounding the plug core.

For the Meter model, Equations (2.13), (4.5) and (4.23) combine to give

$$\begin{aligned} u(r) = \frac{R\tau_R}{2\mu_0}\Bigg\{ & \left[1-\left(\frac{r}{R}\right)^2\right] + \frac{2}{a+1}\left[\frac{\tau_R}{\tau_m}\right]^{a-1}\left[1-\left(\frac{r}{R}\right)^{a+1}\right] \\ & - \left[\frac{\mu_\infty}{\mu_0}\right]\left[\frac{\tau_R}{\tau_m}\right]^{a-1}\left[\left[\frac{2}{a+1}\right]\left[1-\left(\frac{r}{R}\right)^{a+1}\right]\right. \\ & \left. + \frac{1}{a}\left[\frac{\tau_R}{\tau_m}\right]^{a-1}\left[1-\left(\frac{r}{R}\right)^{2a}\right]\right]\Bigg\} + O\left[\left[\frac{\mu_\infty}{\mu_0}\right]^2\right]. \end{aligned} \tag{4.30}$$

The $O$ term is usually very small, and neglected to yield a good first order approximation.

## 4.3 Critical flow Equations

Ryan and Johnson [54] proposed a stability parameter based on small fluctuations about a mean velocity. The stability parameter is the ratio of the rate of energy supplied by the fluctuations to the rate the energy is dissipated, and is given as

$$\zeta(r) = \frac{\rho u(r) R \dot{\gamma}(r)}{\tau_R}, \tag{4.31}$$

where $\rho$ is density, $u(r)$ is the velocity distribution, $R$ is the pipe radius, $\dot{\gamma}(r) = -\mathrm{d}u/\mathrm{d}r$, and $\tau_R$ is the pipe wall stress. $\zeta$ is zero at the pipe wall and at the pipe centre line, but reaches a unique maximum value $Z$ at some radial point. Unlike the Reynolds number, the stability parameter is applicable to non-Newtonian fluids, though it can be interpreted as proportional to the Reynolds number (4.7) for point values of $r/R$. The parameter has been successful when tested on much data of Bingham plastic fluids [55], and pseudoplastic fluids [56]. Further confidence in its applicability comes from Hanks [57] who took a completely different approach to derive a generalised stability parameter applicable to any geometry which becomes equivalent to Ryan and Johnson's for pipe flow geometry.

For a Newtonian fluid, applying the Hagen-Poiseuille equation (4.12) and the Newtonian velocity distribution (4.24) to Equation (4.31), the maximum value of $\zeta$ occurs at the point $r/R = 1/\sqrt{3}$, and is given by

$$Z = \mathrm{Re}\sqrt{\frac{4}{27}}, \tag{4.32}$$

where Re is the Reynolds number. Critical flow is the upper bound of laminar flow—the point at which laminar flow becomes unstable. If the critical Reynolds number is taken to be $\mathrm{Re}_c = 2\,100$, then the critical value of $Z$ is

$$Z_c = 808. \tag{4.33}$$

For $Z < Z_c$, the flow can be regarded as laminar, and for $Z > Z_c$, the flow becomes unstable and can be regarded as non-laminar.

The stability parameter could be used in its naked form, but is often instead used to derive more meaningful non-Newtonian Reynolds numbers and critical quantities. For a Bingham plastic fluid, Hanks and Pratt [55] defined a modified Reynolds number as

$$\mathrm{Re}_B = \frac{\rho U D}{\eta}, \tag{4.34}$$

where the coefficient of rigidity $\eta$ replaces the Newtonian viscosity $\mu$. Although this

Reynolds number clearly resembles the Newtonian Reynolds number (4.7), it does not, incidentally, satisfy the generalised Reynolds number proposed by Metzner and Reed [20]. Using analysis based on the Ryan and Johnson stability parameter, Hanks showed that the critical Reynolds number is no longer the constant value 2 100, but an expression in terms of a dimensionless group called the Hedström number [50]. This expression is given as

$$(\mathrm{Re}_B)_c = \frac{\mathrm{He}}{8\xi_c}\left[1 - \frac{4}{3}\xi_c + \frac{1}{3}\xi_c^4\right], \tag{4.35}$$

where the Hedström number is

$$\mathrm{He} = \frac{\rho D^2 \tau_y}{\eta^2}. \tag{4.36}$$

$\xi_c = \tau_y/(\tau_R)_c$ is the ratio of yield stress to critical wall stress defined by the relation

$$\mathrm{He} = 16\,800\frac{\xi_c}{(1 - \xi_c)^3}. \tag{4.37}$$

$\xi_c$ may be obtained from this equation using an iterative scheme, and used to estimate $(\mathrm{Re}_B)_c$ from Equation (4.35). Alternatively, $\xi_c$ could be used to estimate a critical pressure gradient from Equation (4.4), or a critical velocity using the Buckingham [51] equation (4.14).

For the power law case, Hanks and Christiansen [56] defined a Reynolds number from the generalised Reynolds number of Metzner and Reed [20]:

$$\mathrm{Re}_P = 8\left[\frac{n}{6n + 2}\right]^n \frac{\rho U^{2-n} D^n}{K}. \tag{4.38}$$

This expression can also, incidentally, be obtained from Newtonian Re by substituting the Newtonian viscosity $\mu$ with the effective viscosity [58] $\mu_e = \tau_R/\Gamma$. Using the Ryan and Johnson stability criterion of Equations (4.31) and (4.33), critical $\mathrm{Re}_P$ becomes

$$(\mathrm{Re}_P)_c = \frac{6464\,n}{(3n + 1)^2}(n + 2)^{\frac{n+2}{n+1}}, \tag{4.39}$$

and reduces to the Newtonian critical Re, 2 100, for n = 1. A critical velocity can be obtained from these equations, but a critical pressure gradient also requires Equation (4.17).

For the general Bingham case, Hanks and Ricks [59] combined the definition of a Reynolds numbers for the Bingham plastic fluid and the power law fluid to give

$$\mathrm{Re}_{GB} = 8\left[\frac{n}{6n + 2}\right]^n \frac{\rho U^{2-n} D^n}{K}. \tag{4.40}$$

This expression has the same form as Equation (4.38), but whereas $K$ for a general Bingham

fluid reduces to Bingham $\eta$ for $n = 1$, $K$ for a power law fluid reduces to Newtonian $\mu$ for $n = 1$. Using the Ryan and Johnson stability criterion, Hanks and Ricks obtained an expression for the critical Reynolds number, which is

$$(\mathrm{Re}_{GB})_c = \frac{6464n(n+2)^{\frac{n+2}{n+1}}}{[(3n+1)(1-\xi_c)]^2}\left\{1 - \frac{\xi_c}{2n+1}\left[1 + \frac{2n\xi_c}{n+1}(1+n\xi_c)\right]\right\}^{2-n}, \qquad (4.41)$$

where $\xi_c = \tau_y/(\tau_R)_c$ is the ratio of yield stress to critical wall stress defined by the relation

$$\mathrm{He}_{GB} = \frac{3232}{n}(n+2)^{\frac{n+2}{n+1}}\xi_c^{\frac{2-n}{n}}\left(\frac{1}{1-\xi_c}\right)^{\frac{n+2}{n}}, \qquad (4.42)$$

and $\mathrm{He}_{GB}$ is the following Hedström number modified for a general Bingham fluid:

$$\mathrm{He}_{GB} = \frac{\rho D^2 \tau_y^{(2-n)/n}}{K^{2/n}}. \qquad (4.43)$$

Analogous to the Bingham case, $\xi_c$ may be obtained from these equations using an iterative scheme and used to estimate $(\mathrm{Re}_{GB})_c$ from Equation (4.41). Alternatively, $\xi_c$ could be used to estimate a critical pressure gradient from Equation (4.4), or a critical velocity using Equation (4.18).

Slatter and Lazarus [60] reverted to the original Newtonian interpretation of the Reynolds number as the ratio of inertial to viscous forces to derive the following general Bingham Reynolds number:

$$\mathrm{Re}_{SL} = \frac{8\rho U^2}{\tau_y + K\left[\frac{8U}{D}\right]^n}. \qquad (4.44)$$

General Bingham pipe flow has a plug core—an indisputable fact for upper bound laminar flow. Slatter [61] later modified this Reynolds number to account for the plug core as follows:

$$\mathrm{Re}_S = \frac{8\rho U_{ann}^2}{\tau_y + K\left[\frac{8U_{ann}}{D - D_y}\right]^n}, \qquad (4.45)$$

where $U_{ann}$ is the mean cross-sectional velocity of the annular flow, and $D_y$ is the diameter of plug flow. Both these Reynolds numbers are assumed to have a critical value the same as a Newtonian Reynolds number, ie 2 100.

For critical flow specifically of a general Bingham liquid, there seems to be little else in the literature. Slatter correctly points out that some general Bingham Reynolds numbers do not

have a yield stress, and therefore do not account for the plug core. For Equation (4.40) this is true, but does not matter since the corresponding critical relation, Equation (4.41), is not constant and accounts for the yield stress via the Hedström number. The key point is that defining a Reynolds number can, to some degree, be an arbitrary process because it is the critical flow relation that determines the stability criterion.

For any pseudoplastic fluid in general, Metzner and Reed combined Equations (4.13), (4.6) and (4.22) to derive a generalised Reynolds number, which is given as

$$\mathrm{Re}_{MR} = \frac{\rho U^{2-n'} D^{n'}}{8^{n'-1} K'}, \tag{4.46}$$

and as with Equation (4.21) $n' = \mathrm{d}\ln\tau_R/\mathrm{d}\ln\Gamma$.

## 4.4 Turbulent Flow Equations

Consider the turbulent flow of a fluid through a straight pipe. Equation (4.13) gives the relationship between the friction factor and the Reynolds number for laminar pipe flow. This relation is $f = 16/\mathrm{Re}$, and has been the impetus for obtaining semi-empirical relationships between $f$ and Re for turbulent flow. For a Newtonian fluid, notice that these turbulent flow relations would be a function of viscosity (via the Reynolds number), which is a laminar flow parameter. For non-Newtonian fluids in general, turbulent flow modelling is often based on the parameters of the laminar flow model.

For a Newtonian fluid, Blasius[62] obtained a simple, but widely used equation from a friction plot—a plot of $f$ against Re. This is given as

$$f = 0.079\,\mathrm{Re}^{-0.25}, \tag{4.47}$$

and is suitable for Re = 3 000 to 100 000.

Von Kármán[63] obtained a relationship between $f$ and Re based on the turbulent flow velocity distribution proposed by Prandtl[25]. This equation—which includes two constants determined by Nikuradse[64]—is given as

$$\frac{1}{\sqrt{f}} = 4.0\log_{10}(\mathrm{Re}\sqrt{f}) - 0.40, \tag{4.48}$$

and is suitable for Re = 3 000 to 3 000 000. Clapp[65] followed a similar approach to obtain the relation

$$\frac{1}{\sqrt{f}} = 4.53\log_{10}(\mathrm{Re}\sqrt{f}) - 2.3. \tag{4.49}$$

For a general Bingham fluid Torrance[27] extended Clapp's equation to give

$$\frac{1}{\sqrt{f}} = \frac{4.53}{n}\left[\log_{10}\left(\mathrm{Re}_T f^{1-n/2}\right) + \log_{10}\left(1 - \frac{\tau_y}{\tau_R}\right)\right] - \frac{2.75}{n} + 0.45, \quad (4.50)$$

where $\mathrm{Re}_T$ is a modified Reynolds number defined as

$$\mathrm{Re}_T = \frac{\rho U^{2-n} D^n}{8^{n-1} K}. \quad (4.51)$$

This equation reduces to Equation (4.49) for $\tau_y = 0$ and for $n = 1$.

Slatter[66] argued that a particle suspension has a similar effect on the velocity profile of a slurry as wall roughness has on the velocity profile of a Newtonian fluid. With this assumption, plug flow does not occur, and this is borne out by experimental evidence[67, 68]. The advantage of the method is that wall roughness has been well researched, so derivation of a model was made less daunting. Slatter defined a particle roughness Reynolds number as

$$\mathrm{Re}_r = \frac{8\rho U^{*2}}{\tau_y + K\left[\frac{8U^*}{d_x}\right]^n}, \quad (4.52)$$

where $d_x$ is the representative particle diameter and $U^*$ is the friction velocity $\sqrt{(\tau_w/\rho)}$.
If $\mathrm{Re}_r \leq 3.32$ then

$$\frac{U}{U^*} = 2.5 \ln\left[\frac{R}{d_x}\right] + 2.5 \ln(\mathrm{Re}_r) + 1.75, \quad (4.53)$$

and if $\mathrm{Re}_r > 3.32$ then

$$\frac{U}{U^*} = 2.5 \ln\left[\frac{R}{d_x}\right] + 4.75. \quad (4.54)$$

Although the slurry data that Slatter used are of a fairly broad spread, these equations give a good representation of the data.

Conventional wisdom has it that a plug core always survives for the turbulent flow of a fluid with a yield stress; this must be the case if the turbulent fluctuations are assumed to be infinitesimal. Although the experimental evidence seems to contradict the idea of a plug core, this evidence could hardly be extrapolated to all flow rates for all complex mixtures. For this research, there are no available data of the velocity distributions of a flow situation. Nevertheless, this is unimportant for our modelling requirements. For instance, the magnitude of a mean cross-sectional velocity prediction would come largely from the region of high shear; the remaining 'core' region of a low shear or zero shear would have relatively little significance on the prediction. In fact, there is nothing in the objectives that requires an explicit knowledge of the velocity profile.

The turbulent flow models discussed so far are only relevant for a pipe geometry. Many of these models are based on integration of the velocity distribution with several simplifying assumptions to obtain simple relations. A more direct, though less simple procedure for modelling turbulent flow is obtained by integrating the velocity distribution given by Equation (4.23). The velocity distribution was given as

$$u(r) = \int_{r}^{R} \dot{\gamma}\, dr, \tag{4.55}$$

which integrates to give a relationship between the pseudo-shear rate and wall stress. This has already been defined by Equation (4.11) as

$$\Gamma = \frac{4}{\tau_R^3} \int_{\tau_y}^{\tau_R} \tau^2 \dot{\gamma}\, d\tau. \tag{4.56}$$

The mixing length model (2.23) is a shear flow relation, where the mixing length parameter was defined for Newtonian fluids only. Using $y = R - r$ with Equation (4.5), Hanks [69] proposed a pipe version of this equation, which is given as

$$\boxed{l = \kappa R \left[1 - \frac{\tau}{\tau_R}\right] \left[1 - e^{-\phi\left(1 - \frac{\tau}{\tau_R}\right)}\right],} \tag{4.57}$$

where $\phi$ has been redefined for the appropriate fluid type (see proceeding sections). This model has had success when tested on much data of Newtonian fluids [69], Bingham plastic fluids [70], and pseudoplastic fluids [71].

For the Newtonian case, Hanks [69] defined $\phi$ of the mixing length model (4.57) to be

$$\phi = \frac{B - B_c}{\sqrt{8}\, b},$$

where

$$B = \mathrm{Re}\sqrt{f},$$

which is a slight modification to Equation (2.23) such that $B_c$ is the critical value of $B$, and is given by $2\,100 \times \sqrt{(16/2\,100)} = 183$. For pipe flow, $du/dy$ becomes $-du/dr$, which is the rate of shearing strain. Therefore, Equations (2.7) and (2.24) give a total stress as

$$\tau = \mu\dot{\gamma} + \rho l^2 \dot{\gamma}^2. \tag{4.58}$$

This equation is a quadratic shear flow function, and can be rearranged in terms of $\dot{\gamma}(\tau)$ and substituted into Equation (4.56). Since Equation (4.56) cannot be integrated analytically, an

integration method would be required to estimate $\Gamma$ and hence the mean cross-sectional velocity $U$. To obtain a pressure gradient prediction via wall stress $\tau_R$, an inverse procedure would have to be employed. Unlike a laminar shear flow function, the shear flow relation now becomes a function of $\dot{\gamma}$, $\tau$ and $\tau_R$ meaning that the Mooney-Rabinowitsch equation (4.21) is irrelevant for this case. Equation (4.58) can be rearranged as the two-variable function $\dot{\gamma}(\tau, \tau_R)$, and substituted into Equation (4.56). A search method and an integration method would be required to solve the equation for $\tau_R$; the solution procedure would not be simple.

To obtain a turbulent flow velocity distribution of a Newtonian fluid, $\dot{\gamma}(\tau)$ can be substituted into Equation (4.55) and, via the linear relation (4.5), can used to calculate point values of $u(r)$ via an iterative scheme. Figure 4-4 compares the laminar and turbulent flow velocity profiles of a Newtonian fluid. The turbulent flow profile is expectedly flatter than the laminar flow profile as energy is dissipated as random velocity fluctuations.

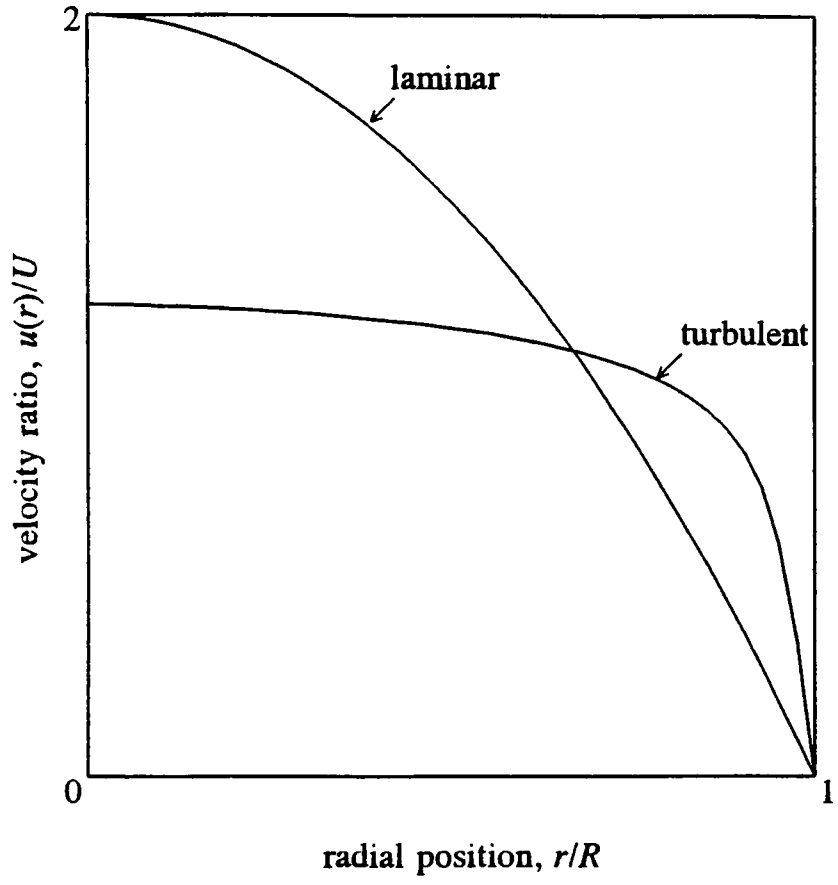


**Figure 4-4** Velocity profiles of a Newtonian fluid. Turbulent flow has a much flatter profile than the laminar flow equivalent.

For the Bingham case, the shear flow function becomes

$$\tau = \tau_y + \eta\dot{\gamma} + \rho l^2 \dot{\gamma}^2. \tag{4.59}$$

Hanks and Dadia [70] redefined $\phi$ of the mixing length model (4.57) to be

$$\phi_B = \frac{B_B - (B_B)_c}{\sqrt{8}\, b(\mathrm{He})}, \tag{4.60}$$

where

$$B_B = \mathrm{Re}_B \sqrt{f},$$

and $\mathrm{Re}_B$ is a Reynolds number based on Bingham flow defined by Equation (4.34). Critical

$\mathrm{Re}_B$, required to calculate $(B_B)_c$, is given by Equation (4.35), and critical $f$ can be calculated from Equation (4.6) using the critical flow equations of Section 4.3. Hanks[26] found $b$ to no longer be constant as in the Newtonian case, but the following function of the Hedström number:

$$b(\mathrm{He}) = 22\left[1 + \frac{0.00352\,\mathrm{He}}{(1 + 0.000504\,\mathrm{He})^2}\right], \tag{4.61}$$

where He is defined by Equation (4.36). For He = 0, Equation (4.61) clearly reduces to $b = 22$ for a Newtonian fluid. Like the Newtonian case, Equation (4.59) is quadratic in $\dot{\gamma}$, and pipe flow estimates can be obtained in much the same way.

For the power law case, the shear flow function becomes

$$\tau = K\dot{\gamma}^n + \rho l^2\dot{\gamma}^2. \tag{4.62}$$

Hanks and Ricks[71] redefined $\phi$ of the mixing length model (4.57) to be

$$\phi_P = \frac{B_P - (B_P)_c}{\sqrt{8}\,b(n)}, \tag{4.63}$$

where

$$B_P = \left[\frac{3n + 1}{n}\right]\left[\mathrm{Re}_P\left(\frac{f}{16}\right)^{\frac{2-n}{2}}\right]^{\frac{1}{n}},$$

and $\mathrm{Re}_P$ is a Reynolds number based on a power law fluid defined by Equation (4.38). $B_P$ reduces to Newtonian $B$ for $n = 1$. Critical $\mathrm{Re}_P$, required to calculate $(B_p)_c$, is given by Equation (4.39), and critical $f$ is given as $f_c = \sqrt{[16/(\mathrm{Re}_P)_c]}$. For a power law fluid version of $b$, Hanks and Ricks obtained the following function of consistency index:

$$b(n) = \frac{22}{n}, \tag{4.64}$$

where for $n = 1$ this reduces to $b = 22$, the Newtonian value of $b$. Unlike the Bingham case, Equation (4.62) cannot be directly expressed in terms of $\dot{\gamma}$, but is a three-valued function of the form $H(\dot{\gamma}, \tau, \tau_R)$. A numerical scheme to solve for pressure gradient would therefore be very complicated. However, Hanks and Ricks presented methods for obtaining dimensionless plots—such as friction plots—for a particular fluid type.

For the general Bingham case, the shear flow function becomes

$$\tau = \tau_y + K\dot{\gamma}^n + \rho l^2\dot{\gamma}^2. \tag{4.65}$$

Hanks[26] redefined $\phi$ of the mixing length model (4.57) to be

$$\phi_{GB} = \frac{B_{GB} - (B_{GB})_c}{\sqrt{8}\,b(n,\ \mathrm{He}_{GB})}, \tag{4.66}$$

where

$$B_{GB} = \left[\frac{3n + 1}{n}\right]\left[\mathrm{Re}_{GB}\left(\frac{f}{16}\right)^{\frac{2-n}{2}}\right]^{\frac{1}{n}},$$

and $\mathrm{Re}_{GB}$ is a Reynolds number based on a general Bingham fluid as defined by Equation (4.40). Critical $\mathrm{Re}_{GB}$, required to calculate $(B_{GB})_c$, is given by Equation (4.41), and critical $f$ can be calculated from Equation (4.6) using the critical flow equations of Section 4.3. For a general Bingham version of $b$, Hanks suggested using the product of $b$ for the Bingham and power law cases, which is

$$b(n,\ \mathrm{He}_{GB}) = \frac{22}{n}\left[1 + \frac{0.00352\,\mathrm{He}_{GB}}{(1 + 0.000504\,\mathrm{He}_{GB})^2}\right], \qquad (4.67)$$

though this conjecture was not verified for any data. Solution methods and design procedures for a general Bingham fluid are essentially the same as for a power law fluid. The laminar and turbulent flow velocity profiles for the general Bingham case are compared on Figure 4-5. Notice that the size of the unsheared core is reduced for the higher shear required of turbulent flow.

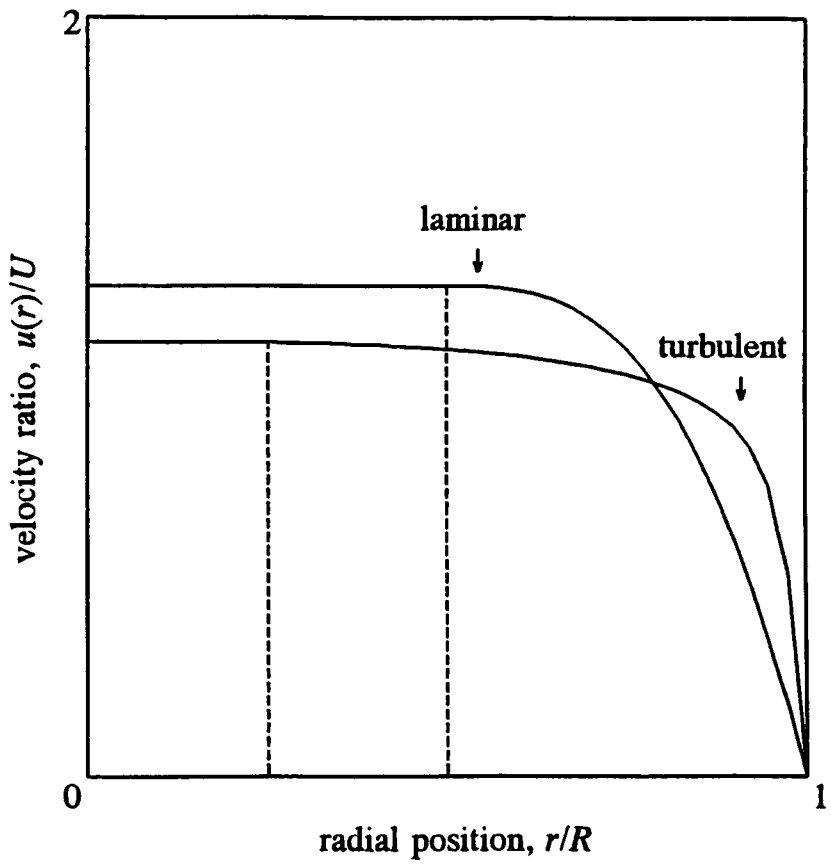


**Figure 4-5** Velocity profiles of a general Bingham fluid. Notice that the solid core reduces in size at higher shear.

For any pseudoplastic fluid in general, Dodge and Metzner[21] obtained the following turbulent equation based on the Metzner and Reed generalized Reynolds number (4.46):

$$\frac{1}{\sqrt{f}} = \frac{4.0}{n'^{0.75}}\log_{10}\left(\mathrm{Re}_{MR}\, f^{\frac{1-n'}{2}}\right) - \frac{0.40}{n'^{1.2}}, \qquad (4.68)$$

where

$$n' = \frac{d\ln\tau_R}{d\ln\Gamma}.$$

Equation (4.68) is suitable for values of $n'$ from 0.36 to 1.0, and $Re_{MR}$ from 2900 to 36000, and reduces to Nikuradse's equation (4.48) for $n' = 1$.

Tam and Tiu [72] derived a simpler expression by considering the relation between two other dimensionless groups, namely a loss coefficient [73]

$$\varphi = \frac{\rho D^2 \tau_R}{\mu_R^2}, \tag{4.69}$$

and the modified Reynolds number

$$Re^{**} = \left[\frac{3n' + 1}{4n'}\right]\left[\frac{\rho UD}{\mu_R}\right]. \tag{4.70}$$

The wall viscosity is defined as $\mu_R = \tau_R/\dot{\gamma}_R$, and from Equations (4.21) and (4.22) is

$$\mu_R = K'\left[\frac{4n'}{3n' + 1}\right]\Gamma^{n'-1}. \tag{4.71}$$

The relationship between $\varphi$ and $Re^{**}$ is

$$\varphi\left[\frac{3n' + 1}{4n'}\right]^4 = 3.96 \times 10^{-2}\, Re^{**\,1.75}, \tag{4.72}$$

where $n' = 0.4$ to 1.35, and reduces to the Blasius equation (4.47) for $n' = 1$. Tam and Tiu's work also extends to ducts of arbitrary cross-section.

Dziubiński [74] took a similar approach but converted the final expression back into the usual frictional form:

$$f = 0.01382\left[\frac{3n' + 1}{4n'}\right]^{-3.5}\exp\left[1.745\left[\frac{3n' + 1}{4n'}\right]\right]Re_{MR}^{-0.25}. \tag{4.73}$$

where $Re_{MR}$ is the Metzner-Reed Reynolds number given by Equation (4.46).

### 4.4.1 Pipe Roughness

For this research, the impetus for pipe flow modelling is primarily to analyse the data. All of the data of this research are of smooth pipe flow, so pipe roughness is of no direct concern to us. Pipe roughness can significantly affect the turbulent flow of a fluid, and a straightforward way of dealing with this is to use the Moody chart [75]. This chart is only applicable to Newtonian fluids, but can be extended to non-Newtonian fluids [24]. The method involves calculating the pressure gradient prediction for a smooth pipe, and multiplying the result with an adjustment factor. This factor is calculated from the Moody chart as the ratio of the friction factor for a rough pipe to the friction factor for a smooth pipe at the non-Newtonian Reynolds number instead of the Newtonian Reynolds number.

### 4.4.2 Solids Concentration Relations

For the turbulent flow of sewage sludge through straight pipes, Frost[8] has developed empirical relations between the sludge-to-water head loss ratio, HLR, and the concentration of solids in percent by mass, $C_w$. For a primary sludge,

$$\text{HLR} = 1.0,$$

where the solids concentration—which is independent of the head loss ratio—has a range of about 2 to 6 percent by mass. For an activated sludge

$$\text{HLR} = 0.88 + 0.24\,C_w,$$

where the range of $C_w$ is about 0.5 to 4 percent. For digested sludge

$$\text{HLR} = 0.80 + 0.16\,C_w,$$

where the range of $C_w$ is about 1.5 to 6 percent.

These models are markedly different to those of the previous sections in that they are empirical models of the effect of solids concentration. The main objectives of this research are to derive models that are based on the analysis of the previous sections but include the effect of solids concentration.

## 4.5 Wall Slippage Equations

So far in this chapter, the assumption has been of the flow of a smooth, pseudohomogeneous fluid through a straight pipe. Wall slippage is a misleading term used to describe the separation of solids from the liquid medium close to the pipe wall, and is therefore a basic inhomogeneous model[76]. Separation occurs during flow, firstly because the particles tend to migrate radially inwards towards the region of higher shear, and secondly because the finite sizes of particles cause a decreasing solids concentration of fluid close to the wall. These effects can be realistically modelled as a discontinuity of the rate of shear at the pipe wall. The assumption is that wall slippage is suppressed for rough pipes[77], and being more significant at low shear[78], the effect is less important for turbulent flow. The assumption of this chapter has so far been of a zero fluid velocity at the pipe wall, ie $u(R) = 0$, but now a slip velocity can be introduced such that $u(R) = U_s$. This slip velocity has been found to be a function of both wall stress $\tau_R$ and pipe diameter $D$[78], and is typically modelled as

$$U_s = \frac{\beta \tau_R}{D^\alpha}, \tag{4.74}$$

where $\alpha$ and $\beta$ are constants established from data. $\alpha$ frequently lies between one and two.

Equation (4.11) gave a relationship between pseudo-shear rate $\Gamma$ and wall stress $\tau_R$ relevant for both laminar and turbulent flow. Adding a slip pseudo-shear rate, $\Gamma_s = 8U_s/D$, to this equation yields

$$\Gamma = \frac{8\beta\tau_R}{D^{\alpha+1}} + \frac{4}{\tau_R^3}\int_{\tau_y}^{\tau_R}\tau^2\dot{\gamma}\,d\tau. \tag{4.75}$$

For laminar flow, this equation reduces to a version of the Mooney-Rabinowitsch equation (4.21) adapted for wall slip, and is given by

$$\dot{\gamma}_R = \left[\frac{3n'' + 1}{4n''}\right](\Gamma - \Gamma_s), \tag{4.76}$$

where

$$n'' = \frac{d\ln\tau_R}{d\ln(\Gamma - \Gamma_s)}.$$

Extending a quantity to allow for wall slippage can often be trivial. For instance, the velocity distribution given by Equation (4.23) can be redefined as

$$u(r) \rightarrow u(r) + U_s.$$

Similarly, a critical velocity can be redefined as

$$U_c \rightarrow U_c + U_s.$$

Wall slip modelling will be a topic of the next chapter.

# 5 Pipe Flow Modelling

In this chapter, a discussion is given of the mathematical modelling of time-independent non-Newtonian viscous fluids through a straight pipe. Algorithms are presented of laminar, critical and turbulent flow, and velocity distributions. The fluid will primarily be regarded as pseudohomogeneous, but in the final section, wall slip will be introduced into the model. The work takes the first step away from graphical methods or simple iterative methods, and towards more complex numerical solutions. The numerics are still relatively simple compared to those of computational fluid dynamics discussed in Chapter 1 where complex three-dimensional geometries with complex flow fields are solved. Judging by the literature, the work is original as numerical methods have only been derived for the complex pipe flow situations discussed in Chapter 1, such as the transient flow of a liquid in a pipe[29], or the numerical simulation of turbulent flow through a pipe[30, 31].

In the previous chapter, models were reviewed of straight pipe flow for yield pseudoplastic fluids with a particular shear flow function. In this chapter, algorithms are derived for such a system that permits the end-user to define *any* shear flow function (though how this function would be specified—ie as a program subroutine—is of no particular concern to this research). The flexibility of the methods are still comparable to friction plots since on-the-job predictions can now be made using notebook computers which have become widely available. The Water Research Centre also wishes to extend the algorithms to include pipe bends and other fittings enabling pipe networks to be defined. This chapter does not use any computer terminology. However, the algorithms have been implemented in Fortran 77 and Appendix B gives the subroutine declaration (name and argument list) of each associated algorithm of this chapter.

## 5.1 Laminar Flow Modelling

The *shear flow function* (the relationship between shear stress and rate of shearing strain) was discussed in Section 2.1, and is either of the explicit form

$$\tau = g(\dot{\gamma}), \tag{5.1}$$

or the implicit form

$$G(\dot{\gamma}, \tau) = 0. \tag{5.2}$$

Every numerical algorithm discussed in this chapter will require a shear flow relation of one of the above two forms, so before discussing any algorithm in detail, brief consideration will be given to the difference between the explicit and implicit cases. In particular, a numerical algorithm that requires an evaluation of an explicit function would receive a value of $\tau$ for a given $\dot{\gamma}$, but for an implicit function, both values of $\dot{\gamma}$ and $\tau$ would be required for an

evaluation. It could be possible to adapt any numerical algorithm that uses Equation (5.1) to be compatible with Equation (5.2); this would be achieved by numerically solving Equation (5.2) for $\tau$ at each given value of $\dot{\gamma}$. An algorithm for the implicit case could thus be extended to the explicit case by employing an extra numerical method; although such an adaption would be easy to effect, it could seriously jeopardise the efficiency of an algorithm. Therefore, the explicit and implicit cases of an algorithm will be given separate treatment.

Consider the laminar flow of a time-independent non-Newtonian viscous fluid through a straight pipe. The relationship between pressure gradient and mean cross-sectional velocity is more conveniently expressed as a *pseudo-shear flow function*—a relationship between wall shear stress and a pseudo-shear rate. Such relationships were discussed in Section 4.2 for specific time-independent non-Newtonian viscous fluids, but all have been derived from the general relation, Equation (4.11), which was given as

$$\Gamma = \frac{4}{\tau_R^3} \int_{\tau_y}^{\tau_R} \tau^2 \dot{\gamma} \, d\tau, \tag{5.3}$$

where $\tau_R$ is the shear stress at the pipe wall,

$$\tau_R = \frac{D}{4} \frac{\Delta P}{L}, \tag{5.4}$$

and $\Gamma$ is a pseudo-shear rate,

$$\Gamma = \frac{8U}{D}. \tag{5.5}$$

It should be appreciated that any successful numerical algorithm of this equation would also be applicable to the Hagen-Poiseuille equation (4.12) for Newtonian fluids, and the Buckingham [51] equation (4.14) for Bingham fluids etc. Such equations, which are special cases of Equation (5.3), will be useful for checking the validity and accuracy of any numerical algorithm.

### 5.1.1 Mean Cross-Sectional Velocity

For predictions of mean cross-sectional velocity, an algorithm is required for numerical estimates of Equation (5.3). Since the body of the equation is an integral, a suitable integration method would presumably be a useful starting point. The integrand, however, suggests that things are not so straightforward; for an explicit function of type (5.1), the function inverse, $\dot{\gamma} = g^{-1}(\tau)$, becomes part of the integrand. If the inversion is considered independently, then a function inversion method would be employed; the method would be invoked for each and every integrand evaluation. The numerical algorithm of Equation (5.3) would thus require method nesting: a function inversion method nested within an integration

method. Such method nesting would be computationally expensive and not simple to implement, so serious consideration needs to be given to simplify the approach. An obvious solution is to consider rearrangements of Equation (5.3) that would yield a simpler algorithm.

Since the integrand is a multiple of two parts, an arrangement using integration by parts can be attempted. From Equation (5.3) this is given as

$$\Gamma = \frac{4}{\tau_R^3} \int_0^{\dot{\gamma}_R} \frac{\mathrm{d}}{\mathrm{d}\dot{\gamma}} \left[ \frac{\tau^3}{3} \right] \dot{\gamma} \, \mathrm{d}\dot{\gamma},$$

which integrates by parts to give

$$\Gamma = \frac{4}{3} \left[ \dot{\gamma}_R - \frac{1}{\tau_R^3} \int_0^{\dot{\gamma}_R} \tau^3 \mathrm{d}\dot{\gamma} \right]. \tag{5.6}$$

This arrangement of Equation (5.3) is advantageous; it has effectively transferred the inverse function outside of the integrand so that the shear flow function needs inverting only once for the wall value $\dot{\gamma}_R$. This would be performed independent of, and before the integration. The algorithm is therefore a favourable one-tiered system of two distinct methods as opposed to the two-tiered system of nested methods considered earlier.

Having defined the basic structure of the algorithm itself, the next task is to embody some suitable methods. For the inversion, Muller's bracketing method (A.4: Appendix A, Section 4) is used, and for the integration, three methods are compared: adaptive versions of Trapezium, Simpson and Boole (methods that are two-, three-, and five-point respectively. See (A.1)). The accuracy of a scheme is user-defined with a relative tolerance check $\epsilon$. For instance, the convergence criterion $|x_i - x_{i-1}|/|x_i| < \epsilon$ applied to a converging sequence $x_i$, $i = 1,2,...$ will result in an estimate of $x$ with a relative accuracy of at least $\epsilon$.

The required accuracy of a scheme would undoubtedly affect its efficiency, although a way of defining the efficiency of a scheme is needed. Timings are not a good idea as they are machine dependent. The number of iterations is problem dependent as it hinges on what is being iterated (this could be anything from a simple function to another scheme). These problems can be avoided by choosing the number of evaluations of the shear flow function as the measure of efficiency, and this is the measure that shall be adopted.

Although one might intuitively expect Boole's five-point method to outperform the others, this is not actually the case. Consider the example of the flow of a general Bingham fluid through a straight pipe. Arbitrarily take the shear flow function to be $\tau = 10 + \sqrt{\dot{\gamma}}$ with a wall stress of $\tau_R = 25$ Pa and a relative tolerance check of $\epsilon = 5 \times 10^{-5}$. The following table gives estimates of the pseudo-shear rate (the star signifies an estimate) with the number of evaluations of the shear flow function used to obtain it.

| Method | $\Gamma^*/s^{-1}$ | No. of evaluations |
|---|---|---|
| Trapezium | 132.4800 | 55 |
| Simpson | 132.4804 | 45 |
| Boole | 132.4805 | 65 |

It is worth first checking the estimates against the true value given by Equation (4.18) for a general Bingham fluid. Setting $\tau_R$ = 25 Pa, $\tau_y$ = 10 Pa, $K$ = 1 Pa s, $n$ = 0.5 and evaluating Equation (4.18) using a pocket calculator, a pseudo-shear rate of exactly $\Gamma$ = 132.48 $s^{-1}$ is obtained. All of the estimates are correct to the required four significant figures, and for this particular case, it can be seen that Simpson's method is the most efficient. In fact, tested on some other examples, Simpson's method is generally the most efficient typically requiring three dozen evaluations of the shear flow function. The Trapezium method is less efficient because it is of a lower order, and conversely Boole's method is less efficient because it requires more points for an area estimate. It is fair to say that all three methods work perfectly well and efficiently, so there is not that much to choose between them. The efficiency tests have helped to put the problem into perspective, but for the rest of the chapter, less emphasis will be given to efficiency.

For many engineering applications, a four significant figure accuracy is unlikely to be required. However, the accuracy of a scheme is, for instance, determined by the number of iterations or steps taken, and not by the complexity of the scheme (this scheme is relatively simple). When testing a scheme, it is often much easier to detect a fault with the logistics when a result is accurate. Furthermore, a scheme such as this needs to be accurate when it is used as part of something bigger, such as parameter estimation scheme, as it is important to avoid error accumulation within the bigger scheme. Finally, if a scheme is used for data analysis, the final result may be sensitive to a particular predicted value. For instance, if a critical flow prediction is too large, a turbulent flow point may be detrimentally included in the laminar flow analysis. Therefore, all of the schemes of this chapter will be tested for accuracy. Figure 5-1 illustrates the final version of the algorithm in the form of a structured chart [79].

For implicit shear flow functions of type (5.2), things become a little less straightforward. In this case, both Equations (5.3) and (5.6) have integrands with implicit variables: for the first equation, the integrand is a function of $\tau$, whereas for the second, the integrand is a function of $\dot{\gamma}$. An algorithm based on either equation would require a method to solve Equation (5.2) for $\dot{\gamma}$ or $\tau$ to be nested within an integration method. Since this is undesirable, a rearrangement is again needed that would alleviate the problem; this time, none can be found. Since algorithms based on Equations (5.3) and (5.6) would both have

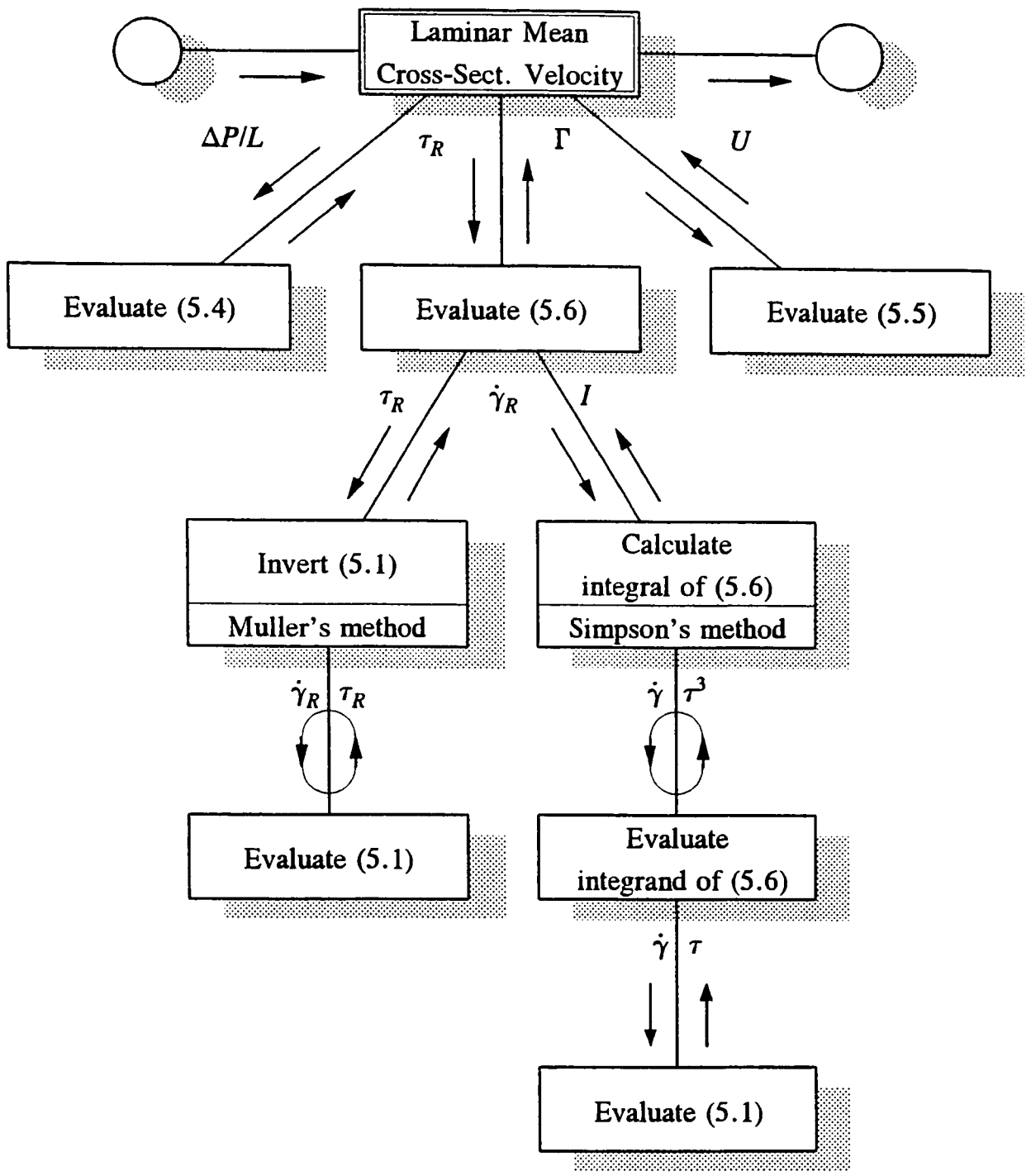


**Figure 5-1** The algorithm to predict the mean cross-sectional velocity for the laminar flow of a time-independent, non-Newtonian, viscous fluid through a straight pipe.

similar structures, both are implemented to compare their efficiencies. In devising an algorithm for Equation (5.6), the obvious thing is done in extending the explicit case to deal with implicit shear flow functions. This is accomplished by nesting a method to solve Equation (5.2) for values of $\tau$ within the integration method. The algorithm for Equation (5.3), although similar, is derived from scratch, though this time a method to solve Equation (5.2) for values of $\dot{\gamma}$ is nested within the integration method. Adaptive Simpson's method is used in both algorithms for the integration, and Muller's method is used as the nested method in both cases. Relative tolerance checks are used, though since Muller's method is nested, its tolerance is further reduced by a factor of ten. Tested on some data, Equation (5.6) proves to yield a more efficient algorithm than Equation (5.3)—sometimes by orders of magnitude. Equation (5.6) is therefore endorsed for the purpose.

As an example of the implicit case, the Meter model (2.13) can be used with the following arbitrarily chosen values: $\mu_0 = 1$ Pa s, $\mu_\infty = .001$ Pa s, $\tau_m = 10$ Pa, $a = 1.5$. Using the algorithm with a wall stress of $\tau_R = 25$ Pa and a relative tolerance check of $\epsilon = 5 \times 10^{-5}$, a

pseudo-shear rate estimate of $\Gamma^\star$ = 60.0514 $s^{-1}$ is obtained in 119 function evaluations. This estimate needs some verification, so it can be compared to the first order approximation given by Equation (4.20). Placing $\tau_R$ = 25 Pa into Equation (4.20) yields $\Gamma \approx 60.0513\ s^{-1}$, which agrees with the estimate to at least four significant figures. One might have expected the first order approximation to fare worse than this, but this approximation is accurate for small $\mu_\infty/\mu_0$. For this example, the algorithm requires 119 evaluations of the shear flow function, which compares to 45 evaluations for the general Bingham example. In general, the algorithm for the implicit case loses ground on method nesting, typically requiring three times as many shear flow function evaluations as the explicit case.

### 5.1.2 Pressure Gradient

A pressure gradient prediction is essentially the inverse of a velocity prediction. Evaluating Equation (5.6) for $\Gamma$ to obtain a velocity prediction is straightforward enough, but in order to obtain a pressure gradient prediction, the equation would have to be solved for $\dot{\gamma}_R$. Viewed as $\Gamma(\dot{\gamma}_R)$, Equation (5.6) is an integral, but viewed as $\dot{\gamma}_R(\Gamma)$, the equation becomes an *integral equation* with a variable upper limit of integration. This equation could still be solved with a root-finding method, but every iteration of this method would require a re-evaluation of the integral. In essence, the integration method would be nested within the root-finding method, and since this would be a computationally expensive option, a better alternative shall be sought.

As discussed in Section 4.2, the Mooney-Rabinowitsch [52, 53] equation (4.21) is an alternative arrangement of Equation (5.3), and when arranged as a linear differential equation, becomes

$$\frac{d\tau_R}{d\Gamma} = \frac{\tau_R}{4\dot{\gamma}_R - 3\Gamma}, \qquad \tau_R(0) = \tau_y. \tag{5.7}$$

This is therefore Equation (5.3) or (5.6) set up as an initial value problem (IVP) of the form $y' = f(x, y)$, $y(a) = b$. However, as a function of $\Gamma$ and $\tau_R$, this equation is not entirely satisfactory as it contains the inverse of the shear flow function $\dot{\gamma}_R = g^{-1}(\tau_R)$. So, after giving the problem some consideration, Equation (5.7) is transformed to be a function of $\Gamma$ and $\dot{\gamma}_R$ by dividing both sides of the equation by the derivative of the shear flow function at the pipe wall, $d\tau_R/d\dot{\gamma}_R$:

$$\frac{d\dot{\gamma}_R}{d\Gamma} = \frac{\tau_R}{4\dot{\gamma}_R - 3\Gamma} \Big/ \left(\frac{d\tau_R}{d\dot{\gamma}_R}\right), \qquad \dot{\gamma}_R(0) = 0. \tag{5.8}$$

Although this equation has a derivative term, it is easier to deal with in terms of numerical methods than Equation (5.7) which contains the inverse of the shear flow function. The derivative term, $d\tau_R/d\dot{\gamma}_R$, on the right hand side of Equation (5.8) is the derivative of the shear flow function at the pipe wall. If the derivative is not specified by the end-user, a

fresh estimate of this derivative is required for every evaluation of the right-hand side of the equation, so the following forward difference formula is used

$$\frac{d\tau_R}{d\dot{\gamma}_R} \approx \frac{\tau(\dot{\gamma}_R + \Delta\dot{\gamma}_R) - \tau(\dot{\gamma}_R)}{\Delta\dot{\gamma}_R}. \tag{5.9}$$

Runge-Kutta Fehlberg's fifth-order method (A.6), which has automatic step-size control, is used to solve Equation (5.8). However, the functional part of the equation (the right-hand side) cannot be evaluated at the initial value ($\Gamma = 0$, $\dot{\gamma}_R = 0$) as the denominator would always be zero and the numerator would be zero for functions without a yield stress. This is no real problem as a standard approach to this situation is to choose an arbitrarily small starting value that is smaller than the required tolerance. In our case, for instance, consider a relative tolerance check of $\epsilon$. If an arbitrary starting value for $(\Gamma, \dot{\gamma}_R)$ is chosen to be $(\epsilon\Gamma, \epsilon\Gamma)$, from Equation (4.21) it is clear that $\dot{\gamma}_R < \Gamma$ for all pseudoplastic fluids, and that $\epsilon\Gamma$ contributes relatively less than $\epsilon$ to the final error.

For example, consider again the general Bingham fluid $\tau = 10 + \sqrt{\dot{\gamma}}$, a pseudo-shear rate of $\Gamma = 100\ s^{-1}$, and Fehlberg's method with a relative tolerance check of $\epsilon = 5 \times 10^{-5}$. Using the above criterion, the starting value is $(\Gamma_0 = 5 \times 10^{-3}\ s^{-1}, (\dot{\gamma}_R)_0 = 5 \times 10^{-3}\ s^{-1})$. The method takes 35 steps to reach the solution where the first and last five steps are shown in the following table:

| $m$ | $\Gamma/s^{-1}$ | $\dot{\gamma}_R/s^{-1}$ |
|---|---|---|
| 0 | $5.0000 \times 10^{-3}$ | $5.0000 \times 10^{-3}$ |
| 1 | $5.0010 \times 10^{-3}$ | $5.2614 \times 10^{-3}$ |
| 2 | $5.0037 \times 10^{-3}$ | $5.8227 \times 10^{-3}$ |
| 3 | $5.0078 \times 10^{-3}$ | $6.4957 \times 10^{-3}$ |
| 4 | $5.0147 \times 10^{-3}$ | $7.4134 \times 10^{-3}$ |
| ⋮ | ⋮ | ⋮ |
| 31 | 14.0829 | 34.4542 |
| 32 | 24.1760 | 53.2627 |
| 33 | 42.1578 | 84.2983 |
| 34 | 75.3325 | 137.8183 |
| 35 | 100.0000 | 175.9859 |

Although a solution is reached, this is still slow for a fifth-order method. The objectives of this research require data analysis and parameter estimation of an extensive set of pipe flow data, so it is worth trying to improve the scheme. Fehlberg's method has an automatic step-size control, so there is no way of improving the efficiency in that respect. The idea of using a starting value closer to the solution can be examined. Since Eq's (5.6) and (5.8) are

completely different arrangements of the same equation, this advantage can be exploited in a major way. Values of $\Gamma$ and $\dot{\gamma}_R$ that satisfy Equation (5.6) will also, of course, satisfy Equation (5.8). If, for Fehlberg's scheme, a starting value of $\dot{\gamma}_R$ is known to be relatively close to the solution, then the corresponding value of $\Gamma$ can be calculated (to within the required relative tolerance) from Equation (5.6) using numerical integration (such as the scheme presented in the previous subsection). Since $\Gamma$ will make a far better starting value for $\dot{\gamma}_R$ than the original $\epsilon\,\Gamma$, it shall be chosen in preference.

In terms of the example, the initial rate of shear is now set to $(\dot{\gamma}_R)_0 = 100\ \mathrm{s}^{-1}$, and Equation (5.6) is used to find the corresponding value of $\Gamma_0$ to within the required tolerance. Fehlberg's method is then employed and, as shown in the following table, takes just one step to reach the solution.

| $m$ | $\Gamma/\mathrm{s}^{-1}$ | $\dot{\gamma}_R/\mathrm{s}^{-1}$ |
|---|---|---|
| 0 | 51.6669 | 100.0000 |
| 1 | 100.0000 | 175.9856 |

Many other test cases were tried using this method and, by virtue of the excellent starting value, a solution was usually reached in just one step. As the step size was often big for the method, Fehlberg is therefore not too powerful for the job. The number of steps of a method is *not* a good measure of efficiency as the computation of a step is bound to vary considerably between methods. Using the measure adopted by this research, the number of shear flow function evaluations (with the difference formula (5.9) implemented) is 52. In fact, for any test problem, the algorithm typically requires about 50 evaluations of the shear flow function.

For completeness, it is worth checking the solution of the above table against the pipe flow Equation (4.18) for a general Bingham fluid. However, $\tau_R$ cannot be obtained from Equation (4.18) directly, so it is instead preferable to substitute in our estimate of $\tau_R$ into the equation to yield an estimate of $\Gamma$, which can be compared to the original value of $\Gamma = 100.0000\ \mathrm{s}^{-1}$. Firstly, $\tau_R^\star = (10 + \sqrt{175.986})\ \mathrm{Pa} = 23.2660\ \mathrm{Pa}$. Furthermore, $\tau_y = 10\ \mathrm{Pa}$, $K = 1\ \mathrm{Pa\,s}$ and $n = 0.5$, so evaluating Equation (4.18) using a pocket calculator yields an estimate of $\Gamma^\star = 100.0000\ \mathrm{s}^{-1}$, which is wholly valid. A more systematic validation of the algorithm will be discussed in Subsection 5.1.4.

For an implicit shear flow function, both Equations (5.7) and (5.8) become implicit. However, the extra derivative term of Equation (5.8) now makes it less appealing to use as an algorithm than Equation (5.7). To solve Equation (5.7), Runge-Kutta Fehlberg's method

is used (as with Equation (5.8)). For the nested method required to solve Equation (5.2) for values of $\dot{\gamma}_R$ and $\tau_R$ (see Figure 5-2), Muller's bracketing method (A.4) is used. Being nested, the tolerance of Muller is naturally reduced, using the factor ten. The starting value needs consideration as the solution variable is now wall shear stress rather than wall shear rate as in the explicit case. $\Gamma$ made a good starting value for $\dot{\gamma}_R$, but it may not be so close to a solution for $\tau_R$. However, the problem is overcome by numerically solving the shear flow function at $\dot{\gamma}_R = \Gamma$ to obtain an initial value for $\tau_R$ that is reasonably close to the solution. As with the explicit case, Equation (5.6) can then be numerically integrated at $\dot{\gamma}_R = \Gamma$ to yield the corresponding value of $\Gamma_0$. Analogous to the explicit case, the resulting initial value $(\Gamma_0, (\tau_R)_0)$ would satisfy Equation (5.7) to within the required tolerance.

As an example of the implicit case, the Meter model (2.13) can again be used with the following arbitrarily chosen values: $\mu_0 = 1$ Pa s, $\mu_\infty = .001$ Pa s, $\tau_m = 10$ Pa, $a = 1.5$. Using the algorithm with a pseudo-shear rate of $\Gamma = 100\ s^{-1}$, and a relative tolerance check of $\epsilon = 5 \times 10^{-5}$, Fehlberg's method takes just one step to reach the solution (see table below).

| $m$ | $\Gamma/s^{-1}$ | $\tau_R$/Pa |
|---|---|---|
| 0 | 92.7802 | 34.9232 |
| 1 | 100.0000 | 36.9745 |

This solution needs some verification. A first order approximation of $\Gamma$ for the Meter fluid is given by Equation (4.20). Placing our estimate of $\tau_R$ which is 36.9745 Pa into Equation (4.20) yields $\Gamma^\star \approx 99.9996\ s^{-1}$ (an approximation based on an estimate) which agrees with $\Gamma$ to four significant figures. One might have expected the first order approximation to fare worse than this, but as mentioned in the previous subsection, this approximation is accurate for small $\mu_\infty/\mu_0$. For this example, the algorithm required 116 evaluations of the shear flow function, which compares to 52 evaluations for the general Bingham example.

For any test problem in general, the implicit case typically makes eighty to one hundred and fifty evaluations of the shear flow function—about three times as many as the explicit case. Suspicions arose as one would not expect the implicit case to fare three times as badly: both algorithms use Fehlberg's method and both algorithms require method nesting (forward differencing for the explicit case and root-finding for the implicit case). However, it should be noticed that Equation (5.8) is dimensionless doubtlessly making the equation well-behaved in terms of convergence.

As a point of interest, if the derivative term of Equation (5.8) is known by the end user, it would show more promise for an algorithm than Equation (5.7). Is it possible to obtain the

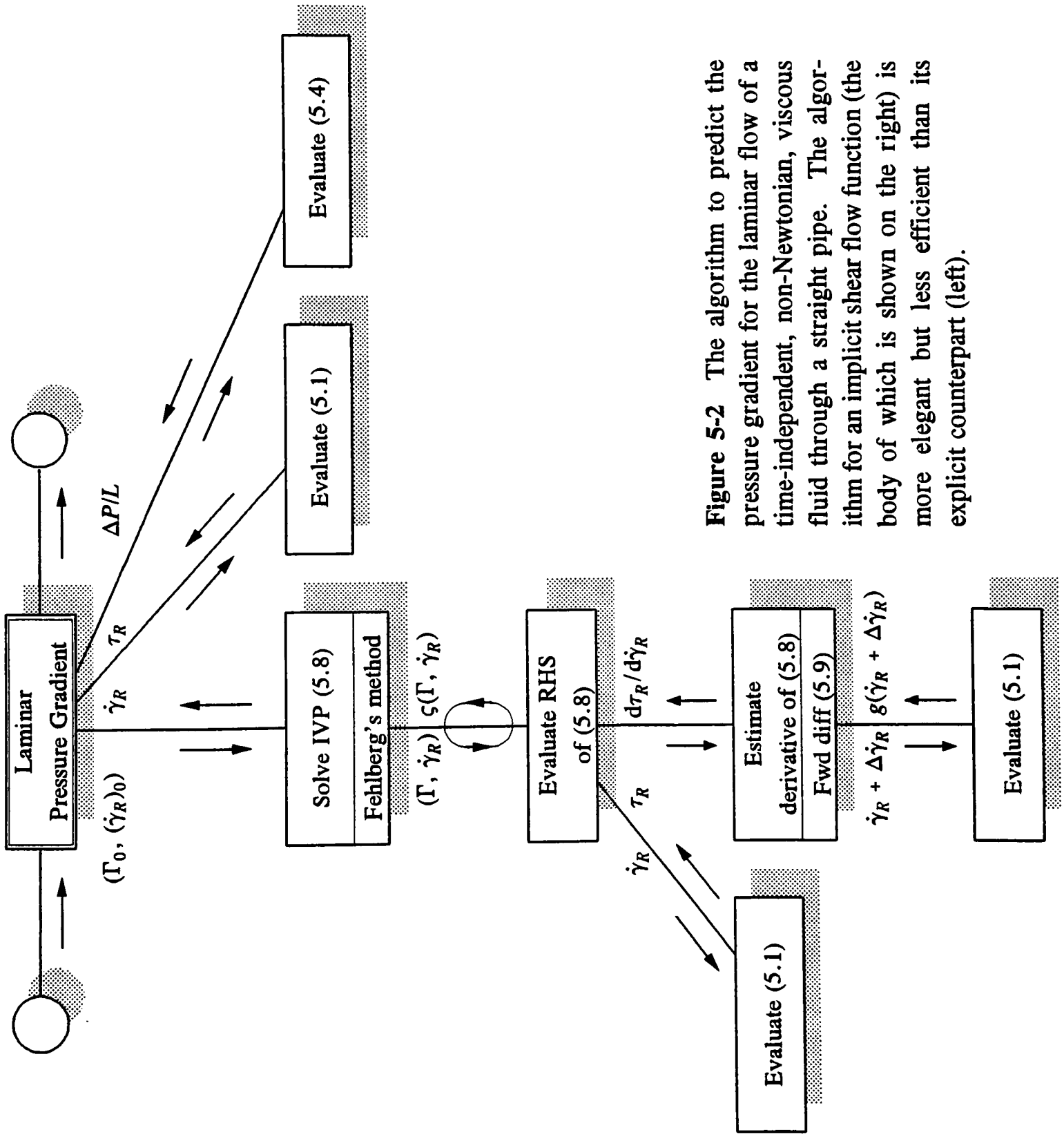


**Figure 5-2** The algorithm to predict the pressure gradient for the laminar flow of a time-independent, non-Newtonian, viscous fluid through a straight pipe. The algorithm for an implicit shear flow function (the body of which is shown on the right) is more elegant but less efficient than its explicit counterpart (left).

derivative term of Equation (5.8) from Equation (5.2)? Applying the chain rule to the derivative with the observation that the total differential of the implicit shear flow function is zero, $dG = 0$, we have

$$\frac{d\tau_R}{d\dot{\gamma}_R} = -\left(\frac{\partial G}{\partial \dot{\gamma}_R}\right) \Big/ \left(\frac{\partial G}{\partial \tau_R}\right).$$

So the answer is yes, the user would need to only specify the partial derivatives of the shear flow function with respect to rate of shear and shear stress.

### 5.1.3 Velocity Distribution

Subsection 4.2.1 gave a general discussion of fully-developed velocity profiles: for Newtonian fluids, the velocity profile is parabolic; for pseudoplastic fluids, the velocity profile is flatter than a parabola, whereas for dilatant fluids, the velocity profile is sharper. It was also asserted that a fluid with a yield stress always (at least theoretically) flows with an unsheared solid plug core. The radius of the solid core is surprisingly simple to formulate. From Equation (4.5), the linear relationship between $r$ and $\tau$ is

$$\frac{r}{R} = \frac{\tau}{\tau_R}, \tag{5.10}$$

therefore the radius of the plug core is given by

$$r_y = R\frac{\tau_y}{\tau_R}. \tag{5.11}$$

For the sheared region of fluid where $r > r_y$, the velocity distribution is calculated from the definition of the rate of shear, $\dot{\gamma} = -du/dr$. Assuming $u(R) = 0$ (no slippage against the pipe wall), this integrates to give

$$u(r) = \int_r^R \dot{\gamma}\, dr. \tag{5.12}$$

For the core region of the fluid where $r \leq r_y$, the velocity profile is flat and the velocity has constant maximum value—the value of Equation (5.12) evaluated at $r_y$.

If the shear flow function is of the explicit type, then the required relationship between $\dot{\gamma}$ and $r$ of Equation (5.12) is given via Equations (5.1) and (5.10). However, the integrand of Equation (5.12) contains the inverse of the shear flow function $\dot{\gamma} = g^{-1}(\tau)$. Since a similar problem arose with the mean cross-sectional velocity case, this problem can be dealt with in much the same way. Equation (5.12) can be rearranged as

$$u(r) = \int_{\dot{\gamma}}^{\dot{\gamma}_R} \frac{dr}{d\dot{\gamma}}\dot{\gamma}\, d\dot{\gamma},$$

which integrates by parts to give

$$u(r) = R\dot{\gamma}_R - r\dot{\gamma} - \int_{\dot{\gamma}}^{\dot{\gamma}_R} r\mathrm{d}\dot{\gamma}. \tag{5.13}$$

This velocity distribution would be of practical use (for velocity profile plots etc) at a set of $W$ equally spaced radial points. Since the initial condition $u(R) = 0$ is at the pipe wall, the following 'discretisation' of $r$ from the wall to the centre line can be chosen:

$$r_s = R\frac{W - s}{W - 1}, \qquad s = 1,2,...,W. \tag{5.14}$$

Let us assume that the first $T$ points of the distribution define the sheared region of fluid, whereas the subsequent $T + 1$ to $W$ points of the distribution define the plug core. Point values of Equation (5.13) are given by

$$u(r_s) = R\dot{\gamma}_R - r_s\dot{\gamma}_s - \int_{\dot{\gamma}_s}^{\dot{\gamma}_R} r\mathrm{d}\dot{\gamma}, \qquad s = 1,2,...,T.$$

From this equation, it can clearly been seen that the range of integration for the $s - 1$th point ($\dot{\gamma}_{s-1}$ to $\dot{\gamma}_R$) covers much of the range of integration for the $s$th point ($\dot{\gamma}_s$ to $\dot{\gamma}_R$). From a computational viewpoint, it would be much more economical to calculate an $s$th integral for the range $\dot{\gamma}_s$ to $\dot{\gamma}_{s-1}$ (noting that $\dot{\gamma}_s$ is less than $\dot{\gamma}_{s-1}$) and augment this value to a running total. Effecting these changes to the equation above yields

$$u(r_s) = R\dot{\gamma}_R - r_s\dot{\gamma}_s - I_s, \qquad s = 2,...,T, \tag{5.15}$$

where

$$I_s = I_{s-1} + \int_{\dot{\gamma}_s}^{\dot{\gamma}_{s-1}} r\mathrm{d}\dot{\gamma}, \qquad I_1 = 0. \tag{5.16}$$

Equation (5.15) requires an inversion of the shear flow function for the pipe wall value $\dot{\gamma}_R$, and (considering the relationship between $\tau$ and $r$ defined by (5.10)) for each $\dot{\gamma}_s$. For these inversions, Muller's bracketing method (A.4) is used.

Consider Equation (5.16). For any value of $s$, the region of integration is likely to be small. On this premise, it would be logical to suggest that the discrete points of the integration method should match those of the velocity distribution. However, since the integration method would become inextricably embedded within the velocity distribution scheme, this would not be a good idea from a design viewpoint. For the algorithm to be modular, flexible, and easy to understand, the integration should be performed independently on each and every interval of the velocity distribution. Using the test data, adaptive versions of the Trapezium, Simpson and Boole methods (A.1)—two-, three-, and five-point methods respectively—are compared. For a distribution of many points—hence small intervals—a

powerful integration method is found to be unnecessary, whereas for a distribution of few points—hence large intervals—a powerful method is found to be desirable. As it transpires, this is no problem as the integration methods (as discussed in (A.1)) initially check using lower-point methods. Our implementation of adaptive Simpson's method, for instance, does an initial check of two Trapezium estimates against a Simpson estimate. For Boole's method, a further initial check of Simpson against Boole is conducted. Such initial checks provide the necessary computational economy for integration over relatively small intervals. It has thus been found that our implementation of Boole's method is well suited to any given number of velocity distribution points. For distributions of few points, the algorithm typically requires about fifty to eighty shear flow function evaluations, whereas for distributions of many points, the number of shear flow function evaluations is about seven to ten times the number of distribution points, and there is no considerable difference in the efficiency of the algorithm for any particular test problem. The final version of the algorithm is illustrated by Figure 5-3.

The velocity profiles of Figure 4-2 were all created using this algorithm by defining each curve as a series of straight lines joining a set of closely spaced points. As an example, consider the general Bingham fluid $\tau = 10 + \sqrt{\dot{\gamma}}$ with a mean cross-sectional velocity of $U = 1\ \mathrm{m\ s^{-1}}$ and a pipe of diameter of $D = 0.04\ \mathrm{m}$. The numerical estimates can be compared with the analytical values of Equation (4.29). Taking a relative tolerance check of $\epsilon = 5 \times 10^{-5}$ and $W = 11$ profile points, the following table gives the estimates in the starred column and the actual values in the far right column.

| $s$ | $r_s$/mm | $u^\star(r_s)$/m s$^{-1}$ | $u(r_s)$/m s$^{-1}$ |
|---|---|---|---|
| 1 | 20. | 0.000000 | 0.000000 |
| 2 | 18. | 0.552613 | 0.552613 |
| 3 | 16. | 0.934939 | 0.934939 |
| 4 | 14. | 1.178344 | 1.178344 |
| 5 | 12. | 1.314194 | 1.314194 |
| 6 | 10. | 1.373857 | 1.373856 |
| 7 | 8. | 1.388716 | 1.388696 |
| 8 | 6. | 1.389164 | 1.389109 |
| 9 | 4. | 1.389164 | 1.389109 |
| 10 | 2. | 1.389164 | 1.389109 |
| 11 | 0. | 1.389164 | 1.389109 |

There is a plug core of about 7 mm which explains why the last values are the same. The numerical estimates are all accurate to the required four significant figures, but notice that the estimates become less accurate further from the wall where error from the numerical integration accumulates.

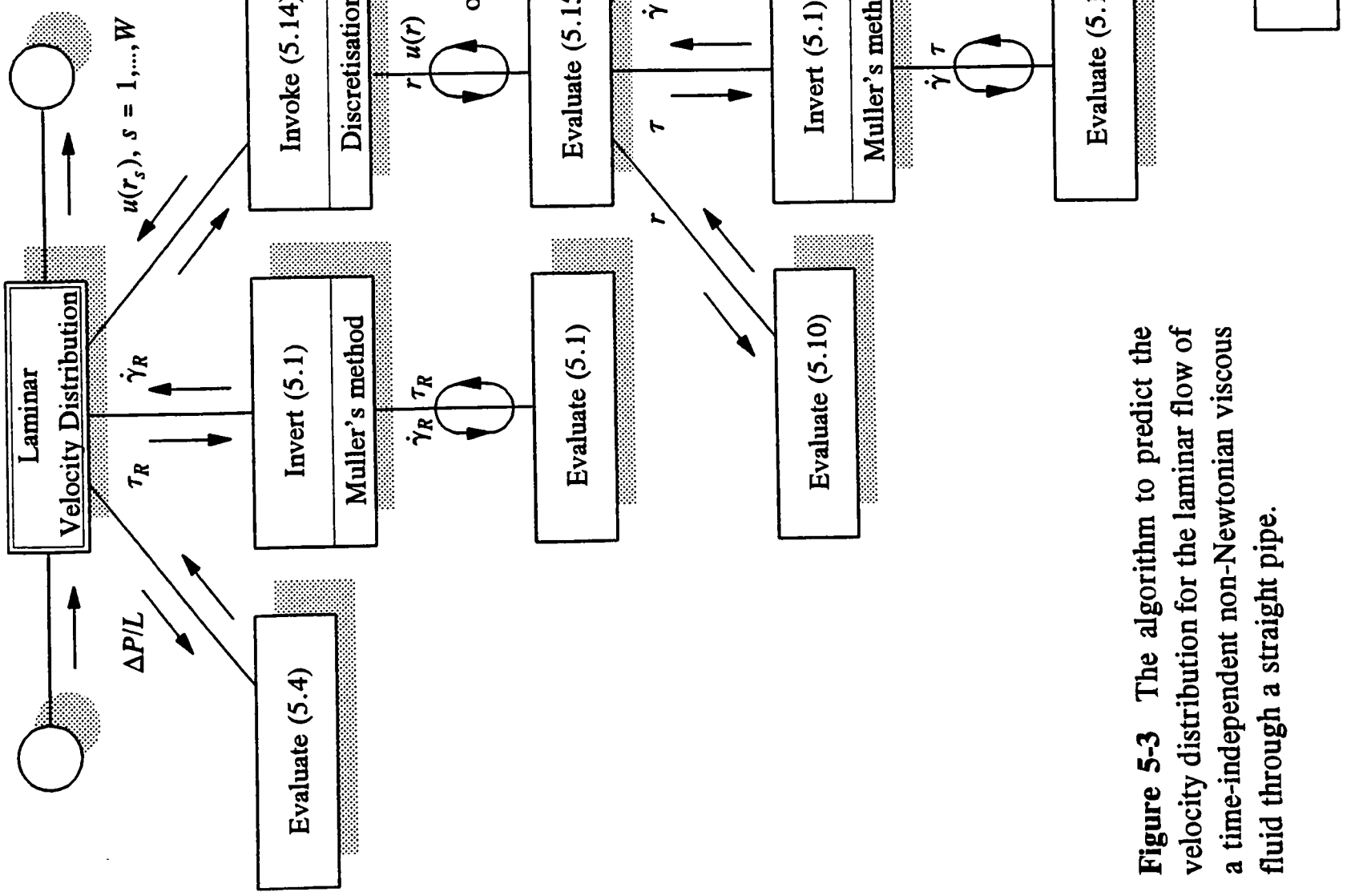


**Figure 5-3** The algorithm to predict the velocity distribution for the laminar flow of a time-independent non-Newtonian viscous fluid through a straight pipe.

For implicit shear flow functions of type (5.2), either Equation (5.12) or (5.13) can be used for an algorithm. However, via Equation (5.10), they are both handicapped with implicit integrands so, from this perspective, there is nothing to choose between them. Analogous to the implicit case of mean cross-sectional velocity, algorithms can be developed for both equations to compare their efficiencies. The algorithm for Equation (5.13) is an extension of the explicit case. Boole's method is used for the integration, and Muller's method is used to solve Equation (5.2) for values of $\dot{\gamma}$ or $\tau$. Since Muller's method is nested, the tolerance is, as usual, reduced by a factor of ten. Tested on some data, the algorithm based on (5.12) proves to be about twice as efficient as the algorithm based on (5.13) and, much as expected, two and a half times less efficient than the explicit case.

As an example, the Meter model (2.13) can again be used with the following values: $\mu_0 = 1\,\text{Pa s}$, $\mu_\infty = .001\,\text{Pa s}$, $\tau_m = 10\,\text{Pa}$, $a = 1.5$, and compared to the first order approximation given by Equation (4.30). Taking a pipe diameter of $D = 0.04\,\text{m}$, a mean cross-sectional velocity of $U = 1\,\text{m s}^{-1}$, and a relative tolerance check of $\epsilon = 5 \times 10^{-5}$, the following table compares the numerical estimates (marked with a star) with the first order approximations.

| $s$ | $r_s$/mm | $u^\star(r_s)$/m s$^{-1}$ | $u(r_s)$/m s$^{-1}$ |
|---|---|---|---|
| 1 | 20. | 0.000000 | 0.000000 |
| 2 | 18. | 0.405299 | 0.405297 |
| 3 | 16. | 0.754099 | 0.754095 |
| 4 | 14. | 1.048914 | 1.048908 |
| 5 | 12. | 1.292422 | 1.292416 |
| 6 | 10. | 1.487504 | 1.487496 |
| 7 | 8. | 1.637295 | 1.637286 |
| 8 | 6. | 1.745267 | 1.745258 |
| 9 | 4. | 1.815375 | 1.815364 |
| 10 | 2. | 1.852335 | 1.852325 |
| 11 | 0. | 1.862499 | 1.862479 |

The values all compare to four significant figures, which is more than one might expect when comparing an estimate with a first order approximation. As mentioned earlier in the chapter however, such first order approximations are good for small $\mu_\infty/\mu_0$.

For completeness, Figure 5-4 compares the general Bingham profile with the Meter profile generated from the above two tables. However, the smooth curve appearance has been achieved using twice as many points. Note that these profiles are based on two completely different hypothetical shear flow models, but they could both conceivably represent thick

sludges. The profiles are of comparable size, as one would expect, since the mean cross-sectional velocity is 1 m $s^{-1}$ in both cases.

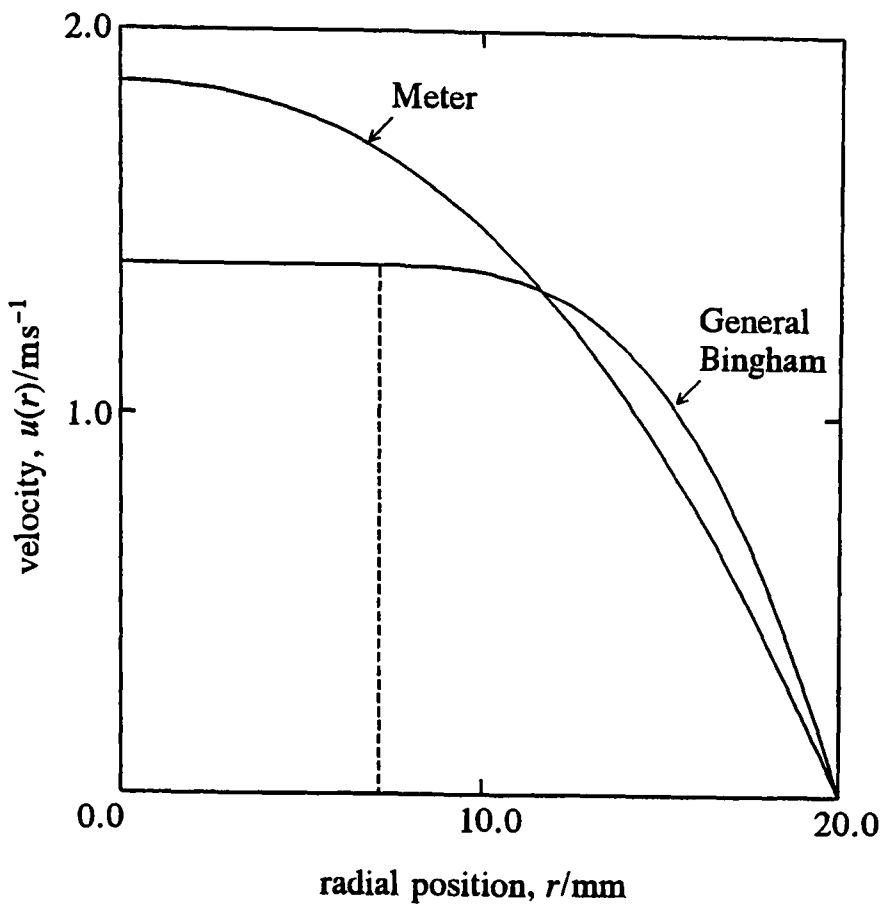


**Figure 5-4** Laminar flow velocity profiles of a general Bingham fluid and a Meter fluid.

## 5.1.4 Scope of Use

The limitations of an algorithm are difficult to define since many of the variables and parameters are interdependent. The general Bingham model (2.10) is a particular example of an explicit shear flow function, and given as

$$\tau = \tau_y + K\dot{\gamma}^n.$$

This is an empirical relation, and being a good model of any time-independent, non-Newtonian, viscous fluid makes it an excellent choice for validation. Section 4.2 discussed the equations for laminar flow of a general Bingham fluid (and its special cases) through a straight pipe; they are straightforward, and can be evaluated directly, or using a simple iterative method.

The second validation procedure requires inverting a prediction to see if it reverts back to its original value. For instance, a mean cross-sectional velocity value can be used to make a pressure gradient prediction which, in turn, can be used to make a mean cross-sectional prediction which is then compared to its original value.

After some exploratory tests using the two validation methods, the scope of the algorithms are presented in Table 5-1, but there may be some absurd combinations of these values that may not actually meet the required tolerance. Since the usable parameter ranges are so extensive, they would easily encompass any real life problem. The algorithms may seem

excessively robust for their application, but this is not the case. An objective of this research is to perform extensive parameter estimation on the data discussed in Chapter 3, and the corresponding method may require the parameters to wildly fluctuate before an optimum solution is reached.

**Table 5-1** Usable ranges of the parameters for the laminar flow algorithms

| Parameter | Range |
|---|---|
| $U$/m s$^{-1}$ | $10^{-3}$ - $10^{3}$ |
| $(\Delta P/L)$/Pa m$^{-1}$ | $10^{-3}$ - $10^{9}$ |
| $D$/m | $10^{-3}$ - $10^{3}$ |
| $\tau_y$/Pa | 0 - $10^{6}$ |
| $K$ | $10^{-6}$ - $10^{6}$ |
| $n$ | 0.1 - 2.0 |

The efficiency of an algorithm is defined as the total number of shear flow function evaluations made by the algorithm. Table 5-2 gives the order of magnitude of efficiency for each algorithm.

**Table 5-2** The number of the shear flow function evaluations in orders of magnitude made by each algorithm.

| Estimate | Explicit | Implicit |
|---|---|---|
| Mean velocity/m s$^{-1}$ | 10 - $10^{2}$ | $10^{2}$ |
| Pressure grad/Pa m$^{-1}$ | 10 - $10^{2}$ | $10^{2}$ |
| Velocity dist'n/m s$^{-1}$ | $10^{2}$ | $10^{2}$ |

## 5.2 Critical Flow Modelling

Critical flow is the upper bound of laminar flow; the point at which laminar flow becomes unstable. As discussed in Chapter 1, the end-user must be allowed to specify their own choice of shear flow relation for an algorithm, so a suitable choice of critical flow model needs to be selected. From Section 4.3, this rules out any model derived for a specific fluid type, such as the Reynolds number of Slatter derived for a general Bingham fluid (see Equation (4.45)). The clear favourite is the Ryan and Johnson stability parameter [54] as not only is it completely general, but as discussed at the beginning of Section 4.3, has been widely tested on many fluid types.

Unlike laminar flow, critical flow is a two-variable problem; for a given pipe diameter and fluid type, the critical flow conditions occur at a particular mean cross-sectional velocity and pressure drop. As with the laminar flow case, the shear flow function is either of the explicit form

$$\tau = g(\dot{\gamma}), \tag{5.17}$$

or the implicit form

$$G(\dot{\gamma}, \tau) = 0, \tag{5.18}$$

and will be treated as separate cases.

Critical flow predictions of non-Newtonian fluids can be made using the Ryan and Johnson [54] general stability parameter, which was discussed in Section 4.3. For straight pipe flow, this is

$$\zeta(r) = \frac{\rho u(r) R \dot{\gamma}(r)}{\tau_R}, \tag{5.19}$$

where $u(r)$ is the velocity distribution. $\zeta$ is zero at the pipe wall and at the pipe centre line, but reaches a unique maximum value $Z$ at some radial point. $Z$ may be used like a generalised Reynolds number whose *critical value* is 808: if $Z \leq 808$, the flow is laminar, whereas if $Z > 808$, the flow is non-laminar. By basic turning point techniques, the radial point at which $\zeta$ has a maximum is the solution of the equation

$$\frac{d\zeta(r)}{dr} = 0, \tag{5.20}$$

which can be substituted into Equation (5.19) to obtain $Z$.

The stability parameter should give results consistent with the Reynolds number (4.7) for Newtonian fluids, and should also be consistent with, for instance, the Reynolds number for power law fluids (4.38) at critical flow (4.39). Such equations are discussed in Section 4.3 and are special cases of Equation (5.19); they will be useful for checking the validity of any algorithm based on Equation (5.19).

### 5.2.1 Critical Rate of Shear

A generally more useful prediction to the one discussed so far is the *critical wall stress*; the wall stress that has a $Z$ value of 808. This is the inverse problem where instead of obtaining $Z$ for a given $\tau_R$, $\tau_R$ is obtained for a given $Z$. In the former case, $Z$ would be calculated for a particular $\tau_R$, then compared to its critical value 808, but in the latter case, $Z$ would be set to its critical value in order to obtain the critical $\tau_R$. There is an important distinction here since the first sort of prediction depends on a particular flow and is compared with a critical flow criterion, whereas the second sort of prediction is derived at critical flow conditions only.

Critical wall stress $(\tau_R)_c$ could accordingly be found by numerically solving Equation (5.19) for $\tau_R$ whilst, for each iteration, solving Equation (5.20) for $r$. Since this approach would, however, yield a computationally expensive algorithm, the problem needs to be viewed from a different perspective. Equations (5.19) and (5.20) can be validly regarded as a pair of two equations with two unknowns; the unknowns being $r$ and $\tau_R$. Moreover, since Equation (4.5) relates $r$ to shear stress $\tau$ through the simple expression

$$\frac{r}{R} = \frac{\tau}{\tau_R}, \tag{5.21}$$

the two independent variables can both be regarded as stress terms, namely shear stress at the pipe wall and shear stress at a radial point. This observation enables the two equations to be perceive as functions of shear flow variables only. Worthwhile though this observation is, for explicit shear flow functions of type (5.17), there is the unnecessary complexity of the equation pair expressed in terms of stresses. The problem is that the rate of shear variables, $\dot{\gamma}$ and $\dot{\gamma}_R$, of the equation pair are shear flow function inversions. After giving the problem some thought, the equation pair can be transformed to functions of the rate of shear variables, $\dot{\gamma}$ and $\dot{\gamma}_R$, themselves. Setting up Equations (5.19) and (5.20) as a homogeneous pair of the form

$$\mathbf{f}(\dot{\gamma}) = \mathbf{0}, \tag{5.22}$$

we have

$$\begin{aligned} f_1(\dot{\gamma},\ \dot{\gamma}_R) &= \frac{\rho u(\dot{\gamma},\ \dot{\gamma}_R) R \dot{\gamma}}{\tau_R} - 808, \\ f_2(\dot{\gamma},\ \dot{\gamma}_R) &= \frac{\tau_R}{R} u(\dot{\gamma},\ \dot{\gamma}_R) - \dot{\gamma}^2 \frac{\mathrm{d}\tau}{\mathrm{d}\dot{\gamma}}. \end{aligned} \tag{5.23}$$

The velocity distribution, $u$, is given by Equation (5.13), and arranged in terms of the shear rate variables, is

$$u(\dot{\gamma},\ \dot{\gamma}_R) = \frac{R}{\tau_R} \left[ \tau_R \dot{\gamma}_R - \tau \dot{\gamma} - \int_{\dot{\gamma}}^{\dot{\gamma}_R} \tau \mathrm{d}\dot{\gamma} \right]. \tag{5.24}$$

The above equations are thus rid of the shear flow function inversions that afflicted the original equations. Equation (5.24) is particularly fascinating as the lower and upper limits of integration are the two independent variables; the integral varies at both limits! To see if these equations could be simplified further, all conceivable transformations were applied with the result that no transformation could be found where, for instance, one of the variables could be directly eliminated. It must therefore be assumed that the equations cannot be further simplified.

To solve Equation (5.22), general Newton's method (A.5) is used. Pertinent to our problem, this method becomes

$$\dot{\boldsymbol{\gamma}}^{[m+1]} = \dot{\boldsymbol{\gamma}}^{[m]} - J^{-1}(\dot{\boldsymbol{\gamma}}^{[m]})\,\mathbf{f}(\dot{\boldsymbol{\gamma}}^{[m]}), \tag{5.25}$$

where $J$ is the Jacobian matrix $\partial \mathbf{f}/\partial\dot{\gamma}$ whose elements are

$$
\begin{aligned}
j_{11} &= \frac{\partial f_1}{\partial \dot{\gamma}} = \frac{\rho R}{\tau_R}\left[u - \frac{R\dot{\gamma}^2}{\tau_R}\frac{\mathrm{d}\tau}{\mathrm{d}\dot{\gamma}}\right], \\
j_{12} &= \frac{\partial f_1}{\partial \dot{\gamma}_R} = \frac{\rho R\dot{\gamma}(R\dot{\gamma}_R - 2u)}{\tau_R^2}\frac{\mathrm{d}\tau_R}{\mathrm{d}\dot{\gamma}_R}, \\
j_{21} &= \frac{\partial f_2}{\partial \dot{\gamma}} = -\dot{\gamma}^2\frac{\mathrm{d}^2\tau}{\mathrm{d}\dot{\gamma}^2} - 3\dot{\gamma}\frac{\mathrm{d}\tau}{\mathrm{d}\dot{\gamma}}, \\
j_{22} &= \frac{\partial f_2}{\partial \dot{\gamma}_R} = \dot{\gamma}_R\frac{\mathrm{d}\tau_R}{\mathrm{d}\dot{\gamma}_R}.
\end{aligned}
\tag{5.26}
$$

There is an assortment of derivatives of the shear flow function to estimate. Finite differences are chosen whose relative accuracy converges with the solution. These are

$$
\begin{aligned}
\tau'(\dot{\gamma}^{[m]}) &\approx \frac{\Delta\tau^{[m]}}{\Delta\dot{\gamma}^{[m]}}, \\
\tau'(\dot{\gamma}_R^{[m]}) &\approx \frac{\Delta\tau_R^{[m]}}{\Delta\dot{\gamma}_R^{[m]}}, \\
\tau''(\dot{\gamma}^{[m]}) &\approx \frac{2(\Delta\tau^{[m]}\Delta\dot{\gamma}^{[m-1]} - \Delta\tau^{[m-1]}\Delta\dot{\gamma}^{[m]})}{\Delta\dot{\gamma}^{[m]}\Delta\dot{\gamma}^{[m-1]}(\Delta\dot{\gamma}^{[m]} + \Delta\dot{\gamma}^{[m-1]})},
\end{aligned}
\tag{5.27}
$$

where $\Delta\dot{\gamma}^{[m]} = \dot{\gamma}^{[m]} - \dot{\gamma}^{[m-1]}$, and similarly for $\dot{\gamma}_R$ and $\tau$.

For the $m$th iteration of Newton's method, Equation (5.24) requires integration of $\tau$ from $\dot{\gamma}^{[m]}$ to $\dot{\gamma}_R{}^{[m]}$. Hindsight shows that there is actually no a need to integrate over the entire range, but only the difference from the $m$ - 1th interval (see Figures 5-5 and 5-6). The $m$th integral value is thus calculated as

$$
I^{[m]} = I^{[m-1]} + \int_{\dot{\gamma}^{[m]}}^{\dot{\gamma}^{[m-1]}} \tau\,\mathrm{d}\dot{\gamma} + \int_{\dot{\gamma}_R^{[m-1]}}^{\dot{\gamma}_R^{[m]}} \tau\,\mathrm{d}\dot{\gamma}. \tag{5.28}
$$

Boole's method (A.1) is used for the integration with a relative tolerance check, and since the method is nested within Newton's method, its tolerance is fittingly reduced by a factor of ten. It has already been pointed out that the two limits of integration are the solution variables. This means that, in general, the region of integration of Equation (5.28) becomes relatively smaller as convergence of Newton's method is met. To make the computation equivalently less intensive, a two-pronged attack is made on the problem: firstly, the convergence criterion of the integration is set to be relative to the current running total $I^{[m]}$, and secondly, our implementation of adaptive Boole's five-point method makes initial estimates using the Trapezium two-point method and Simpson's three-point method; simply stated, low powered methods are used for the relatively small intervals of integration.

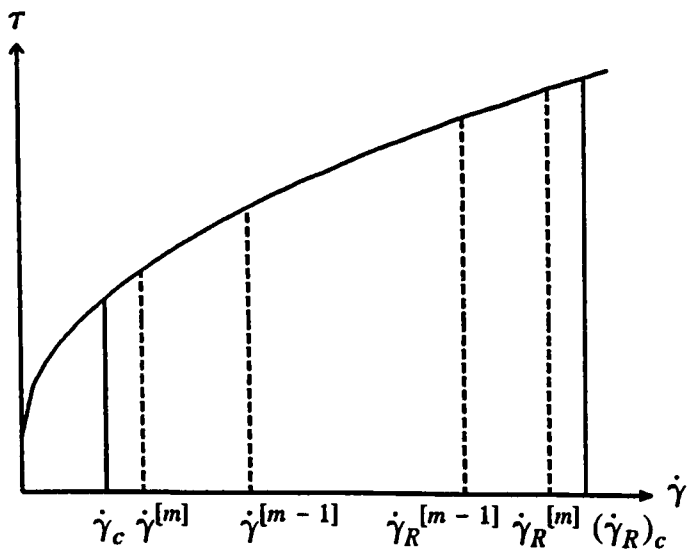


**Figure 5-5** A schema representing the converging limits of integration of Equation (5.24) to the critical flow solution $(\dot{\gamma}_c, (\dot{\gamma}_R)_c)$ of Eq's (5.23).

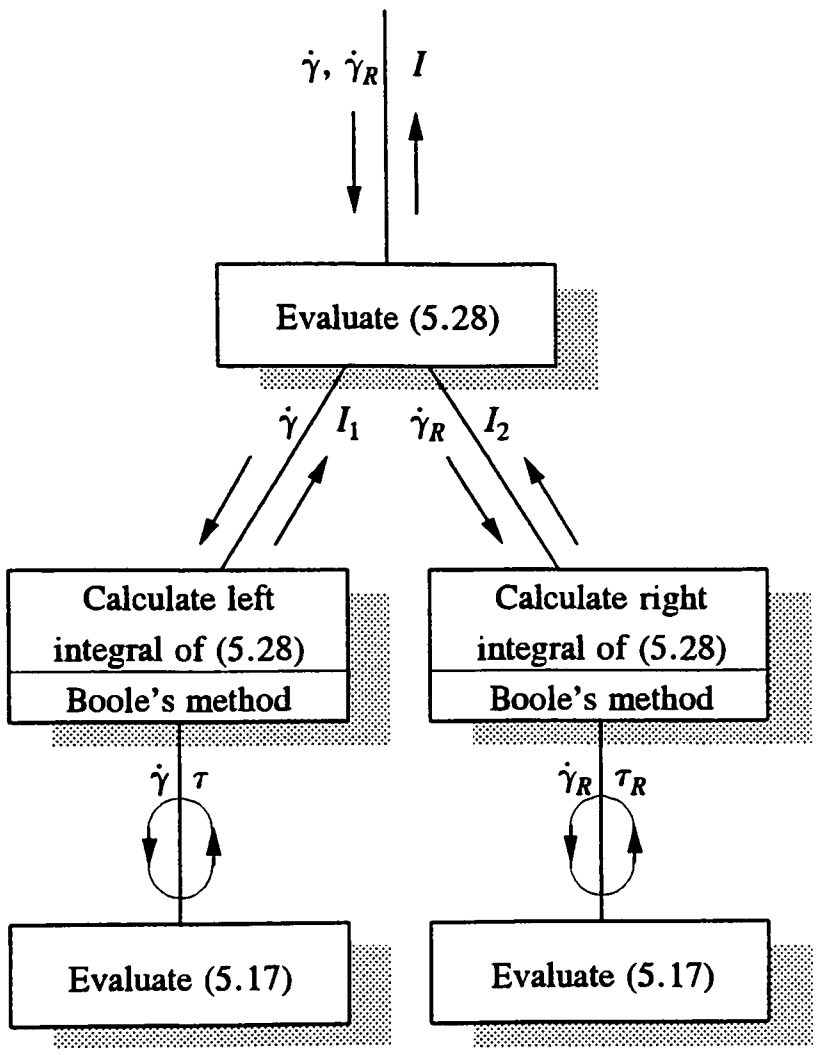


**Figure 5-6** The algorithm of Equation (5.28) where the total integral $I$ is updated by the new integrals $I_1$ and $I_2$

The final version of the algorithm is illustrated by Figure 5-7 overleaf.

As an example, consider again the flow of the general Bingham fluid $\tau = 10 + \sqrt{\dot{\gamma}}$ of density $\rho = 1000$ kg/m$^3$ through a pipe of diameter $D = 0.1$ m. Using a relative tolerance check of $\epsilon = 5 \times 10^{-5}$, the scheme takes 9 iterations to reach convergence (see table below). The final wall rate estimate gives a wall stress estimate of $(\tau_R)_c^\star = 29.0584$ Pa and a mean cross-sectional velocity estimate of $U_c^\star = 2.83919$ m s$^{-1}$.

| $m$ | 0 | 1 | 2 | 3 | 4 |
|---|---|---|---|---|---|
| $\dot{\gamma}$/s$^{-1}$ | 201.431 | 201.500 | 195.812 | 197.715 | 196.959 |
| $\dot{\gamma}_R$/s$^{-1}$ | 201.834 | 333.981 | 358.125 | 363.078 | 363.147 |

| $m$ | 5 | 6 | 7 | 8 | 9 |
|---|---|---|---|---|---|
| $\dot{\gamma}$/s$^{-1}$ | 197.225 | 197.123 | 197.160 | 197.146 | 197.151 |
| $\dot{\gamma}_R$/s$^{-1}$ | 363.152 | 363.153 | 363.153 | 363.153 | 363.153 |

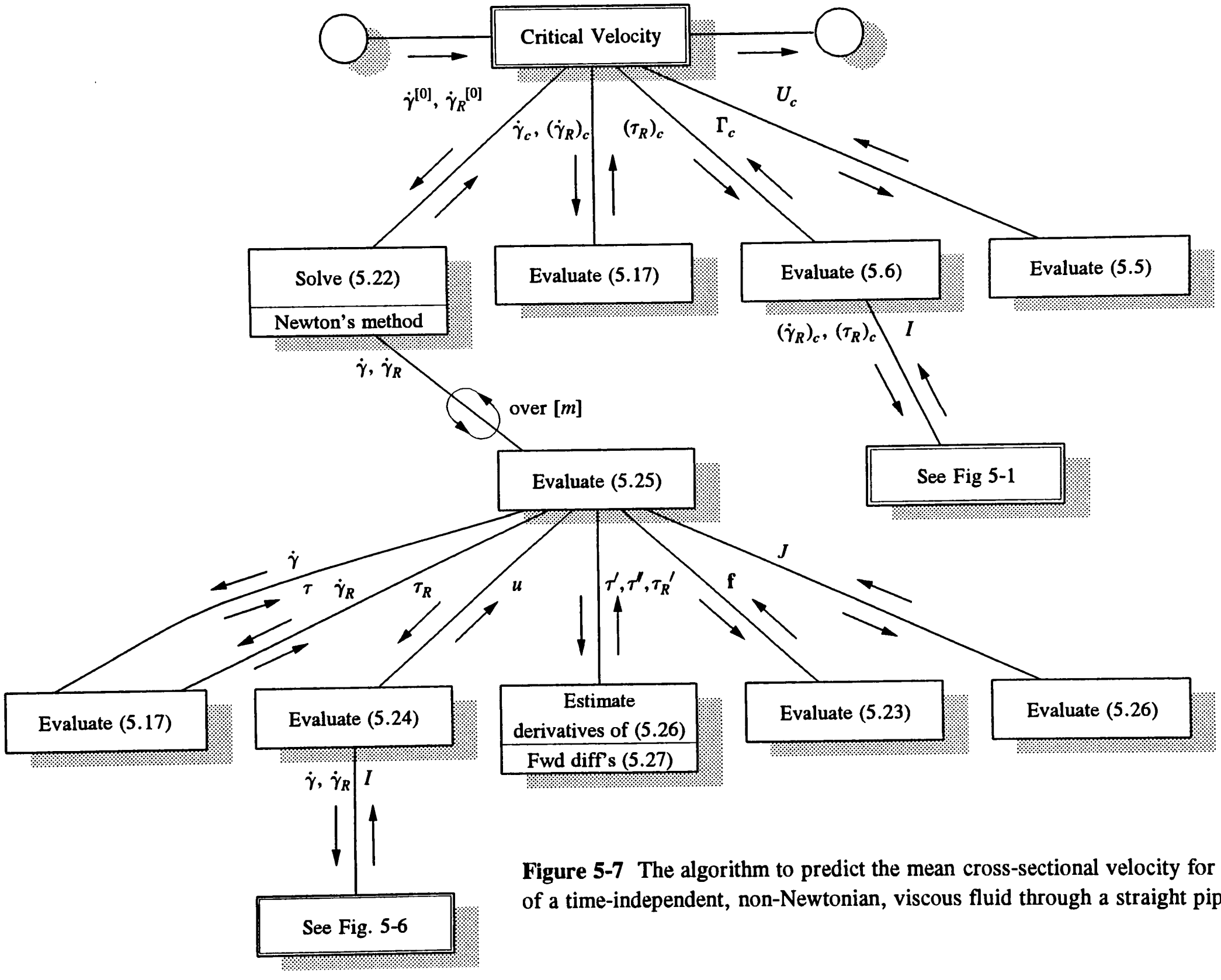


**Figure 5-7** The algorithm to predict the mean cross-sectional velocity for the critical flow of a time-independent, non-Newtonian, viscous fluid through a straight pipe.

The estimates can be checked against the critical flow equations for a general Bingham fluid—Equations (4.40) to (4.43). Normally an iterative scheme would be used to solve Equations (4.42) and (4.43) for $\xi_c = \tau_y/(\tau_R)_c$, and this value would then be substituted into Equation (4.41) to derive a critical Reynolds number. However, by substituting our estimates for $U_c$ and $\xi_c$ into the four equations, each dimensionless pair should have comparable values. These comparisons are presented in the table below where the estimates are given stars. The Second Hedström number is therefore a true value.

| Equation | Estimate |
|---|---|
| (4.40) | $Re^\star = 3825.97$ |
| (4.41) | $Re_c^\star = 3825.95$ |
| (4.42) | $He^\star = 10000.00$ |
| (4.43) | $He = 10000.00$ |

It can be seen that the values compare comfortably to the required four significant figures, which is wholly acceptable. For this particular example, the algorithm made 128 evaluations of the shear flow function and is the type of efficiency achieved for other test cases as well. A more systematic validation of the algorithm will be discussed in Subsection 5.2.3.

For implicit shear flow functions of type (5.18), no simpler way of dealing with the problem can be found than by extending the explicit case. Whereas values of $\tau$ and $\tau_R$ can be evaluated directly from Equation (5.17), they must be solved for when using Equation (5.18). For this, Muller's bracketing method (A.4) is used. This involves method nesting of up to three levels, so the relative tolerance of each successive level is reduced by a factor of ten.

As an example, consider again the Meter model (2.13) with the following values: $\mu_0 = 1$ Pa s, $\mu_\infty = .001$ Pa s, $\tau_m = 10$ Pa, $a = 1.5$. Take a density of $\rho = 1000$ kg/m$^3$, a pipe of diameter $D = 0.1$ m, and a relative tolerance check of $\epsilon = 5 \times 10^{-5}$. For the Meter model, there is no known Ryan and Johnson critical flow equation of a simplified form. Nevertheless, there are other clever ways of checking the algorithm. Although the algorithm solves for shear rate and wall rate, rather than examine the convergence of these two variables, the corresponding stability parameter $\zeta(r)$ and its derivative $d\zeta/dr$ can be examined instead; by virtue of Equations (5.19) and (5.20), they should converge to 808 and zero respectively. Note that the stability parameter is not often used in this basic form.

The table overleaf shows that the variables do indeed converge as anticipated. The magnitude of the derivative decreases to a point where it is relatively much smaller than at first. The radial point of instability is also given; its final estimate is about two-thirds of the

| $m$ | $r$/mm | $\zeta(r)$ | $d\zeta/dr$ |
|---|---|---|---|
| 0 | 49.9275 | 6.082 | $-8.37267 \times 10^{4}$ |
| 1 | 42.1450 | 629.132 | $-9.65606 \times 10^{3}$ |
| 2 | 34.6571 | 685.811 | $-9.19683 \times 10^{3}$ |
| 3 | 33.1338 | 805.206 | $-6.62480 \times 10^{2}$ |
| 4 | 32.6367 | 807.358 | $4.42269 \times 10^{1}$ |
| 5 | 32.7237 | 807.976 | $-3.17143 \times 10^{1}$ |
| 6 | 32.6933 | 807.998 | $6.87284 \times 10^{0}$ |
| 7 | 32.7004 | 808.000 | $-2.00439 \times 10^{0}$ |
| 8 | 32.6984 | 808.000 | $4.90311 \times 10^{-1}$ |

way out from the pipe axis. In terms of efficiency, the algorithm makes 431 evaluations of the shear flow function which compares to the 128 evaluations made for the general Bingham model. In general, the implicit case requires about three times as many evaluations as the explicit case.

### 5.2.2 Critical Mean Cross-Sectional Velocity

So far, the critical rate of shear predictions have been discussed; values that are generally impractical as they stand. Of particular interest is the critical mean cross-sectional velocity $U_c$, and since critical flow is laminar flow at the upper bound, $U_c$ can be calculated from Equation (5.6) at $(\dot{\gamma}_R)_c$.

### 5.2.3 Scope of Use

An indication of the scope of the critical flow algorithms is, like the laminar flow case, accomplished using the general Bingham shear flow function (2.10),

$$\tau = \tau_y + K\dot{\gamma}^n.$$

Section 4.3 discussed the equations for critical flow of a general Bingham fluid (and its special cases) through a straight pipe; they are fairly straightforward, and are suitable for validating the critical flow algorithms. After some exploratory analysis, the usable parameter ranges are extensive and are given by Table 5-3, but some absurd combinations of these values may not actually meet the required tolerance. Critical flow conditions are not always possible for a dilatant fluid (where $n > 1$) since shear thickening may develop faster than flow instability.

**Table 5-3** Usable ranges of the parameters for the laminar flow algorithms

| Parameter | Range |
|---|---|
| $D$/m | $10^{-3}$ - $10^{3}$ |
| $\tau_y$ /Pa | 0 - $10^{3}$ |
| $K$ | $10^{-6}$ - $10^{3}$ |
| $n$ | 0.1 - 1.0 |

The efficiency of an algorithm is defined as the total number of shear flow function evaluations made by the algorithm. Table 5-4 gives the order of magnitude of efficiency for each algorithm.

**Table 5-4** The number of the shear flow function evaluations in orders of magnitude made by each algorithm.

| Estimate | Explicit | Implicit |
|---|---|---|
| Mean velocity/m $s^{-1}$<br>Pressure grad/Pa $m^{-1}$ | $10^2$ | $10^2$ |

## 5.3 Turbulent Flow Modelling

Many models have been developed for the turbulent flow of non-Newtonian fluids through a straight pipe. As discussed in Chapter 1, there is a need for a turbulent shear flow function, so this rules out the friction relations discussed in Section 4.4 such as Dodge-Metzner [21] and Torrance [27]. The model proposed by Hanks [26] was suggested as a good choice since it is based on few underlying assumptions, and is suitable for both transitional and turbulent flow. In fact, the widely used Torrance relation is based on the same mixing length model as Hanks but without the Van Driest [46] wall damping factor, and several further simplifying assumptions were made when integrating the velocity profile. A frictional relation can still be obtained from the model of Hanks, so a comparison with other frictional relations will be discussed in Chapter 7.

From the viewpoint of creating an algorithm, there is a continuity in basing both the laminar and turbulent flow models on a shear flow function, but there is a difference of form; the turbulent flow model includes a *mixing length* term given as a function of wall distance. Consequently, the laminar flow algorithms are not wholly applicable to the turbulent flow case—a difficulty that is to be addressed. The main problem with the model of Hanks is that

it is restricted to general Bingham fluids only. Yet our objectives are to allow for any time-independent non-Newtonian viscous fluid, so a way of generalising the model will be considered.

The turbulent shear flow function, Equation (2.24), is the sum of the laminar and turbulent stresses, given as

$$\tau = \tau_L + \tau_T. \tag{5.29}$$

The laminar stress term is given from the laminar shear flow function which is, as usual, either of the explicit form

$$\tau_L = g(\dot{\gamma}), \tag{5.30}$$

or of the implicit form

$$G(\dot{\gamma}, \tau_L) = 0, \tag{5.31}$$

though in this case, the subscript $L$ has been used to signify a laminar stress. Since Equation (5.29) is a shear flow function, the *pseudo-shear flow function* (4.11) which was used for the laminar flow modelling is still applicable. The equation, which relates the mean cross-sectional velocity to the pressure gradient, is given by

$$\Gamma = \frac{4}{\tau_R^3} \int_{\tau_y}^{\tau_R} \tau^2 \dot{\gamma} \, d\tau, \tag{5.32}$$

where $\tau_R$ is the shear stress at the pipe wall,

$$\tau_R = \frac{D}{4} \frac{\Delta P}{L}, \tag{5.33}$$

and $\Gamma$ is a pseudo-shear rate,

$$\Gamma = \frac{8U}{D}. \tag{5.34}$$

A full discussion of the model proposed by Hanks was given in Section 4.4. As noted already, the model is restricted to general Bingham fluids with the shear flow function (2.10), namely

$$\tau = \tau_y + K\dot{\gamma}^n. \tag{5.35}$$

This defines the laminar stress term of Equation (5.29), though in our case, any equation of the form (5.30) or (5.31) would be permitted. Now, the turbulent stress term of Equation (5.29) is given as

$$\tau_T = \rho l^2 \dot{\gamma}^2, \tag{5.36}$$

where $l$ is a mixing length defined as

$$l = \kappa R \left[ 1 - \frac{\tau}{\tau_R} \right] \left[ 1 - e^{-\phi_{GB}\left(1 - \frac{\tau}{\tau_R}\right)} \right], \tag{5.37}$$

and

$$\phi_{GB} = \frac{B_{GB} - (B_{GB})_c}{\sqrt{8}\, b(n,\ \mathrm{He}_{GB})}. \tag{5.38}$$

$\phi_{GB}$ is relevant to general Bingham fluids only as $B_{GB}$ contains parameters of Equation (5.35) as does its critical value $(B_{GB})_c$. The parameter $b$ is empirical, and Hanks defined $b$ to be a relation of both the consistency index $n$, and a general Bingham Hedström number $\mathrm{He}_{GB}$. Since $b$ is empirical, it has the advantage in that specific relationships for $b$ can be derived for specific fluid types. An objective of this research is to develop relationships for $b$ based on the data of Chapter 3.

Since the turbulent stress component (5.36) contains the parameters $\tau_y$, $K$ and $n$ of the general Bingham function, the parameters can be rewritten more generally as functions of Equations (5.30) and (5.31). If the shear flow function is of the explicit type (5.30), the parameters of Equation (5.35) can be expressed as the following functions of $\dot{\gamma}$:

$$\begin{aligned} \tau_y &= g(0), \\ n(\dot{\gamma}) &= \frac{\dot{\gamma}}{g(\dot{\gamma}) - g(0)} \frac{\mathrm{d}g(\dot{\gamma})}{\mathrm{d}\dot{\gamma}}, \\ K(\dot{\gamma}) &= \frac{g(\dot{\gamma}) - g(0)}{\dot{\gamma}^{n(\dot{\gamma})}}, \end{aligned} \tag{5.39}$$

where the derivative term $\mathrm{d}g/\mathrm{d}\dot{\gamma}$ is simply the derivative of the shear flow function. If the shear flow function is of the implicit type (5.31), the derivative term $\mathrm{d}g/\mathrm{d}\dot{\gamma}$ is no longer relevant, but since the total differential of the implicit shear flow function is zero, $\mathrm{d}G = 0$, the chain rule can be applied to give an equivalent partial derivative term. The general Bingham parameters of Equation (5.35) can therefore be rearranged as the following functions of $\dot{\gamma}$ and $\tau$:

$$\begin{aligned} G(0,\ \tau_y) &= 0, \\ n(\dot{\gamma},\ \tau) &= -\frac{\dot{\gamma}}{\tau - \tau_y} \frac{\partial G}{\partial \dot{\gamma}} \Big/ \frac{\partial G}{\partial \tau}, \\ K(\dot{\gamma},\ \tau) &= \frac{\tau - \tau_y}{\dot{\gamma}^{n(\dot{\gamma},\ \tau)}}. \end{aligned} \tag{5.40}$$

where the derivatives are the partial derivatives of the shear flow function with respect to rate of shear and shear stress.

### 5.3.1 Mean Cross-Sectional Velocity

For turbulent flow predictions of mean cross-sectional velocity $U$, Equation (5.32) can be used. For known wall stress $\tau_R$, close examination of Equations (5.29) to (5.31) and (5.36)

reveal that the turbulent shear flow function is implicit, and of the form

$$H(\dot{\gamma},\ \tau) = 0. \tag{5.41}$$

This is true regardless of whether the laminar stress component is explicit or implicit. The equations are therefore of the same form as the laminar flow equations for the implicit case discussed in Subsection 5.1.1. Referring back to the laminar flow case, two algorithms were compared, one based on the flow equation given here as Equation (5.32), and the other based on a rearrangement of it, namely Equation (5.6). For the turbulent flow case, the same comparisons can be made.

For the integration required of these equations, Simpson's method (A.1) is used. Since the integrands of these equations are functions of $\dot{\gamma}$ and $\tau$, Muller's bracketing method (A.4) is used to solve Equation (5.41) for values of $\dot{\gamma}$ or $\tau$ as necessary. This method is a nested method as Equation (5.41) is solved for each and every integrand evaluation required of Simpson's method. The tolerance of Muller's method is therefore reduced over Simpson by a factor of ten.

The derivative terms of Equations (5.39) and (5.40) also need considering. The derivative term of Equation (5.39) is the derivative $\mathrm{d}g/\mathrm{d}\dot{\gamma}$ of the shear flow function (5.30). If this is undefined, then the following forward difference formula can be used

$$\frac{\mathrm{d}g}{\mathrm{d}\dot{\gamma}} \approx \frac{g(\dot{\gamma} + \Delta\dot{\gamma}) - g(\dot{\gamma})}{\Delta\dot{\gamma}}. \tag{5.42}$$

The derivative terms of Equation (5.40) are the partial derivatives $\partial G/\partial\dot{\gamma}$, $\partial G/\partial\tau$ of the implicit shear flow function (5.31). If these are undefined, then the following forward difference formulae can be used:

$$\begin{aligned} \frac{\partial G}{\partial\dot{\gamma}} &\approx \frac{G(\dot{\gamma} + \Delta\dot{\gamma},\ \tau) - G(\dot{\gamma},\ \tau)}{\Delta\dot{\gamma}}, \\ \frac{\partial G}{\partial\tau} &\approx \frac{G(\dot{\gamma},\ \tau + \Delta\tau) - G(\dot{\gamma},\ \tau)}{\Delta\tau}. \end{aligned} \tag{5.43}$$

The computational efficiency of each algorithm is measured by the number of evaluations of the turbulent shear flow function (5.41). One would expect the efficiencies of the two turbulent flow algorithms to differ by a similar relative amount as their laminar flow counterparts. This is not borne out by observation. For the turbulent flow case, an algorithm based on Equation (5.32) proves significantly more efficient than an algorithm based on the rearranged version of it, whereas for the laminar flow case, the converse was true. This is most likely to be due to the nature of the shear flow functions used; for the laminar flow case, the function always decreases for an increasing rate of shear, whereas for the turbulent flow case, the function may become anything up to a quadratic in rate of shear

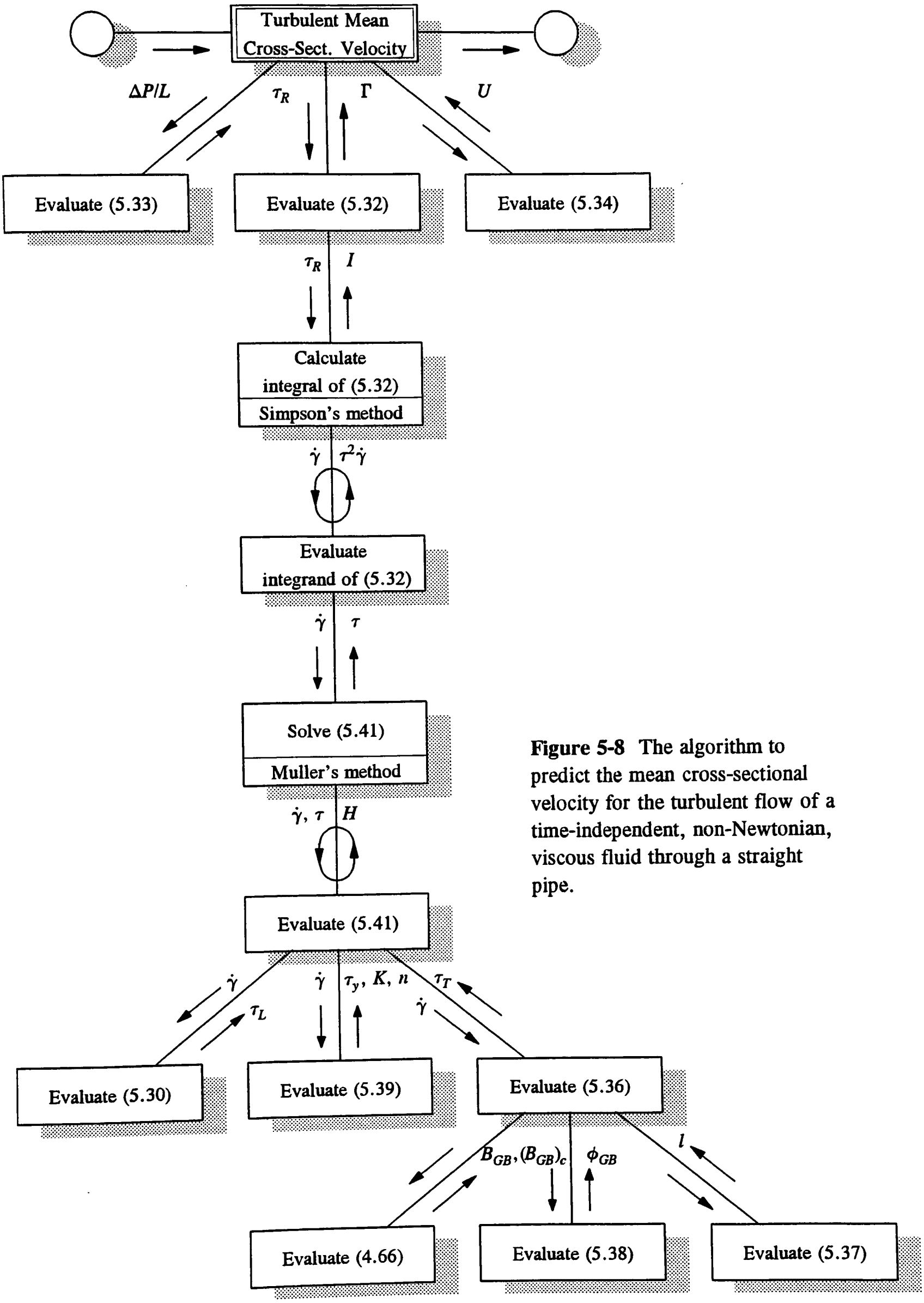


**Figure 5-8** The algorithm to predict the mean cross-sectional velocity for the turbulent flow of a time-independent, non-Newtonian, viscous fluid through a straight pipe.

(see Equation (5.36)). The final algorithm, as illustrated by Figure 5-8, typically requires about three hundred evaluations of the turbulent shear flow function, though this depends on the nature of flow; for near-critical flow, the algorithm requires about one hundred evaluations, whereas for fully-developed turbulent flow, the algorithm requires about eight hundred evaluations.

As an example, consider the flow of the usual general Bingham test case fluid, $\tau = 10 + \sqrt{\dot{\gamma}}$, through a pipe. To make sure that turbulent conditions are met, take a large wall stress of $\tau_R = 100$ Pa and a small pipe diameter of 0.04 m. These conditions give a critical wall stress of about 42 Pa indicating that the turbulent flow is fairly well developed. Using a relative tolerance check of $\epsilon = 5 \times 10^{-5}$, the mean cross-sectional velocity estimate $U^\star = 8.22619 \text{ m s}^{-1}$ is given after 480 shear flow function evaluations. There is no direct way of validating this estimate, but bear in mind that this scheme is essentially the same as the laminar flow scheme for implicit functions that has already been validated. However, the scheme of the next subsection is the inverse of this scheme, so the estimate of $U$ from this scheme can be used by the next scheme to calculate an estimate of $\tau_R$, which can be compared to its original value of 100 Pa. This idea will be explored in the next subsection.

### 5.3.2 Pressure Gradient

A turbulent flow prediction of the pressure gradient is essentially the inverse of a velocity prediction. The velocity prediction algorithm, as discussed in the previous subsection, estimates $\Gamma$ from Equation (5.32) given wall stress $\tau_R$. The pressure gradient algorithm must now *solve* Eq. (5.32) for $\tau_R$ given $\Gamma$. In this case, the variable $\tau_R$ features in the turbulent shear flow function, Equation (5.41) now making it a function of three variables of the form

$$H(\dot{\gamma},\ \tau,\ \tau_R) = 0. \tag{5.44}$$

An algorithm to solve Equation (5.32) for $\tau_R$ could be derived by attaching a front-end, root-finding method to the mean cross-sectional velocity algorithm. Since there are already two levels of method nesting for the velocity algorithm, a third level would produce an inefficient algorithm. For the laminar flow case, the Mooney-Rabinowitsch equation (a differential equation version of (5.32)) was used. However, since the turbulent shear flow function above is also a function of $\tau_R$, there is no Mooney-Rabinowitsch equivalent to this problem. After much investigation, nothing better can be offered than the three-tiered scheme.

Muller's method (A.4) is used as the front-end solver to the mean cross-sectional velocity algorithm. Incidentally, Muller's method is also used in the body of the algorithm, so it becomes nested within itself. The applications are different though since the method is used for root-finding in the mean cross-sectional velocity algorithm, and for inversion in the front-end solver. For an overall relative tolerance of $5 \times 10^{-5}$, the algorithm typically requires

three thousand evaluations of the turbulent shear flow function. As with the mean cross-sectional velocity algorithm, efficiency is better for near-critical flow (making about one thousand function evaluations) than for fully-developed turbulent flow (making several thousand function evaluations). It should be noted that in terms of computer efficiency, the algorithm never took more than a second or two on an IBM compatible PC with a Pentium processor (several seconds on a 386/387 processor). For a single prediction, this caused no problem, but for multiple predictions or large-scale parameter estimation (such as of the data presented in Chapter 3) efficiency becomes a priority. The final version of the algorithm is illustrated by Figure 5-9.

The example of the previous subsection can be validated using this scheme by inverting the mean cross-sectional velocity estimate of the previous scheme to see if the original wall stress value is recovered. Just to recap, the previous example used the general Bingham model $\tau = 10 + \sqrt{\dot{\gamma}}$ with a pipe diameter of 0.04 m. A wall stress value of $\tau_R = 100$ Pa yielded a mean cross-sectional velocity estimate of $U^\star = 8.22619\ \mathrm{m\ s^{-1}}$. Now using the same model and pipe diameter with this scheme, taking a relative tolerance check of $\epsilon = 5 \times 10^{-5}$ and a mean cross-sectional velocity of $U^\star = 8.22619\ \mathrm{m\ s^{-1}}$ yields a wall stress estimate of $\tau_R{}^\star = 100.0005$ Pa. This matches the original value to within the required four significant figures taking 4787 evaluations of the shear flow function to do so.

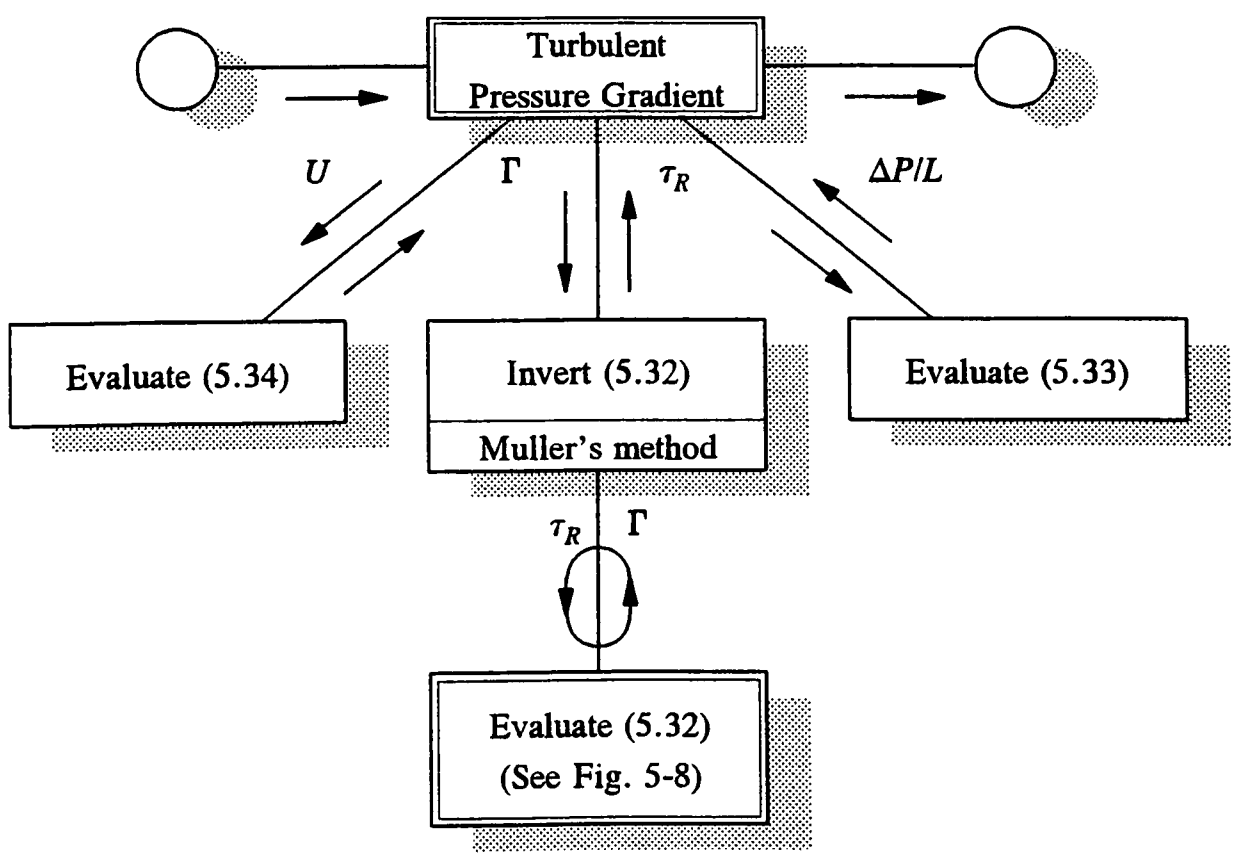


**Figure 5-9** The algorithm to predict the pressure gradient for the turbulent flow of a time-independent, non-Newtonian, viscous fluid through a straight pipe.

### 5.3.3 Velocity Distribution

Consider the velocity distribution of the turbulent flow of a fluid through a straight pipe. Using the turbulent shear flow function proposed by Hanks[26], much of the laminar flow analysis of Subsection 5.1.3 remains applicable. A fluid with a yield stress theoretically flows with an unsheared solid plug core, the radius $r_y$ of which is given by Equation (5.11). For the sheared region of fluid, $r > r_y$, the velocity distribution was given by Equation (5.12) as

$$u(r) = \int_r^R \dot{\gamma}\,dr, \tag{5.45}$$

where $u(R) = 0$. To tie this equation in with the shear variables $\dot{\gamma}$ and $\tau$, there is a linear relationship between $r$ and $\tau$, which was given by Equation (5.10) as

$$\frac{r}{R} = \frac{\tau}{\tau_R}. \tag{5.46}$$

Examination of Equations (5.29) to (5.31) and (5.36) show that, in this case, the turbulent shear flow function is of the implicit form defined by Equation (5.41). This, again, reduces the analysis to that of laminar flow for implicit shear flow functions. However, the laminar flow algorithm worked best for a rearrangement of Equation (5.45), but for the turbulent flow case, an algorithm based directly on Equation (5.45) shall also be considered.

Our objectives are to represent the velocity distribution at a set of $W$ equally spaced radial points. These are given by

$$r_s = R\frac{W - s}{W - 1}, \qquad s = 1,2,...,W. \tag{5.47}$$

Assume that the first $T$ points of the distribution define the sheared region of the fluid, and the subsequent $T + 1$ to $W$ points of the distribution define the solid plug core. Point values of Equation (5.45) are therefore given as

$$u(r_s) = \int_{r_s}^R \dot{\gamma}\,dr, \qquad s = 1,2,...,T.$$

It is clear that the regions of integration overlap for each successive $s$, so we instead use

$$u(r_s) = u(r_{s-1}) + \int_{r_{s-1}}^{r_s} \dot{\gamma}\,dr. \tag{5.48}$$

For this equation, $r$ is linearly related to shear stress $\tau$ through Equation (5.46), whereas the integrand—which is the rate of shear $\dot{\gamma}$—is related to $\tau$ through the turbulent shear flow function (5.41).

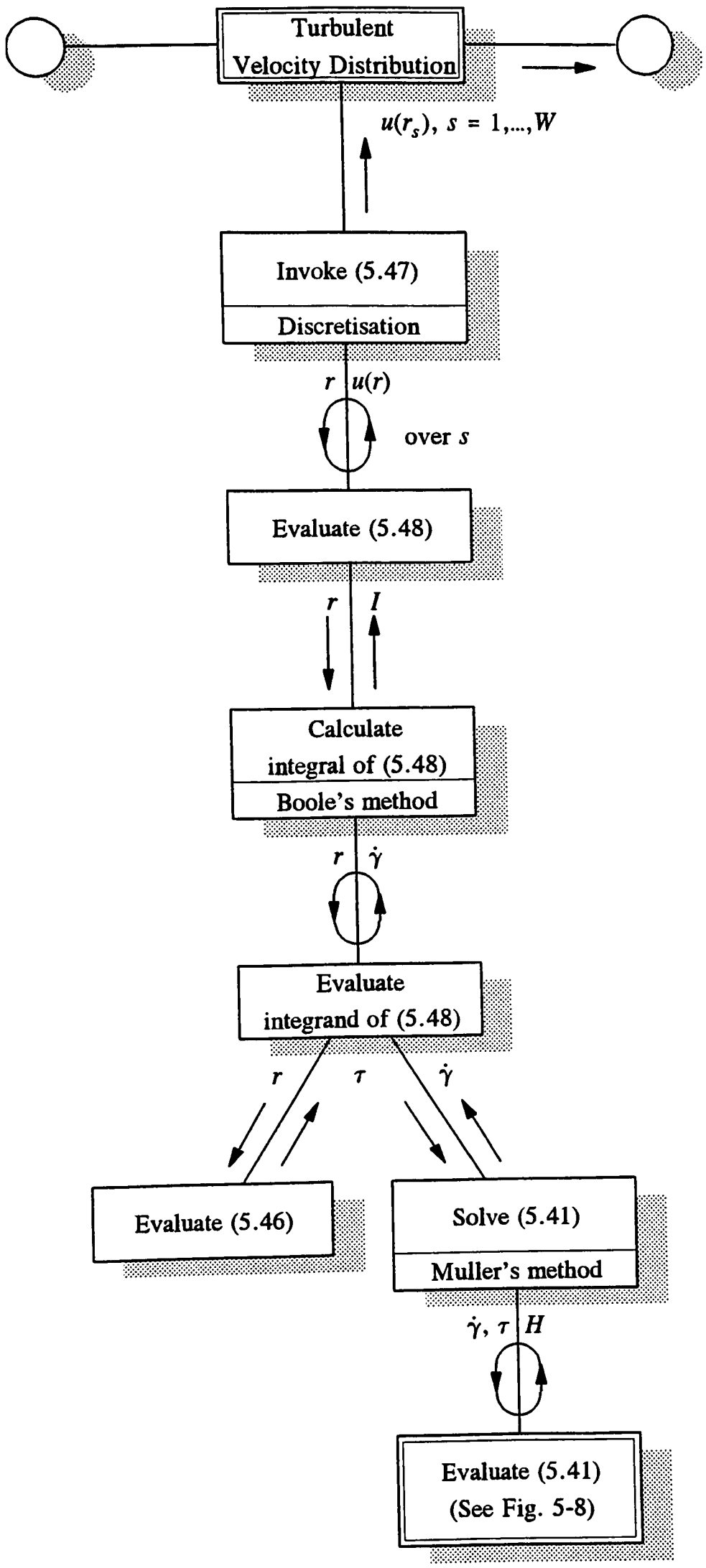


**Figure 5-10** The algorithm to predict the velocity distribution for the turbulent flow of a time-independent, non-Newtonian, viscous fluid through a straight pipe.

For the integration, Boole's five-point method (A.1) is used—the same implementation as for the laminar flow case. This has a computational safeguard for relatively small intervals by using initial tests of Trapezium two-point and Simpson three-point estimates. For the integrand, Muller's bracketing method (A.4) is used as a nested method to solve the turbulent shear flow function for values of $\dot{\gamma}$. Using a relative tolerance check of $5 \times 10^{-5}$, the algorithm requires a few hundred evaluations of the turbulent shear flow function. For near-critical predictions, the algorithm proves more efficient, requiring a couple of hundred evaluations, whereas for fully-developed turbulence, the algorithm requires about one thousand evaluations. The final algorithm is illustrated by Figure 5-10 on the previous page.

There is no simple way of validating this scheme, but it is essentially the same as the laminar flow scheme for implicit functions which has already been validated. The turbulent flow velocity profiles of Figures 4-4 and 4-5 were both created using this scheme by defining each curve as a series of straight lines joining a set of closely spaced points.

### 5.3.4 Scope of Use

An indication of the scope of the turbulent flow algorithms is again accomplished by using the general Bingham shear flow function (2.10),

$$\tau = \tau_y + K\dot{\gamma}^n.$$

Section 4.4 discussed the equations for the turbulent flow of a general Bingham fluid (and its special cases) through a straight pipe. On the whole, the solution procedure to these equations would be no different from the general case under consideration so they would be of limited use for validation. There are, however, useful exceptions such as the Bingham turbulent flow function (4.59) which is quadratic in $\dot{\gamma}$. The second validation procedure (as discussed for laminar flow) requires inverting a prediction to see if it reverts back to its original value, and is particularly useful in this case.

Using the validation procedures, Table 5-5 gives a general idea of the usable ranges of parameters. Although the ranges are not as extensive as for the laminar and critical flow algorithms, they are generally suitable for any practical problem. It would be true to say that the required tolerance is generally met, and if not, a reasonably accurate answer is almost always given. Some inaccuracy does occur for a small percentage of predictions, probably because of the inherent complexity and generality of the algorithms. Anyhow, an end-user could easily validate their own prediction using the inversion method.

The efficiency of an algorithm is defined as the total number of shear flow function evaluations made by the algorithm. Table 5-6 gives the order of magnitude of efficiency for each algorithm.

**Table 5-5** A general guide to the parameter ranges for the turbulent flow algorithms

| Parameter | Range |
|---|---|
| $U$/m s$^{-1}$ | $10^{-3}$ - $10^{3}$ |
| $(\Delta P/L)$/Pa m$^{-1}$ | $10^{-3}$ - $10^{9}$ |
| $D$/m | $10^{-2}$ - 10 |
| $\tau_y$/Pa | 0 - 100 |
| $K$ | $10^{-6}$ - $10^{6}$ |
| $n$ | 0.3 - 1.0 |

**Table 5-6** The number of the shear flow function evaluations in orders of magnitude made by each algorithm.

| Estimate | Efficiency |
|---|---|
| Mean velocity/m s$^{-1}$ | $10^{2}$ - $10^{3}$ |
| Pressure grad/Pa m$^{-1}$ | $10^{3}$ - $10^{4}$ |
| Velocity dist'n/m s$^{-1}$ | $10^{2}$ - $10^{3}$ |

## 5.4 Wall Slippage Modelling

Wall slip of the flow of a suspension through a straight pipe was discussed in Section 4.5. This can be typically modelled using a slip velocity as a function of both shear stress $\tau_R$ and pipe diameter $D$ such as Equation (4.74),

$$U_s = \frac{\beta \tau_R}{D^{\alpha}}, \tag{5.49}$$

where $\alpha$ and $\beta$ are constants established from data. This was used in the derivation of a relation between pseudo-shear rate $\Gamma$ and wall stress $\tau_R$ given by Equation (4.75) as

$$\Gamma = \frac{8\beta \tau_R}{D^{\alpha + 1}} + \frac{4}{\tau_R^3} \int_{\tau_y}^{\tau_R} \tau^2 \dot{\gamma} \, d\tau. \tag{5.50}$$

The schemes for modelling laminar and turbulent flow using this equation remain unchanged as the extra term contains no new variables to solve for. Laminar flow was better modelled using the Mooney-Rabinowitsch equation; the wall slip version was defined by Equation (4.76) as

$$\dot{\gamma}_R = \left[ \frac{3n'' + 1}{4n''} \right] (\Gamma - \Gamma_s), \tag{5.51}$$

where

$$n'' = \frac{\mathrm{d} \ln \tau_R}{\mathrm{d} \ln (\Gamma - \Gamma_s)},$$

and $\Gamma_s = 8U_s/D$. With some straightforward manipulation, Equation (5.51) can be rearranged as the linear differential equation

$$\frac{\mathrm{d}\dot{\gamma}_R}{\mathrm{d}\Gamma} = \frac{\tau_R}{4(\dot{\gamma}_R + \Gamma_s) - 3\Gamma} \Big/ \left( \frac{\mathrm{d}\tau_R}{\mathrm{d}\dot{\gamma}_R} \right), \qquad \dot{\gamma}_R(0) = 0, \tag{5.52}$$

which is the same as Equation (5.8) with a slip term included. This equation can also be obtained by differentiating Equation (5.50) with respect to $\tau_R$ and rearranging. It should be appreciated that $\tau_R$ and $\Gamma_s$ are themselves both function of $\dot{\gamma}_R$ via the shear flow function.

Consider the first example of the chapter: laminar flow of the general Bingham fluid $\tau = 10 + \sqrt{\dot{\gamma}}$ through a straight pipe. A wall stress value of $\tau_R = 25$ Pa yielded a pseudo-shear rate value of $\Gamma = 132.48\ s^{-1}$. This is essentially an evaluation of the right-hand term of Equation (5.50). Taking a pipe diameter of $D = 0.1$ m and slip parameters of $\alpha = 1$ and $\beta = .001$, the slip term of Equation (5.50) is, after a simple calculation, $20\ s^{-1}$. The total pseudo-shear rate evaluation for Equation (5.50) is therefore $\Gamma = 152.48^{-1}$. So far, this is not very exciting, but the problem can be inverted using Equation (5.52) to see if the wall stress estimate matches the original value of $\tau_R = 25$ Pa. Of course, the slip term of Equation (5.52) is now unknown as it is a function of $\tau_R$, which is effectively the solution variable. The scheme for numerically solving Equation (5.52) remains the same as the Runge-Kutta Fehlberg scheme of Subsect. 5.1.2. The starting value idea remains unchanged. From Equation (5.51) it is clear that $(\dot{\gamma}_R)_0 = (\Gamma - \Gamma_s)$ would lie reasonably close to the solution; the corresponding value of $\Gamma_0$ would then be estimated from Equation (5.50). Taking a relative tolerance check of $\epsilon = 5 \times 10^{-5}$, and using the appropriate values and function above, the scheme gives a wall stress estimate of $\tau_R^{\star} = 25.0000$ Pa, which lies well within the required four significant figure accuracy. Much as expected, the scheme is still efficient taking one step of Fehlberg's method and 52 evaluations of the shear flow function.

## 5.5 Conclusions

In this chapter, a discussion has been given of the mathematical modelling of time-independent, non-Newtonian, viscous fluids through a straight pipe for any explicit or implicit shear flow function. Algorithms have been presented of laminar, critical and turbulent flow, and velocity distributions. The algorithms have been extensively tested on the three parameter general Bingham shear flow function as it is a good model of any time-independent, non-Newtonian, viscous fluid. Examples using the implicit Meter shear flow function have also been included. The laminar and critical flow algorithms have been validated way beyond any practical range (Tables 5-1 and 5-3) which is desirable for data analysis (Chapters 7 and 8) where robust pipe-to-shear transformations are required. Critical flow does not always occur for dilatant fluids as shear thickening may develop faster than flow instability. The turbulent flow algorithms were found to be less extensive (see Table 5-5) than those of the laminar and critical flow, though the required tolerance was generally met for any realistic test case. In the final section of this chapter, wall slippage was introduced into the models without affecting either the basic structure or the efficiency of any of the algorithms. The next chapter discusses the development and implementation of parameter estimation algorithms where the algorithms of this chapter will be extensively utilised.

# 6 Parameter Estimation

This chapter discusses the parameter estimation for rheological models of time-independent, non-Newtonian, viscous fluids. The work is original as parameter estimation of pipe flow data for any rheological model is considered. There is precious little in the literature about estimating rheological parameters, which is hardly surprising since methods for obtaining least-squares (or other) estimates are well-established[80]. However, there is the added complication that, for practical reasons, the viscometry of sewage sludge is often conducted in tubes or pipes. Due to the pipe geometry, the parameters must be estimated through the Mooney-Rabinowitsch correlation (4.21). Frost[8] resolved this problem for general Bingham fluids by using a second order approximation on a log-log transformation of the data. For a specific model like the general Bingham model, such a simplification may be possible, but the objectives of this research are to consider any rheological model either laminar or turbulent. This has the advantage, for instance, that the analysis could be easily repeated at a later date using a different rheological model. In fact, the method could be used for the analysis of any pipe flow data for any choice of rheological model. This chapter does not use any computer terminology. However, the algorithms have been implemented in Fortran 77 and Appendix B gives the subroutine declaration (name and argument list) of each associated algorithm of this chapter.

## 6.1 Laminar Flow Case

The shear flow function is a relationship between shear stress $\tau$ and rate of shear $\dot{\gamma}$. Including the fitting parameters $\alpha$, an explicit shear flow function is of the form

$$\tau = g(\dot{\gamma};\ \alpha), \tag{6.1}$$

and an implicit shear flow functions is of the form

$$G(\dot{\gamma},\ \tau;\ \alpha) = 0. \tag{6.2}$$

To illustrate the nature of the problem, consider the hypothetical situation where parameter estimation of either of the above two functions was carried out on a set of shear flow coordinates $(\dot{\gamma}_j,\ \tau_j)$, $j = 1,2,...,M$. The problem would be geometrically independent, and therefore straightforward. To obtain estimates of the parameters, the relevant shear flow function would be fitted directly to the coordinates.

In practice, however, the problem is complicated by data which comes from pipes, and are therefore geometrically dependent; they are given as pseudo-shear flow coordinates, $(\Gamma_j,\ (\tau_R)_j)$, $j = 1,2,...,M$, or similar. The pseudo-shear flow function (discussed in Section 4.2) could be fitted; this is a relationship of the form

$$\psi(\Gamma,\ \tau_R;\ \alpha) = 0, \tag{6.3}$$

where the shear stress at the pipe wall is

$$\tau_R = \frac{D}{4}\frac{\Delta P}{L}, \tag{6.4}$$

and the pseudo-shear rate is

$$\Gamma = \frac{8U}{D}. \tag{6.5}$$

Primarily, this equation can be viewed as a relationship between the pressure gradient $\Delta P/L$ and mean cross-sectional velocity $U$ of a pipe flow situation.

Fitting a pseudo-shear flow function to pseudo-shear flow data is suitable for some shear flow functions such as the power law function, $\tau = K\dot{\gamma}^n$, as the related pseudo-shear flow function is of the similar simple form, $\tau_R = K'(n)\Gamma^n$. The parameters $K'$ and $n$ can first be estimated, then $K$ can be calculated from $K'$ and $n$. For the general Bingham model, $\tau = \tau_y + K\dot{\gamma}^n$, things are less straightforward; the corresponding pseudo-shear flow function (see Equation 4.18) is elaborate and non-linear. Unlike the power law model, the pseudo-shear flow function of the general Bingham model bears no similarity to its corresponding shear flow function. For other explicit and implicit models, the problem becomes more difficult since the pseudo-shear flow function may not be expressible as a simple implicit function of type (6.3). Another drawback of parameter estimation from the pseudo-shear flow function is that, even if the function is known for a particular model, a transformation of the shear flow function itself may be required. For instance, a log transformation of the general Bingham model is $\log(\tau - \tau_y) = \log K + n\log\dot{\gamma}$, and pseudo-shear flow function corresponding to this model would bear no resemblance to that of the non-transformed general-Bingham model.

The first approach to the problem is perhaps the most obvious: the Mooney-Rabinowitsch[52, 53] differential equation (4.21)—or any of its rearrangements—can be regarded as a generalised pseudo-shear flow function. Therefore, the shear flow function parameters could be estimated from such an equation. In essence, the approach would mean fitting an equation such as the Mooney-Rabinowitsch equation to the data—an approach that would be difficult, but still possible. The approach, however, suffers from a drawback: there is no obvious way of dealing with transformations, such as the log-log transformation, of the shear flow function.

For the second approach, the problem is partitioned as follows:

1) Attain geometrical independence by transforming the set of pseudo-shear flow data coordinates to a set of shear flow data coordinates.

2) Once geometrical independence has been attained, fit the shear flow function to the resulting shear flow data coordinates.

The algorithm would be iterative and somewhat more elaborate than this, but it acts as a general outline. Step 1 can be achieved by making laminar flow predictions of the data; an algorithm for making such laminar flow predictions was presented in Section 5.1 and was essentially based on the Mooney-Rabinowitsch equation. Once geometrical independence has been achieved, Step 2 becomes the same as the hypothetical situation discussed earlier. To pose the algorithm in more formal terms: for each pseudo-shear rate data value $\Gamma_j$, a prediction of the corresponding wall shear rate value $(\dot{\gamma}_R)_j$ can be made. However, to make laminar flow predictions, the parameters $\alpha$ of the shear flow function are needed. For the first iteration, guesses of the fitting parameters are used with each $\Gamma_j$ to make the initial laminar flow predictions of $(\dot{\gamma}_R)_j$, $j = 1,2,...,M$. The shear flow function is then fitted to estimates of the shear flow coordinates $((\dot{\gamma}_R)_j, (\tau_R)_j)$, $j = 1,2,...,M$, to give a fresh estimate of $\alpha$—a process that is repeated to convergence. The algorithm is illustrated by Figure 6-1.

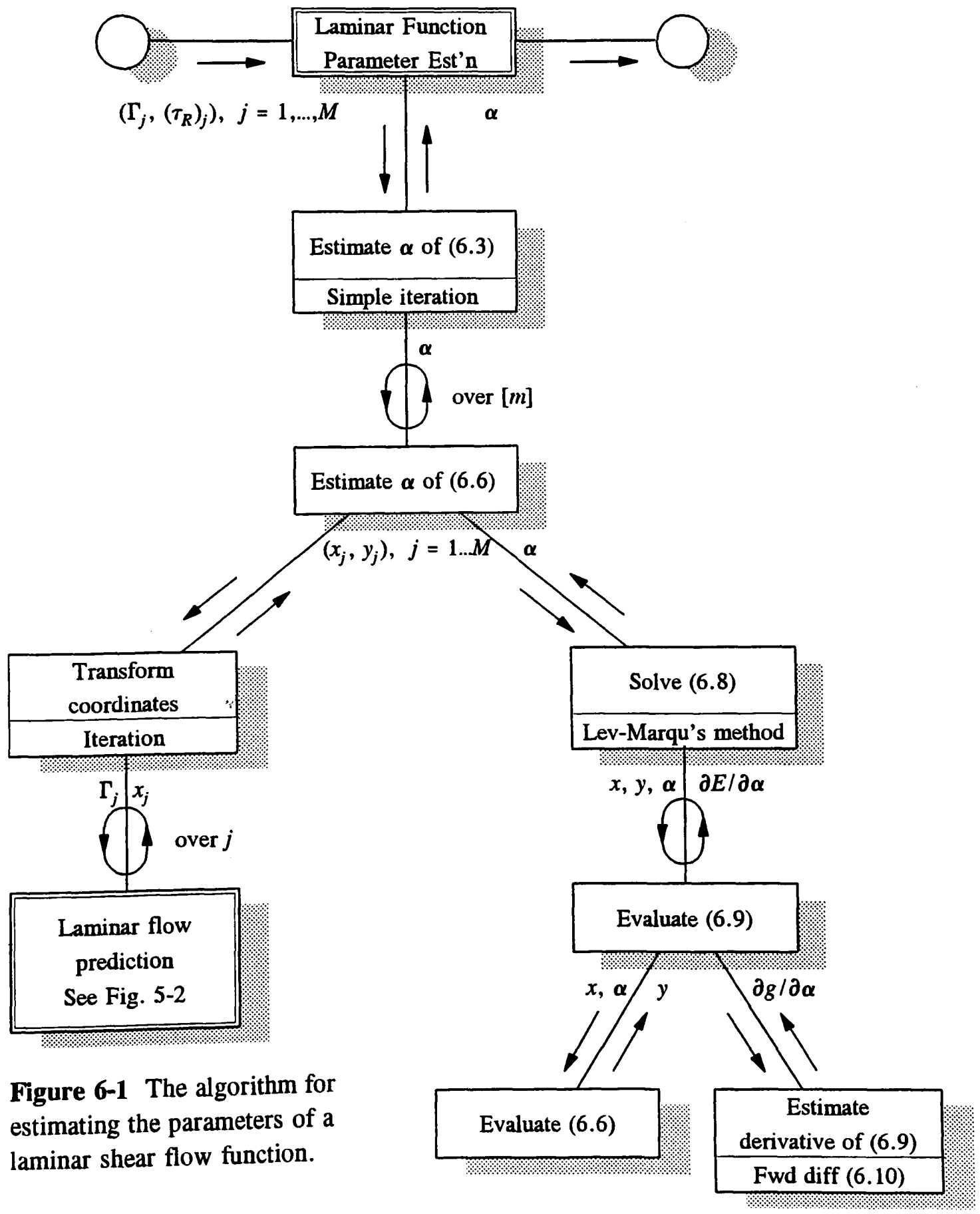


**Figure 6-1** The algorithm for estimating the parameters of a laminar shear flow function.

Notice that, for each iteration, the algorithm makes successive transformations (namely laminar flow predictions) of the independent variable $\dot{\gamma}_R$. The dependent variable $\tau_R$, however, remains unaffected, enabling the assumptions of an estimating method—such as the least squares method—to remain valid. The algorithm is nested, iterating $\alpha$ at the top-level and estimating $\alpha$ at the lower-level. Using $\alpha$ itself as the convergence criterion at either of the levels would be unwise for obvious reasons. For convergence of the top-level method, the standard error between the $m$ - 1th and $m$th estimates of the shear rate points $(\dot{\gamma}_R)_j$, $j = 1,2,...,M$, are compared using a relative convergence criterion. For the lower-level method, the same convergence criterion is used, but on the dependent variable $\tau_R$ rather than the independent variable $\dot{\gamma}_R$ using a factor-of-ten reduction of tolerance. One of the great advantages of the algorithm is that it effectively separates the parameter estimation of the shear flow function from the transformation of the pseudo-shear flow function. If a transformation of the shear flow function is to be required (such as the log transformation), then this can be regarded as secondary to the pipe-to-shear transformation.

At the core of the algorithm is the method of estimating shear flow function parameters from a set of shear flow coordinates. For this, *least squares estimates* are chosen. For convenience, we denote

$$x_j \equiv (\dot{\gamma}_R)_j^{[m]}, \quad j = 1,2,...,M,$$

which are the $m$th estimates of the wall shear rate values, and

$$y_j \equiv (\tau_R)_j, \quad j = 1,2,...,M,$$

which are the wall stress values.

For the explicit case, Equation (6.1) can be written as

$$y = g(x;\ \alpha). \tag{6.6}$$

The error sum of squares is the sum of squares of each data value minus the predicted value, and is given as

$$E = \sum_{j=1}^{M} [y_j - g(x_j;\ \alpha)]^2. \tag{6.7}$$

The least squares estimates of $\alpha$ are given at the minimum value of $E$ with respect to $\alpha$; they are given by the solution of the equations

$$\frac{\partial E}{\partial \hat{\alpha}_k} = 0, \qquad k = 1,2,...,Q, \tag{6.8}$$

where

$$\frac{\partial E}{\partial \hat{\alpha}_k} = -2 \sum_{j=1}^{M} [y_j - g(x_j;\ \hat{\alpha})] \frac{\partial g(x_j;\ \hat{\alpha})}{\partial \hat{\alpha}_k}, \tag{6.9}$$

and the hat is used to signify estimates.

Equation (6.8) is a system of $Q$ equations in $Q$ unknowns. To solve this system, Levenberg-Marquardt's method (A.2: Appendix A, Section 2) is used. The derivatives of Equation (6.9) are the partial derivatives of the shear flow function with respect to each of its parameters. If these derivatives are undefined then the following forward difference formulae would be used:

$$\frac{\partial g(x_i;\,\alpha)}{\partial \alpha_k} \approx \frac{g(x_i;\,\alpha_1,\ldots,\alpha_k + \Delta\alpha_k,\ldots,\alpha_Q) - g(x_i;\,\alpha_1,\ldots,\alpha_k,\ldots,\alpha_Q)}{\Delta\alpha_k},\quad k = 1\ldots Q. \tag{6.10}$$

For the implicit case, Equation (6.2) can be written as

$$G(x,\,y;\,\alpha) = 0. \tag{6.11}$$

The value of $y$ at $x_j$ can no longer be evaluated directly from this equation, so a method to solve for $y$ can be used. Letting $\tilde{y}_j$ to be the value of $y$ at $x_j$, we have

$$G(x_j,\,\tilde{y}_j;\,\alpha) = 0, \qquad j = 1,\ldots,M, \tag{6.12}$$

and the error sum of squares becomes

$$E = \sum_{j=1}^{M} [y_j - \tilde{y}_j]^2. \tag{6.13}$$

Minimizing this equation with respect to $\alpha$, the least squares estimates are given by the solution of

$$\frac{\partial E}{\partial \hat{\alpha}_k} = 0, \qquad k = 1,2,\ldots,Q, \tag{6.14}$$

where

$$\frac{\partial E}{\partial \hat{\alpha}_k} = -2\sum_{j=1}^{M} [y_j - \hat{y}_j]\frac{\partial \hat{y}_j}{\partial \hat{\alpha}_k}, \tag{6.15}$$

and the hat is used to signify estimates. The derivatives are the partial derivatives of $y$ with respect to each of the shear flow function parameters, but evaluated at $x_j$. As $y$ is implicitly defined via (6.12), these derivatives are not available directly, so applying the chain rule to the partial derivatives of implicit functions[81] gives

$$\frac{\partial y}{\partial \alpha_k} = -\left(\frac{\partial G}{\partial \alpha_k}\right)\Big/\left(\frac{\partial G}{\partial y}\right). \tag{6.16}$$

Since the function $G$ is explicit in terms $y$ and $\alpha$, the partial derivatives are now definable.

Equation (6.14) is a system of $Q$ equations in $Q$ unknowns. To solve this system, Levenberg-Marquardt's method (A.2) is again used. The nested method used to solve Equation (6.12) for specific values of $y$ is Muller's method (A.4) with a reduction of the main tolerance by a factor of ten. Computations of the derivative terms of Equation (6.16) are also a nested part of the main method. If these derivatives are undefined, then the

following forward difference formulae can be used:

$$\frac{\partial G}{\partial \alpha_k} \approx \frac{G(x, y; \alpha_1,...,\alpha_k + \Delta\alpha_k,...,\alpha_Q) - G(x, y; \alpha_1,...,\alpha_k,...,\alpha_Q)}{\Delta\alpha_k}, \quad k = 1...Q,$$
$$\frac{\partial G}{\partial y} \approx \frac{G(x, y + \Delta y; \alpha) - G(x, y; \alpha)}{\Delta y}. \tag{6.17}$$

## 6.1.1 General Bingham Case

In this section, fitting the general Bingham model to shear flow data shall be discussed. This particular example of an explicit shear flow function has been singled out as the choice of model used for analysing the data (to be discussed in the next chapter). The general Bingham model is an interesting case as Levenberg-Marquardt's method is not needed, but the rest of the algorithm—the pipe-to-shear transformation—remains unchanged. Since the general Bingham function is really the only model under consideration, one might ask why algorithms have been developed to utilise any appropriate explicit or implicit shear flow function: why have these general cases been considered? Apart from the obvious—satisfying the objectives—there are many other reasons for working with the general case. Firstly, in Chapter 8, the general Bingham model will be extended as a function of solids concentration, effectively resulting in an entirely new function with a completely different pseudo-shear flow function. Secondly, when the general Bingham model is fitted to a data set, to satisfy the requirements of the residual analysis, a transformation may be required [82] (this will be a topic of the next chapter). Although the general Bingham model will conceptually be unaffected by the transformation, it will strictly be a different function, and its corresponding pseudo-shear flow function will be completely different. Thirdly, any further work may repeat the data analysis using functions other than the general Bingham model; working with the general case now would avoid much repetition of the developmental work. It should further be noted that an algorithm based exclusively on the general Bingham model is not likely to be trivial anyway, so the advantages of working with the general case are considerable.

The problem is to fit the general Bingham model

$$\tau = \tau_y + K\dot{\gamma}^n, \tag{6.18}$$

to a set of shear flow coordinates $(\dot{\gamma}_j, \tau_j)$, $j = 1,2,...,M$. Notice that for constant $n$, the problem reduces to that of linear regression [83]. The error sum of squares is

$$E = \sum_{j=1}^{M} (\tau_j - \bar{\tau})^2 - \frac{\left[\sum_{j=1}^{M} (\dot{\gamma}_j^n - \overline{\dot{\gamma}^n}) \sum_{j=1}^{M} (\tau_j - \bar{\tau})\right]^2}{\sum_{j=1}^{M} (\dot{\gamma}_j^n - \overline{\dot{\gamma}^n})^2}, \tag{6.19}$$

where $\bar{\tau}$ is the average value of $\tau$, and similarly for $\dot{\gamma}^n$. The solution of the equation pair

$$\frac{\partial E}{\partial \hat{\tau}_y} = 0,$$
$$\frac{\partial E}{\partial \hat{K}} = 0, \tag{6.20}$$

yield the least squares estimates

$$\hat{K} = \frac{\sum_{j=1}^{M} (\dot{\gamma}_j^n - \overline{\dot{\gamma}^n}) \sum_{j=1}^{M} (\tau_j - \bar{\tau})}{\sum_{j=1}^{M} (\dot{\gamma}_j^n - \overline{\dot{\gamma}^n})^2},$$
$$\hat{\tau}_y = \bar{\tau} - \hat{K}\overline{\dot{\gamma}^n}, \tag{6.21}$$

where the hat is used to distinguish the parameters as estimates. For fixed $n$, the problem becomes a linear regression one where the parameters are explicitly given. But when fitting the general Bingham model, $n$ must be treated as variable, so a solution is also required of

$$\frac{\partial E}{\partial \hat{n}} = 0. \tag{6.22}$$

Since there is no obvious analytical solution for $n$, Newton's method is used to solve this equation. For this case, it is

$$n^{[m+1]} = n^{[m]} - \frac{\partial E}{\partial n} \Big/ \frac{\partial^2 E}{\partial n^2}, \tag{6.23}$$

where the derivatives are themselves functions of $n$, and are evaluated at each $n^{[m]}$.

### 6.1.2 Log General Bingham Case

A log version of the general Bingham model is given as

$$\log(\tau - \tau_y) = \log K + n \log \dot{\gamma}. \tag{6.24}$$

This would be fitted to log values of the shear flow coordinates, ie $(\log \dot{\gamma}_j, \log(\tau_j - \tau_y))$, $j = 1,2,...,M$. In this case, if the parameter $\tau_y$ is considered constant, the equation is linear in terms of the log variables. Using linear regression, estimates for $\log K$ and $n$ can be obtained. However, $\tau_y$ is variable, so the equation

$$\frac{\partial E}{\partial \hat{\tau}_y} = 0, \tag{6.25}$$

must also be solved. This bears much analogy to the non-transformed case, so Newton's method is likewise employed to solve the equation for $\tau_y$.

It should be appreciated that, although the log general Bingham model is conceptually the same as the ordinary version, they are strictly different functions. The equations that yield the least squares estimates would be different, and therefore some differences would be expected of the estimates of $\tau_y$, $K$ and $n$ themselves, though the differences would probably be minimal. The better model to use—ordinary or transformed—depends on the spread of residuals. Both models are to be used to analyse the data discussed in Chapter 3, the results of which will be discussed in Section 7.1.

## 6.2 Turbulent Flow Case

The turbulent shear flow function proposed by Hanks [26] (discussed in Section 4.4) is an implicit function of shear stress and rate of shear. The turbulent flow model has a single fitting parameter $b$ of its own, so it is of the form

$$H(\dot{\gamma},\ \tau;\ b) = 0. \tag{6.26}$$

The turbulent flow case bares much analogy to the laminar flow case for implicit functions, but because turbulent predictions are so computationally intensive, and because the turbulent shear flow function has only one fitting parameter, it merits its own special consideration. The pseudo-shear flow function for turbulence would be of a similar form to the laminar Equation (6.3), but with the one parameter:

$$\omega(\Gamma,\ \tau_R;\ b) = 0. \tag{6.27}$$

For convenience, denote

$$x_j \equiv (\dot{\gamma}_R)_j,\ \ j = 1,2,...,M,$$

which are the wall shear rate values, and

$$y_j \equiv (\tau_R)_j^{[m]},\ \ j = 1,2,...,M,$$

which are the $m$th estimates of the wall stress values. Equation (6.26) now becomes

$$H(x,\ y;\ b) = 0. \tag{6.28}$$

Letting $\tilde{y}_j$ to be the value of $y$ at $x_j$, the error sum of squares is

$$E = \sum_{j=1}^{M} [y_j - \tilde{y}_j]^2. \tag{6.29}$$

The objectives are to find the value of $b$ that yields the minimum error, $E$. There are alternative ways of minimising the error, such as equating the derivative of (6.29) to zero, or just simply searching for the minimum. As there is only one parameter to estimate, the search option is considered to be better. Since turbulent flow predictions are computationally intensive, it is sensible to use an effective search method; this is chosen to be quadratic

interpolation (A.3) to successively reduce the interval containing the minimum to convergence. The final algorithm is shown by Figure 6-2.

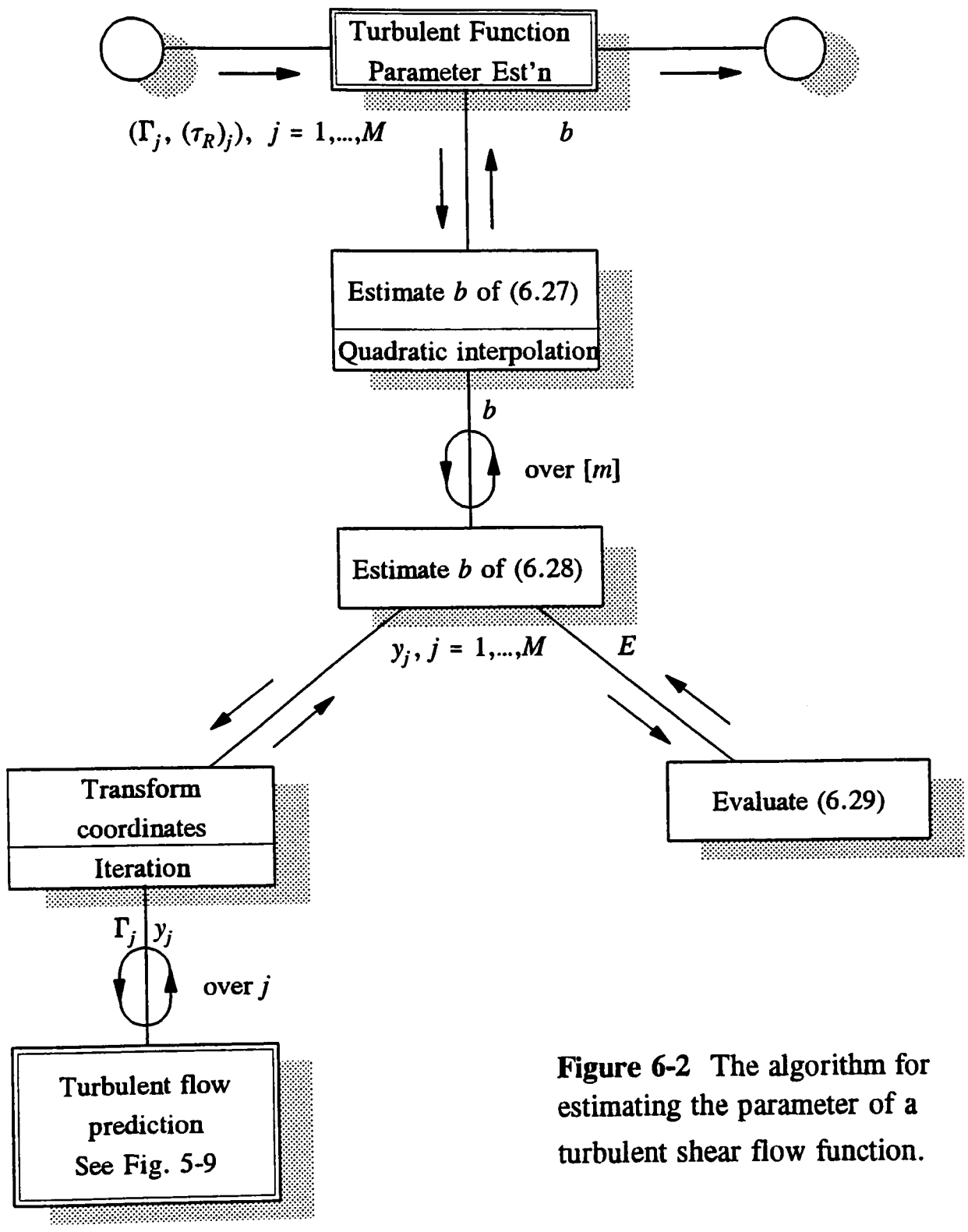


**Figure 6-2** The algorithm for estimating the parameter of a turbulent shear flow function.

## 6.3 General Case

This chapter has so far only considered parameter estimation for a single sludge sample test. But there are three sludge types—primary, activated and digested—and many sludge samples to consider. For each sludge type, let there be $i = 1,...,N$ samples of sludge and $j = 1,...,M_i$ viscometric measurements of each sample. First consider a model for the $i$th sludge sample of a particular sludge type. For dependent variable $y$, the error sum of squares is given as

$$E_i = \sum_{j=1}^{M_i} (y_{ij} - \hat{y}_i)^2, \tag{6.30}$$

where $\hat{y}_i$ is the $i$th predicted model.

The standard error of this model is given as

$$S_i = \sqrt{\frac{E_i}{M_i - Q}}, \tag{6.31}$$

where $Q$ is the number of parameters of the model.

Now consider a model for a particular sludge type. The *total* error sum of squares of the model can be partitioned into the error *between* the sludge samples, and the error *within* each sludge sample. In terms of error sum of squares this equates to

$$E_T = E_B + E_W. \tag{6.32}$$

Algebraically, each of these terms are given by

$$\begin{aligned} E_T &= \sum_{i=1}^{N} \sum_{j=1}^{M_i} (y_{ij} - \hat{y})^2, \\ E_B &= \sum_{i=1}^{N} M_i (\hat{y}_i - \hat{y})^2, \\ E_W &= \sum_{i=1}^{N} E_i = \sum_{i=1}^{N} \sum_{j=1}^{M_i} (y_{ij} - \hat{y}_i)^2, \end{aligned} \tag{6.33}$$

where $\hat{y}$ is the overall predicted model for the sludge type, and $\hat{y}_i$ is the predicted model of the $i$th sludge sample. The total standard error for this model is given by

$$S = \sqrt{\frac{E_T}{\Sigma_1^N M_i - Q}}. \tag{6.34}$$

## 6.4 Confidence Intervals

Individual predictions, such as obtaining a pressure gradient from a given mean cross-sectional velocity, were discussed in Chapter 5. Such predictions can be made using the estimated values of the parameters. A confidence interval is a statistical interval of confidence on a prediction. Confidence intervals can be very important for fluids such as sewage sludge since there may be large random errors when measuring the viscosity of sludge.

A $100(1 - a)\%$ confidence interval for a prediction $x_0$ of a regression curve[83] such as Equation (6.6) or (6.11) is given by

$$\hat{y}_0 \pm t_{a/2;\, M-Q} \times S, \tag{6.35}$$

where $\hat{y}$ is the predicted model, $M$ is the number of measured values, $Q$ is the number of parameters of the model, and $t$ is the $t$ statistic. $S$, the standard error between the data and the fitted curve, is given as

$$S = \sqrt{\frac{\Sigma_{j=1}^{M}(y_j - \hat{y}_j)^2}{M - Q}} \,. \tag{6.36}$$

For statistical reasons, this is strictly a *prediction interval*, but the term *confidence interval* is used here for clarity. This model assumes that the confidence interval is constant for the whole $x$ range, and ignores the variation associated with the predicted curve $\hat{y}$ itself. To have include this variation would have made the confidence interval a function of $x$, narrower at the centre of the $x$ range, and wider at the extremities. The analysis for this effect would have been difficult for the types of non-linear functions that we are dealing with. Since the variance of the data is expectedly greater than that of the predicted curve, the variance of the predicted curve has been excluded to greatly simplify the analysis. A further advantage of the confidence interval being independent of $x$ is that transformations can be applied to the $x$ variable without affecting the interval.

## 6.5 Conclusions

This chapter discussed the development of algorithms for the parameter estimation of laminar and turbulent flow models. Three models have been discussed in particular: the general Bingham model, the log general Bingham model and a turbulent flow model. The extensive use of these models to examine the data discussed in Chapter 3 will be the subject of the next chapter. Parameter estimation for the general case has also been discussed, and the extensive use of these algorithms to yield models as a function of volume fraction of solids will be the topic of Chapter 8.

# 7 Data Analysis

This chapter discusses the analysis of concentrated sewage sludge flow data of the laboratory report [10] using the algorithms developed in Chapters 5 and 6. As mentioned in Chapter 3 (where a discussion was given of the data), sludge is lumpy and inhomogeneous, so tubes and pipes were used to measure the viscosity of the sewage. The objectives of this part of the research are to obtain laminar, critical and turbulent flow models of each sludge type. For the analysis of the laminar flow data, the three parameter general Bingham shear flow function (2.10) is fitted to all of the sound laminar flow data, and statistical tests are conducted to see if all three parameters of the model are necessary; if they are not, then the modelling can be greatly simplified. For the critical flow analysis, the predictions of the Ryan and Johnson [54] stability parameter (4.31) are qualitatively assessed for pipe flow data and, to a lesser extent, tube flow data that extend into the transitional regime. For the turbulent flow analysis, the model proposed by Hanks [26] is fitted to all of the sound turbulent flow data, and is based on the three parameters of the general Bingham model and one further fitting parameter of its own. Error and residual analysis will be used extensively to gauge the accuracy and validity of a model, and admit any transformations required. Outlier analysis will also be conducted (to detect and remove irregular data) using both qualitative and statistical techniques. Since the body of data is not extensive enough (see Chapter 3), time dependent and wall slippage effects will be excluded from the analysis.

Statistical packages were considered for analysing the data, such as Glim, Genstat or SPSS, but since the data requires far more than standard statistical methods, these packages were deemed to be inadequate. For instance, the analysis of the laminar flow data requires schemes for predicting both laminar pipe flow and critical flow. Much of the analysis involves combining the schemes of Chapters 5 and 6 whilst including some basic statistical methods, such as analysis of variance. The task in hand therefore involves combining a wide selection of simple tools to perform a difficult task, and most of the tools used for the analysis are not offered by any statistical package.

## 7.1 Laminar Flow Analysis

For the laminar flow analysis, the tube flow data are of relevance as they mainly cover the laminar flow regime (the pipe flow data give more emphasis to the transitional and turbulent flow regimes). The tube flow data are given as pseudo-shear flow data (wall stress, $\tau_R$ versus pseudo-shear rate, $8U/D$), and as they stand, are of little practical value since they depend on the pipe diameter. However, the objective is to achieve geometrical independence by modelling the true shear flow function on the pseudo-shear flow data using the methods presented in Chapter 6.

Observations made in Chapter 3 of the pseudo-shear flow data were that sewage sludge exhibits pseudoplastic behaviour (the viscosity of the sludge decreases with increasing shear) and that it has a yield stress (an initial yield resistance to shearing). With reference to Chapter 2, there are many possible shear flow functions that would model these effects. However, the three parameter General Bingham model will now be used for the data analysis as it is well-established and widely used. It has limitations for very low and very high shear which are not expected to be violated by the data. None-the-less, to be prudent, the model shall be graphically appraised for the lowest and highest shear rate values of the data. The general Bingham model shall be compared with its special cases; collectively these are

$$\text{General Bingham:} \qquad \tau = \tau_y + K\dot{\gamma}^n, \tag{7.1}$$

$$\text{Power law:} \qquad \tau = K\dot{\gamma}^n, \tag{7.2}$$

$$\text{Bingham:} \qquad \tau = \tau_y + \eta\dot{\gamma}, \tag{7.3}$$

$$\text{Newtonian:} \qquad \tau = \mu\dot{\gamma}. \tag{7.4}$$

The power law parameters $K$ and $n$ are purely empirical since they are conventionally obtained by fitting a straight line through a log-log plot of the data (the curved part of a shear flow relationship depends on so many factors that a completely theoretical function has never been derived). In contrast, yield stress $\tau_y$, coefficient of rigidity $\eta$, and viscosity $\mu$ can be considered as actual properties of the fluid itself.

The first stage of the analysis involves fitting the general Bingham model to all of the sound tube flow data and examining the residuals. At this stage, the objectives are to establish the suitability of the general Bingham model for the tube flow data, so there would be no point in being selective about the type of tube flow data to analyse. It also follows that, if the general Bingham model fails the assumptions required of the least squares model, then there would be no point in using any of the special cases of the general Bingham model. This is because the residuals of any of the special cases would, at best, be as good as the general Bingham model. A full discussion of a least squares fit of the general Bingham model to a set of data points was given in Section 6.1.1. To ensure that the least squares method is employed correctly, residual analysis is carried out at each stage of the analysis. Now, the residuals are the difference between the observed and the fitted values, and for pseudo-shear flow data, are given as

$$e_j = (\tau_R)_j - (\hat{\tau}_R)_j, \qquad j = 1,\ldots,M, \tag{7.5}$$

where $(\tau_R)_j$ is the $j$th observation of the wall stress and the hat quantity denotes the $j$th prediction. The assumptions for the residuals of a least squares fit are that they follow a normal distribution about the independent axis, and have a constant variance[83].

Figures 7-1 and 7-2 show tube flow data of a sludge from Letchworth and its corresponding residual plot. Since only the laminar flow regime is of concern, Figure 7-1 includes the critical velocity prediction (ideally, the horizonal scale of the two plots should have been matched to make comparison of the two graphs easier). The residual plot (Figure 7-2) shows that there is no systematic increase, decrease or interdependence of the residuals, hence the residual assumptions are valid. Since there were several hundred such sludge samples to check, a computer program was written to access, fit and display the residual plots for any selected sludge sample. It was found that the other residual plots were equally sound, so on this evidence, the general Bingham function (7.1) is considered to be a sound model.

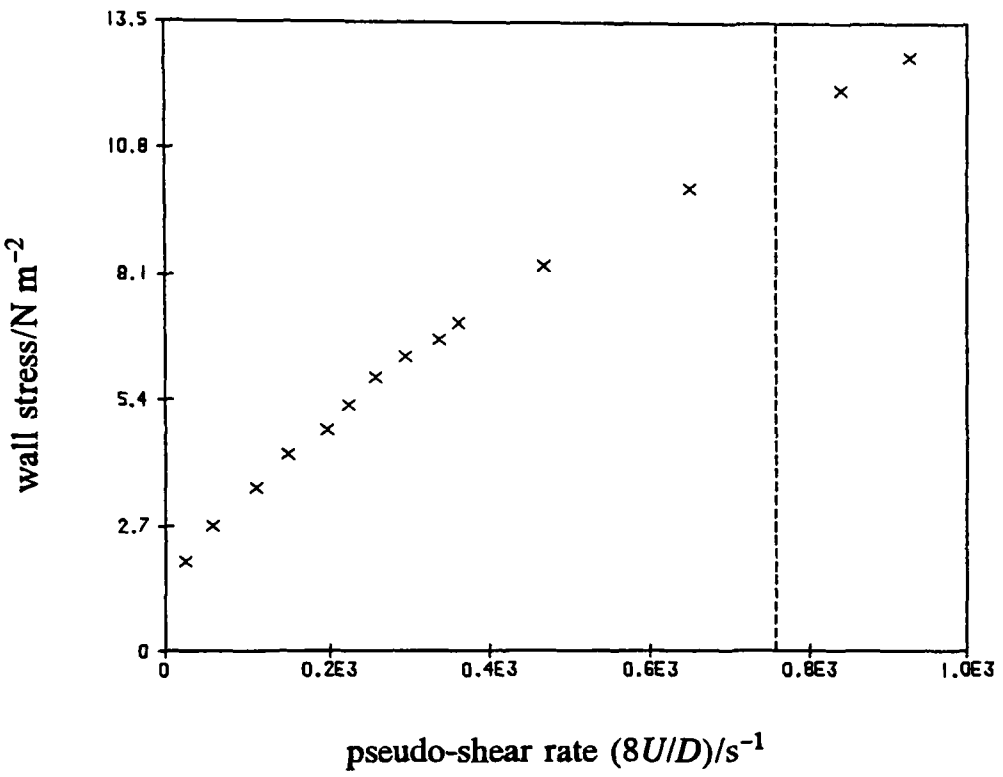


**Figure 7-1** Tube flow data of a digested sludge from Letchworth with a critical velocity prediction based on Ryan and Johnson's stability parameter.

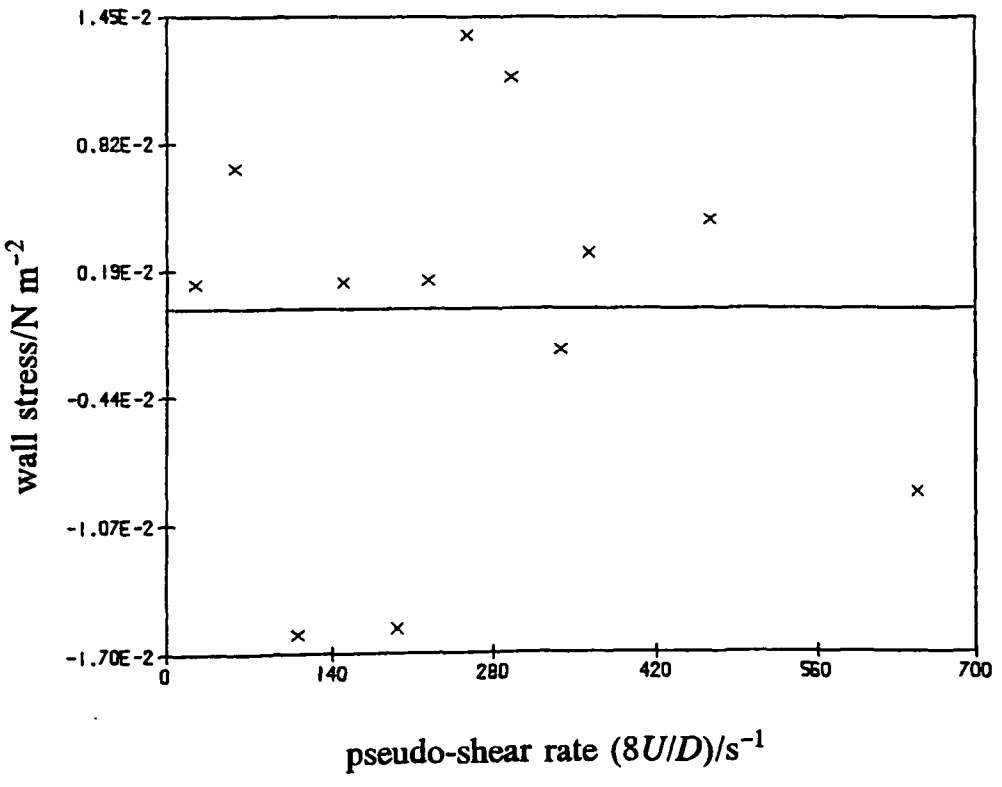


**Figure 7-2** The residual plot of the general Bingham model fitted to the data of Figure 7-1.

For any particular sample, the residual analysis is therefore a success and can be regarded as the residual analysis *within* each sample. However, the second stage of the analysis (the subject of the next chapter) is to introduce solids concentration into the model in order to obtain a generalised shear flow function for each sludge type. For this to be feasible, the

residual analysis must also be carried out *between* the sludge samples. For least squares estimates to be valid on a global scale, the standard errors between each general Bingham fit must be independent and have a constant spread. In fact, the constant value about the spread of standard errors can be regarded as a global standard error. A convenient way of examining this is to plot the standard error of each fit (defined by Equation (6.36)) against their respective wall stress means. Another computer program was written to perform this analysis where a particular sludge batch or sludge type could be selected. The standard errors of digested, activated and primary sludges for the tube flow data are shown on Figures 7-3, 7-4 and 7-5 respectively.

Without loss of generality, Figure 7-3 includes only a batch of Perry Oaks digested sludge as there were so many points on the complete plot that they fused together into a black mass. The three figures show that the standard errors are clearly non-constant, particularly digested sludge. The results indicate that the greater the range of data for a particular sludge, the greater the variation within the data. It may be generally true that higher wall stress values have larger residuals.

The problem of having a set of non-constant standard deviations is solved by applying a *variance stabilizing transformation*[82]. Since the relationship between $S$ and $\bar{\tau}_R$ is roughly linear, a log-log transformation of the data would be appropriate[82]. For the general Bingham model (7.1), this transformation is given as

$$\log_{10}(\tau - \tau_y) = \log_{10}K + n\log_{10}\dot{\gamma}. \tag{7.6}$$

This is not quite a pure log transformation of the general Bingham model since the yield stress has been moved to the left-hand side; the advantages of this simplification are self-evident. Note that this is, of course, still the general Bingham model, but rearranged in a different form.

As with the ordinary general Bingham model, the analysis now involves fitting the log general Bingham model to all of the sound tube flow data, and examine the residuals. A full discussion of a least squares fit of the log general Bingham model to a set of data points was given in Section 6.1.2. It is convenient to use the notation $q = \log_{10}(\tau - \tau_y)$ so that the error sum of squares for the $i$th sludge sample (Section 6.3) is given as

$$E_i = \sum_{j=1}^{M_i} (q_{ij} - \hat{q}_i)^2, \tag{7.7}$$

where the hat denotes a prediction. Least squares estimates of $\tau_y$, $K$ and $n$ are obtained from minimizing Equation (7.7) with respect to each of these parameters. Estimates of the parameters for this log model are expected to be similar to those of the ordinary version, but the residuals of each fit and the standard errors between these fits are expected to be generally different.

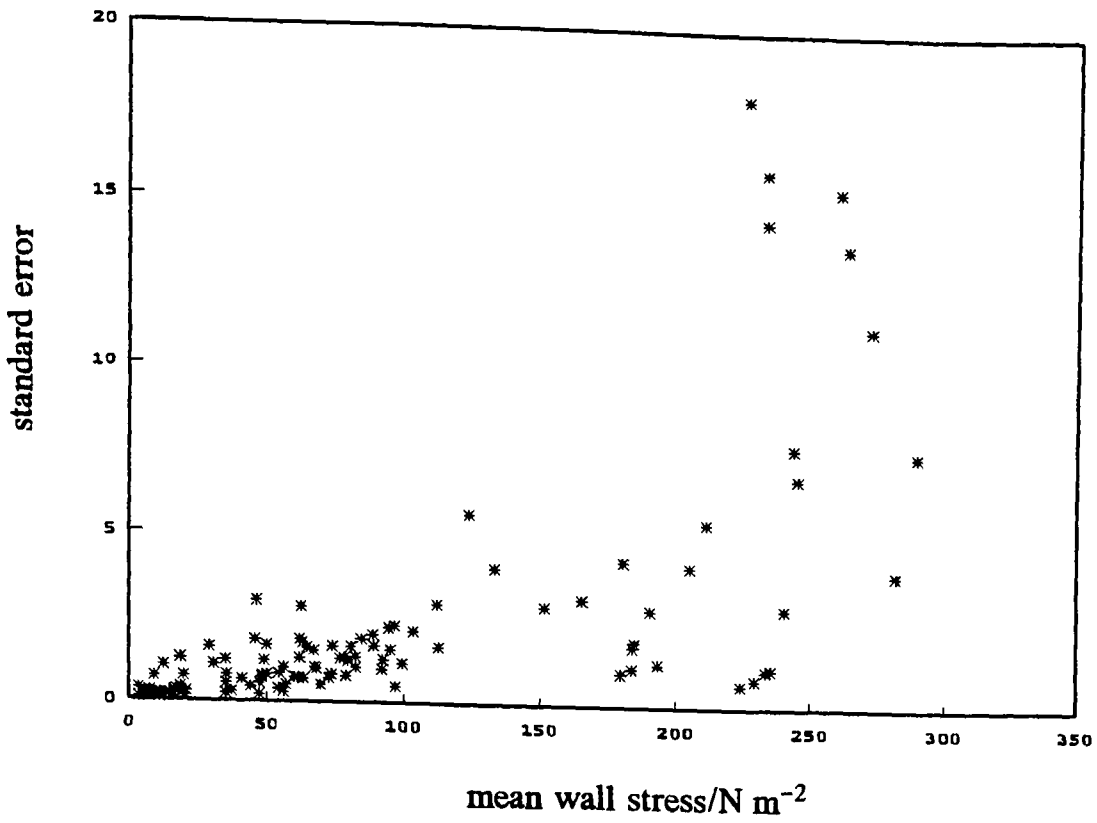


**Figure 7-3** The standard errors of the general Bingham model for the Perry Oaks digested sludges.

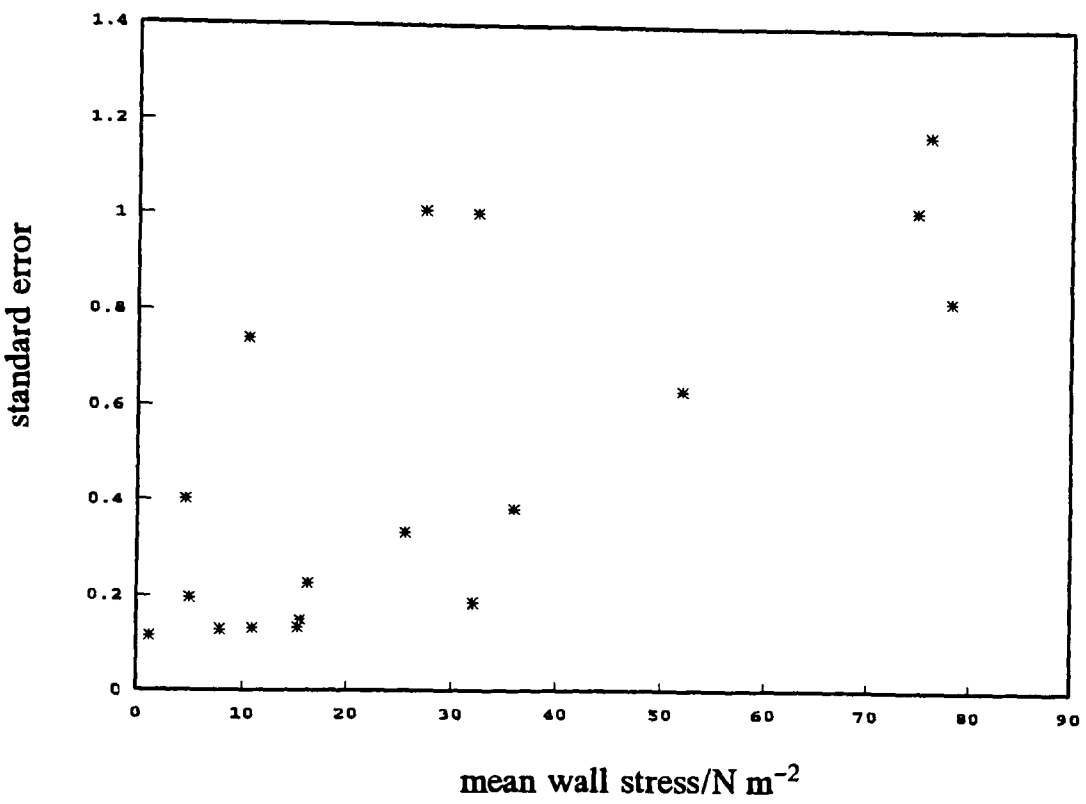


**Figure 7-4** The standard errors of the general Bingham model for the activated sludges.

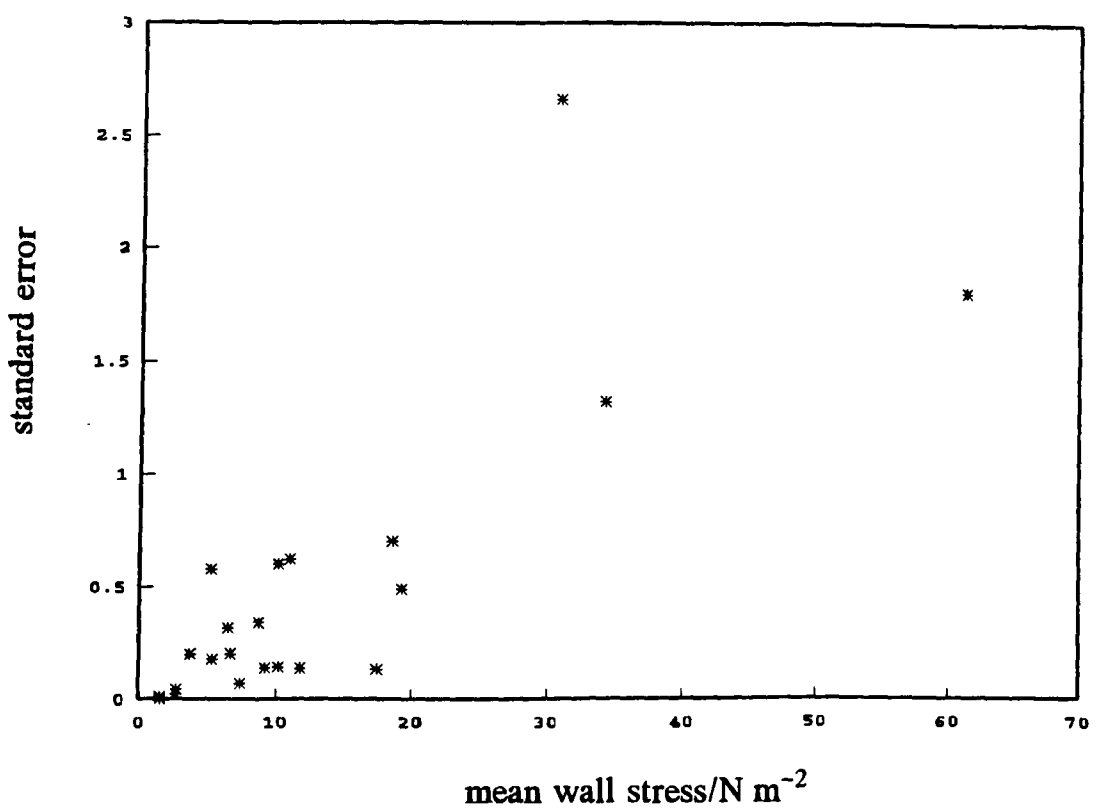


**Figure 7-5** The standard errors of the general Bingham model for the primary sludges.

As with the ordinary general Bingham model, residual analysis has to be repeated for the log general Bingham model for all of the sound tube flow data. Analogous to Equation (7.5), the residuals of the log model are redefined as

$$\epsilon_j = \log_{10}[(\tau_R)_j - \tau_y] - \log_{10}[(\hat{\tau}_R)_j - \tau_y], \qquad j = 1,...,M. \tag{7.8}$$

The least-squares assumptions for the residuals must apply; they must follow a normal distribution about the independent axis and have a constant variance. The computer program that was used to perform residual analysis on the ordinary model was modified to also apply to the log model. Figure 7-6 now shows the residuals of the log fit to the data of Figure 7-1, and since the plot shows that there is no systematic increase, decrease or interdependence of the residuals, on this evidence, the log general Bingham model (7.6) is sound.

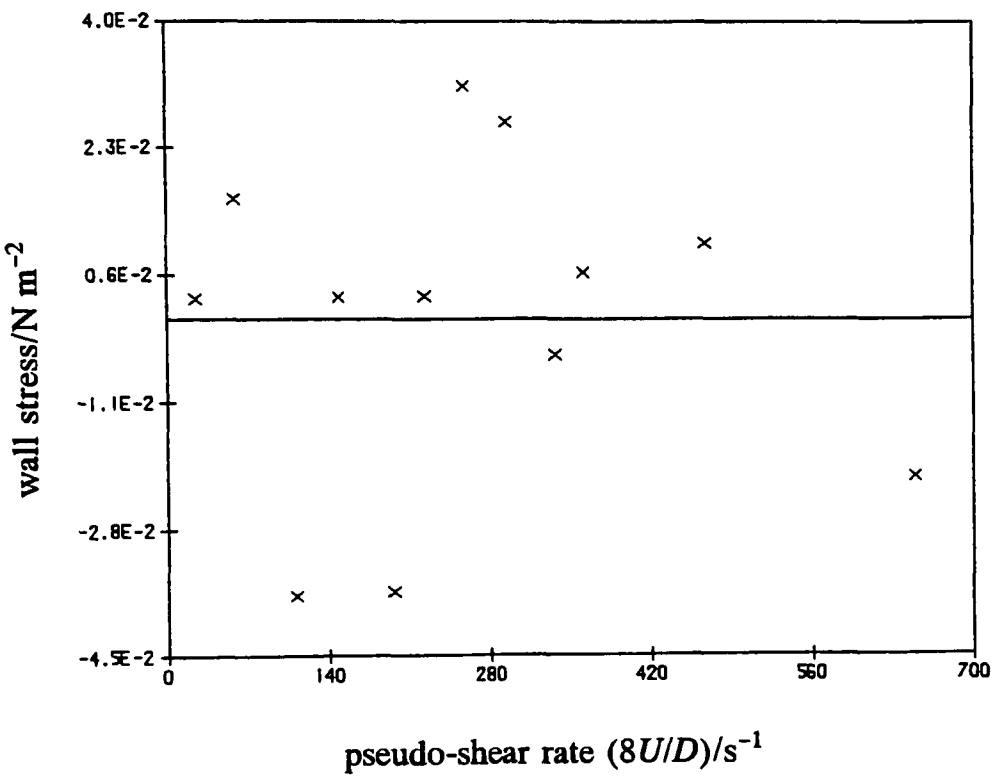


**Figure 7-6** A residual plot of the log general Bingham model fitted to the data of Figure 7-1.

Residual analysis must also include the detection and removal of outliers; Figure 7-7—a tube flow test of a Perry Oaks digested sludge—is such an example. Unless there was either a clear typing error in the laboratory report, or a mistake on our behalf entering the data, it is not possible to determine the reason for the outlier. Outliers may represent a genuine, if not haphazard property of the sludge. Since sewage sludge is lumpy and ill-behaved, some outliers in the data are to be expected. For Figure 7-7, the tube's inside diameter is only 12.52 mm—rather narrow for carrying out viscometric measurements. Anyway, such values are either erroneous or unquantifiable and have to be removed.

To identify outliers, the *externally studentised residual test*[84] is used. This involves *studentising* the residuals by dividing each residual with its respective standard error. This yields residuals that are expectedly from the $t$ (or student) distribution. The residuals are, however, *externally* studentised by dividing each $j$ th residual with the $j$ th value missing from its respective standard error. A residual is thus assumed to be an outlier unless otherwise

tested. For a set of $(x_j, y_j), j = 1,...,M$ data points, the $t$ statistic of the $j$th point is therefore

$$t_j = \frac{y_j - \hat{y}_j}{S_{(j)}\sqrt{1 - \lambda_j}},$$

where the hat denotes a prediction. Conveniently, $S_{(j)}$ is the standard error of the model with the $j$th value missing, and when multiplied with the right-hand term of the denominator, gives the standard error of the individual residual itself. The term

$$\lambda_j = \frac{1}{M} + (x_j - \bar{x})^2 \Big/ \sum_{j=1}^{M} (x_j - \bar{x})^2,$$

is known as the leverage of the $j$th value.

The residual analysis program was extended to identify the outliers automatically, and give user-control over their fate. The program—which uses a $t$ distribution to give 95% confidence on any outlier—detected several possible outliers. Figure 7-8 shows the residual plot for the data of Figure 7-7, and for the least squares assumptions to be valid, the residuals should be normally distributed and spread evenly about the shear rate axis. For this case, the absolute value of the $t$ statistic is 7.11, and the critical value of the $t$ distribution is 1.89; the outlier is so extreme that the other residuals arc over the horizontal axis. Having removed the outlier, the updated residual plot is shown in Figure 7-10 where the residuals are now evenly spread around the horizonal axis.

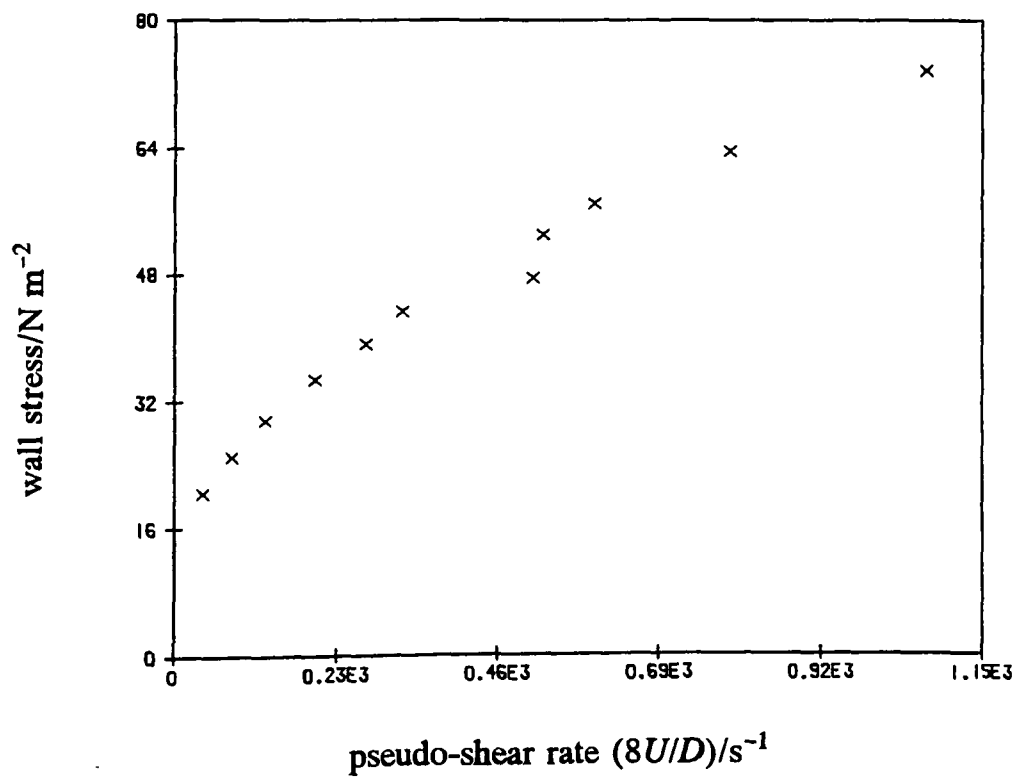


**Figure 7-7** Tube flow data of a digested sludge from Perry Oaks. One of the values is a suspected outlier.

Figure 7-9 shows the accuracy of the fit of the predicted shear flow model for the data of Figure 7-7, and with reference to Equation (7.6), the gradient of the curve is $n$ and the intercept of the curve is $\log_{10} K$. However, it should be noted that the data of Figure 7-9 are not the raw data, but a *prediction* of the log shear flow data. In other words the independent variable has been given a log pipe-to-shear transformation to make the data linear. Whereas

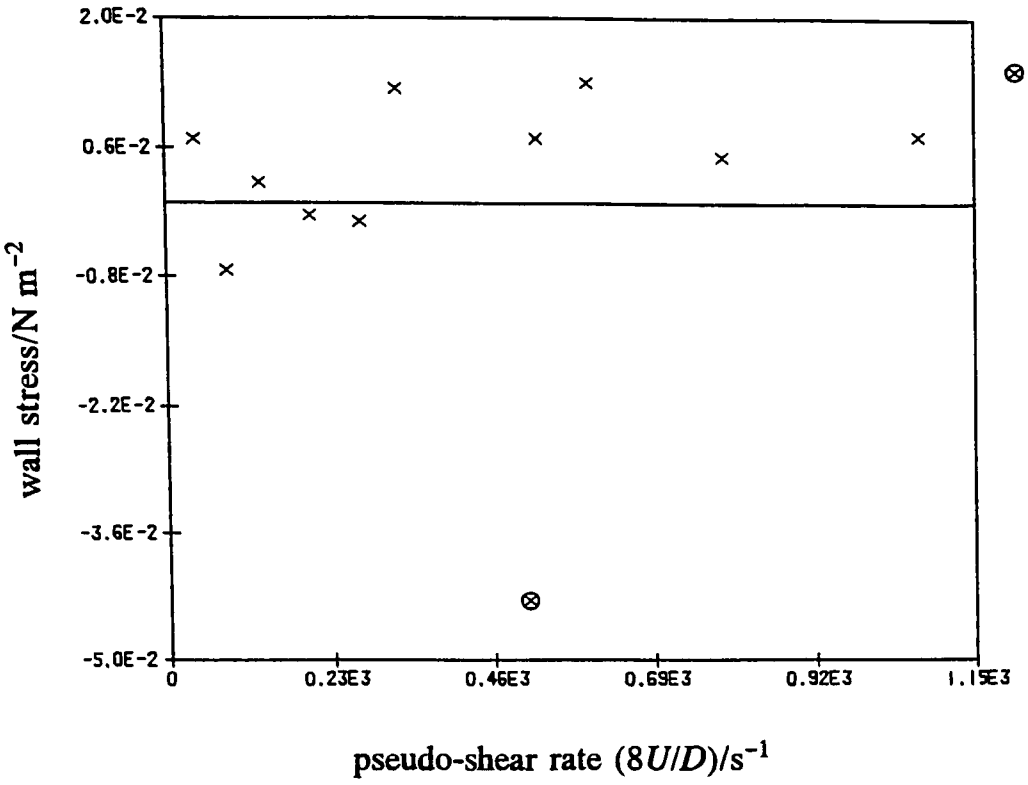


**Figure 7-8** The residual plot of the log general Bingham model fitted to the data of Figure 7-7. The plot emphasises the outlier.

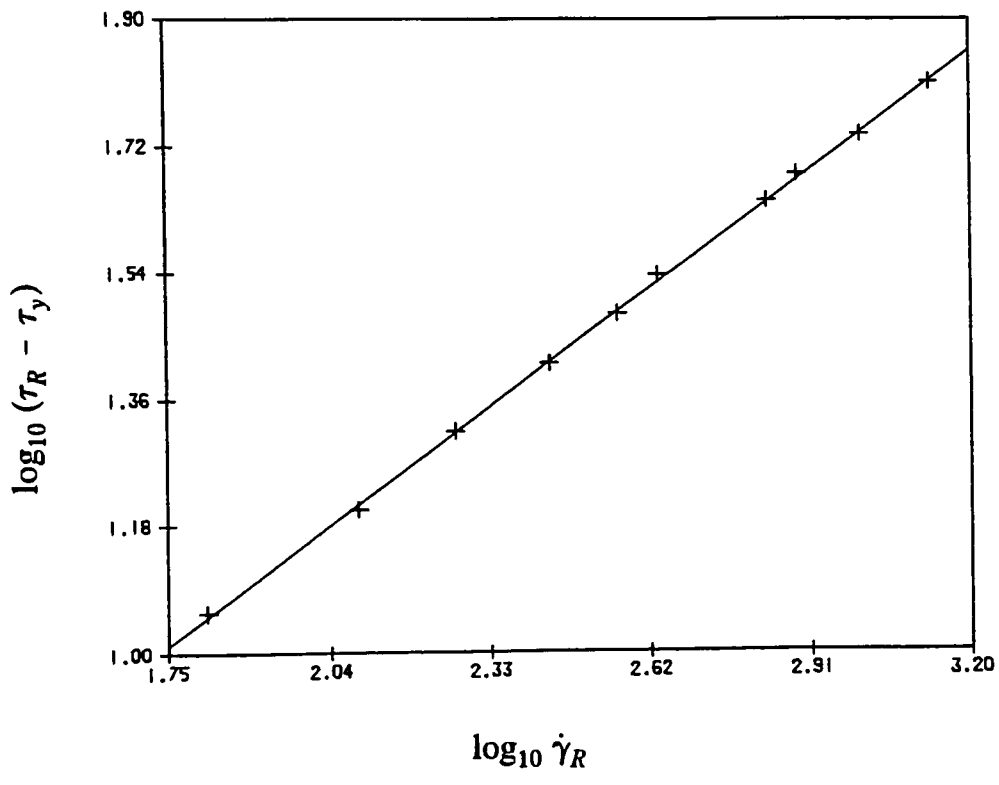


**Figure 7-9** The log general Bingham model fitted to the data of Figure 7-7, but with the outlier removed.

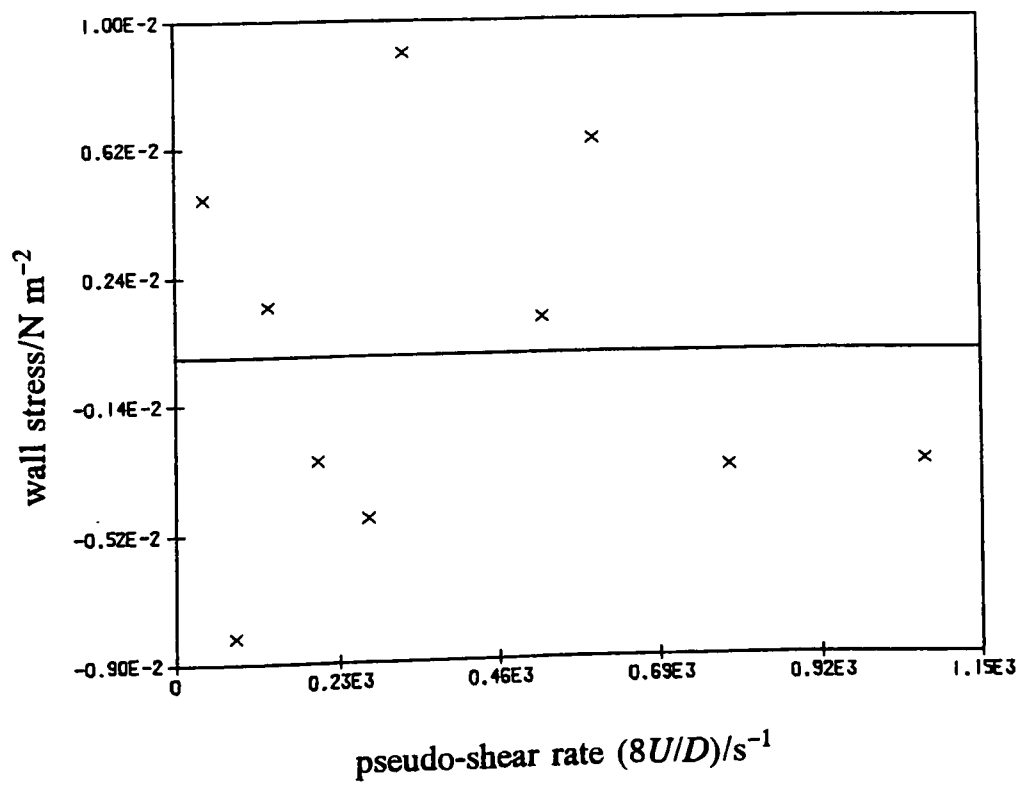


**Figure 7-10** The residual plot corresponding to Figure 7-9. With the removal of the outlier, the residuals are now much more evenly distributed than those of Figure 7-8.

Figure 7-10 shows the actual distribution of the residuals, Figure 7-9 gives a clearer indication of the magnitude of the residuals and the accuracy of the fit; in this case, it is a good fit. All of the tube flow data have been checked and edited for residuals in this way, and the residuals *within* each sludge sample were found to be well-behaved for the log general Bingham model (7.6).

The residual analysis *between* each sludge sample must be repeated again for the log general Bingham model, so the computer program for the ordinary fit was extended to deal with the log fit. The standard error versus the logarithm of the mean wall stress for the tube flow data of a batch of digested, activated, and primary sludges are shown by Figures 7-11, 7-12 and 7-13 respectively; these figures are the transformed versions of Figures 7-3, 7-4 and 7-5 respectively. For the model to be valid, the standard errors must be evenly spread throughout the independent variable. There no evidence of a systematic dependence on the mean wall stress for both the digested and primary sludges (Figures 7-11 and 7-13) (though for the primary case, the conclusion is based on little data). For activated sludge (Figure 7-12) there is a little negative correlation between the variables, but since the least-squares method is known to be robust against minor residual violations, the log general Bingham model is a good model for the data. Global standard errors can be estimated visually from Figures 7-11 to 7-13 to be about 0.01 for digested sludge, and about 0.02 for activated and primary sludges.

The next stage of the analysis involves fitting log versions of the general Bingham model and its special cases, the power law, the Bingham and the Newtonian models to the tube flow data. It becomes apparent that, if any of the special cases of the log general Bingham model fit the data well, then the log general Bingham model must also. This is equivalent to saying that, if a one or two parameter special case model fits the data well, then so must the full three parameter model. A special case model would be much preferable to the general Bingham model as there are less parameters for both fitting to the data and for simplifying a final application. To judge whether or not one model is more suitable than another, visual comparison is considered to be too subjective and tedious in light of all of the data, so the $F$ test (or variance ratio test) can be employed. For the $F$ test, an $F$ statistic is calculated as the ratio between two variances and compared with the $F$ distribution.

To systematically compare the log general Bingham model (7.6) and its special cases, a regression technique known as the *backward elimination method*[83] is used. For this method, all parameters are fitted, then each parameter is tested in turn, and if found to be insignificant, dropped from the model. This results in a selection of the model with the least number of parameters necessary. For our problem in full: the general Bingham model is compared with the power law and Bingham models; if either or both of these two-parameter models are tested as significant, then the general Bingham model is discarded, and the two-parameter model is tested against the Newtonian model.

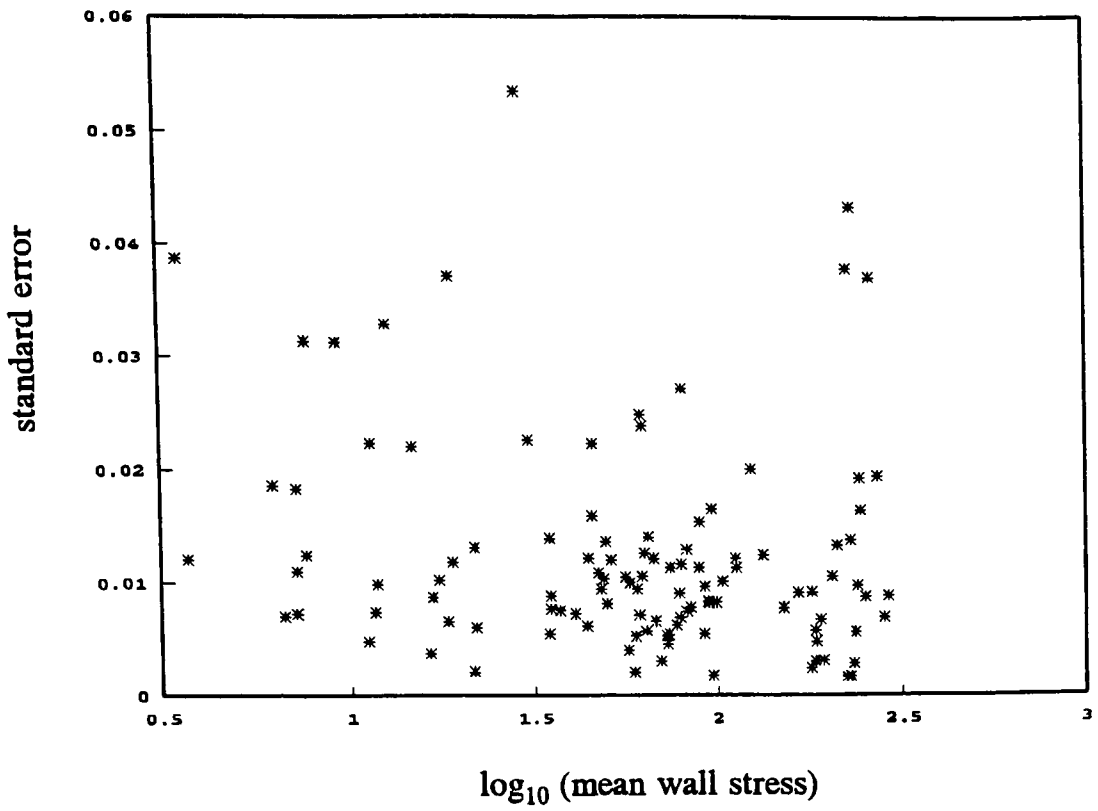


**Figure 7-11** The standard errors of the log general Bingham model for the Perry Oaks digested sludges.

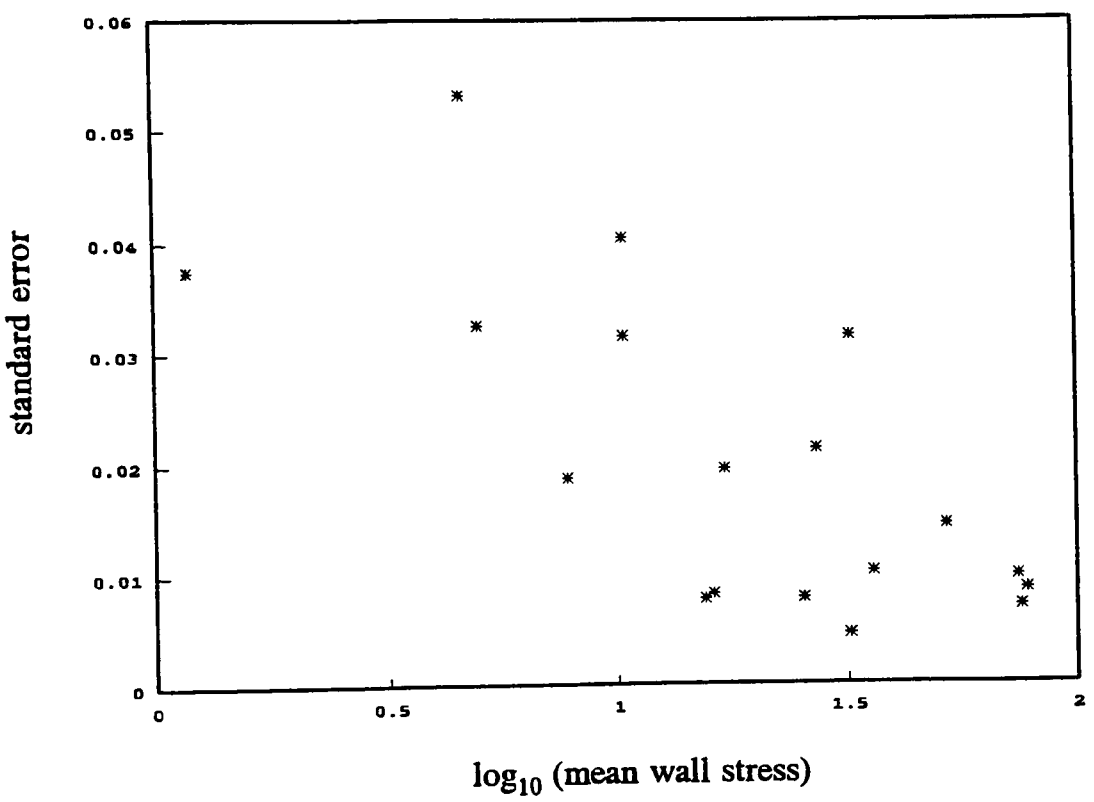


**Figure 7-12** The standard errors of the log general Bingham model for the activated sludges.

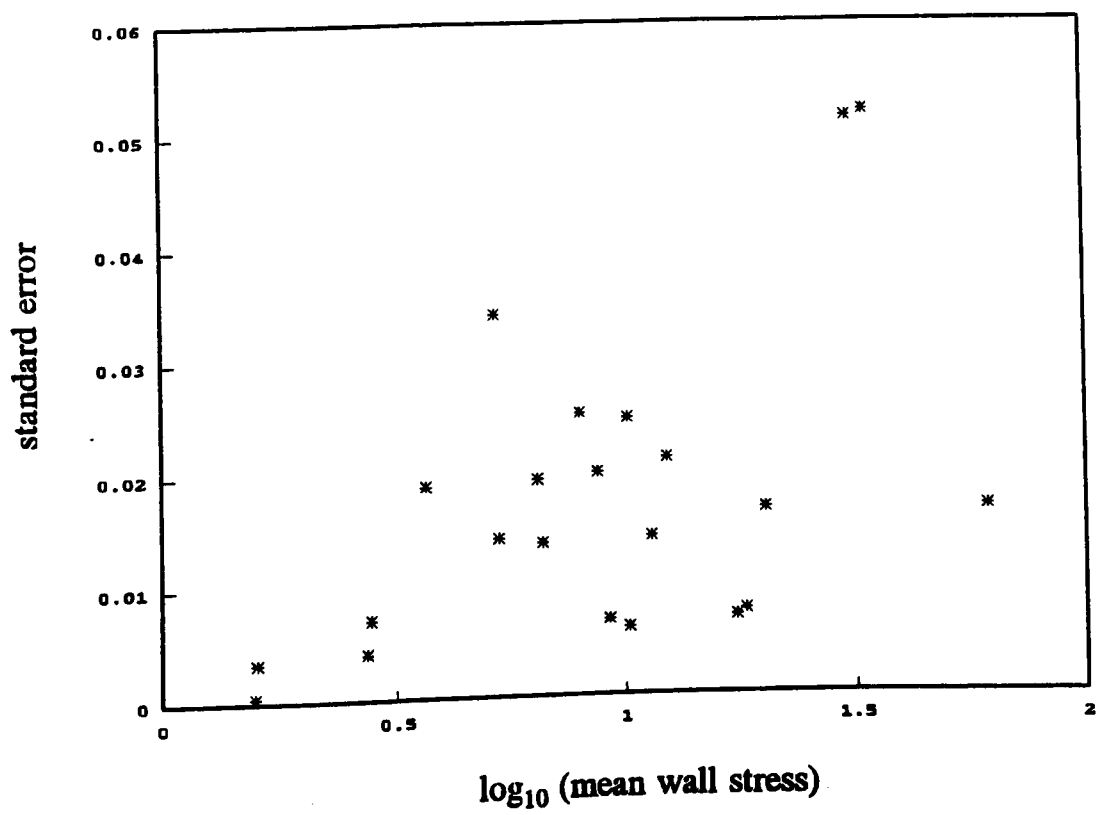


**Figure 7-13** The standard errors of the log general Bingham model for the primary sludges.

A computer program was written to automatically perform the backward elimination method on all of the tube flow data. Rather than present the results in full, Table 7-1 gives the number of times each model was selected for each sludge type.

**Table 7-1** The results of the backward elimination method applied to the tube flow data. The table gives the number of times each model was selected for each sludge type.

| Sludge type | Gen. Bingham | Power | Bingham | Newtonian |
|---|---|---|---|---|
| Digest | 84 | 58 | 3 | 2 |
| Activated | 16 | 2 | 0 | 0 |
| Primary | 4 | 17 | 1 | 0 |

From Table 7-1, the most suitable model for digested sludge is either the general Bingham model or power law model; for activated sludge it is the general Bingham model, and for primary sludge it is almost certainly the power law model. There are only really two models to consider: the general Bingham model and the power law model. Table 7-1 gives the number of times each model is significantly different, but does nothing to quantify the differences. To do this, the general Bingham standard error plots of Figures 7-11 to 7-13 have been extended to include the power law fit; Figures 7-14 to 7-16 show the updated versions. For the digested sludge case, the supremacy of the general Bingham model over the power law model can clearly be seen. For the activated sludge case, the improvement is not as clear cut; in general terms, however, the general Bingham model should be conservatively chosen in preference to the power law model. For the primary sludge, there is little difference between the two models, so there is no reason to choose the general Bingham model in preference to the power law model. Notice that for the primary sludge, the power law model often has smaller standard errors than the general Bingham model, which is counter-intuitive considering that it is a simplified version of the general Bingham model. However, the power law model has one less parameter and therefore one more degree of freedom than the general Bingham model (see Equation (6.36)), and this accounts for the difference. Table 7-2 summarises the choice of model for each sludge type.

**Table 7-2** Choice of model for each sludge type

| Sludge type | Selected model |
|---|---|
| Digested | General Bingham |
| Activated | General Bingham |
| Primary | Power law |

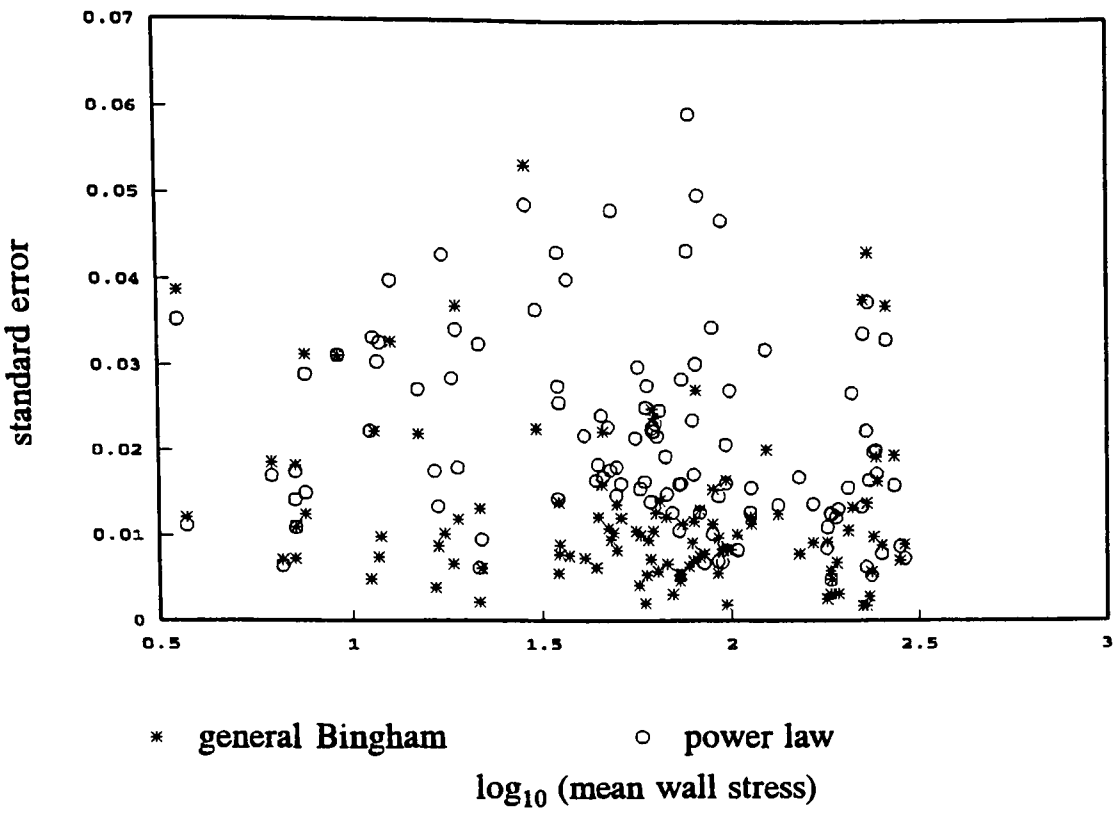


**Figure 7-14** The standard errors of the log general Bingham and log power law models for the Perry Oaks digested sludges.

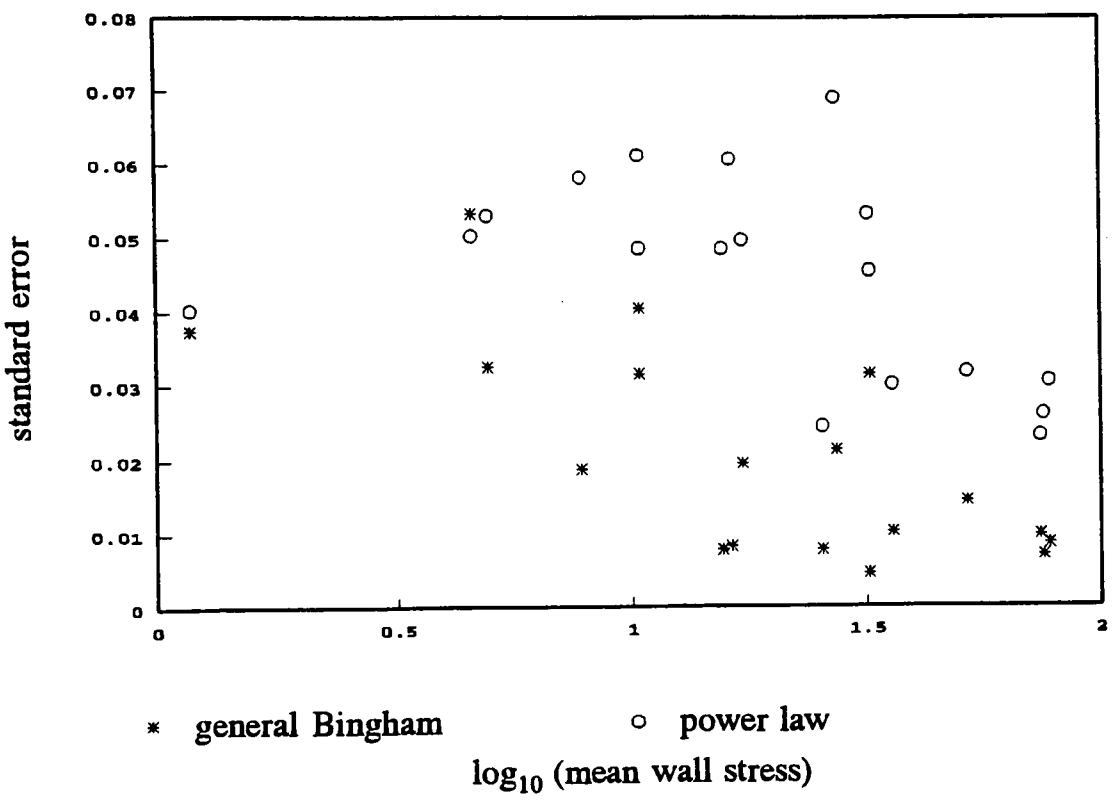


**Figure 7-15** The standard errors of the log general Bingham and log power law models for the activated sludges.

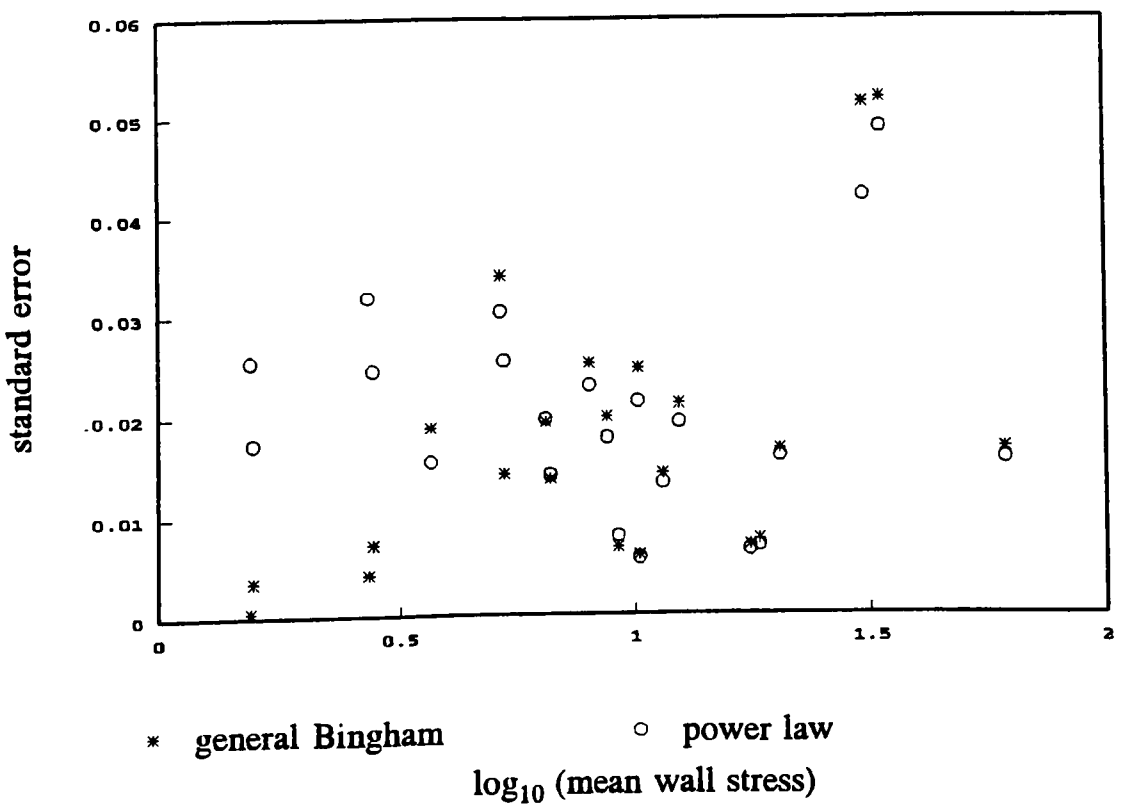


**Figure 7-16** The standard errors of the log general Bingham and log power law models for the primary sludges.

Establishing the rate of shear ranges for each of the three sludge models is not easy as the data are given in terms of a pseudo-shear rate rather than the actual shear rate. Therefore the models of Table 7-2 are used to estimate the ranges for each of the sludge types using all of the relevant laminar flow data, and the results are presented in Table 7-3. The ranges have been estimated from laminar flow data only, and will not therefore be applicable to non-laminar flow situations. Chapter 2 discussed the limitations of the general Bingham and power law models for both low and high and shears and, so far, the residual analysis for these models has proved wholly successful for the data. For completeness however, some of the fitted models at the lower and higher ends of the ranges shall be examined.

**Table 7-3** Rate of shear ranges for the models.

| Sludge | Shear rate range, $\dot{\gamma}_{min}$ /s$^{-1}$ - $\dot{\gamma}_{max}$ /s$^{-1}$ |
|---|---|
| Digested | 1.9 - 2 400 |
| Activated | 6.3 - 1 600 |
| Primary | 7.8 - 1 100 |

For digested sludge, Figure 7-17 shows the laminar flow model fitted to data of the low predicted shear rate range 3.6 $s^{-1}$ - 1 102 $s^{-1}$, and Figure 7-18 shows a similar thing for the high predicted shear rate range 141 $s^{-1}$ - 2 418 $s^{-1}$. For both cases, the fits are remarkably good, and the residuals are evenly spread throughout the pseudo-shear rate ranges. For activated sludge, Figure 7-19 covers the predicted shear rate range 6.34 $s^{-1}$ - 1 207 $s^{-1}$ which is much of the complete range given in Table 7-3. Again the fit is impressive, though notice that the residuals do not seem to be spread constantly throughout the range as they are positive at the ends and negative in the middle. The limitations of the general Bingham model were discussed in Section 2.1, and it appears that they have been breached in this case. However, the fit is still excellent as the standard error is only $8.2 \times 10^{-3}$, and clearly lower than the average shown in Figure 7-12. It appears that the sludge sample was particularly well-behaved or maybe the measurements were more accurate. A more elaborate model such as the Meter model (2.13) may have been slightly better in this case, but when considering the data collectively, the general Bingham model is perfectly suitable. For primary sludge, Figure 7-20 covers the predicted shear rate range 77.4 $s^{-1}$ - 1 086 $s^{-1}$, and shows an excellent fit to many points.

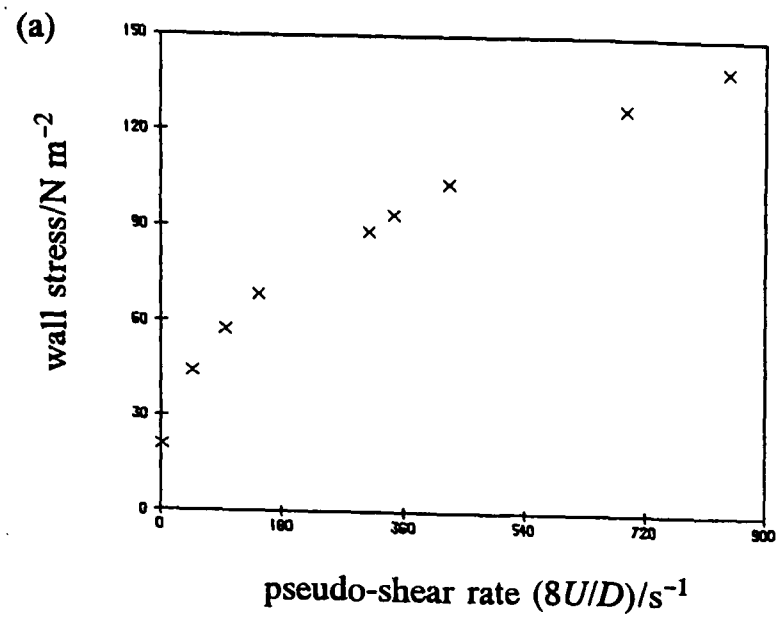


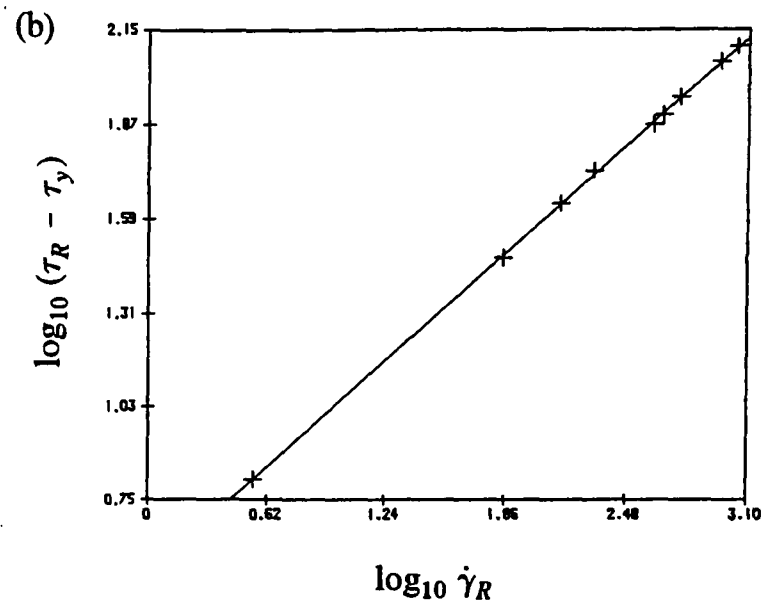


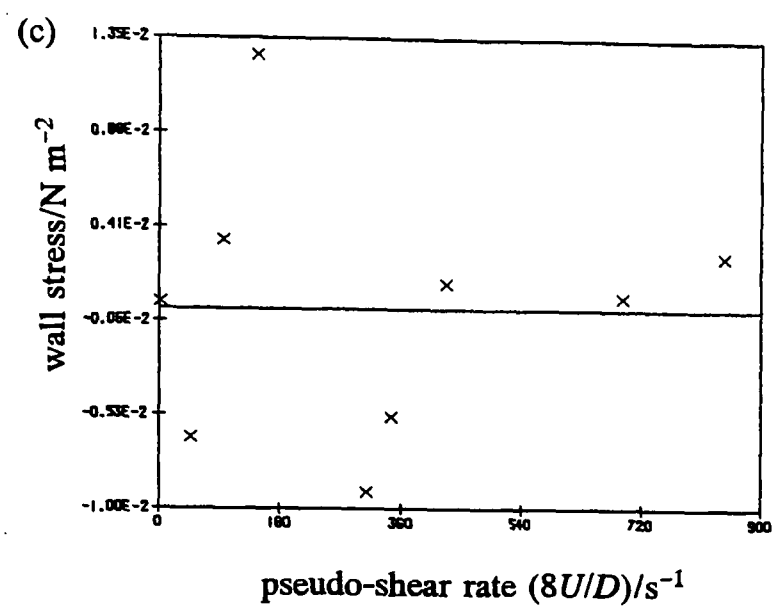


**Figure 7-17** Digested sludge flow data of a low shear rate range: (a) the data, (b) the fit, (c) the residuals.

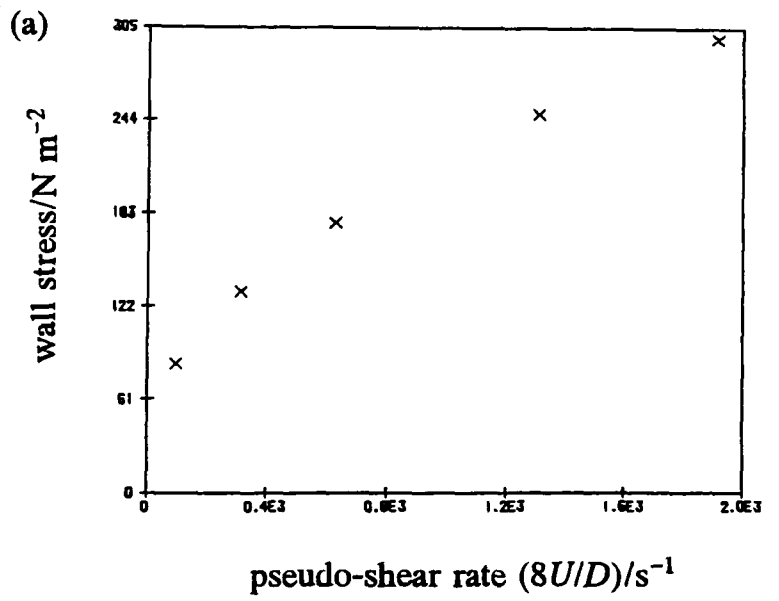


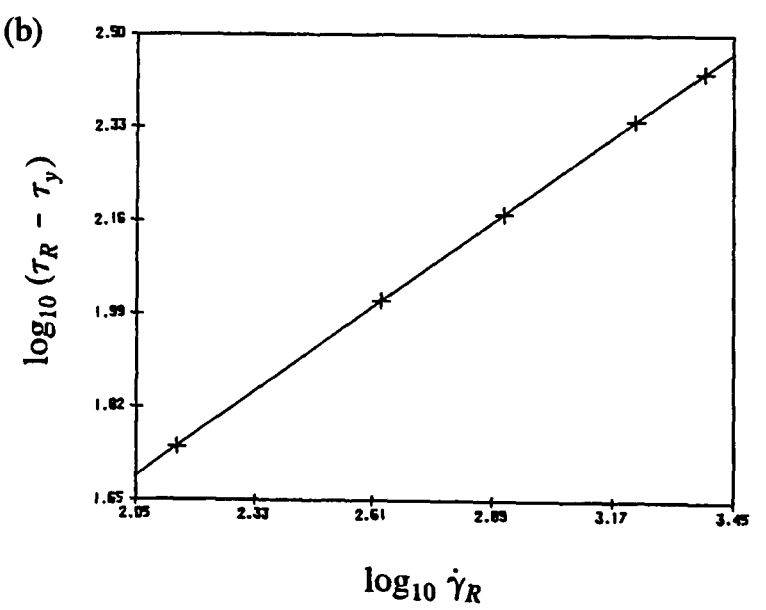


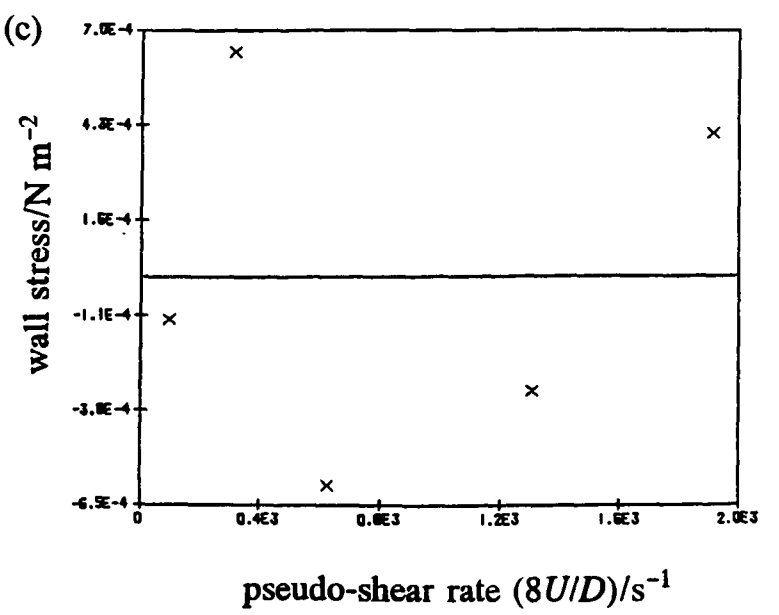


**Figure 7-18** Digested sludge flow data of a high shear rate range: (a) the data, (b) the fit, (c) the residuals.

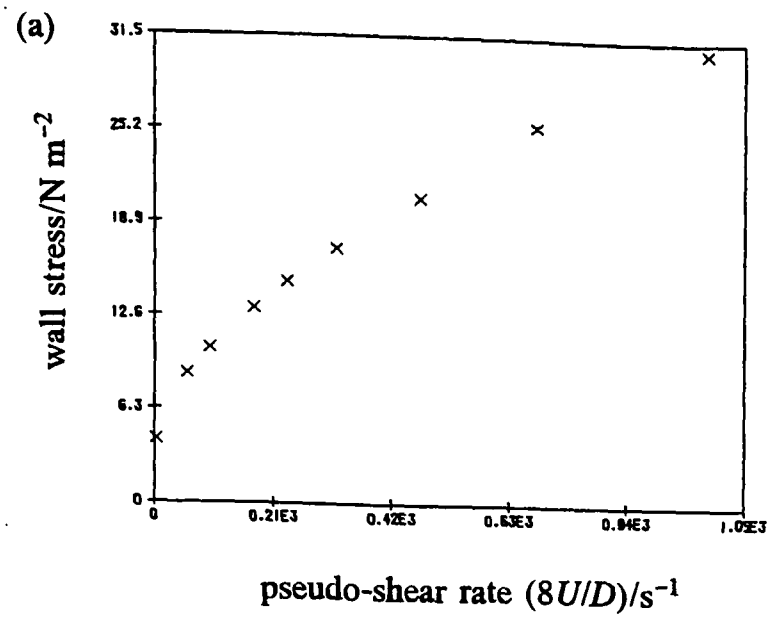


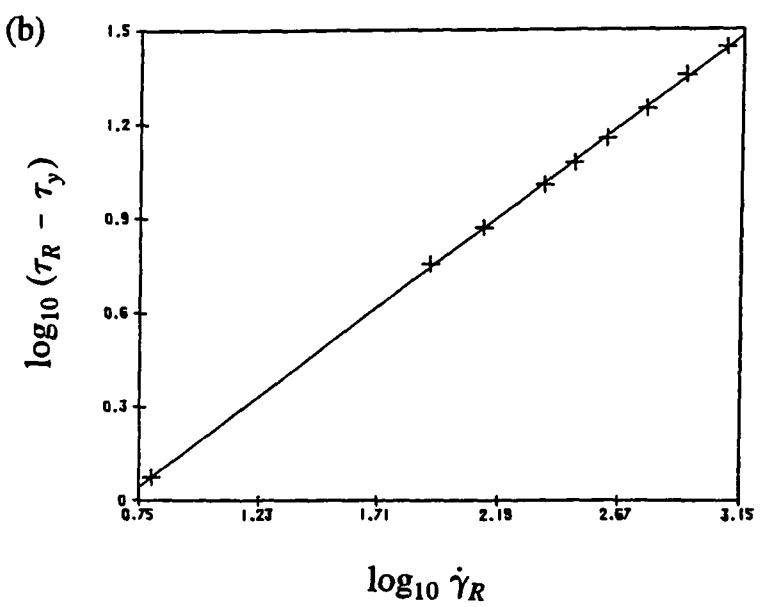


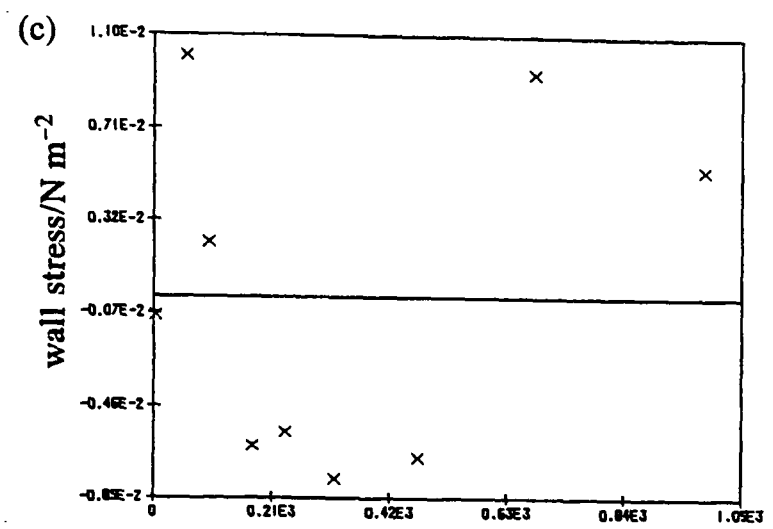


**Figures 7-19** Activated sludge flow data covering most of the shear rate: (a) the data, (b) the fit, (c) the residuals.

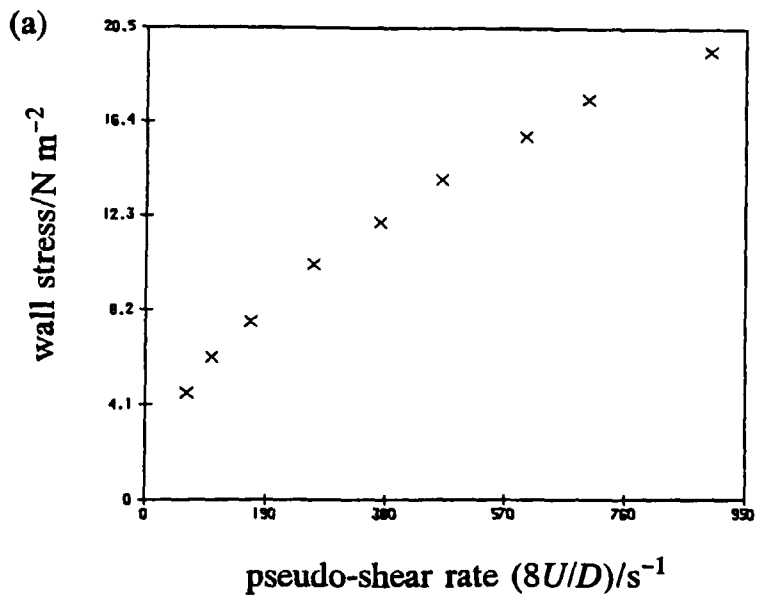


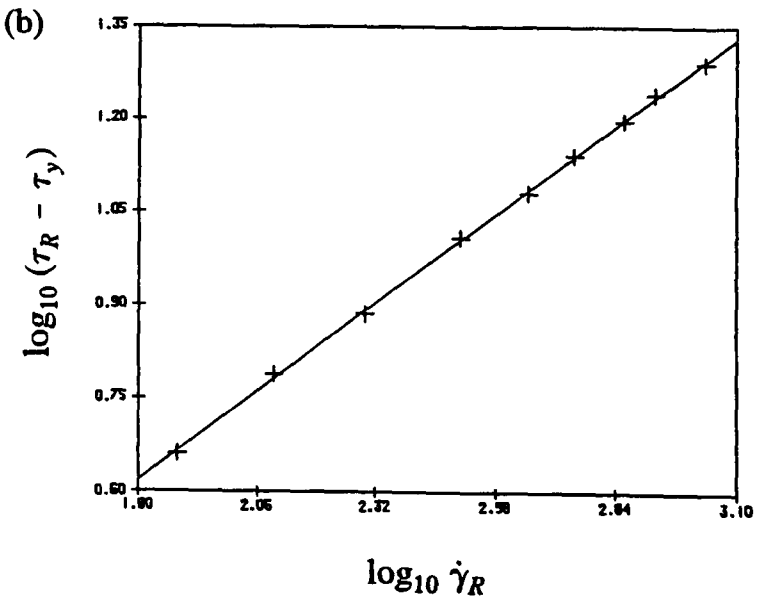


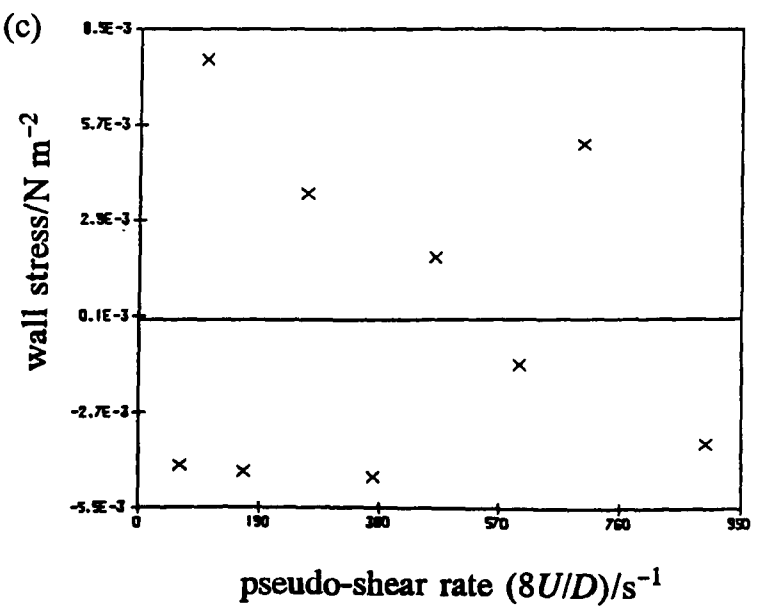


**Figures 7-20** Primary sludge flow data of a higher shear rate range: (a) the data, (b) the fit, (c) the residuals.

## 7.2 Critical Flow Assessment

Critical flow is the upper bound of laminar flow; the point at which laminar flow becomes unstable. Sound critical flow predictions are clearly important for identifying the upper bound of the laminar flow regime. They are also necessary for estimating the laminar shear flow function parameters to ensure that only laminar flow data are used for parameter estimation. However, the converse is also true: laminar flow parameter estimates are required for making critical flow predictions. In other words, laminar and critical flow predictions are interdependent; the scheme for predicting laminar flow parameters iterates over the critical flow prediction (such a procedure was used for the critical flow prediction of Figure 7-1). In this section, laminar and critical flow scale-up predictions are assessed qualitatively for sludge flow data.

In Section 4.3, the Ryan and Johnson stability parameter [54] was cited as being suitable for critical flow modelling of any time-independent, viscous fluid. Since the general Bingham model has been chosen for the data analysis, a simple model such as the Reynolds number proposed by Slatter [61] could be used for critical flow. However, in Section 5.2, a numerical algorithm was presented to solve the stability equation for a straight pipe geometry with any arbitrary shear flow function. The tools are therefore at our disposal for a general Bingham version of Ryan and Johnson with analysis that could easily be repeated with another shear flow function. Another advantage of the Ryan and Johnson stability parameter is that it is well established, and has been tested on a wide variety of data (see introduction to Section 4.3). In contrast, Slatter derived his model with some brave assumptions that has proved successful for his data (mainly Kaolin), but has not been widely tested on other data.

The main problem with critical flow analysis is that the critical flow point is hard to ascertain for high Hedström numbers [26]. In fact, Figure 3-2 showed that repeated measurements of the same sludge sample can produce both smooth and sharp transitions from laminar to turbulent flow. For most of the data, the transitions are smooth, so this makes identification of the critical point difficult. The best approach is to turn the problem on its head and examine each critical flow prediction for a sludge sample. This can be done graphically, and would be more difficult for a smoother transition, but at least a qualitative assessment of the prediction is possible. The approach has the disadvantage of being very tedious for the extensive data, so only Ryan and Johnson's method will be assessed in this way. However, if this method fails, then other methods must be considered. It should be appreciated that there are very few methods available for critical flow modelling of complex fluids, so the choice is limited anyway.

Figure 7-21 shows tube flow data of a digested sludge from Perry Oaks taken before the pump-pipe trials. Included on this figure is the critical flow prediction which looks sound

as it marks a change in the trend of the data. A further qualitative assessment of critical flow predictions was carried out on much of the other tube flow data, and as a result of this initial investigation, were found to be good for activated and digested sludge, but poor for primary sludge. The main problem in assessing the validity of a critical flow prediction in this way is that much of the tube flow data—like that of Figure 7-21—are laminar and, in this respect, the pipe flow data are regarded to be more appropriate as they cover the laminar and fully-developed turbulent flow regimes.

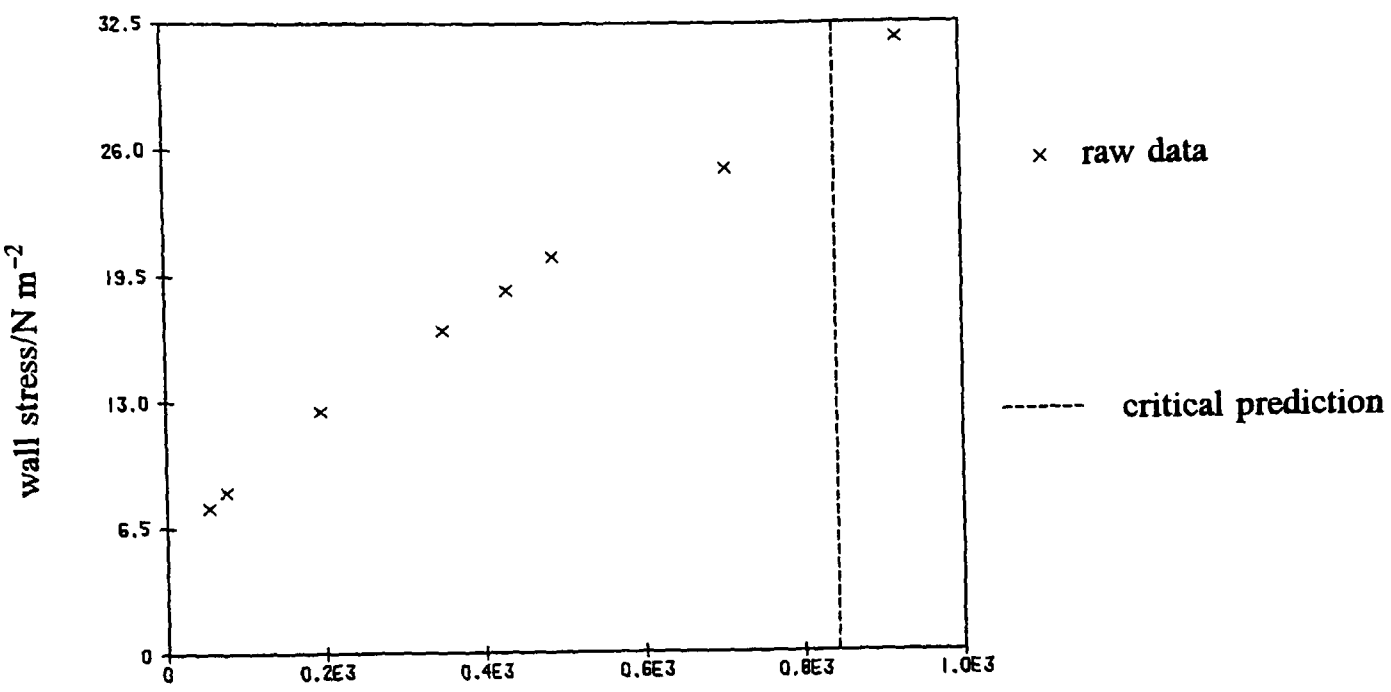


**Figure 7-21** Tube flow data of a digested sludge from Perry Oaks including the critical (upper bound laminar) flow prediction.

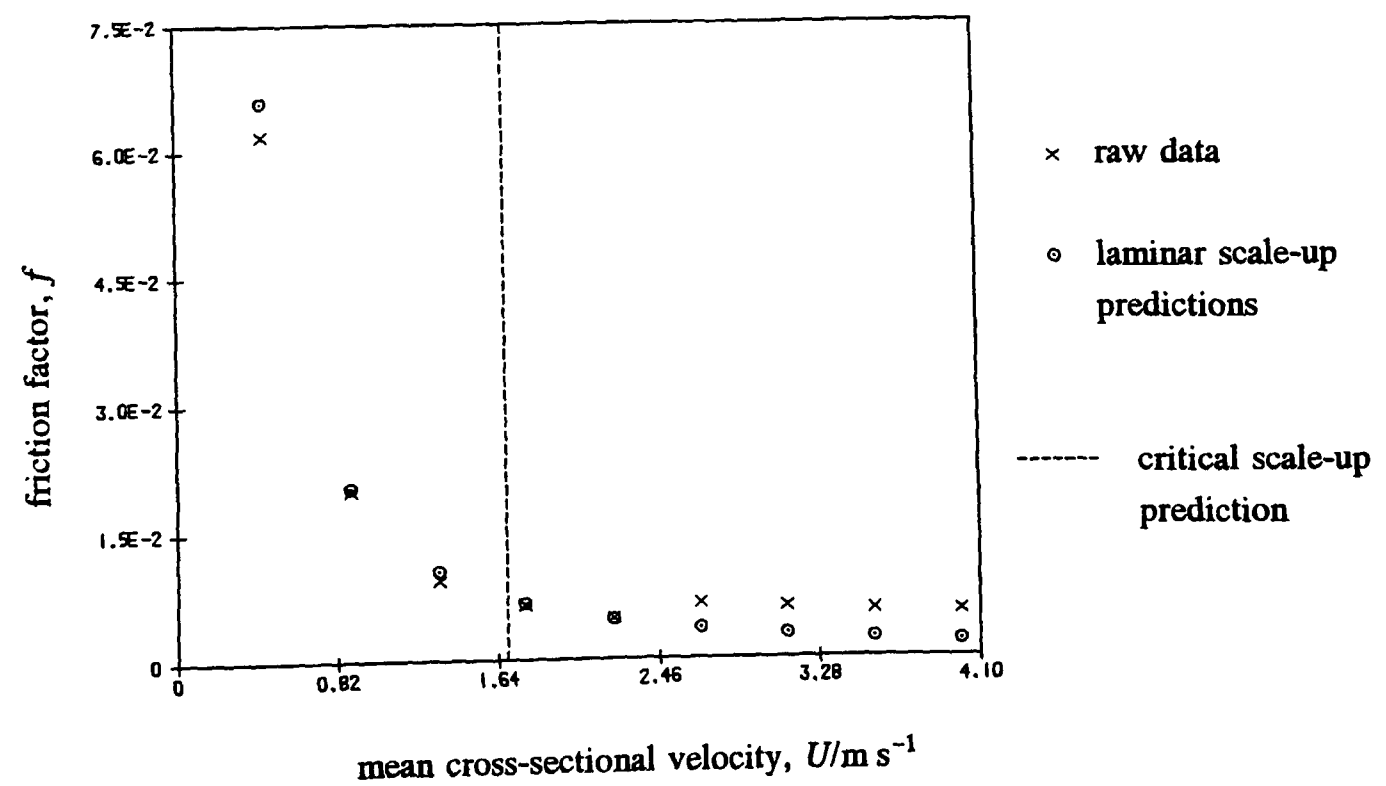


**Figure 7-22** Pipe flow data of the digested sludge sample of Figure 7-21 with laminar and critical flow scale-up predictions.

Figure 7-22 shows the corresponding pipe flow data for the sludge of Figure 7-21. Assessment of the critical flow prediction is much easier since the full laminar and turbulent flow ranges are included. However, the pipe diameter is larger than that of the tube, so the critical flow prediction has been recalculated using the pipe geometry, which is no problem except that now the critical flow prediction is scaled up rather than direct. The figure shows that there are barely enough laminar flow data for parameter estimation and, as this difficulty applies to much of the other pipe flow data, much of the assessment of laminar and critical flow predictions must be carried out using scale-up predictions rather than direct predictions.

Referring again to Figure 7-22, the true critical velocity lies at the intersection of the laminar and fully-developed turbulent flow curves; these curves are defined by the first three, and the last four points respectively. They intersect undiscernibly close to the predicted critical velocity, thus verifying a successful critical velocity prediction. Laminar flow scale-up predictions have been included on the figure showing that the first prediction is an under-prediction and, interestingly, the predictions also appear to be valid for the transitional flow values. Nothing conclusive was drawn from the latter observation since (as noted in Chapter 3) the behaviour of the transitional region can vary from one sludge to another.

Figure 7-23 shows the pipe flow data of an activated sludge from Maple Lodge which includes a critical velocity prediction again made from corresponding tube flow data. A feature of these data is that the transition from laminar to turbulent flow is very clearly defined and, applying the same qualitative methods discussed above, shows the critical flow prediction to be valid. For the laminar flow predictions, it is interesting to note that much the same applies as for the previous figure: an under-prediction for the first value, and an agreement with the transitional flow values.

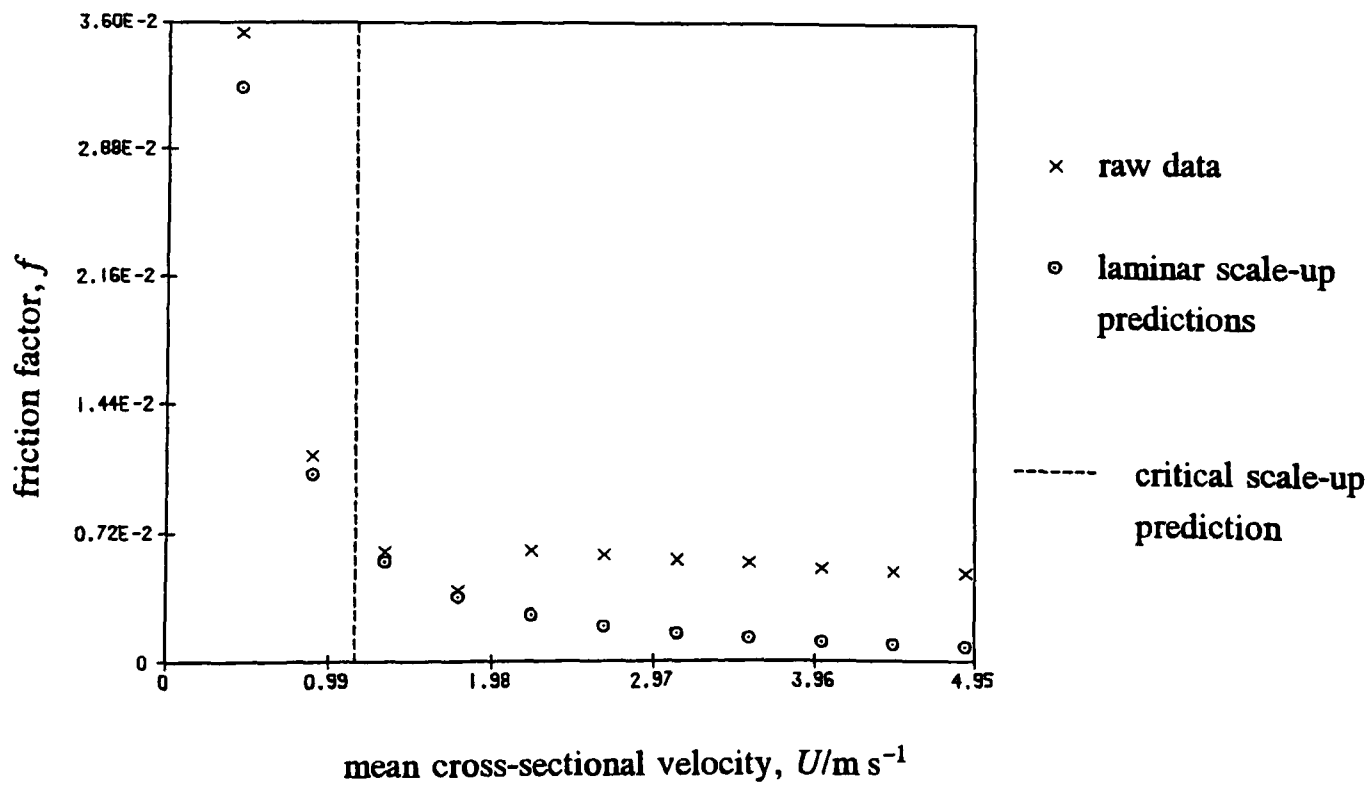


**Figure 7-23** Pipe flow data of an activated sludge from Maple Lodge with laminar and critical flow scale-up predictions.

Why is it that the first laminar flow prediction of the pipe flow data consistently under-predicts? Wall slippage is likely to be the answer to this question because, according to Jastrzebski [78] who wrote an authoritative paper on wall effects, correction for wall slip is particularly important at low shear. In context of our problem, a pseudó-shear rate relation adjusted for wall slippage (see Section 4.5) is given as

$$\Gamma = \frac{8(U - U_s)}{D},$$

where

$$U_s = \frac{\beta \tau_R}{D^{\alpha}}.$$

$U_s$ is the slip velocity, $D$ is pipe diameter, $\tau_R$ is the wall stress, and $\beta$ and $\alpha$ are a parameters for fitting to the data. Firstly notice that, since $\alpha$ must be greater than one, wall slippage becomes less important for larger diameters. Also notice that by definition of a pseudoplastic fluid, when $\Gamma$ increases, $\tau_R$ increases less rapidly. The slip term thus becomes less important for higher shear, and this is borne out by Figures 7-22 and 7-23.

Figure 7-24 shows the pipe flow data of a primary sludge from Ipswich. Unlike the previous figures, the critical velocity prediction is a gross under-prediction of the true critical velocity. An examination of other pipe flow data of primary sludges also showed the critical velocity predictions to be too small. Since these are scale-up predictions, it is not possible from the pipe flow data to establish whether the under-predictions are due to the differences in the pipe diameter, or due to the sludge itself. To rule out the differences in diameter, the tube flow predictions can be re-examined. One such example is Figure 7-25—tube flow data of a primary sludge from Southend—which gives a clear indication that the critical flow prediction is too small, therefore showing that the under-prediction must (at least in part) be due to the sludge itself. Critical flow predictions using other primary sludge tube flow data suggest the same thing: critical flow predictions of primary sludge underestimate the true critical values. Although simple solutions to the problem could be considered (such as a scaling factor), there are certain qualms about altering a credible model that proves inadequate for primary sludge. Needless to say, simple fixes to the problem were sought out of curiosity, but none could be found.

A close inspection of Figures 7-24, 7-25, and of other related primary sludge data suggests that there is more to primary sludge flow than just a late onset of turbulence. For instance, for Figure 7-24, the point immediately proceeding the critical velocity prediction is clearly non-laminar; for Figure 7-25, the gradient of the curve proceeding the critical flow prediction increases with increasing flow rate; an indication of non-laminar flow. Primary sludge therefore has some rather unusual flow behavioral effects that are not investigated here.

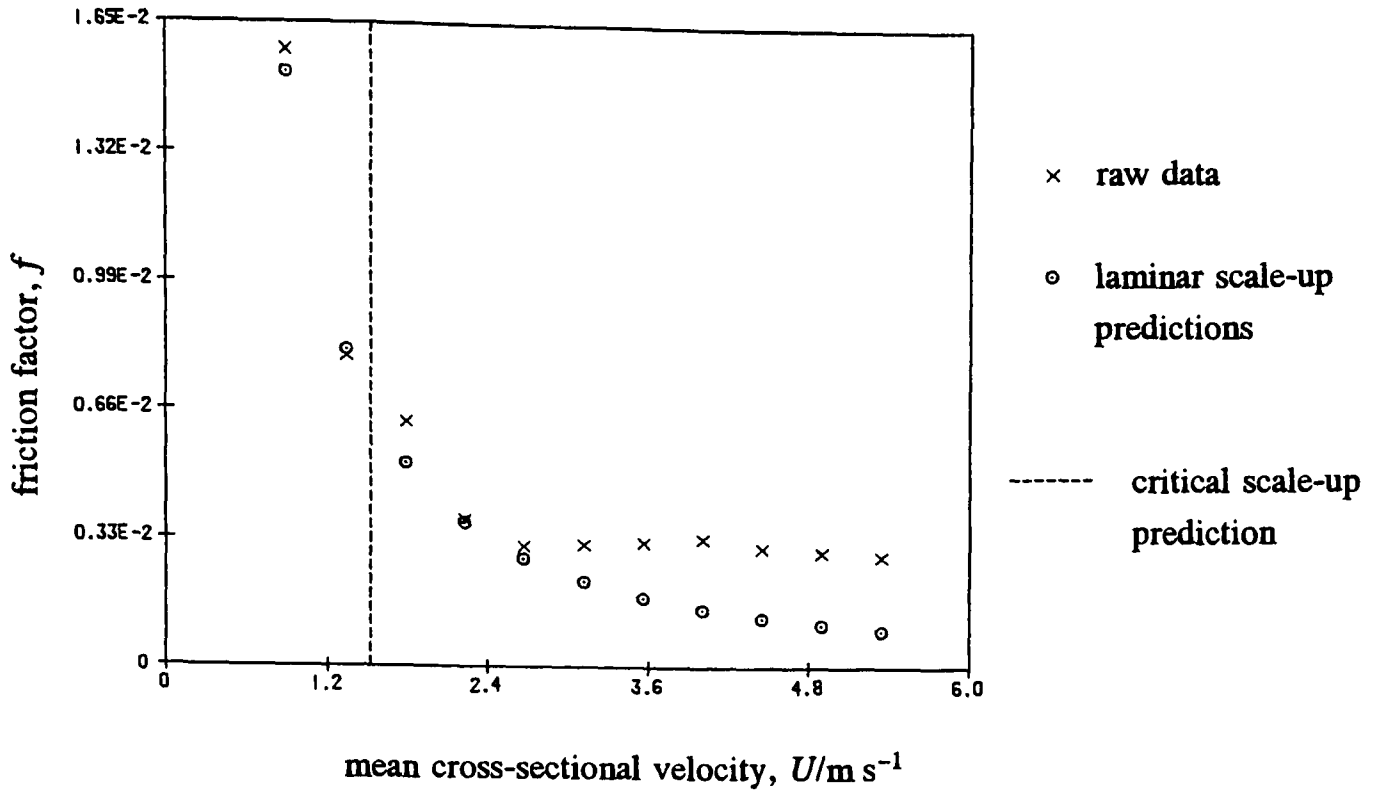


**Figure 7-24** Pipe flow data of a primary sludge from Ipswich with laminar and critical flow scale-up predictions.

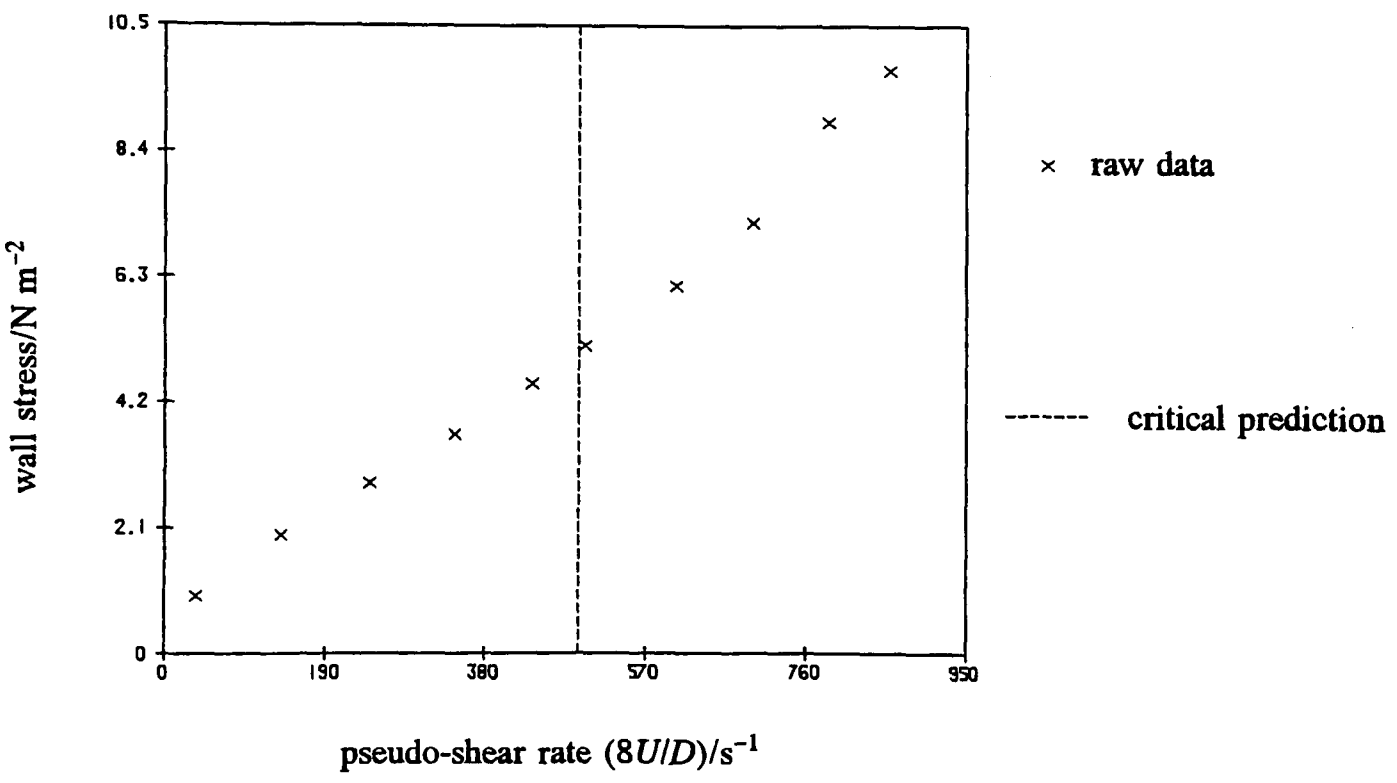


**Figure 7-25** Tube flow data of a primary sludge from Southend including the critical flow prediction.

The reason that the critical flow model does not work well for primary sludge undoubtedly lies in the pseudohomogeneous assumption. Primary sludge has a particularly large distribution of particles sizes (up to one centimetre) and fibrous material that has not been accounted for in the modelling. The fibres themselves could suppress the random fluctuations associated with turbulent flow, and induce a late onset of turbulence. However, any quantitative analysis of these effects is not possible in absence of data.

Since laminar and critical flow predictions are interdependent, there must naturally be some concern about the validity of the laminar flow models of primary sludge. However, there is nothing in the data to suggest that laminar flow of primary sludge is peculiar, and since the critical flow predictions are clearly laminar (upper bound or otherwise), the laminar flow model remains valid. This argument is borne out by good laminar flow scale-up predictions, such as those of Figure 7-24.

It can be concluded that the critical flow predictions of activated and digested sludges are qualitatively sound, but those of primary sludge are erroneously small. For laminar flow modelling, this does not matter as only laminar flow data are utilised. However, based on the current assumptions, turbulent flow modelling of primary sludge is not possible since the pseudohomogeneous assumption that affected critical flow modelling would undoubtedly affect turbulent flow modelling too. Even if this were not the case, the turbulent flow model, Equation (4.65), possesses a wall damping term that is invoked from critical flow onwards. Since the critical flow conditions of primary sludge cannot be correctly predicted, turbulent flow modelling of primary sludge will not be included in this research.

## 7.3 Turbulent Flow Analysis

For the turbulent flow analysis, the pipe flow data (rather than the tube flow data) are of relevance as they cover the full laminar to fully-developed turbulent flow regimes (with less emphasis on laminar flow). In Section 4.4, a discussion was given of a turbulent flow model for non-Newtonian fluids proposed by Hanks[26], which is

$$\tau = \tau_y + K\dot{\gamma}^n + \rho l^2 \dot{\gamma}^2, \tag{7.9}$$

where $l$ is the mixing length defined as

$$l = \kappa R \left[1 - \frac{\tau}{\tau_R}\right] \left[1 - e^{-\phi_{GB}\left(1 - \frac{\tau}{\tau_R}\right)}\right], \tag{7.10}$$

and

$$\phi_{GB} = \frac{B_{GB} - (B_{GB})_c}{\sqrt{8}\, b(n,\ \mathrm{He}_{GB})}. \tag{7.11}$$

$\phi_{GB}$, $B_{GB}$ and its critical value $(B_{GB})_c$ contain parameters of the general Bingham laminar shear flow function (2.10). The parameter $b$ is empirical, and the objectives of this section are to fit the parameter $b$ to all of the sound pipe flow data using the algorithm presented in Section 6.2.

Figure 7-26 is an example of turbulent flow data that contains an outlier. As discussed in Section 7.1, such outlying points may be due to measurement or typing errors, or may represent the haphazard nature of sludge flow behaviour itself. Either way, such outliers may overtly affect the model and must therefore be removed from the data. For the laminar flow data discussed in Section 7.1, a statistical test was used to recognise potential outliers. However, for the turbulent flow data, such a statistical test becomes an unattractive proposition. In Section 6.2, it was recognised that estimating the turbulence parameter $b$ was a computationally intensive process, so outlier analysis would be time consuming to both implement and execute. Furthermore, whereas there have been a considerable amount of laminar flow data in the form of tube flow tests, there are much fewer turbulent flow data to analyse. Outliers of the turbulent flow data can therefore be recognised and removed by visual inspection. A computer program was written in Fortran 77 to display the data and—with a user-controlled facility—remove any chosen point of datum. In this way, all of the suspected outliers were removed from the turbulent flow data.

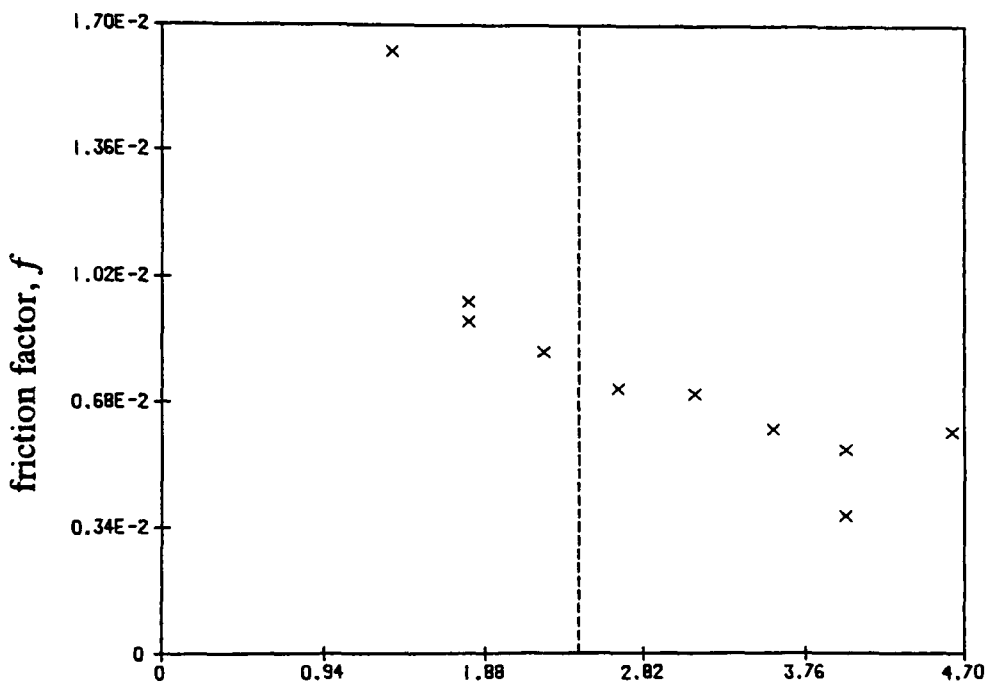


**Figure 7-26** Pipe flow data of a digested sludge from Perry Oaks with a suspected outlier in the turbulent flow regime.

In Chapter 3, it was remarked that pipe flow tests were conducted in two modes of operation: once-through and recirculation. During any particular day's testing, the sludge had either been pumped to make one pass through the pipe (once-through), or the sludge had been recirculated back through the tank to make several passes through the pipe. Examples of recirculated flow are shown in Figures 7-27 and 7-28; they are respectively of a digested sludge from Perry Oaks and an activated sludge from Maple Lodge. The data are presented as pseudo-shear flow plots to give a general idea of the shape of the true shear flow function. The gradients of the curves thus give an idea of the viscosity of the sludge for any particular shear rate. One would expect the overall viscosity of sludge to decrease with each consecutive pipe flow test; such behaviour was identified for laminar flow where a sludge before pumping is never more viscous during pumping, and likewise for during and after.

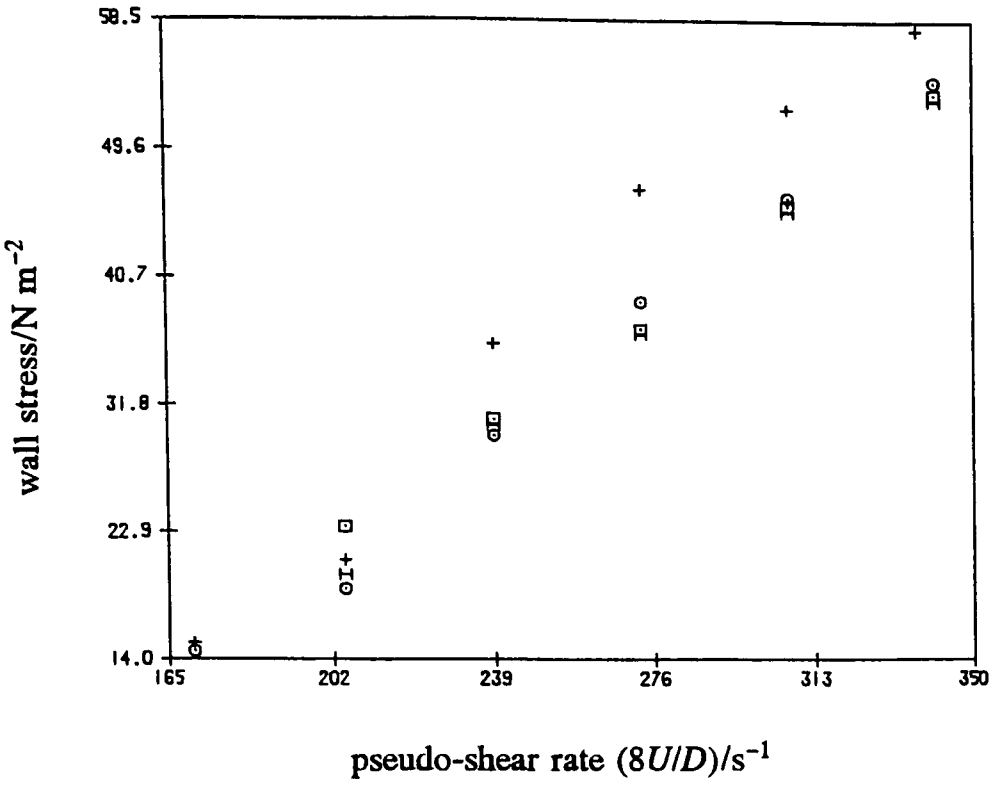


**Figure 7-27** A pseudo-shear plot for the pipe flow data of a digested sludge from Perry Oaks.

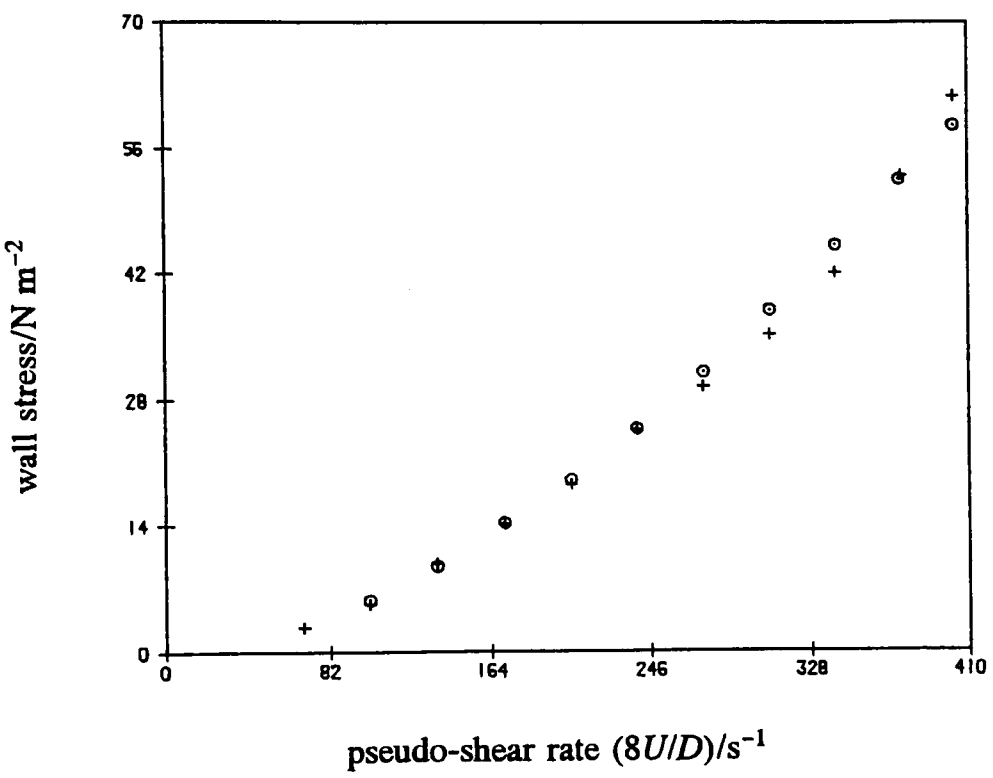


**Figure 7-28** A pseudo-shear plot for the pipe flow data of an activated sludge from Maple Lodge.

It comes as a surprise to find that there is no systematic reduction in turbulent flow viscosity for each consecutive pipe flow test. In fact, some arbitrary variation is evident between the turbulent flow tests; Test 2 of Figure 7-27 illustrates the point beautifully. For these cases there is no clear explanation for the difference of a particular test other than the variation of material content within the sludge.

The objectives are to fit the turbulent flow model (7.9) to the sound pipe flow data and examine the residuals. A full discussion of a least squares fit of the model to a set of data points was given in Section 6.2. At this stage, the objectives are to establish the suitability of the model for the pipe flow data, so there would be no reason for being selective about the type of pipe flow data to analyse. Since the log transformation proved successful for the laminar flow model, it seems reasonable to apply it to the turbulent flow model also. This gives continuity to the data analysis, but it should nevertheless be appreciated that, if the log transformation fails the residual analysis, alternatives will have to be sought.

The log transformation of the turbulent shear flow function (7.9) is

$$\log_{10}(\tau - \tau_y) = \log_{10}(K\dot{\gamma}^n + \rho l^2\dot{\gamma}^2). \tag{7.12}$$

The left-hand side of the equation remains the same as the log laminar shear flow function, but the right-hand side of the equation no longer conveniently reduces to the form of Equation (7.6). Analogous to the laminar flow case, it is convenient to use the notation $q = \log_{10}(\tau - \tau_y)$ to give an error sum of squares for the $i$th sludge sample (Section 6.3) as

$$E_i = \sum_{j=1}^{M_i} (q_{ij} - \hat{q}_i)^2, \tag{7.13}$$

where the hat denotes a prediction. Estimation of $b$ was discussed in Section 6.2, and requires minimizing the error of the turbulent flow model with respect to $b$. It was shown that the minimum was difficult to obtain by the usual turning point techniques, so quadratic interpolation was used as a bracketing method (A.3: Appendix A, Section 3) to obtain the minimum of $E_i$ with respect to $b$. A Fortran 77 program was written to fit the turbulent flow model to all of the sound pipe flow data.

Figures 7-29 and 7-30 show the turbulent flow predictions of a digested sludge from Perry Oaks and an activated sludge from Maple Lodge respectively. As discussed in Section 6.2, estimating $b$ is a computationally intensive process. Using an IBM compatible PC with a Pentium processor and setting a relative convergence value of $5 \times 10^{-4}$, each estimate took roughly twenty seconds. It should be acknowledged that, whereas the laminar flow predictions are scaled up from the tube flow data, the turbulent flow predictions are based on the actual turbulent pipe flow data. Examining Figures 7-29 and 7-30, the turbulent flow model is agreeable for most of the data, which is the least to be expected of a one parameter model. The curvature of the data is of more interest and the model gives a fair portrayal of this. Other data have been examined, and as with Figure 7-29, there is evidence that the data fluctuate about the predicted values, which implies that no more can realistically be expected of a one parameter model. Predictions are at their poorest for the transitional region between laminar and fully-developed turbulent flow. For Figure 7-30, the second non-laminar point was taken to be an outlier and excluded from the analysis. Instead, there is good argument for using the laminar flow predictions of the transitional region. However, as noted in Chapter 3, transitional flow can behave unpredictably, so it may be wiser to be conservative and use the turbulent flow over-predictions.

As discussed in Section 4.4, Hanks derived a turbulent flow model for general Bingham fluids where $b$ is based on an empirical relationship of the consistency index $n$, and the non-Newtonian Hedström number $\mathrm{He}_{GB}$. For the data of Figure 7-29, the fitted value of $b$ is 37.24, whereas Hanks' prediction of $b$ is 71.31. There is a large discrepancy between these two values, though how the discrepancy translates to turbulent flow predictions depends on the sensitivity of $b$. The predictions of Hanks are included on Figure 7-29; they are poor and show that $b$ is indeed a sensitive parameter.

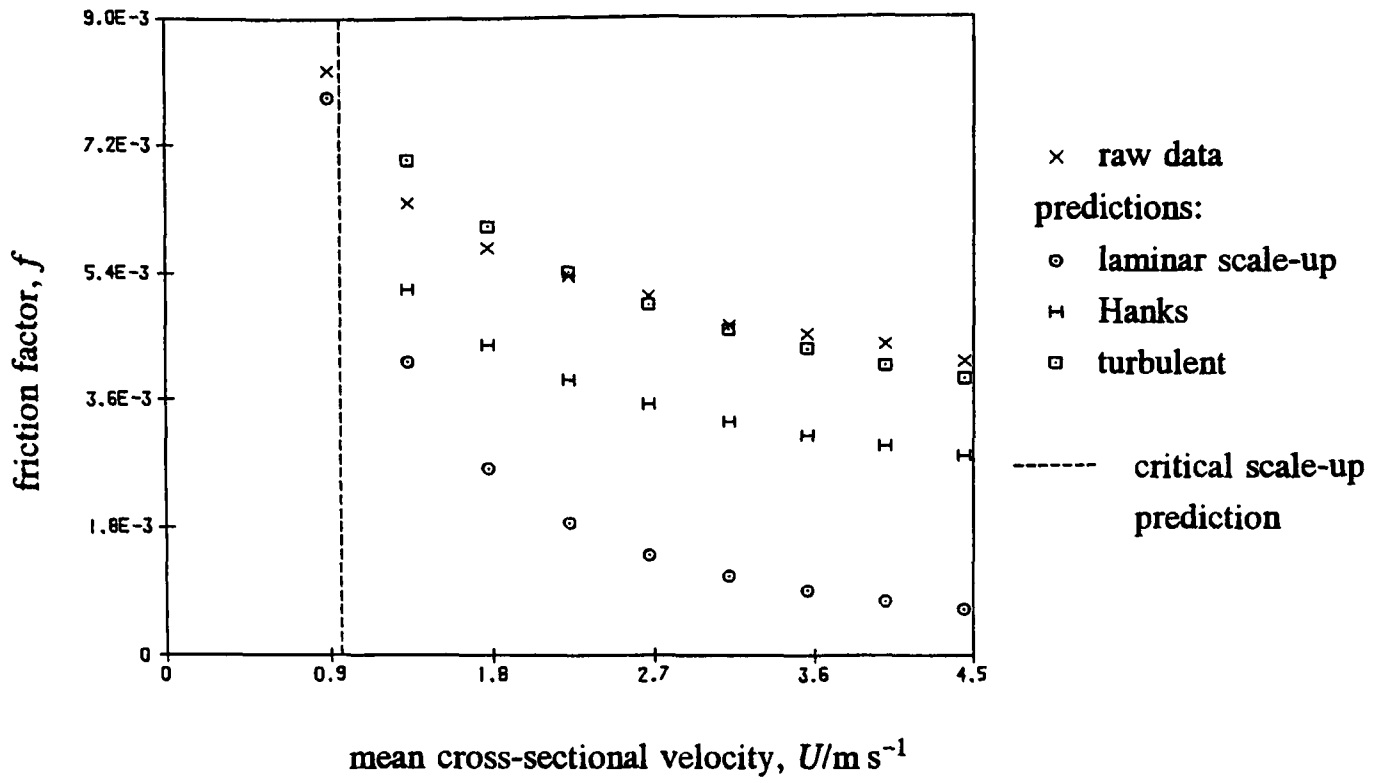


**Figure 7-29** Turbulent flow predictions for the pipe flow data of a digested sludge from Perry Oaks.

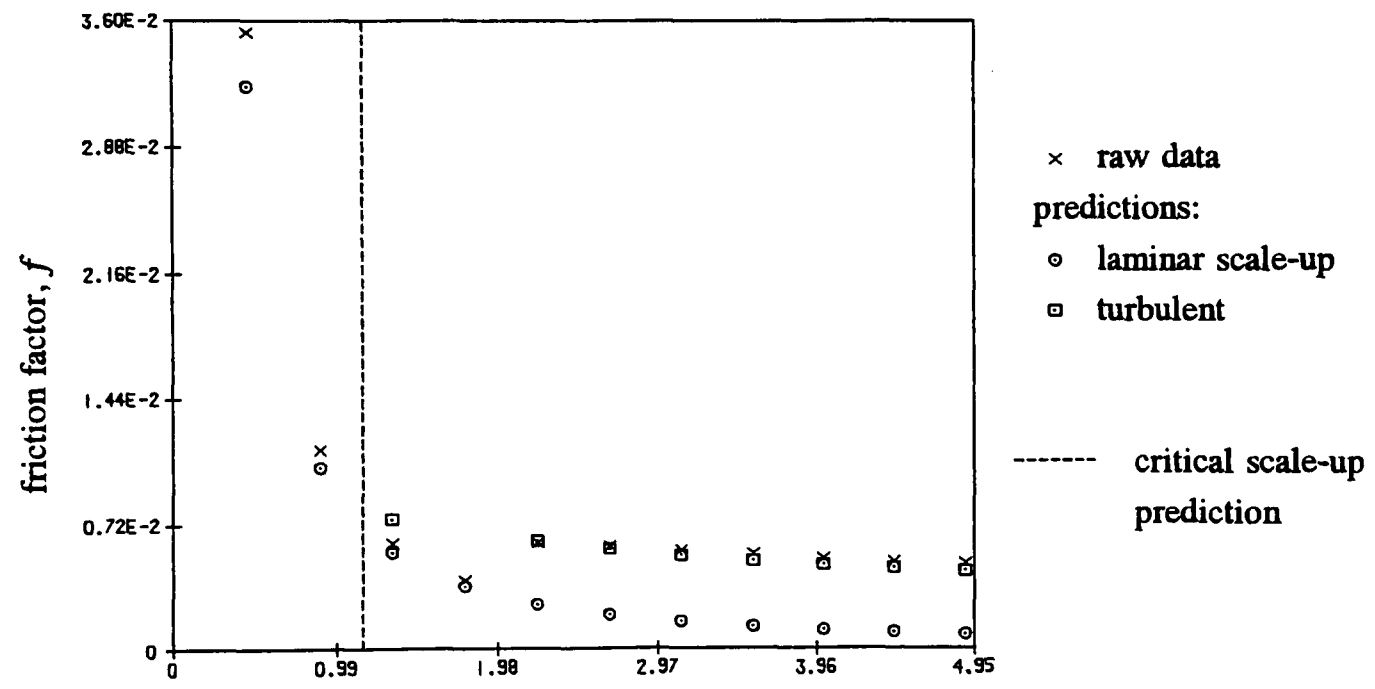


**Figure 7-30** Turbulent flow predictions for the pipe flow data of an activated sludge from Maple Lodge.

As the turbulent flow model is based on only one parameter, there is little point in examining the residuals of individual data sets. A qualitative assessment of the fit such as that given above is more than sufficient. However, for the log transformation to be valid, the standard errors of each fit must be constantly spread over the mean value of the independent variable[82]. Figure 7-31 shows a plot of standard error against mean wall stress for activated and digested sludges. There is no evidence of any systematic variation of standard error with mean wall stress. The log transformation of the turbulent flow model is therefore valid.

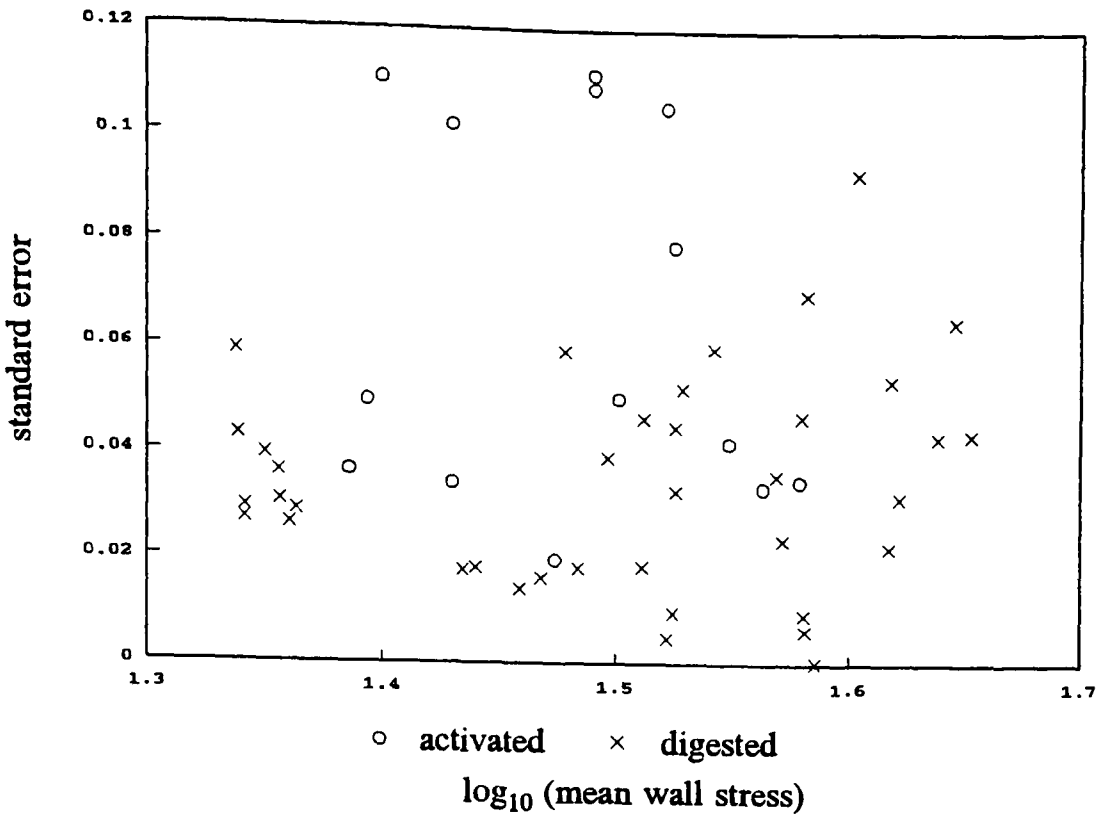


**Figure 7-31** The standard errors of turbulence model fitted to the pipe flow data.

Global standard errors of the log turbulent flow model are estimated directly from Figure 7-31 as being about 0.04 for activated sludge and 0.03 for digested sludge. (For the laminar flow model the standard errors were about 0.02 and 0.01 for activated and digested sludges respectively.) Considering that the turbulent flow model has only one parameter to estimate, this is a significant result; although reasons for this can only be surmised, it may be that the shear thinning effects are less significant for turbulent flow.

The turbulence model has been used to estimate the shear rate range for both sludge types using all of the relevant transitional and turbulent flow data, and the results are given in Table 7-4. These ranges do not include laminar flow as these have already been dealt with at the end of Section 7.1.

**Table 7-4** Rate of shear ranges for the models.

| Sludge | Shear rate range, $\dot{\gamma}_{min}/s^{-1}$ - $\dot{\gamma}_{max}/s^{-1}$ |
|---|---|
| Digested | 190 - 33 000 |
| Activated | 44 - 57 000 |

For completeness, some of the fitted models at the lower and higher ends of the ranges shall be examined. For digested sludge, Figure 7-32 shows the turbulent flow model fitted to data of the low predicted shear rate range 337 $s^{-1}$ - 13 157 $s^{-1}$ and the high predicted shear rate range 824 $s^{-1}$ - 32 881 $s^{-1}$. For the lower range, the fit is very good and this is borne out by the other data with ranges of up to about 13 000 $s^{-1}$. However, for the higher range, the fit is not so impressive and, as verified using other data, the model is not so good for these higher shears. Much the same conclusion was drawn for activated sludge, and a good example of a fit to the lower range 140 $s^{-1}$ - 10 174 $s^{-1}$ is offered by Figure 7-33.

(a)

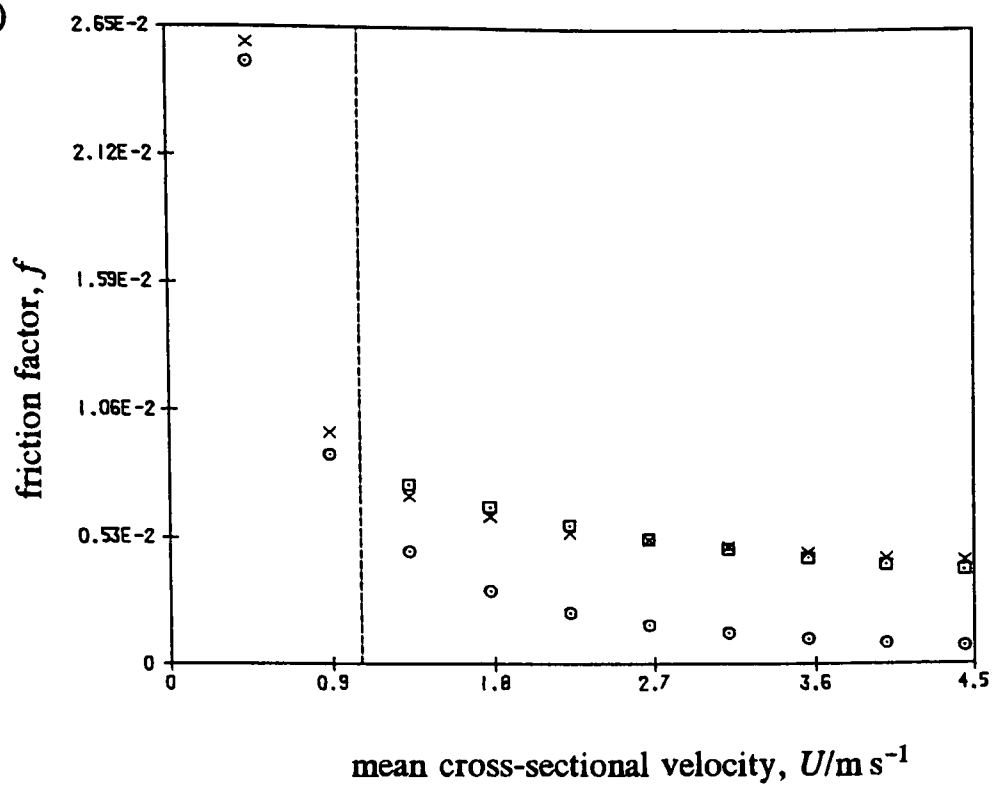


× raw data
predictions:
⊙ laminar scale-up
⊡ turbulent

------- critical scale-up prediction

(b)

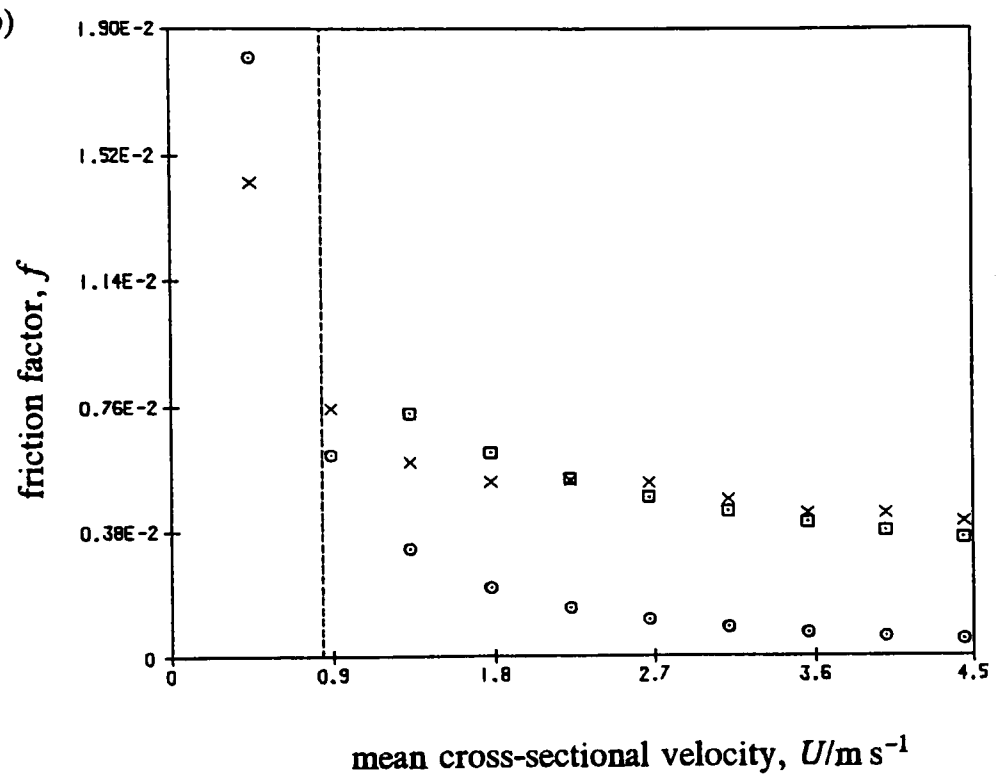


× raw data
predictions:
⊙ laminar scale-up
⊡ turbulent

------- critical scale-up prediction

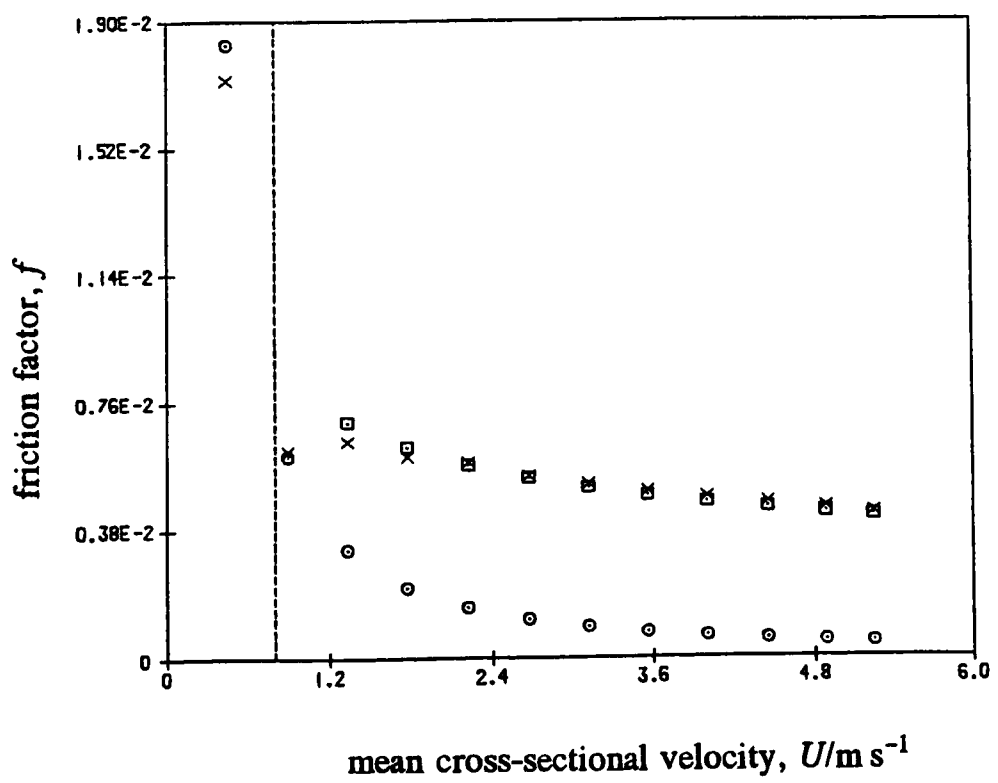


× raw data
predictions:
⊙ laminar scale-up
⊡ turbulent

------- critical scale-up prediction

**Figure 7-32** (top) Turbulent flow fits for digested sludge of (a) low (b) high shear.
**Figure 7-33** (above) Turbulent flow fit for activated sludge of low shear.

## 7.4 Friction Plots

Non-Newtonian systems have often relied on graphical methods for obtaining predictions, and since these methods are well-founded, many engineers still use them. In this section, some non-Newtonian friction plots and prediction curves of the sewage sludge data will be presented. The emphasis of the research has so far been placed on rheological models appropriate to any geometry, but since the data comes from pipe flow measurements, friction plots are a convenient way of representing it. These plots are based on the pipe flow data which cover the full laminar to turbulent flow regimes. Only the first pipe flow result of a trial will be used where the sludge is assumed to be at its least agitated (this is important where conservative estimates are required for design purposes). These plots are also useful for comparing different models of flow prediction. For instance, our turbulent flow model with one fitted parameter will be compared against the widely used Dodge-Metzner relation. A friction plot conventionally contains both the laminar and turbulent flow regime of the data, which will be the case for primary sludge. For the activated and digested sludges where good critical flow predictions are available, the laminar and transitional/turbulent flow regimes will be presented on separate plots.

For non-Newtonian fluids, the Metzner-Reed [20] friction plot is often used, and based on the usual definition of friction factor $f$ and Metzner-Reed Reynolds number $\mathrm{Re}_{MR}$ as defined by Equations (4.6) and (4.46) respectively. Figures 7-34 and 7-35 are two such plots of the digested and activated sludges respectively. It is important to note that the $f$-axis has been scaled up for turbulent flow to show the data more clearly, but the scale of the $\mathrm{Re}_{GB}$-axis remains the same (normally turbulent flow would be represented on the same plot as laminar flow, though with a significantly shallower gradient). The Reynolds number is based on two parameters $K'$ and $n'$ that are not required to be constant, but can be calculated from a logarithmic plot of the laminar flow data. In our case, it is advantageous that the corresponding tube flow data are virtually all laminar, and almost always of a greater $\Gamma$ range than the pipe flow data. Since the first pipe flow data of each trail are being used, it makes sense to use the corresponding tube flow data taken before the pipe trials. This is because it was recognised in Section 3.4 that these measurements are of the sludge at its least agitated. A computer program was written to automatically estimate the tangent of the log-log transformation of the tube flow data, and hence estimate $K'$ and $n'$ at each $\Gamma$.

From the definition of the Metzner-Reed Reynolds number, the laminar flow relation $f = 16/\mathrm{Re}_{MR}$ should hold true. This prediction line has been placed on all four plots, and has a slope of minus one when the scale is taken into account. The prediction holds true for the laminar flow data, but this is to be expected from the definition of the Reynolds number. This consequently supports the no-slip argument as this version of the Metzner-Reed Reynolds number includes no wall slippage term. The adjusted volume percentage of solids for each sludge sample is shown in the legend where they have been sorted into an ascending order.

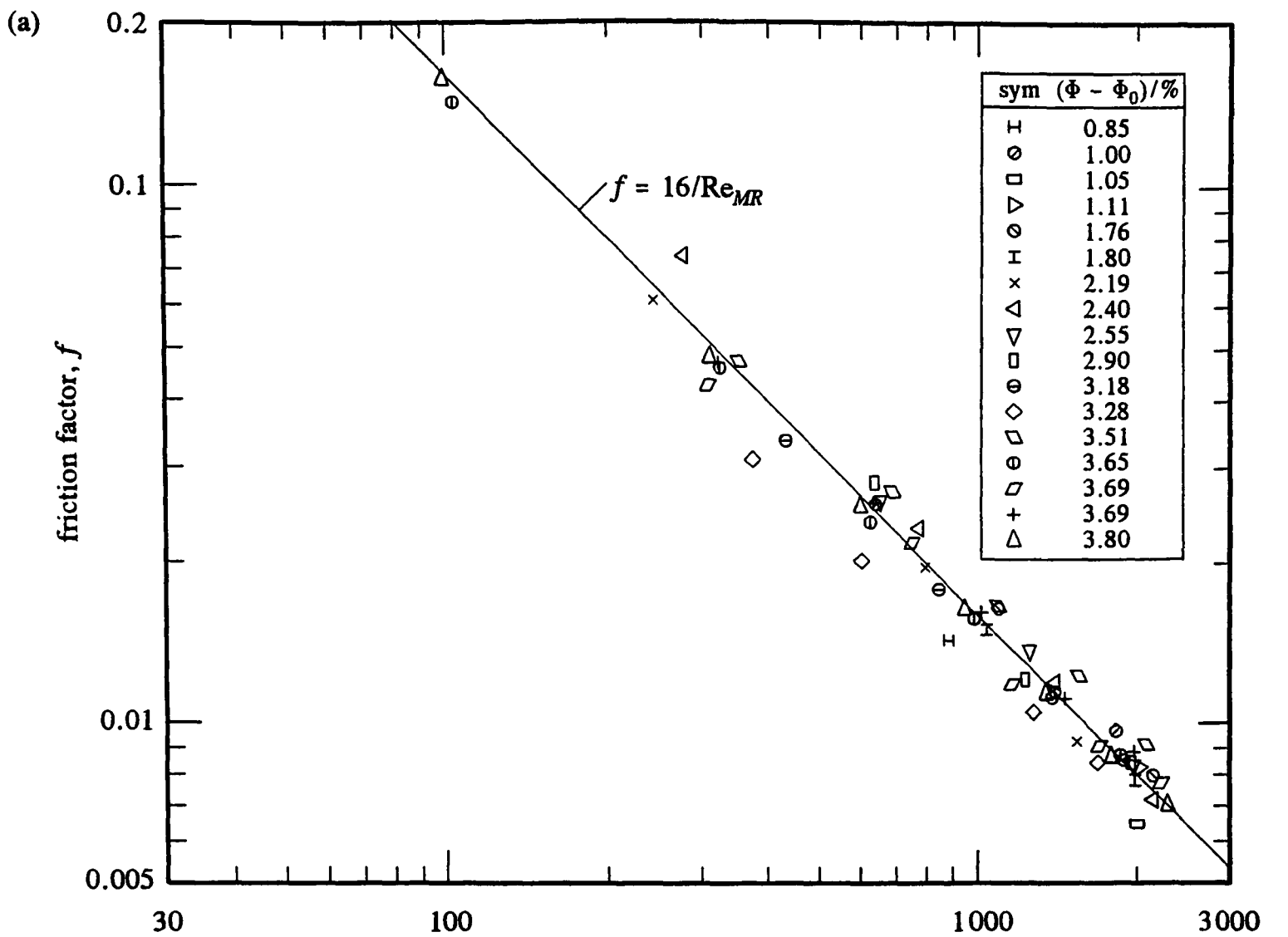


**Figure 7-34** Digested sludge: Metzner-Reed friction plots of (a) laminar and (b) turbulent flow with varying volume percentage of solids.

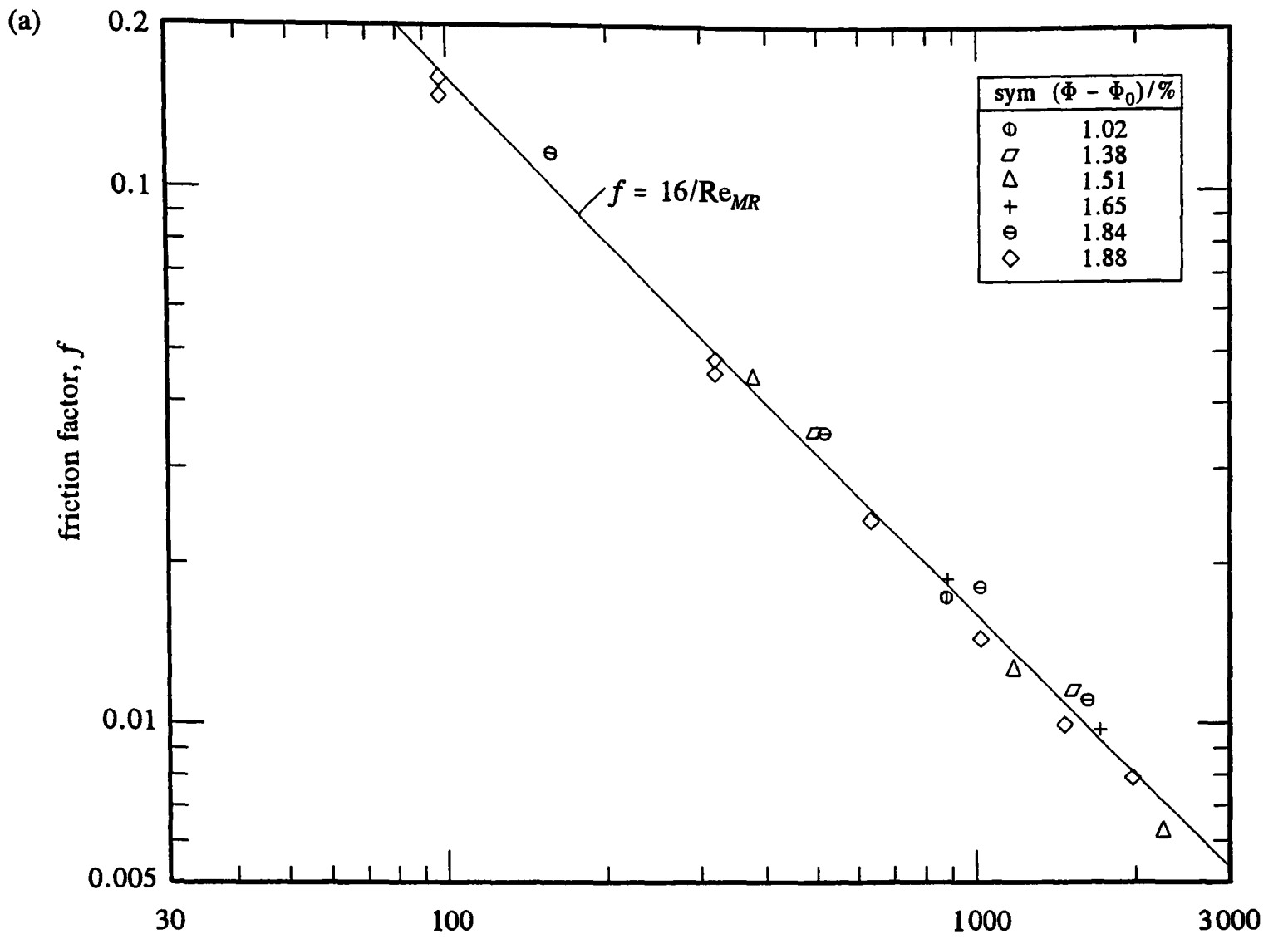


**Figure 7-35** Activated sludge: Metzner-Reed friction plots of (a) laminar and (b) turbulent flow with varying volume percentage of solids.

The two turbulent flow figures show a strong correlation between the gradient of the curves and the concentration of the sludge: the higher the concentration the steeper the gradient. As one would expect, there is much more scatter in the data for higher solids concentrations—an effect that shall be examined in the next chapter. The turbulent flow plots also reveal another interesting result: to some extent the data of the thicker sludges tend to remain laminar. This may be a failure to correctly predict the critical flow velocity, but this is unlikely considering the amount of scatter in the data. It may be that the sludge is unpredictable at these concentrations and does not easily settle into laminar or turbulent flow. It may also be that the transition between laminar and turbulent flow is inherently complex.

The Dodge-Metzner relation for turbulent flow was discussed in Section 4.4 and is based on the Metzner-Reed Reynolds number. It is a widely used relation for non-Newtonian fluids, but is ill-considered for all complex mixtures[85]. Figure 7-36 includes Dodge-Metzner prediction curves on the two turbulent flow friction plots. The predictions are poor, probably because the relation does not account for the yield stress of the fluid in an explicit way, and probably because sewage sludges are inherently complex mixtures. There is clearly no ordering of the curves with volume percentage of solids. So what is it that determines the order of the curves and why, for instance, do two of the curves from the first plot deviate markedly to the left? With foresight, it is known that the curves vary with the Hedström number which, as discussed in Section 4.3, is a measure of the yield stress of the fluid. The curves increase with the Hedström number from left to right with the two curves referred to on the first plot having a Hedström number of more than twice any of the others on the plot.

Recent work by Dziubiński[74] has been based on the Metzner-Reed Reynolds number (see section 4.4), and the prediction curves are shown on Figure 7-37. The predictions are higher and constrained to a narrower band than Dodge-Metzner, but equally poor. Considering that the two relations are completely different, it surprising to find that the trends of the curves are so similar (notice again the two curves of the first plot that branch away). As with Dodge-Metzner's method, however, the Hedström number has a similar implicit effect on the curves.

As the general Bingham model has been used far less in the industry as a whole than the power law and Bingham models, there has been far less research into the turbulent flow of general Bingham fluids. Torrance[27] (see Section 4.4) derived a non-Newtonian Reynolds number for general Bingham fluids and subsequently a turbulent flow relation. Figure 7-38 shows the friction plots of digested and activated sludges respectively with Torrance prediction curves included. The curves look more promising than those of Dodge-Metzner's with a clear indication that the Hedström number increases from left to right, but the results are still poor. Although the model includes yield stress in an explicit way, no experimental work was included in the derivation of Torrance's model, which was probably intended for far less complex mixtures than those of sewage sludges.

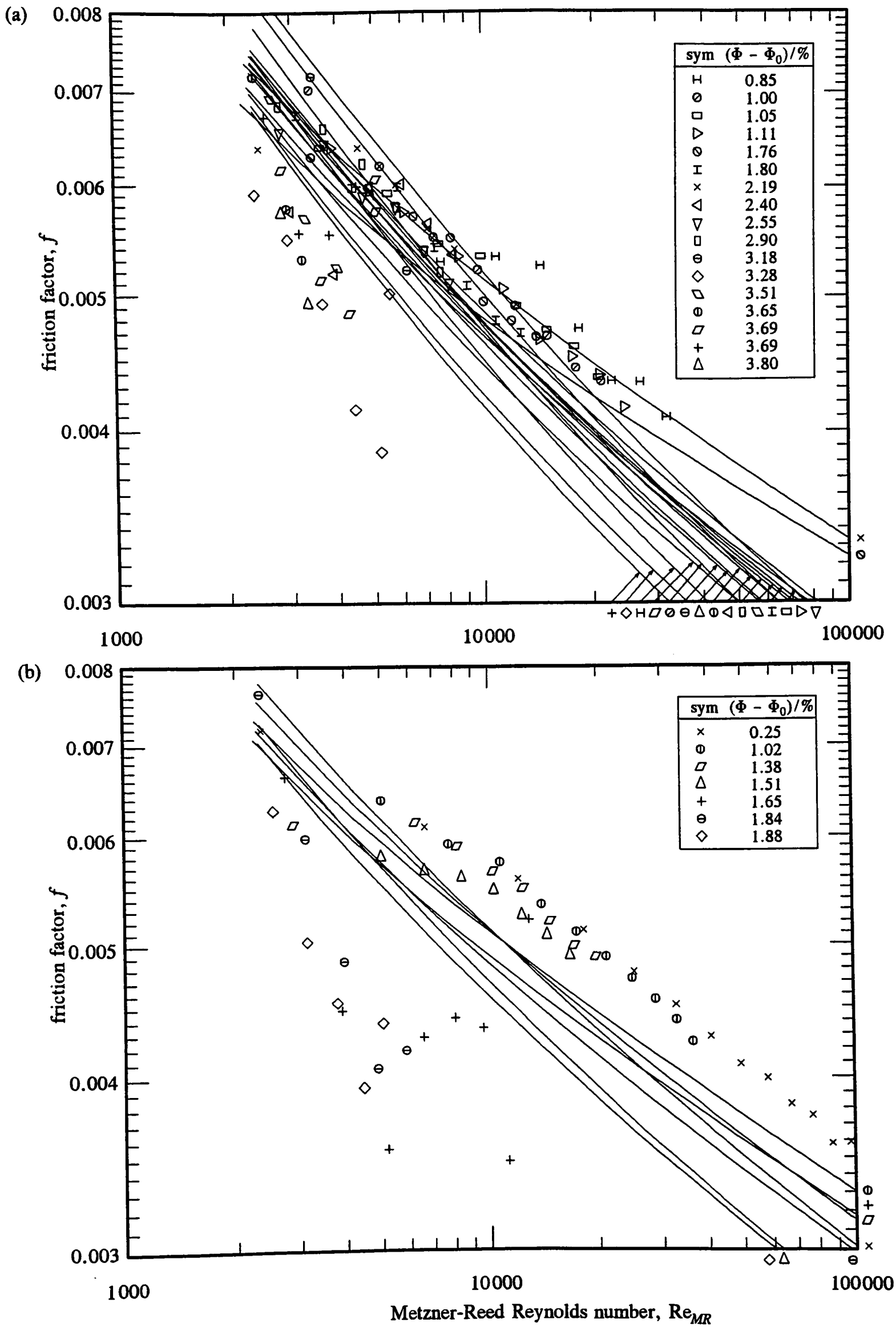


**Figure 7-36** (a) Digested and (b) activated sludge: Dodge-Metzner prediction curves of turbulent flow with varying volume percentage of solids.

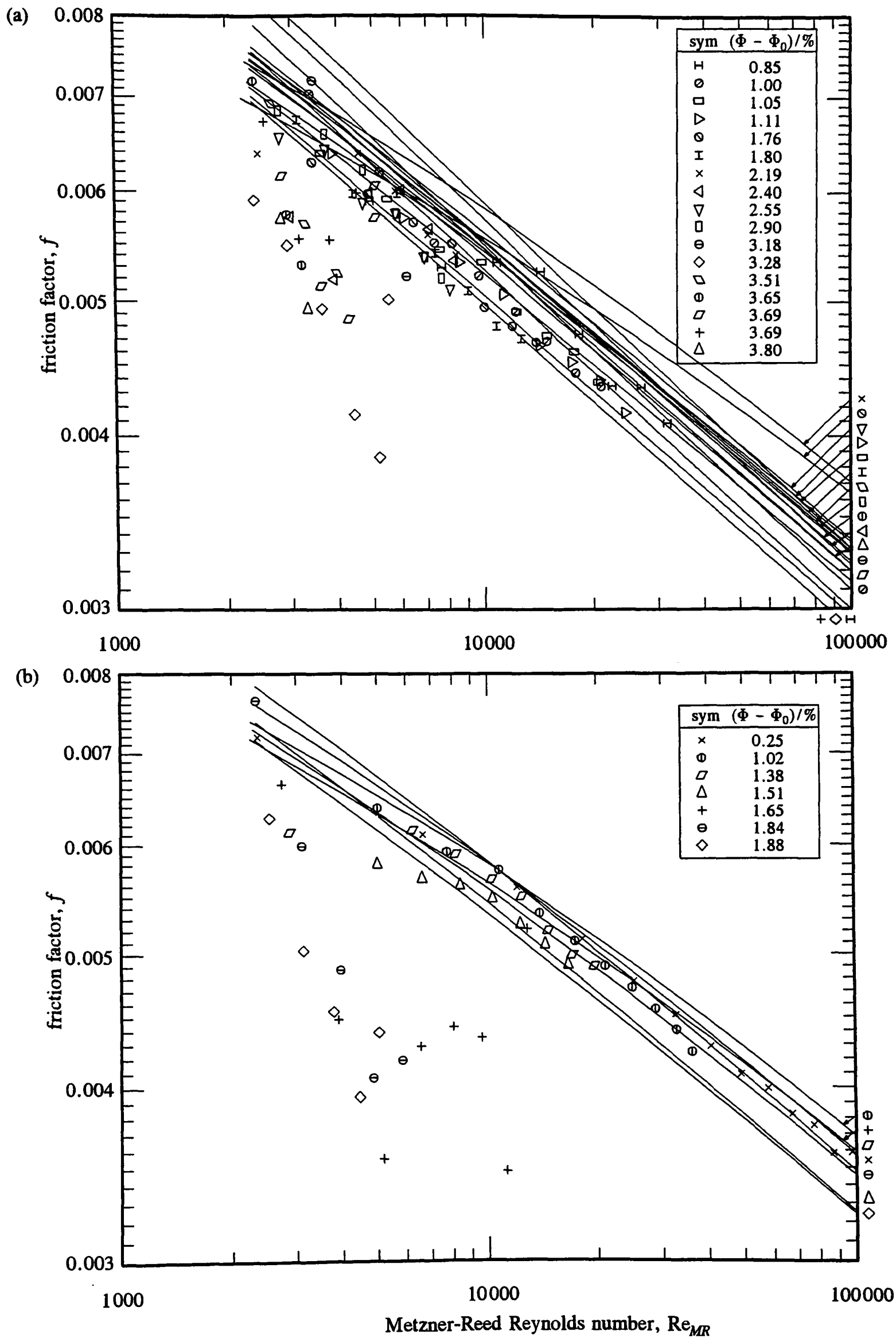


**Figure 7-37** (a) Digested and (b) activated sludge: Dziubiński prediction curves of turbulent flow with varying volume percentage of solids.

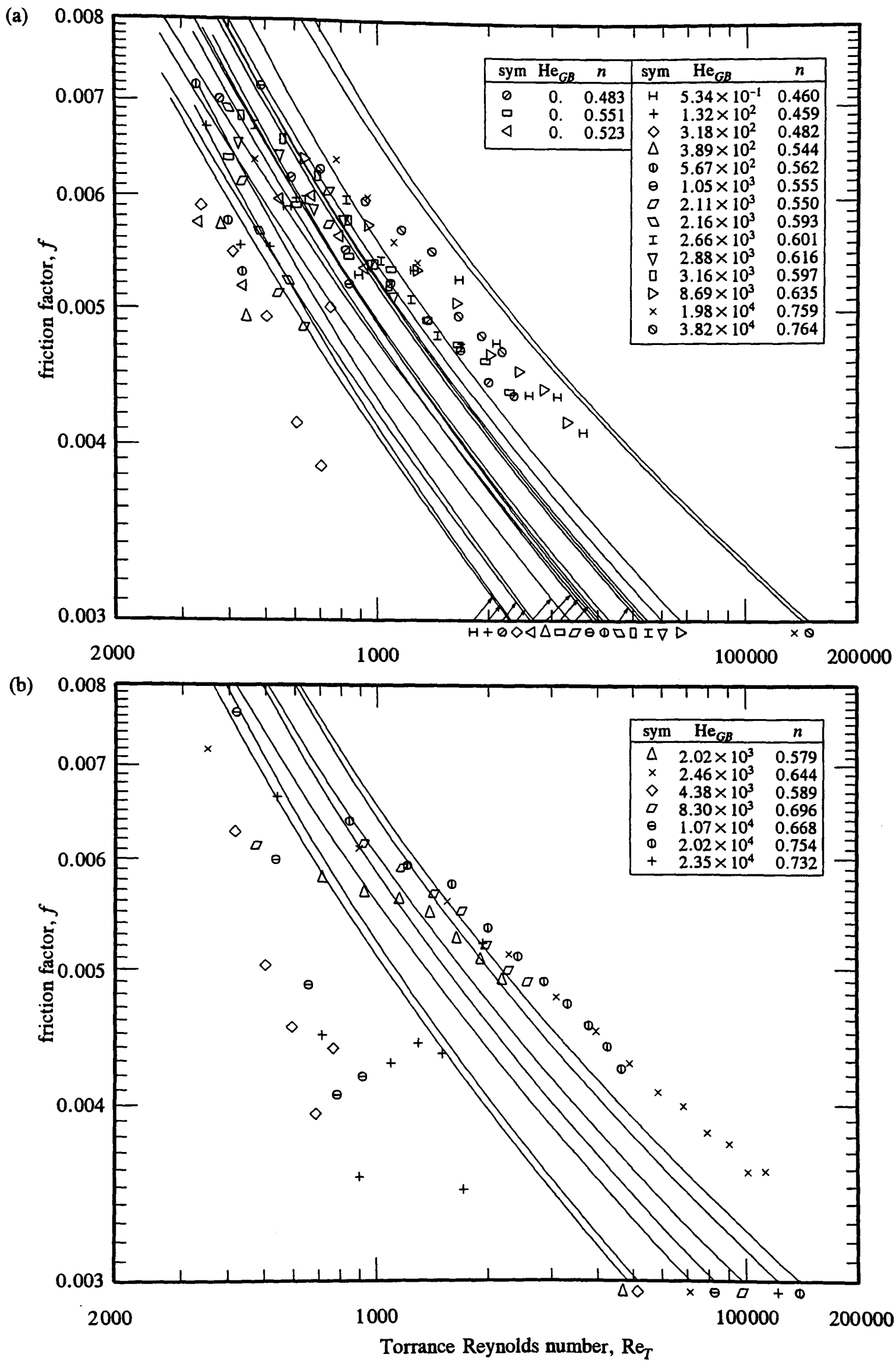


**Figures 7-38** (a) Digested and (b) activated sludge: Torrance prediction curves of turbulence with varying Hedström number and consistency index.

Since the turbulent flow analysis of Section 7.3 was based on a model by Hanks[26], it is worth summarising the data on friction plots proposed by Hanks. Figures 7-39 and 7-40 show the data of the digested and activated sludges respectively. Since the three parameters of the general Bingham model are considered to be constant (see Section 7.1), Hanks' plots are much easier to develop and interpret than Metzner-Reed plots. However, each plot is a function of both the non-Newtonian Hedström number and the consistency index so, for instance, the laminar flow curves are not simply given by $f = 16/\mathrm{Re}_{GB}$ as with Metzner-Reed. The legends contain both of these groups, but are arranged in ascending order of $\mathrm{He}_{GB}$. The use of symbols are consistent with the Metzner-Reed plots, ie the sludge samples are represented by the same symbols for both types of plot.

The turbulent flow analysis of Section 7.3 was based on Hanks, so prediction curves of the turbulent flow data are given on Figure 7-41. The prediction curves are far better than any other model examined so far and make sense of data that contains so much scatter. However, the model has had the advantage of being a one-parameter model where the parameter was fitted to the shear flow relation of each sludge sample. Apart from the free parameter, the main reason for having high expectations of Hanks' method is that few assumptions were made in formulating it. In fact, the Torrance relation is based on the same mixing length model as Hanks but without the Van Driest wall damping factor of Equation (2.22). Furthermore, Torrance made several simplifying assumptions when integrating the velocity profile to obtain the relatively simple friction factor relation.

Referring to Figure 7-41b, although these prediction curves are better than others that have been assessed, there is still some disagreement. A closer look shows that there is some good agreement as well, such as the ◇ curve, and the ⊙ curve (easily confused with the × curve); these curves represent the transitional regime well. The + curve is irrelevant as the + data are so erratic. The poorest predictions are the △ curve and the × curve. There is no obvious reason why these particular predictions fare worse than the others; it may be due to a bad transitional prediction from poor lamina flow data. Note also that these models were derived from shear flow relations and transformed to a frictional relations, so something would have been lost in the transformation.

A major drawback of Hanks' shear flow relation is its complexity. Deriving the prediction curves for Figure 7-41 was a major task as it required the numerical scheme of Section 5.3. Each curve was constructed by discretising wall stress over the friction plot range and calculating the corresponding mean cross-sectional velocity values as described in Subsection 5.3.1—a calculation that involves iteration under integration. Then from the resulting values of $U$, a series of friction factors and Reynolds numbers was calculated. Hanks[26] also developed a set of friction plots in much the same way for varying $\mathrm{He}_{GB}$ and $n$, though he chose to discretise a dimensionless form. Figure 7-41 looks curious as some of the curves

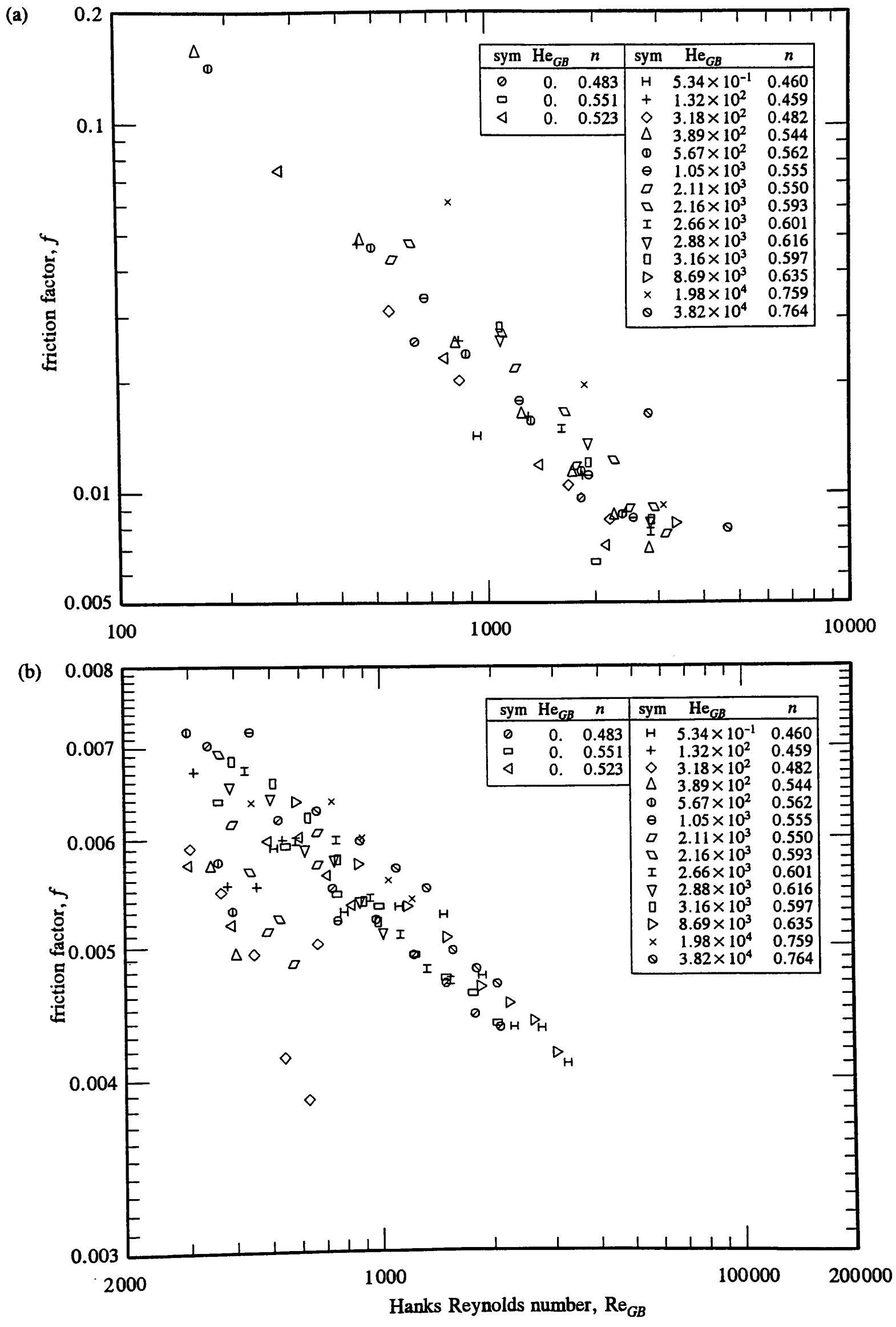


**Figure 7-39** Digested sludge: Hanks friction plots of (a) laminar and (b) turbulent flow with varying Hedström number and consistency index.

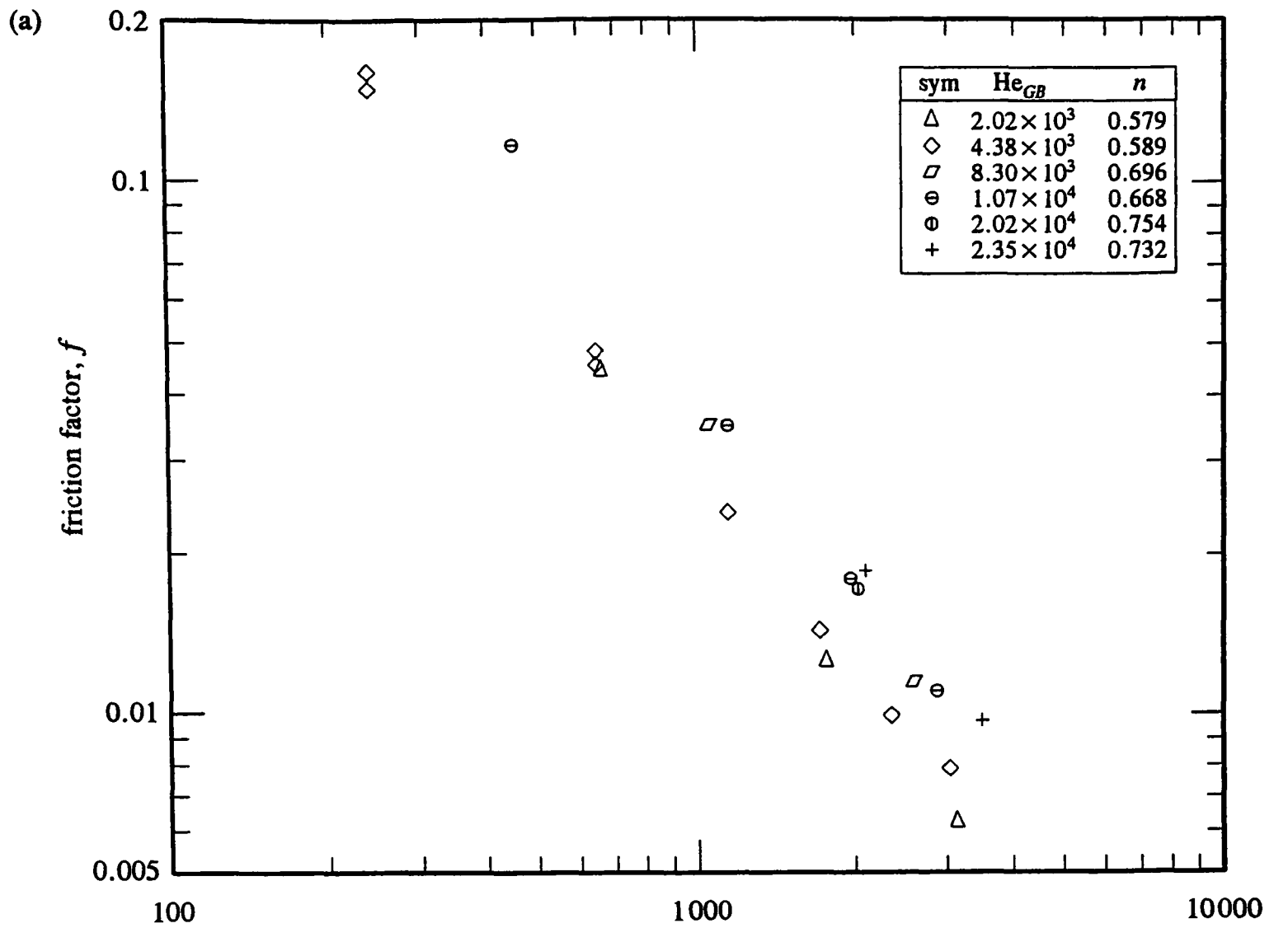


**Figure 7-40** Activated sludge: Hanks friction plots of (a) laminar and (b) turbulent flow with varying Hedström number and consistency index.

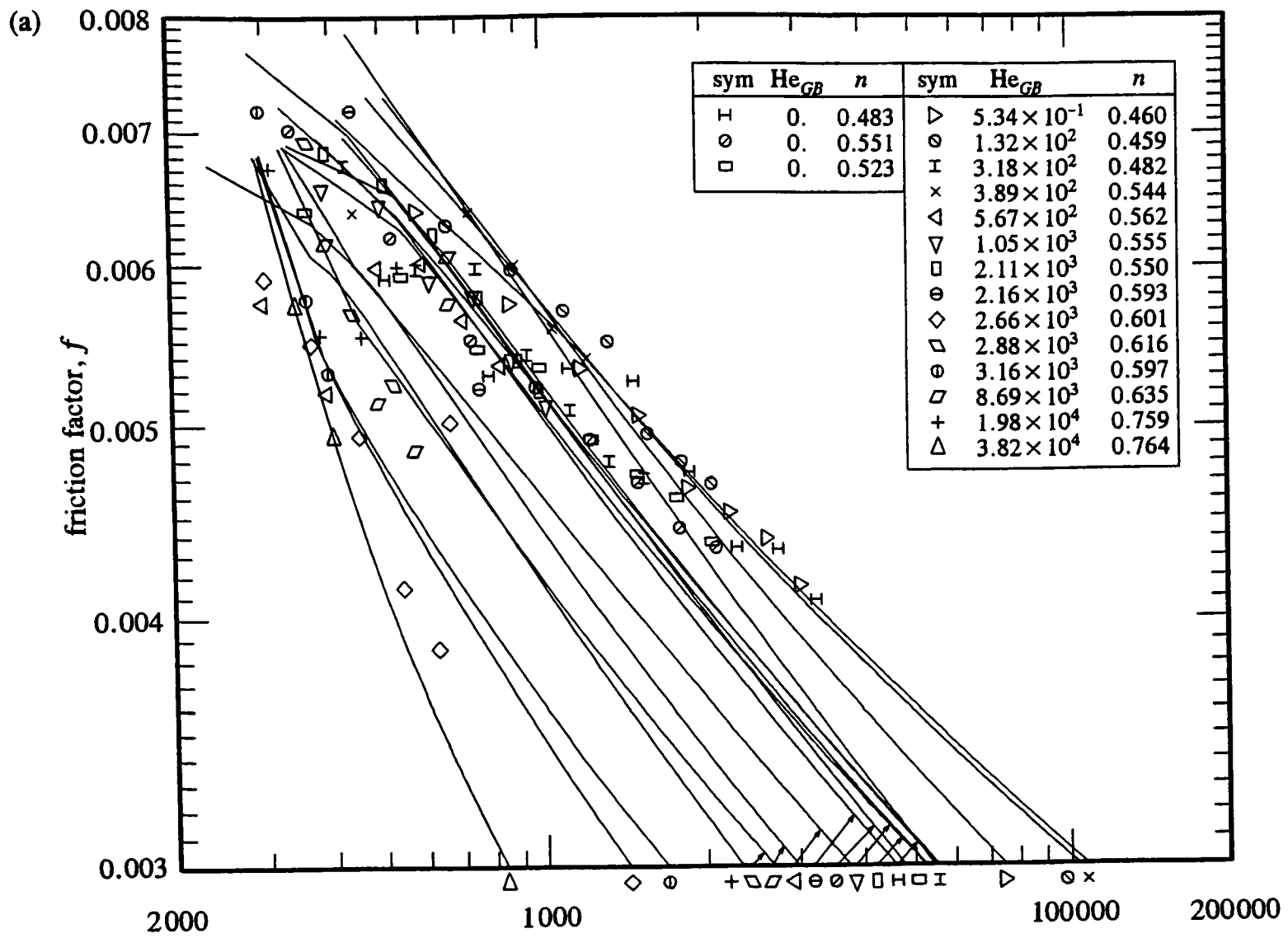


**Figures 7-41** (a) Digested and (b) activated sludge: prediction curves of the turbulence model with one fitted parameter.

inflect in an unusual manner, though this is not wrong as Hanks' original paper shows precisely the same thing. When resolved for pipe geometry, the complexity of Hanks' shear flow relation has undoubtedly weighed against it. Nevertheless such a relation is advantageous for computational fluid dynamics codes as discussed in Chapter 1.

Although the turbulent flow of primary sludge has not yet been considered, Figure 7-42 follows the usual convention by including both the laminar and turbulent flow data on one friction plot. In Section 7.1, primary sludge was statistically shown to be well-modelled by the two-parameter power law model. Therefore $K'$ and $n'$ are constant for the whole of the measured $\Gamma$ range, and Metzner-Reed and Hanks friction plots become the same. The legend includes both volume percentage of solids and $n$, but arranged in ascending order of the former. The laminar flow line, $f = 16/\mathrm{Re}_{MR}$, does not fare well probably because wall slippage is an important effect. This would hardly be surprising considering that primary sludge is known to contain a large distribution of particle sizes (up to 10 mm in diameter), and a significant amount of fibrous material that causes drag. As with the other plots, the solids concentration has a significant effect on the flow behaviour of the sludge.

Since primary sludge has no significant yield stress, one might tentatively hope the Dodge-Metzner relation to be applicable. This hypothesis is tested in Figure 7-43, and it comes as no surprise to obtain a poor result. There has been far more research into the turbulent flow of power law fluids than of general Bingham fluids, so many other relations have been tried on the primary sludge data. Unsurprisingly, none of the relations made satisfactory predictions, though the predictions were surprisingly different. It would be pointless to plot all of these relations, so to summarise, Thomas [86] performed slightly better than Dodge-Metzner, Clapp [65] about the same, Shaver *et al* [87] somewhat worse than Dodge-Metzner, and Tomita [88] and Kemblowski *et al* [89] performed rather poorly.

Similar comparisons of turbulent pipe flow methods were carried out by Heywood and Cheng [90] using the sewage flow data of Hayes *et al* [12]. The sewage was modelled using the general Bingham relation, but Heywood and Cheng still examined power law relations for friction based on the assumption that $\tau_y$ was unimportant for turbulent flow (this was based on conjecture rather than experimental evidence). Heywood and Cheng also examined the method of Hanks straight from plots of the original paper (Hanks only presented two plots—one for $n = 1.0$ and the other for $n = 0.7$). The body of data that Heywood and Cheng used was—by their own admission—limited, so they were unable to draw any definite conclusions from it.

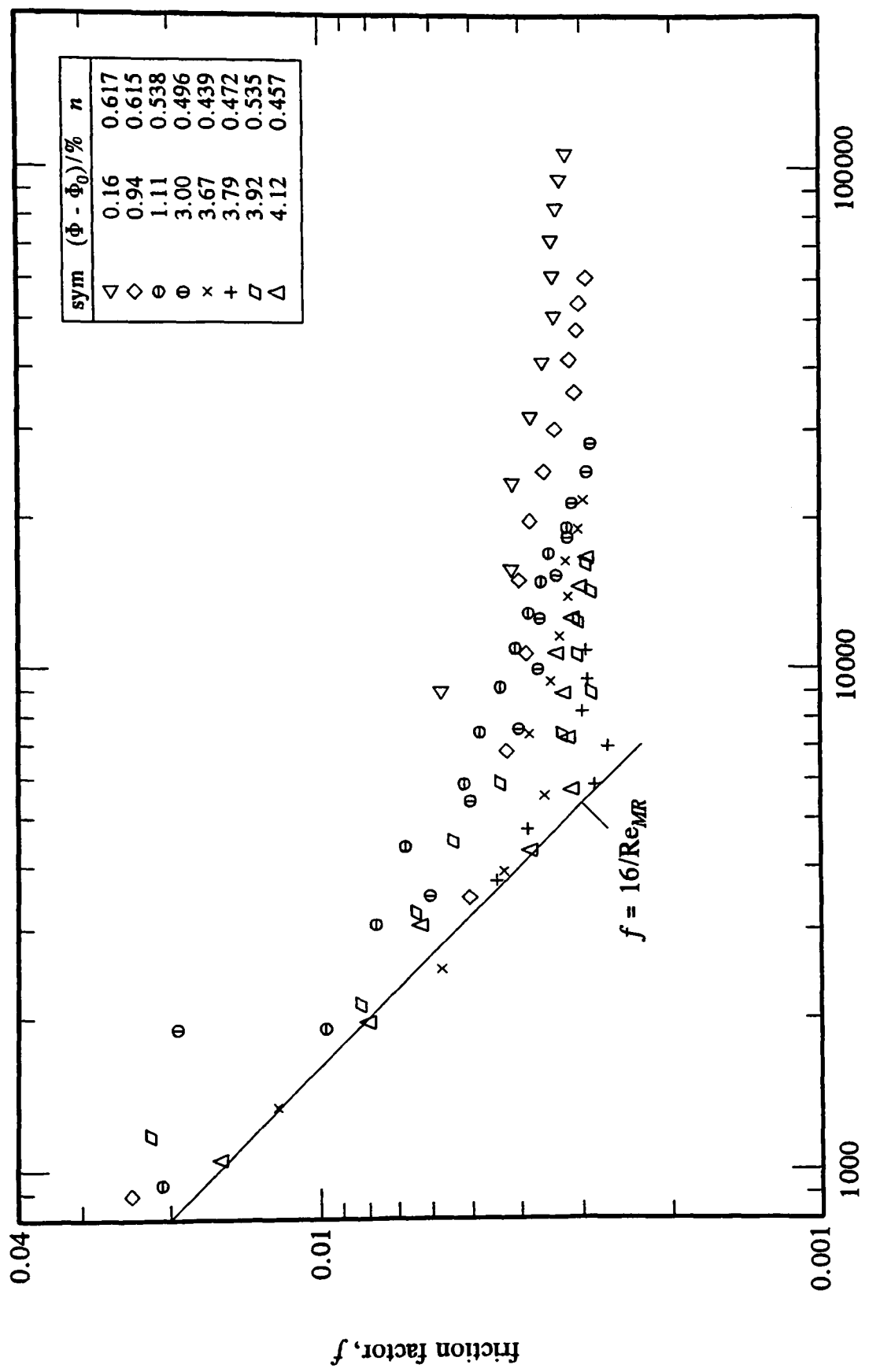


**Figure 7-42** Primary sludge: Metzner-Reed friction plot of laminar and turbulent flow with varying volume percentage of solids and consistency index.

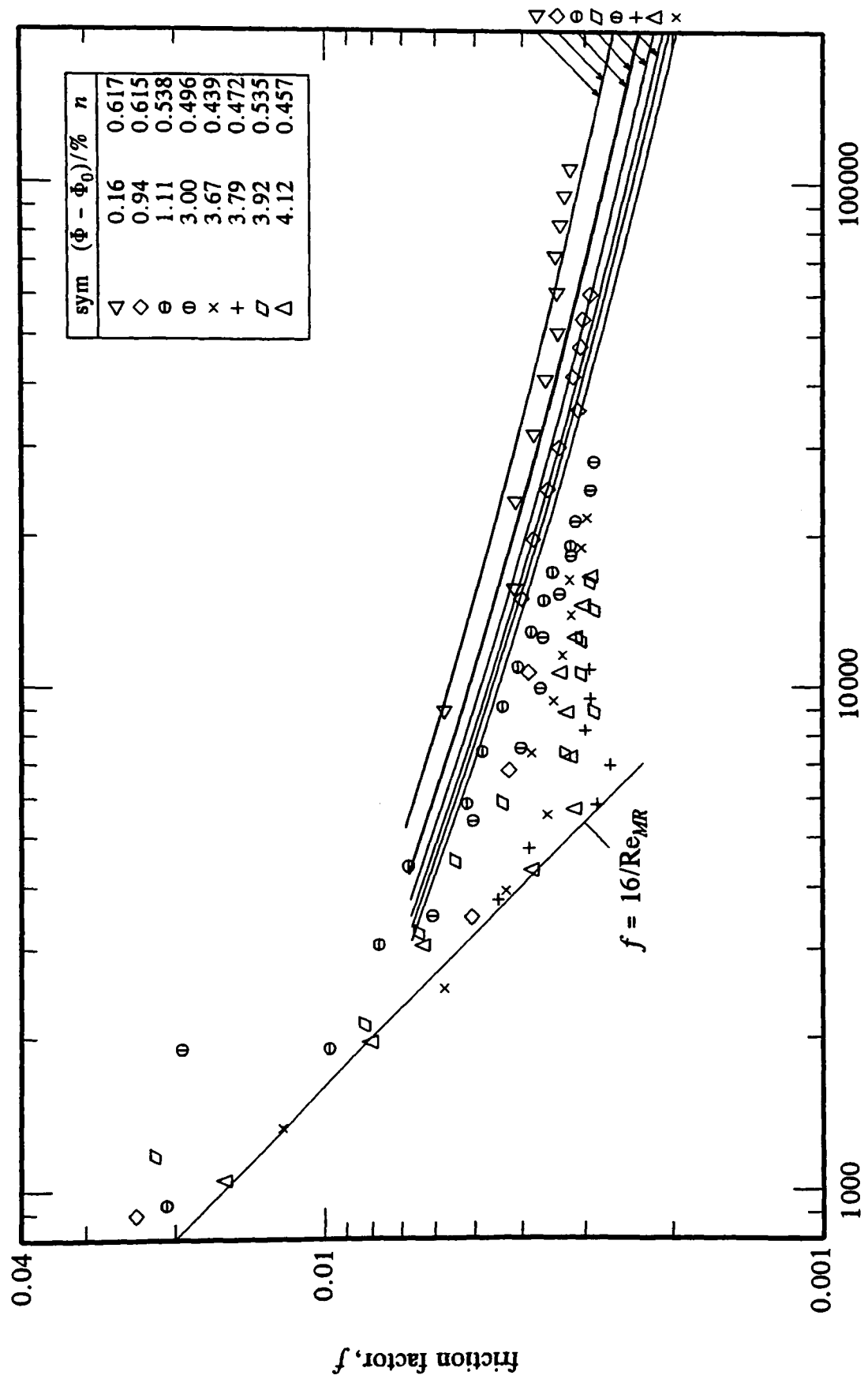


**Figure 7-43** Primary sludge: Dodge-Metzner prediction curves of turbulent flow with varying volume percentage of solids and consistency index.

## 7.5 Conclusions

In this chapter, a large body of concentrated sewage sludge flow data[10] was analysed with the objectives of obtaining laminar, critical and turbulent flow models for each of the primary, activated and digested sludge types. For laminar flow, the three parameter general Bingham model (7.1) was found to fit excellently to all of the sound tube flow data. For the activated and digested sludges, all of the three parameters were tested to be significant, but for primary sludge, the yield stress parameter $\tau_y$ was tested to be insignificant, so the power law model (7.2) was found to be appropriate. Residual analysis was conducted showing that log versions of the general Bingham (7.6) and power law models gave a much better spread of standard errors between each fit than ordinary versions. Critical flow analysis based on the Ryan and Johnson stability parameter[54] was conducted on the data. Critical flow predictions were very good for activated and digested sludges, but no good for primary sludges. No alternative critical flow model for primary sludge was considered, and since the turbulent flow model proposed by Hanks[26] depends on critical flow predictions, turbulent flow analysis of primary sludge was excluded. To concur with the laminar flow analysis, the log version of the turbulent flow model was used. With just one fitting parameter, the turbulent flow model gave a good fit to the turbulent flow data of the activated and digested sludges. In the final section, friction plots were presented to show that the laminar flow relation $f = 16/\mathrm{Re}_{MR}$ held true for activated and digested sludge, but not for primary sludge. The turbulent flow model with one fitting parameter represented the turbulent flow data far better than any of the other widely used methods in the literature.

# 8 Effect of Solids Concentration

In Section 3.6, plots of sewage sludge flow data revealed the striking effect that solids concentration could have on sewage flow behaviour; a full investigation of this effect—both laminar and turbulence—is the subject of this chapter, where the associated error analysis is included. Shear flow models are derived with zero, one, or two user-fitting parameters with the respective reduction of error that each parameter is likely to yield. (The more parameters the user fits to a model, the smaller the associated error of the model is likely to be.) This chapter draws heavily on the data analysis of the previous chapter.

## 8.1 Laminar Flow

Section 7.1 discussed some extensive data analysis of laminar sewage sludge flow through a straight pipe. Statistical analysis revealed that the shear flow behaviour of activated and digested sludges was well modelled using the log version of the three parameter general Bingham model,

$$\log_{10}(\tau - \tau_y) = \log_{10}K + n\log_{10}\dot{\gamma}, \tag{8.1}$$

whereas primary sludge was well modelled using the log version of the two parameter power law model,

$$\log_{10}\tau = \log_{10}K + n\log_{10}\dot{\gamma}. \tag{8.2}$$

Although these models have proved suitable for the sludges of *this* research, would they be suitable for *any* digested, activated or primary sludge? This is a key question without a definite answer, though it would be difficult to believe that Equation (8.1)—with all its three parameters—would not model any sludge; this conjecture has been sustained by a considerable amount of data. The objectives of Section 7.1 were not merely to suggest models for the sludges, but to actually estimate the parameters $\tau_y$, $K$, and $n$ of these models. Because these estimates are sludge specific, they are worthless as they stand. However, the estimates of each parameter can be used to suggest an empirical relation with sludge solids concentration. These relations would then admit generalised versions of Equation (8.1) and (8.2) each as a function of solids concentration.

Significant effects on the viscosity of sewage recognised in Section 3.4 are those of time-dependency. Since the data include no quantitative assessment of these effects, only the qualitative assessment is possible; it is effects such as these that dominate the overall error of a generalised model. One general observation made about time-dependency, however, was that agitated sludge is never more viscous than rested sludge. A model is, of course, intended for practical use. For equipment design purposes, for example, it would be wise

to be conservative about the viscosity of the sludge. Unlike the previous chapter which appraised all of the sound data, the analysis of this chapter will only consider sludge samples at their least agitated. This means that the generalised models are only to be based on tube flow tests taken *before* their respective pipe trials, or more specifically, the first tube flow test of any trial.

### 8.1.1 Effect of Sludge Type

Three general sewage sludge types were identified in Section 3.2 as primary, activated and digested. This is a simplification of the true situation as there are hybrid types and other possible types. Since three distinct types are given, it seems appropriate to develop three generalised models relating to each corresponding type. The possibility must be examined that the types are related enough to unite them into a single generalised model. However, the analysis so far suggests that the three parameter general Bingham model is suitable for activated and digested sludges, whereas the two parameter power law model is suitable for primary sludge; this is not a good premise for uniting them.

Referring back to Section 3.6, the one quantifiable sludge variant of the data that was shown to have a dramatic effect on the viscosity of sewage was solids concentration by mass; this effect must therefore be included in any generalised model. Since it is possible to calculate the volumetric concentration from the data, this may be used in preference to the mass concentration—an idea that will be considered.

### 8.1.2 Effect of Volume Fraction of Solids

In Section 3.6, the solids concentration by mass of a selection of tube flow data was shown to have a marked effect on sewage sludge. There is the question as to whether the solids concentration by volume would not be more suitable for a generalised model. In Chapter 2, Einstein's equation [37] for a suspension of spheres was given as

$$\mu_m = \mu_l(1 + 2.5\,\Phi), \tag{8.3}$$

where $\mu_m$ is the viscosity of the suspension, $\mu_l$ is the viscosity of the liquid, and $\Phi$ is the volume fraction of solids to liquid. This model is limited to Newtonian sludges of solids concentration no greater than one percent by volume. Einstein's equation, which is based purely on theory, has been experimentally verified. This suggests that, since the theoretically derived Newtonian sludge model is based on a volumetric concentration rather than a mass concentration, then an empirically derived non-Newtonian model should also be. While there is some conjecture to the argument, it is our defense for using volumetric concentration rather than mass concentration. The relation [85] between volume fraction of solids $\Phi$ and

mass percentage of solids $C_w$ in terms of the measured values of the test data is given by

$$\Phi = \left[ \frac{C_w}{100} - 1 \right] \frac{\rho_m}{\rho_l} + 1, \tag{8.4}$$

where $\rho_m$ and $\rho_l$ are the densities of the mixture (sludge) and liquid (water) respectively.

A short computer program was written to use Equation (8.4) to find the absolute volume fraction ranges of the laboratory data[10]. For each sludge type, the results are given in Table 8-1; these give the required volume fraction ranges for which the generalised models will be operable. There is an interesting admission about the lower values of ranges as they are actually the *critical volume fractions* (which have nothing to do with critical flow). A critical volume fraction defines the Newtonian/non-Newtonian boundary where the sludge is Newtonian for lower concentrations and non-Newtonian for higher concentrations. The critical volume fractions of Table 8-1 are quoted from the Water Research Centre[91].

**Table 8-1** Applicable ranges of volume fractions for the generalised models. The lower values signify Newtonian/non-Newtonian critical concentrations.

| Sludge | Volume fraction range, $\Phi_0$ - $\Phi_{max}$ |
|---|---|
| Digested | 0.015 - 0.104 |
| Activated | 0.010 - 0.036 |
| Primary | 0.020 - 0.072 |

The analysis of the generalised models shall be performed using the corrected volume fraction $\Phi - \Phi_0$, which is the measured volume fraction corrected by its corresponding critical value. The next stage of the analysis involves relating each of the shear flow function parameters to solids concentration. In the previous chapter, the chosen shear flow function for a digested or activated sludge was the general Bingham model, and for a primary sludge, the power law model. These collectively have the parameters $\tau_y$, $K$ and $n$, so noting that the volume fraction is corrected by its critical value, we seek relationships of the form

$$\tau_y = \tau_y(\Phi - \Phi_0), \tag{8.5}$$

$$K = K(\Phi - \Phi_0), \tag{8.6}$$

$$n = n(\Phi - \Phi_0). \tag{8.7}$$

These relationships are to be empirical, so the obvious first step is to plot them from the results of Section 7.1. The volume fraction plots of $\tau_y$, $K$ and $n$ are shown by Figures 8-1, 8-2 and 8-3 respectively; for comparison, all three sludge types (primary, activated and digested) are included on the plots.

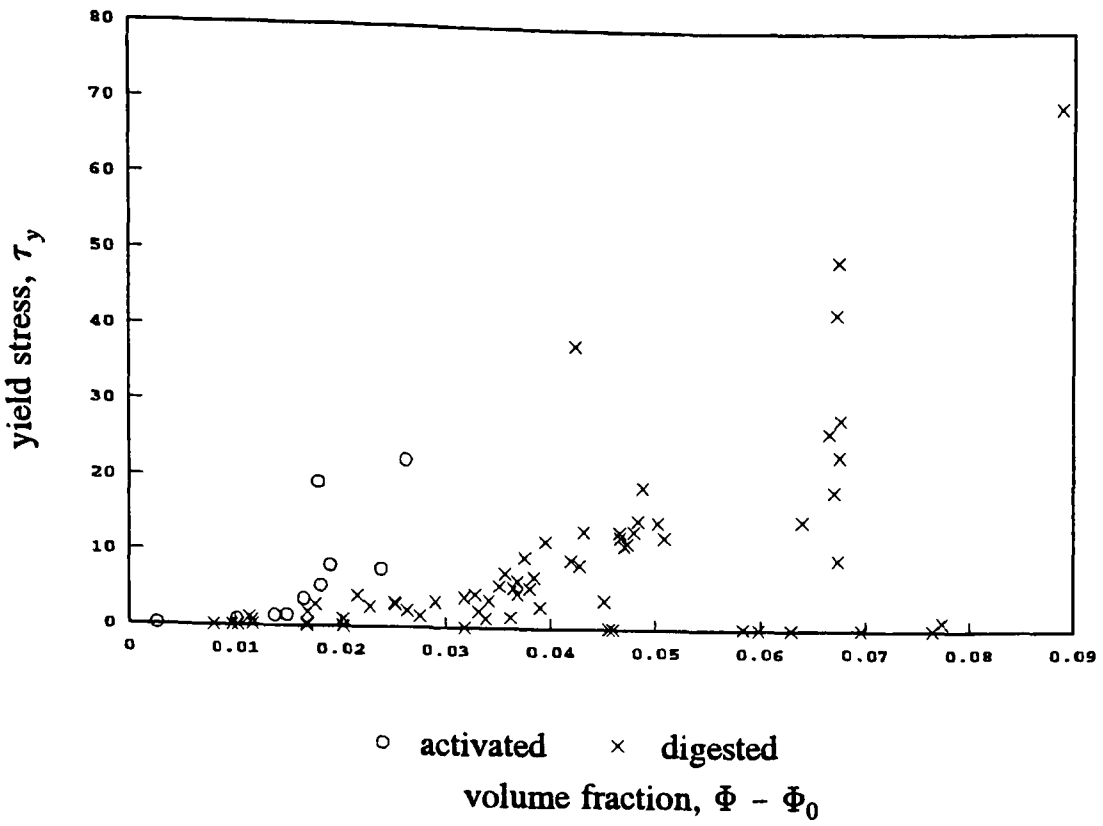


**Figure 8-1** Variation of yield stress with volume fraction for activated and digested sludges.

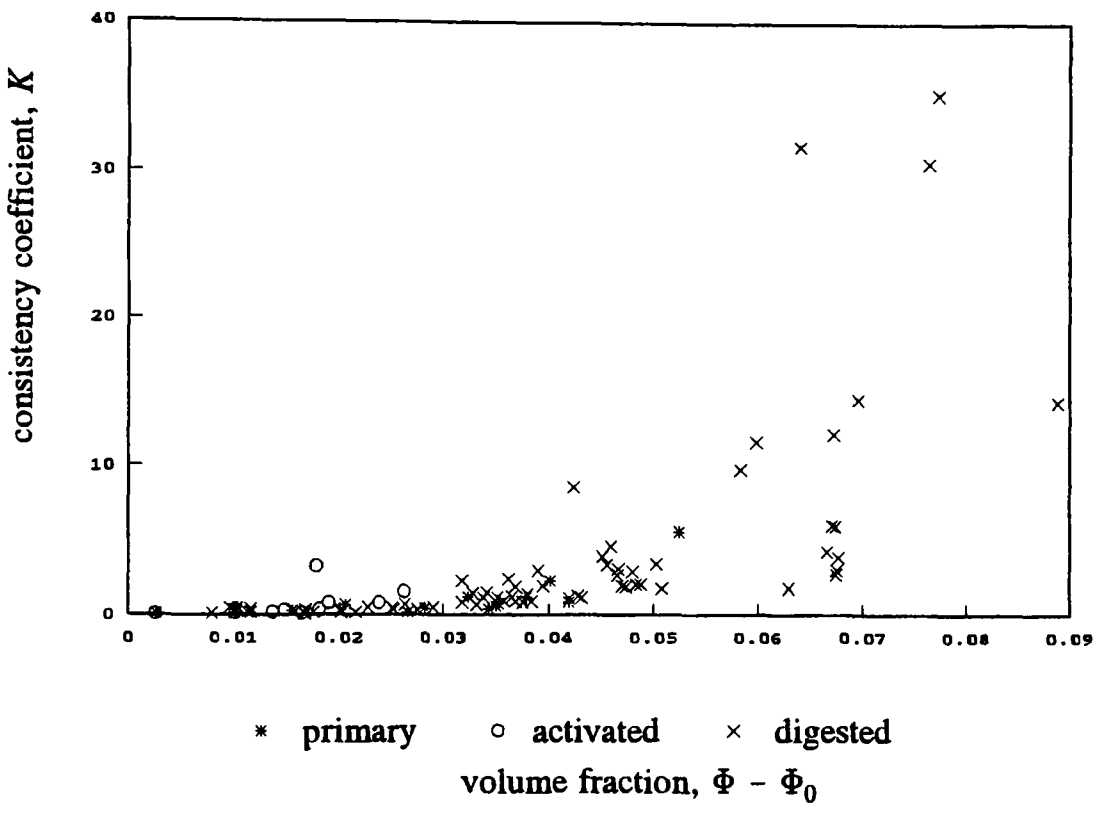


**Figure 8-2** Variation of consistency coefficient with volume fraction for all sludge types.

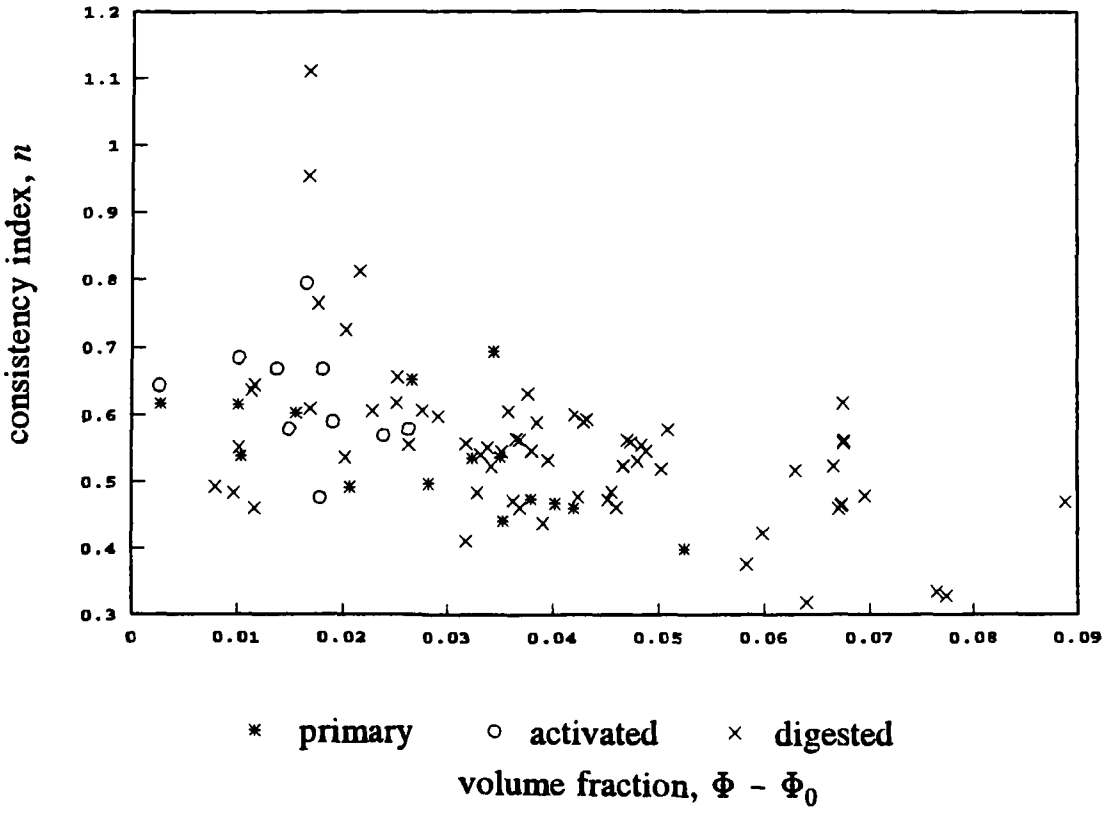


**Figure 8-3** Variation of consistency index with volume fraction for all sludge types

It is important to appreciate that these plots show the general trend of the parameters with volume fraction, but say nothing about the error of a general model. This is because there may be covariation between the parameters, and the extent of this covariation is unknown at this stage. It may, for instance, transpire that considerably different estimates of $\tau_y$, $K$ and $n$ give similar predictions, or conversely that a prediction is very sensitive to parameter variation. These plots, however, provide a very convenient starting point—a means to an end—for generalised modelling.

In Section 7.1, it was concluded that there was no significant yield stress for primary sludge, thus Figure 8-1 excludes primary sludge from the plot. The figure suggests some increase of yield stress with volume fraction, and there appears to be some difference between the increases for activated and digested sludges. For Figure 8-2, there is a dramatic increase of consistency index with volume fraction. Apart from showing such dramatic increases, Figures 8-1 and 8-2 are not very informative since the values are clustered about the origin. This suggests that a transformation is appropriate.

Figure 8-3 shows the variation of consistency index with volume fraction. The trend of the curve shows a decrease of consistency index with volume fraction demonstrating—as one would expect—that the fluid becomes progressively more pseudoplastic for increasing volume fraction of solids. In theory, the sludge should be Newtonian taking a value of $n = 1$ on the vertical axis. From Figure 8-3 this is far from conclusive, but it would be convenient to define an empirical function this way. This would not be erroneous considering that much of the variation for this plot would be due to the covariation property discussed earlier.

The next stage of the analysis is to seek transformations that linearise the values (the term 'linearise' is strictly improper, but its use here means 'form a straight line'). The transformations of the yield stress and consistency coefficient values are log-log and log-linear in both cases, which are shown on Figures 8-4 to 8-8. It can be seen from the four figures that, for both yield stress and consistency coefficient, it is the log-log transformation that linearises the values. This observation is a little tenuous (its weakness is revealed by considering the activated sludge plots); nevertheless, these empirical relations are suitable enough considering their limitations. The consistency index values of Figure 8-3 appear to have a relationship with volume fraction of the form $n(\Phi - \Phi_0) = 1/(1 + \alpha(\Phi - \Phi_0)^\beta)$ where $\alpha$ and $\beta$ are the parameters of the model. For this to be true, it would be expected that a plot of $\log(1/n - 1)$ against $\log(\Phi - \Phi_0)$ would be linear. Such a plot is shown by Figure 8-6 where there is, questionably, a linear trend to the values. This is good enough for our requirements, considering the earlier discussion about the covariation between the parameters.

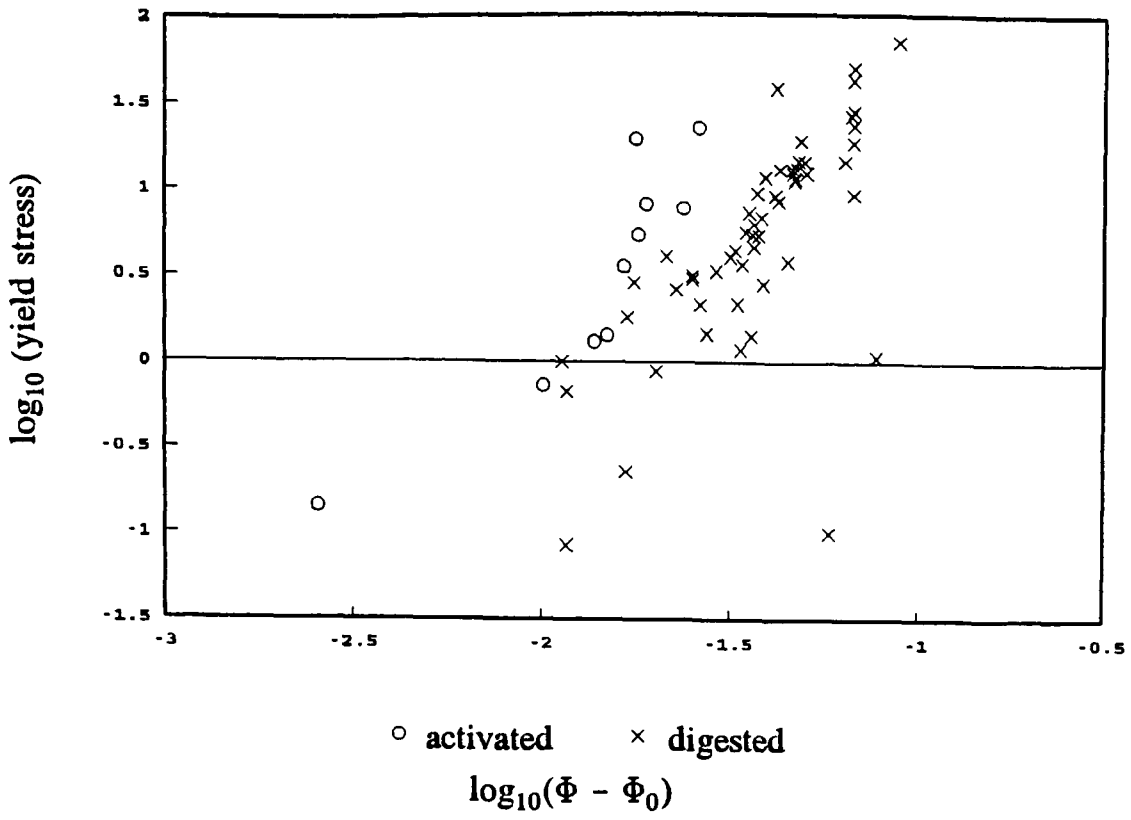


**Figure 8-4** Variation of log yield stress with log volume fraction for activated and digested sludges.

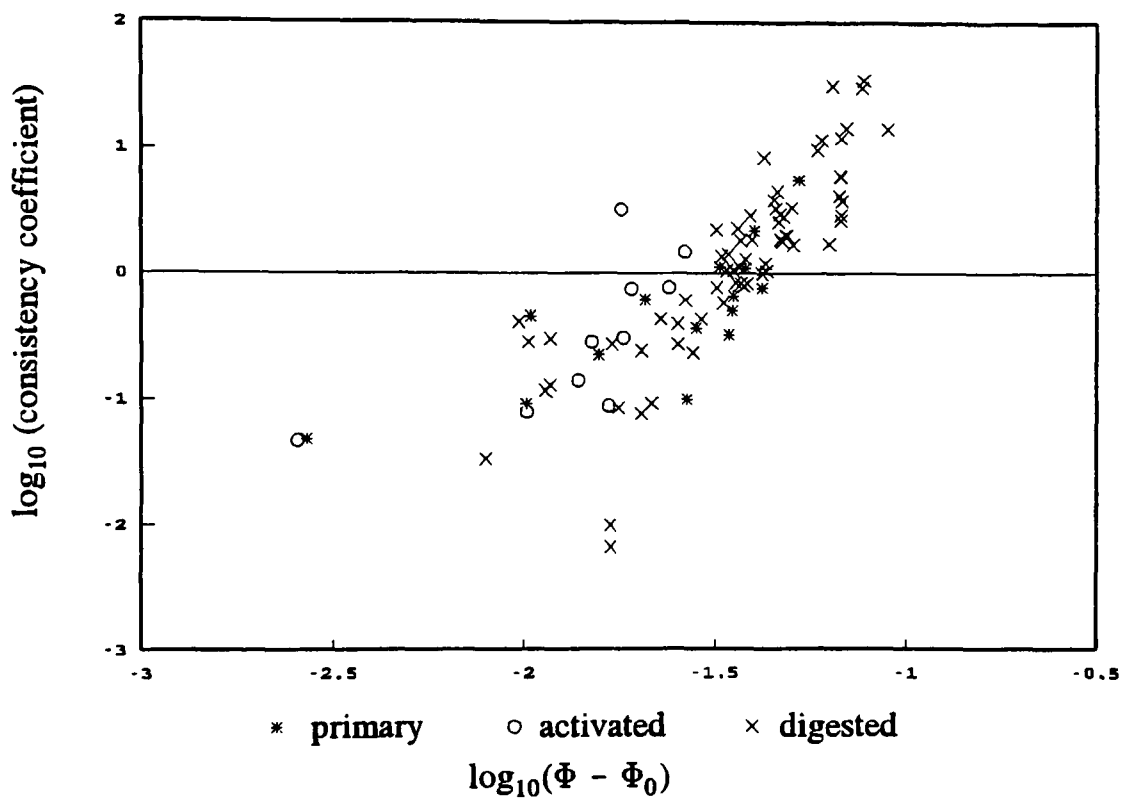


**Figure 8-5** Variation of log consistency coefficient with log volume fraction for all sludge types.

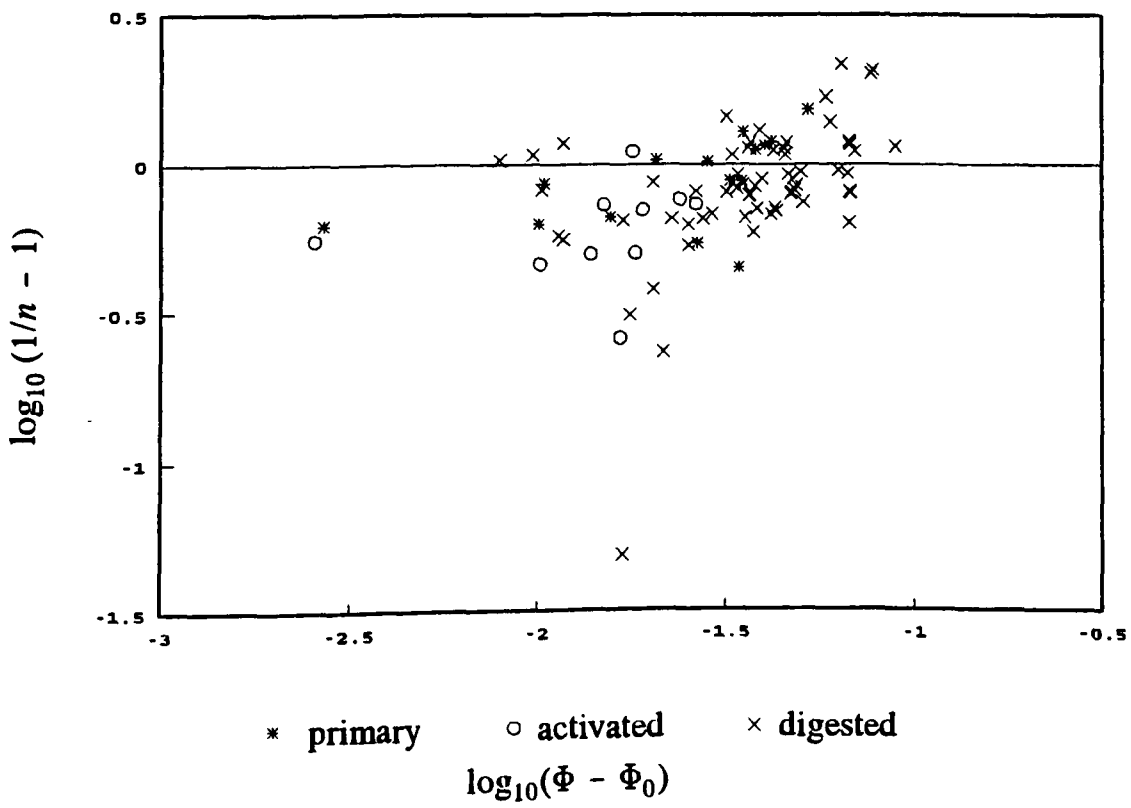


**Figure 8-6** Variation of log $(1/n - 1)$ with log volume fraction for all sludge types.

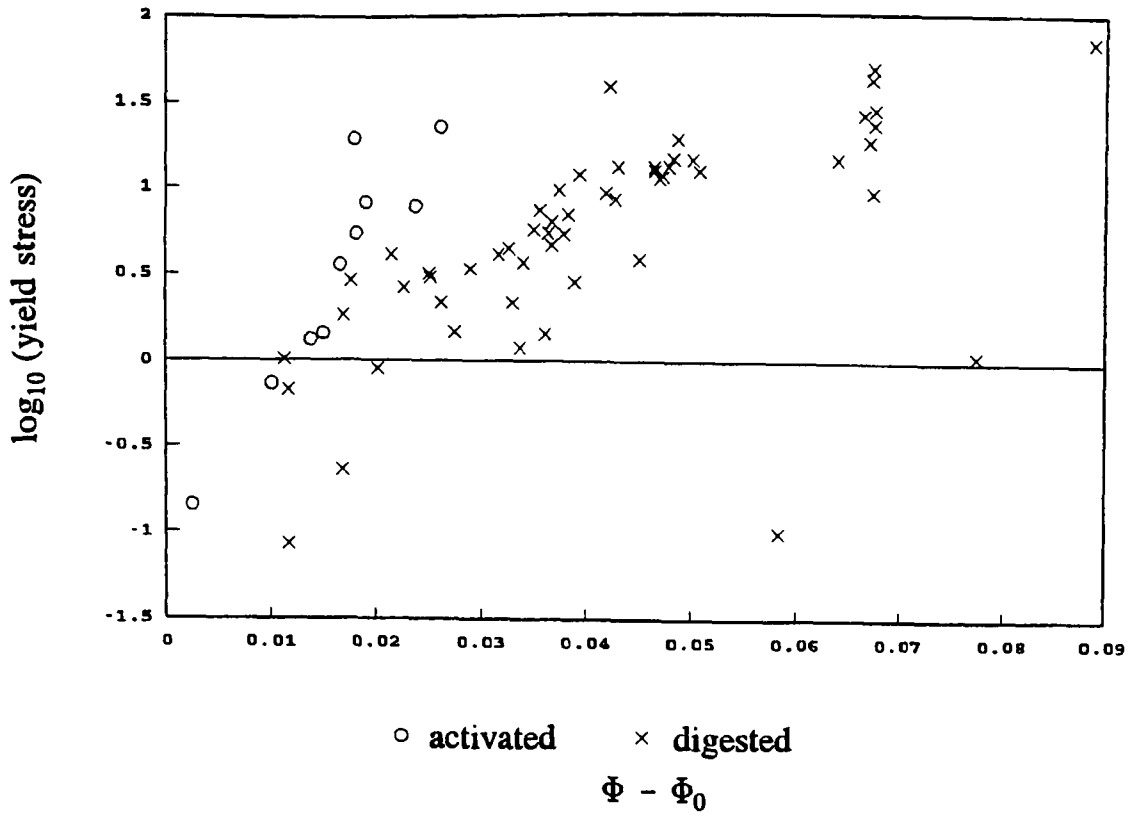


**Figure 8-7** Variation of log yield stress with volume fraction for activated and digested sludges.

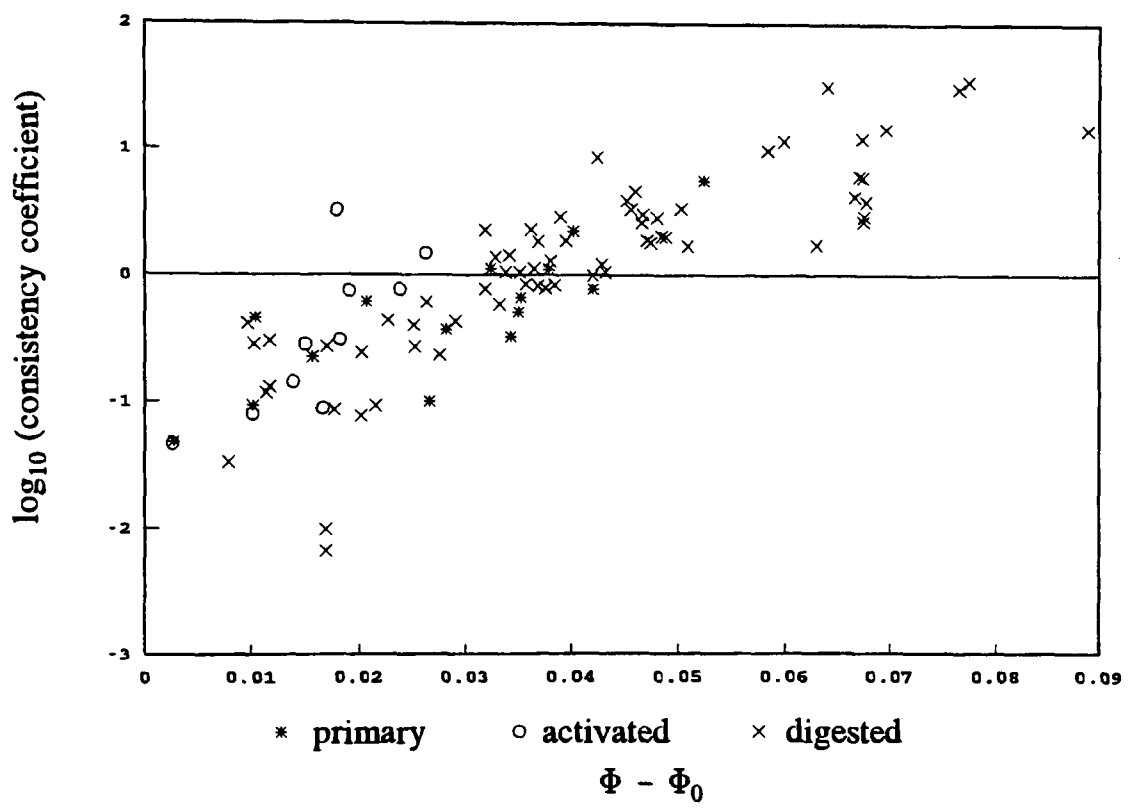


**Figure 8-8** Variation of log consistency coefficient with volume fraction for all sludge types.

Having linearised the parameter values, these now give the following three empirical relationships for each parameter with volume fraction:

$$\tau_y = \alpha_1(\Phi - \Phi_0)^{\alpha_2}, \tag{8.8}$$

$$K = \alpha_3(\Phi - \Phi_0)^{\alpha_4}, \tag{8.9}$$

$$n = \frac{1}{1 + \alpha_5(\Phi - \Phi_0)^{\alpha_6}}, \tag{8.10}$$

where $\alpha_k$, $k = 1,...,6$ are six new parameters of the generalised model. Initial estimates of these parameters are obtained by performing linear regression [83] on the values of Figures 8-4, 8-5 and 8-6 respectively, and are shown in Table 8-2.

**Table 8-2** Parameter estimates for Equations (8.8) to (8.10)

| Sludge Type | Parameter estimate | | | | | |
|---|---|---|---|---|---|---|
| | $\alpha_1$ | $\alpha_2$ | $\alpha_3$ | $\alpha_4$ | $\alpha_5$ | $\alpha_6$ |
| Digested | $1.671 \times 10^4$ | 2.409 | $7.454 \times 10^3$ | 2.617 | 2.407 | 0.3080 |
| Activated | $1.392 \times 10^7$ | 3.683 | $1.958 \times 10^5$ | 3.229 | 6.339 | 0.5837 |
| Primary | — | — | $1.048 \times 10^2$ | 1.452 | 2.032 | 0.2254 |

Earlier in this subsection, it was pointed out that, below some critical volume fraction of solids, ie for $\Phi < \Phi_0$ where $\Phi_0$ depends on the sludge type, the sludge is Newtonian. In this research, the volume fraction of solids has been adjusted by its critical value so that, for instance, the yield stress is zero at $\Phi = \Phi_0$. Other researchers have not done this, probably because critical values were unavailable. For a broad range of materials, Thomas [39] proposed a relationship between yield stress and volume fraction of solids as

$$\tau_y = a\Phi^3. \tag{8.11}$$

This relation is cubic and compares to our indices of about 2.4 and 3.7 for digested and activated sludges respectively (see $\alpha_2$ of Table 8-2). The index of 3.0 proposed by Thomas lies between these two values, though a direct comparison is not possible in light of the critical volume fraction. The one thing that emerges from Figure 8-4 is that the two sludge types of this research have different gradients so, unlike the Thomas relation, cannot be represented by a unique index.

As discussed in Chapter 1, modelling of sewage sludge has often focused on the two parameter Bingham model rather than the three parameter general Bingham model used for this research. However, both models contain a yield stress term, so any yield stress relationship with volume fraction can be compared. This assumes that yield stress is independent of the type of model fitted, but if this were not the case, then the model would anyhow be unsuitable. Other parameters between the Bingham and general Bingham model cannot be compared.

For activated sludge taken from three different plants, Dick and Ewing [40] obtained linear relations between yield stress and volume fraction on log-linear plot. This suggests the following relationship:

$$\tau_y = b\Phi^c. \tag{8.12}$$

Judging by Figure 8-7, the activated sludge data are more or less linear on a log-linear scale, implying that the model would have been suitable for this research as well, though this would not have been true of digested sludge. Dick and Ewing's figure reveals different slopes for each of the three plants; the parameter $c$ in the above relation is therefore different in each

case. For this research, all of the activated sludge samples have been grouped together, and the same goes for the primary and digested sludges as well. This has been necessary to achieve the final goal of generalised models.

Mulbarger *et al*[3] also offer a log-linear plot of $\tau_y$ against $\Phi$ for primary, secondary and digested sludges. There is considerable scatter in their data, and the overall trend is not linear, but similar to that offered by Figure 8-7. However, there is a difference: primary sludge has been included on their plot, but there is no yield stress for the primary sludge of our data. Apart from the primary sludge and taking into account the extra scatter, their curve looks remarkably similar to Figure 8-7. Carthew *et al*[4] supplemented the log-linear plot of Mulbarger with there own data. The data are far less scattered, but only covers the first part of the curve which is almost linear. For the limited data, the exponential model of yield stress would be suitable.

Some of the data used for this research and some of the data used by Frost[8] are the same. Furthermore, the general Bingham model has been used in both cases. Frost estimated the general Bingham parameters through the Mooney-Rabinowitsch equation using a second order approximation on a log-log transformation of the data. In this research, the general Bingham parameters have been estimated through the Mooney-Rabinowitsch equation using a numerical approximation. The similarities and differences of the results are shown on Figure 8-9 where the general Bingham parameters are plotted. The variation of each parameter with solids concentration is very similar in both cases, and it is consoling to find that many points actually or nearly coincide on the plots—these are clearly the points of common data. The second order approximation used by Frost is perfectly suitable for estimating general Bingham parameters. However, for this research, Chapter 6 discussed parameter estimation for any shear flow function so that the analysis could easily be repeated for the parameters of any such function.

### 8.1.3 Generalised Model

It is important to appreciate that the estimates of Table 8-2 are of limited use. These are 'secondary' estimates as they themselves have been derived from other estimates—namely the general Bingham and power law parameters. These estimates are not direct so offer no corresponding error analysis; if these estimates were used for a prediction, there would be no way of obtaining the corresponding magnitude of error for the prediction.

Substituting Equations (8.8) to (8.10) into the log general Bingham model (8.1), the full form of the generalised model becomes

$$q = \log_{10}\alpha_3 + \alpha_4 \log_{10}(\Phi - \Phi_0) + \frac{p}{1 + \alpha_5(\Phi - \Phi_0)^{\alpha_6}}, \qquad (8.13)$$

**Figure 8-9** Comparison of the general Bingham parameters of this research with those of Frost.

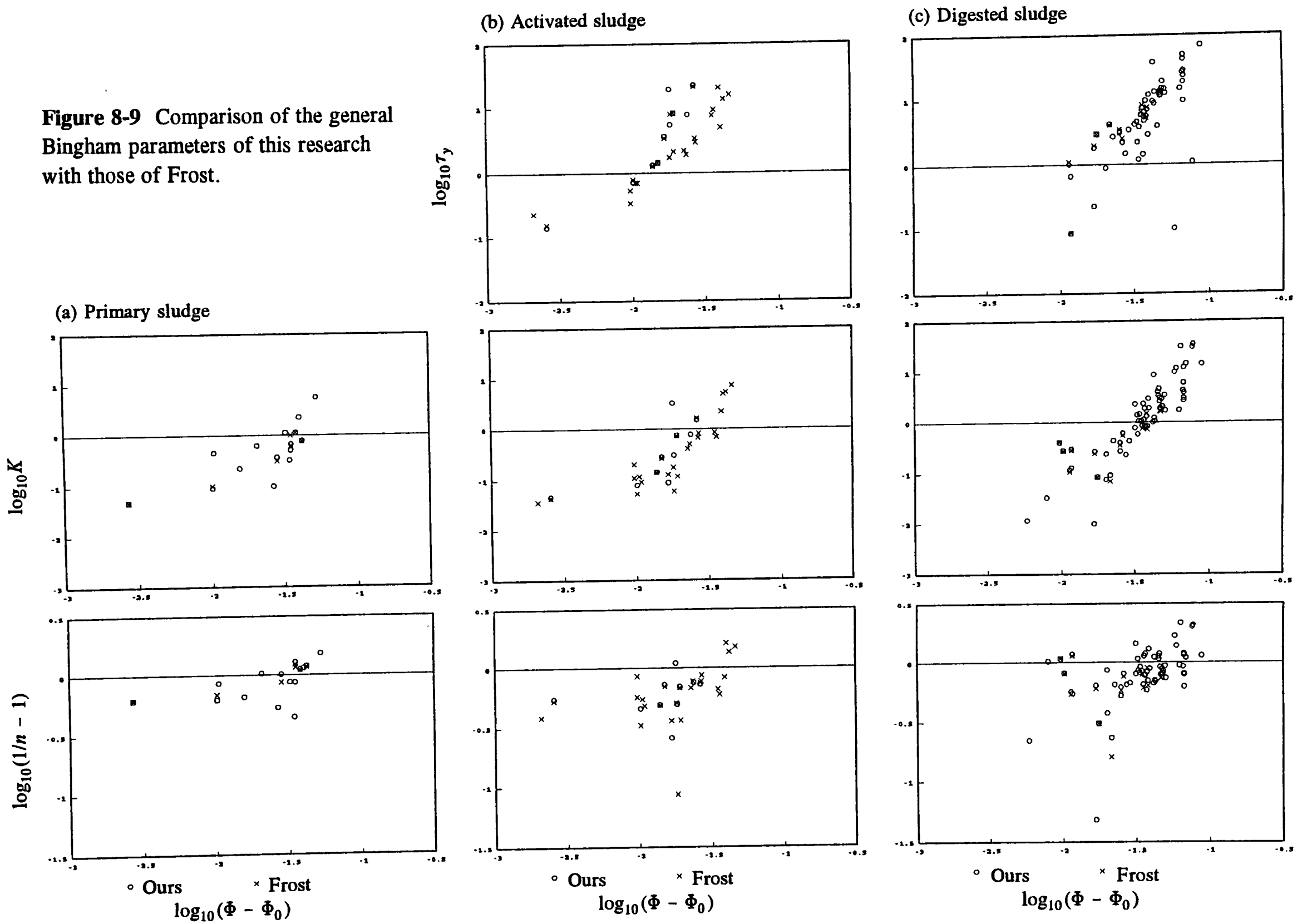

where q and p, the new dependent and independent variables respectively, are

$$q = \log_{10}[\tau - \alpha_1(\Phi - \Phi_0)^{\alpha_2}],$$
$$p = \log_{10}\dot{\gamma}. \tag{8.14}$$

The analysis now involves estimating the parameters $\alpha$ using the least squares method (see Section 6.1) on all of the relevant tube flow data. For each individual sludge sample, the error sum of squares was given by Equation (6.7), but for all $N$ laminar flow sludge samples, the error sum of squares (Section 6.3) is now given by

$$E = \sum_{i=1}^{N} \sum_{j=1}^{M_i} (q_{ij} - \hat{q})^2, \tag{8.15}$$

where the hat denotes a prediction. The objectives are therefore to minimise $E$ with respect to the parameters $\alpha$. It would be a nice idea to fit Equation (8.13) to the data of each sludge type, estimating each of the six parameters using the least squares method, and obtain an overall standard error for each of the models. However, the task would be too difficult and computationally intensive: firstly, there is an enormous amount of data to analyse; secondly, the algorithm includes an encumbering pipe-to-shear transformation; thirdly, there are six parameters to estimate.

It is clear that, since the data can be modelled on fewer than six parameters, this would considerably simplify the problem. A sensible way to proceed is to round off and fix three parameters; the index parameters $\alpha_2$, $\alpha_4$ and $\alpha_6$ of the Equations (8.8) to (8.10). It can be observed from Table 8-2 that the parameters $\alpha_2$ are very similar to $\alpha_4$ for the activated and digested sludges (primary sludge has no $\alpha_2$ parameter). The implication behind this observation is that yield stress $\tau_y$ and consistency coefficient $K$ are linearly related. To check this assumption, $\tau_y$ was plotted against $K$, but since many of the points were bunched up at the origin, it was difficult to tell. However, if the relationship between $\tau_y$ and $K$ is linear, then it also follows that the log-log relationship of these two parameters has a gradient of one. This assumption is verified by Figure 8-10 where, for comparison, an arbitrarily placed line of gradient one has been included. From Table 8-2, ensuring that $\alpha_2 = \alpha_4$ for each sludge type and rounding to the nearest half, the parameters $\alpha_2$, $\alpha_4$ and $\alpha_6$ are fixed to the values given in Table 8-3.

**Table 8-3** Fixed, rounded estimates for index parameters of Equations (8.8) to (8.10)

| Sludge Type | Parameter estimate | | |
|---|---|---|---|
| | $\alpha_2$ | $\alpha_4$ | $\alpha_6$ |
| Digested | 2.5 | 2.5 | 0.5 |
| Activated | 3.5 | 3.5 | 0.5 |
| Primary | — | 1.5 | 0.5 |

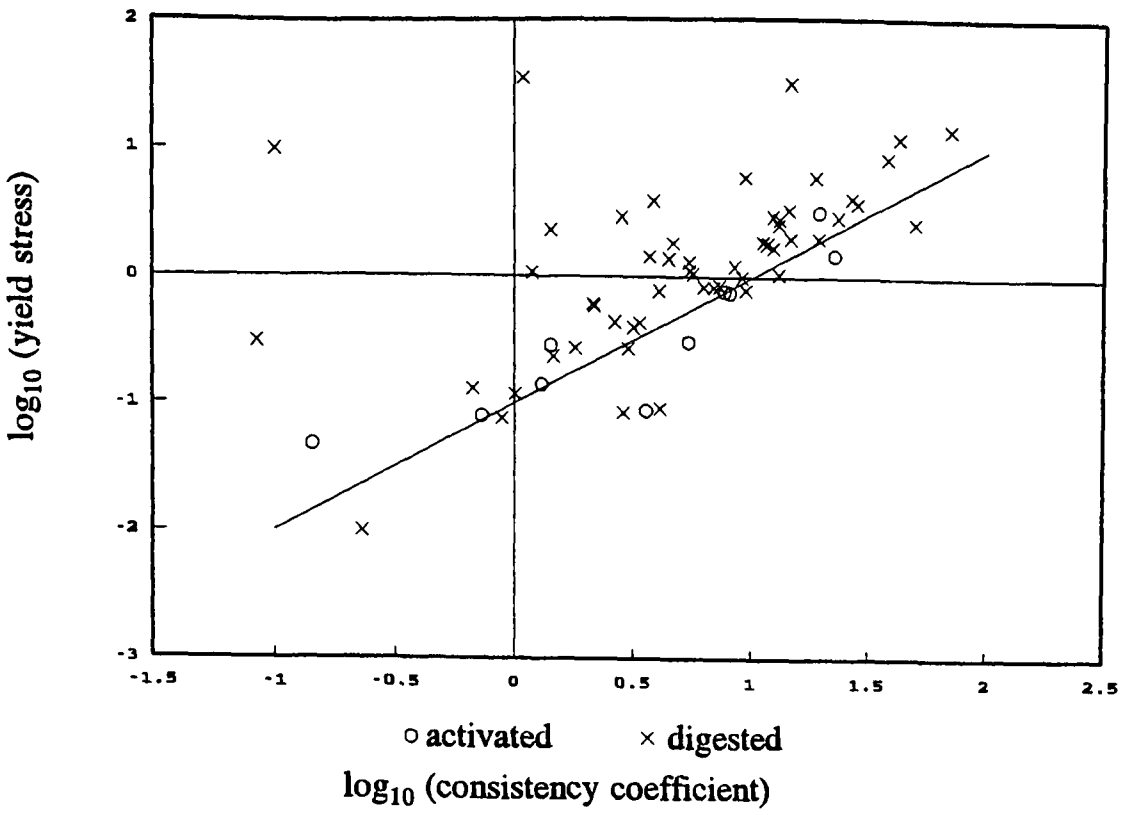


**Figure 8-10** Variation of log yield stress with log consistency coefficient for activated and digested sludges. The line has a gradient of one and the intercept was chosen arbitrarily.

The parameter $\alpha_6$ has been conveniently rounded off to 0.5 in each case. So far, there is only intuitive evidence that these parameters are suitable for a generalised model of each sludge type. A key requirement is that the user can define some parameters of the generalised model with a diminishing standard error for each parameter defined. The first task is to therefore provide a generalised model with all three remaining parameters fitted to the data, thus leaving no parameters for the user to fit. The first model is to include with it the corresponding (and perhaps large) standard error. The next model would have a total of five pre-defined parameters leaving one user-definable parameter and a reduced standard error. A third model would have two user-definable parameters and would perhaps possess the minimum possible standard error.

A full discussion of the algorithm for parameter estimation of laminar flow equations such as Equation (8.13) was given in Section 6.1. The partial derivatives are required of the equation with respect to each of its remaining three fitting parameters. These are given by

$$\frac{\partial q}{\partial \alpha_1} = \frac{-(\Phi - \Phi_0)^{\alpha_2}\log_{10}e}{\alpha_3(\Phi - \Phi_0)^{\alpha_4}10^{p/[1 + \alpha_5(\Phi - \Phi_0)^{\alpha_6}]}},$$

$$\frac{\partial q}{\partial \alpha_3} = \frac{\log_{10}e}{\alpha_3}, \qquad (8.16)$$

$$\frac{\partial q}{\partial \alpha_5} = \frac{-p(\Phi - \Phi_0)^{\alpha_6}}{[1 + \alpha_5(\Phi - \Phi_0)^{\alpha_6}]^2}.$$

A computer program was written to estimate the three fitting parameters for each of the sludge types; the results are given in Table 8-4. Along with the fixed parameters of Table 8-3, they define a generalised model for each of the three sludge types.

**Table 8-4** Least squared estimates for the fixed parameters of Equation (8.13)

| Sludge Type | Parameter estimate $\alpha_1$ | $\alpha_3$ | $\alpha_5$ |
|---|---|---|---|
| Digested | $1.519 \times 10^4$ | $4.335 \times 10^3$ | 3.842 |
| Activated | $5.759 \times 10^6$ | $2.525 \times 10^6$ | 11.345 |
| Primary | — | 97.25 | 4.061 |

## 8.1.4 Error Analysis

The *total* error of a generalised model comes from both *within* a sludge sample and *between* the sludge samples. This equates in terms of error sum of squares (Section 6.3) to be

$$E_T = E_B + E_W. \tag{8.17}$$

An important point to note is that increasing the number of user-definable parameters only decreases the error between the sludge samples but does not affect the error within a sludge sample. The minimum of the total error will therefore come from within the sludge samples.

For a no-parameter model, the standard error came from estimating the parameters of Table 8-3. For the one-parameter model, it has to be decided which parameter to leave as user-definable. The obvious choice is $\alpha_3$ from Equation (8.13) as it is clearly a constant parameter. $\alpha_3$ is fitted to each relevant sludge sample only for the purpose of finding the general standard error of the model. For the two-parameter model, it has to be decided which second parameter to leave as user-definable. The obvious choice is $\alpha_5$ from Equation (8.13) as it is clearly a general curvature parameter. $\alpha_3$ and $\alpha_5$ are fitted to the relevant sludge samples, again only for the purpose of finding the general standard error. Note that $\alpha_1$ would not be a wise choice as a user-definable parameter as this parameter is from the yield stress Equation (8.8), and above all else, primary sludge has no significant yield stress. A computer program was written to fit the one- and two-parameter models to the viscometric data in order to calculate the standard errors. The results are given in Table 8-5.

**Table 8-5** Standard errors for the generalised models

| Sludge Type | Number of user-definable parameters 0 | 1 | 2 |
|---|---|---|---|
| Digested | 0.2940 | $5.901 \times 10^{-2}$ | $1.932 \times 10^{-2}$ |
| Activated | 0.5420 | 0.2012 | $8.106 \times 10^{-2}$ |
| Primary | 0.2491 | $5.323 \times 10^{-2}$ | $2.125 \times 10^{-2}$ |

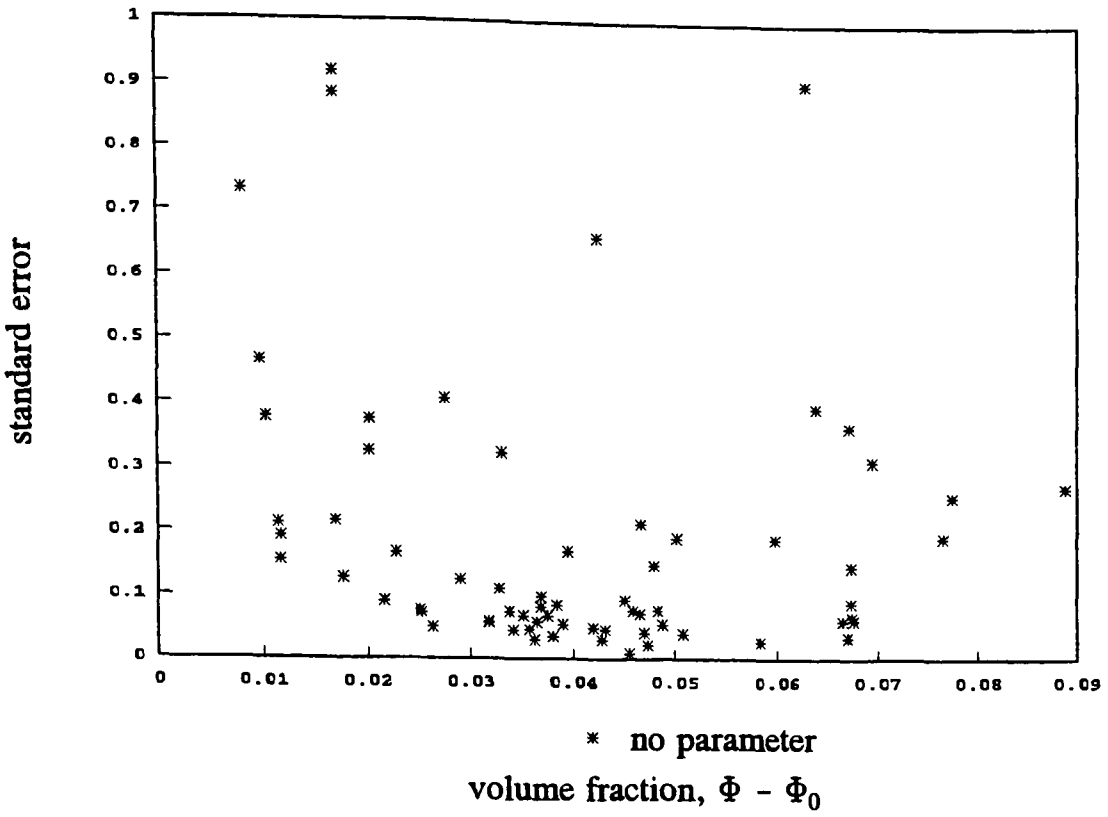


**Figure 8-11**
Expectedly large standard errors of the generalised digested sludge model with no user-fitted parameters.

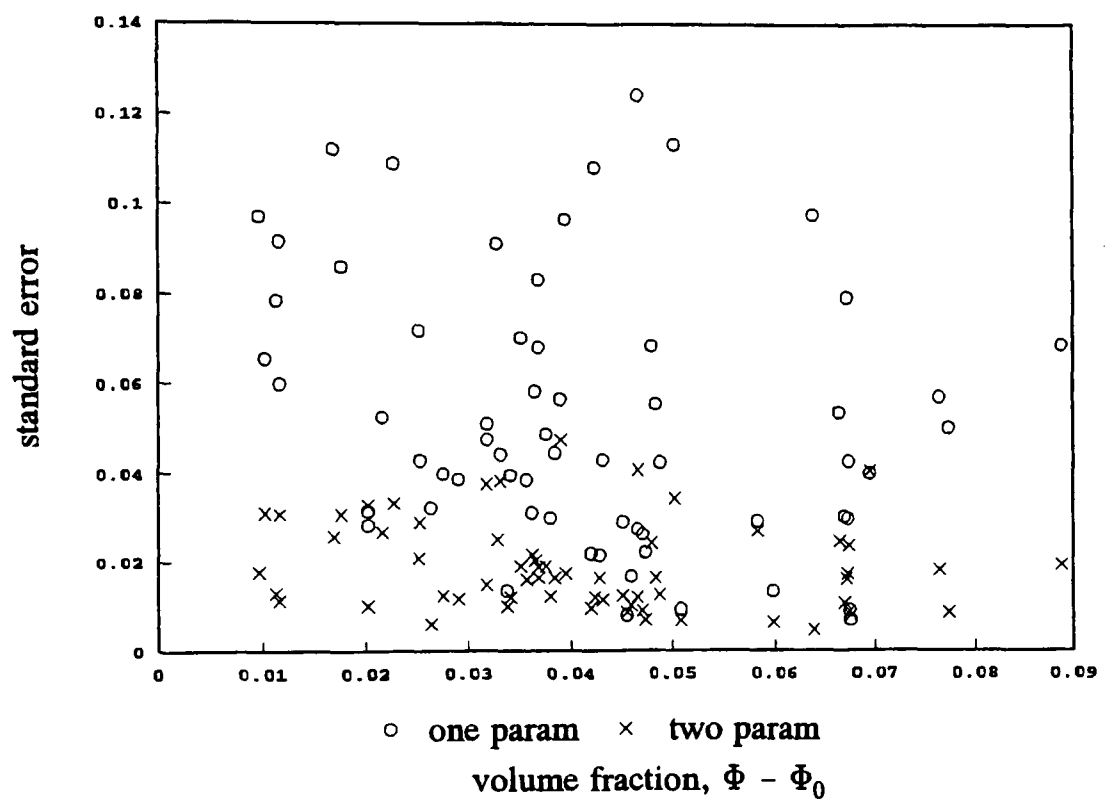


**Figure 8-12** The standard errors of the generalised digested sludge models with one and two user-fitted parameters. Not surprisingly, the two-parameter model has smaller standard errors than that of the one-parameter model.

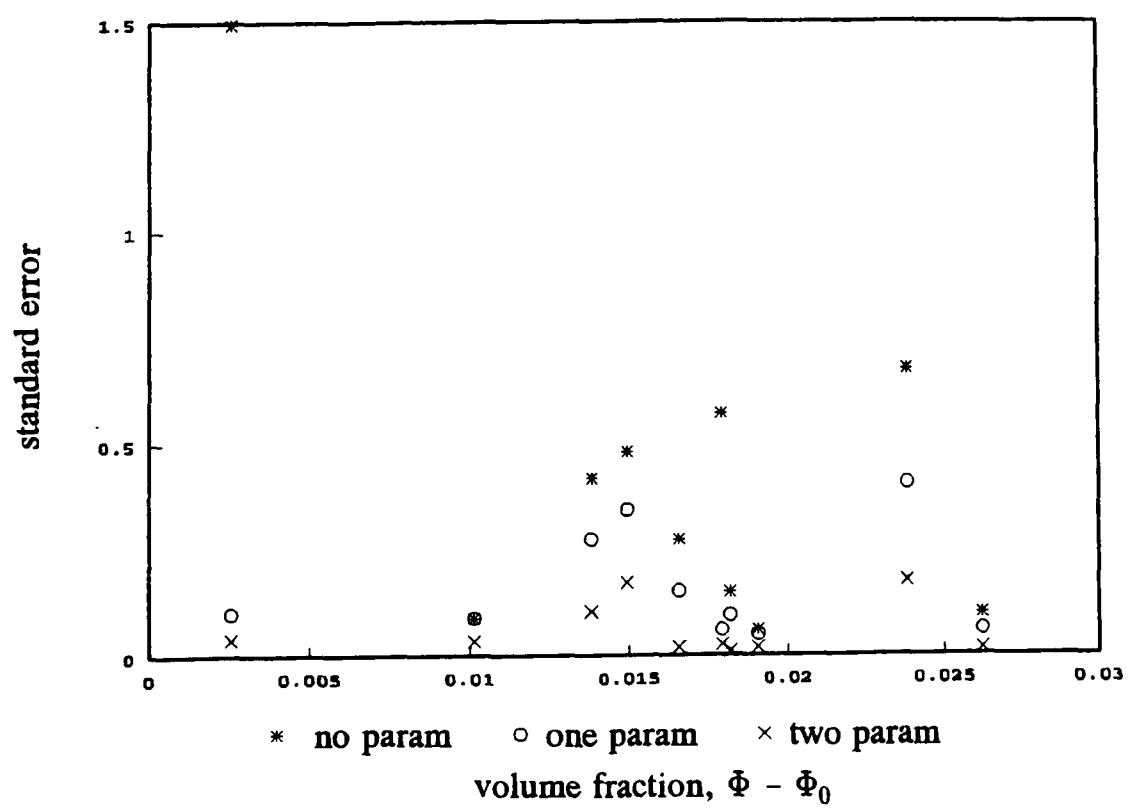


**Figure 8-13** The standard errors of the generalised activated sludge models with no, one and two user-fitted parameters. There is a reduction of standard error with each user-fitted parameter.

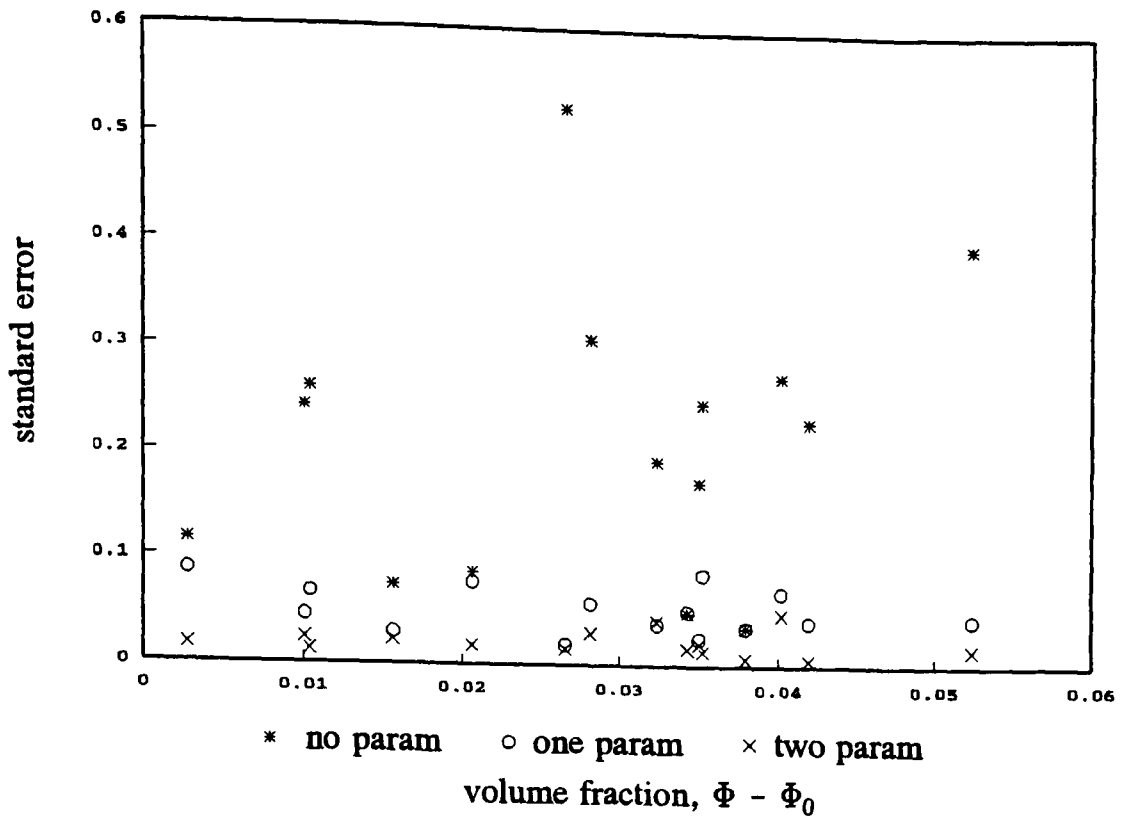


**Figure 8-14** The standard errors of the generalised primary sludge models with no, one and two user-fitted parameters. There is a reduction of standard error with each user-fitted parameter.

Notice that there is a significant reduction of standard error as the number of user-definable parameters increases. However, these errors are global errors for the model and tell nothing of how the error is distributed between each sludge sample. This is shown in Figures 8-11 to 8-14 where the standard errors for the individual sludge tests are plotted. For Figures 8-11 and 8-12—the digested sludge—there is a clear reduction in the standard error for each user-definable parameter. (Figure 8-12 excludes four outliers that distort the spread; these data are, anyhow, of dubious origin as they came from some initial trials.) For the activated sludge, Figure 8-13 shows a similar trend to the digested sludge, but although the standard errors are larger, there are much less data to be certain. The errors of the primary sludge (Figure 8-14) are similar in spread and magnitude to the digested sludge, which is surprising considering the differences between the sludges.

## 8.2 Turbulent Flow

Section 7.3 discussed some extensive data analysis of turbulent sewage sludge flow through a straight pipe. Statistical analysis revealed that the shear flow behaviour of an activated or digested sludge was well modelled using the logarithmic version of a turbulent flow model proposed by Hanks[26]. This is given as

$$\log_{10}(\tau - \tau_y) = \log_{10}(K\dot{\gamma}^n + \rho l^2 \dot{\gamma}^2), \tag{8.18}$$

where the model was fully discussed in Section 4.4. The model contains the three general Bingham parameters $\tau_y$, $K$ and $n$, and the mixing length $l$ contains a turbulence parameter $b$. The model of Hanks is suitable for the laminar-turbulent transitional regime, and is therefore a function of the critical flow conditions. As discussed in Section 7.2, this research was unable to resolve critical flow predictions for primary sludge, so turbulent flow analysis of primary sludge is to be excluded.

In Section 3.4, it was observed that agitated sludge is never more viscous than rested sludge. For practical purposes, it would be wise to be conservative about the viscosity of the sludge. In section 8.1, the laminar flow models were therefore based on tube flow tests taken *before* their respective pipe trials, or more specifically, the first tube flow test of any trial. Turbulent flow will be modelled on the *first* pipe flow test of each trial where the sludge is at its least agitated and closely resembles that of the first tube flow test. The latter point is particularly important for comparing 'scale-up' predictions of different pipe diameters. There is, arguably, some repetition of data since pipe flow tests of the same undiluted sludge had been conducted on different days. However, sludge is such an unpredictable medium that a day can make a significant difference to a result.

### 8.2.1 Effect of Volume Fraction of Solids

To develop a turbulent flow model as a function of volume fraction of solids, $\Phi$, a start can be made by exploring the relationship of the turbulent flow parameter $b$ with $\Phi$. As with the laminar flow modelling of the previous section, the volume fraction of each sludge type, $\Phi$, shall be corrected with its respective Newtonian/non-Newtonian critical volume fraction, $\Phi_0$ (see Table 8-1).

A plot of $b$ against volume fraction for all of the relevant turbulent pipe flow data is given in Figure 8-15. For both sludge types, the results look unusual: both curves gently increase with volume fraction, proceeded by a rapid increase at higher volume fraction. Several attempts have been made to linearise the relation by applying typical transformations —such as the log-log transformation—but without success. An inspection of the figure shows that the curves are very linear with little random variation for most of their range, but at higher values, the points rapidly increase with much more random variation.

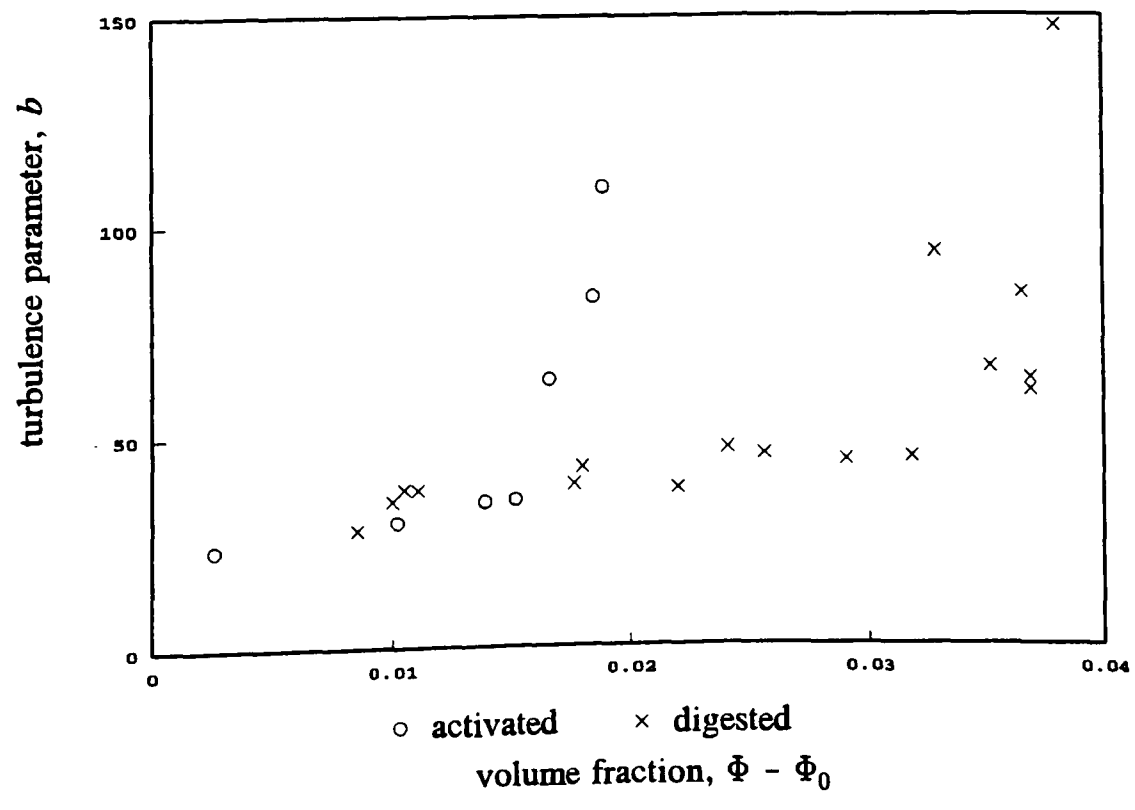


**Figure 8-15** Variation of the turbulence parameter with volume fraction.

Examining Figure 8-15, most of the points on the curves could be well modelled with a linear relationship, and it may be that the model would be valid for the higher values of $b$ on the plot as well. This may give the initial impression of being a ridiculous assumption, but this is not necessarily the case. In Section 7.4, friction plots showed that sludge data of high solids concentration exhibited a considerable amount of scatter. More specifically, the data showed that these sludges did not seem to settle into a laminar or turbulent flow regime—there appeared to be an extended transitional regime. Considering the extreme case where the data remain completely laminar, the mixing length term given by Equation (4.57) would disappear, and this would happen for large values of the turbulence parameter $b$. The most plausible explanation for the large values of $b$ shown in Figure 8-15 is that the flow often becomes unpredictably laminar, and this was borne out by Figures 7-34b and 7-35b. However, for design purposes, an overestimate is preferable to an underestimate, so to be on the safe side, it is best to assume that the thicker sludges develop turbulence earlier rather than later. A conservative estimate of $b$ offered by a linear relation would satisfy this criterion.

Note that the vertical axis of Figure 8-15 is at $\Phi = \Phi_0$ where the sludge is Newtonian (albeit upper bound). The value of $b$ for a turbulent Newtonian fluid was quoted immediately after Equation (2.23) as being 22; this defines the intercept of the line. Ignoring the values that define the steeper part of the curves, linear regression with a fixed intercept[83] is used to find the gradient of the line, which turns out to be 872. The values with this fitted line are shown on Figure 8-16.

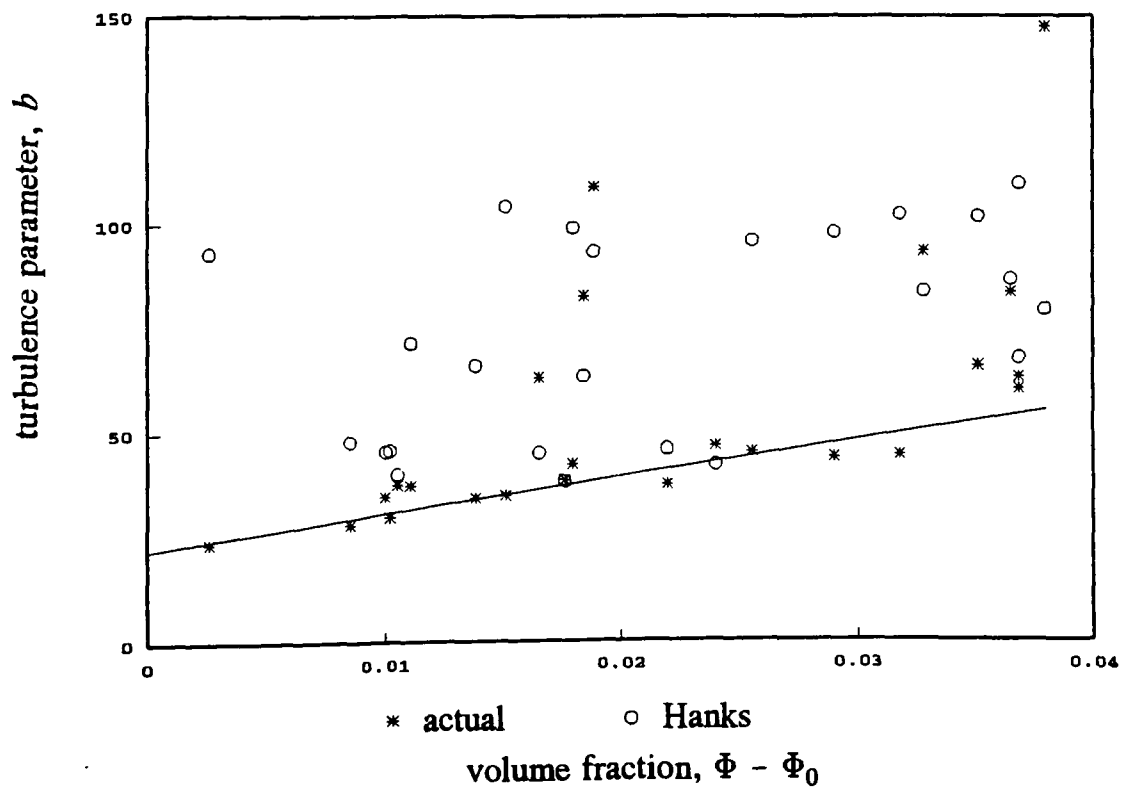


**Figure 8-16** A straight line fit and Hanks' predictions of the turbulence parameters. Hanks' predictions are very poor for these data.

Also included on Figure 8-16 are predictions of $b$ based on the model of Hanks. Most of the predictions are overestimates, so as remarked above, this would translate to underestimates of the final stress predictions (Figure 7-29 clearly supports this reasoning). In

fairness, Hanks tentatively derived $b$ for general Bingham fluids (4.67) by combining $b$ for Bingham fluids (4.61) with $b$ for power law fluids (4.64), but never tested the validity of this assumption on any general Bingham data. For our sludge data, the model of $b$ proposed by Hanks is invalid.

The straight line fit of Figure 8-16 defines a relationship between the turbulence parameter $b$ and the volume fraction of solids $\Phi$ for activated and digested sludges. To assess the effectiveness of the relationship, the standard errors between the raw data and the turbulent predictions must be examined. In particular, the predicted values of $b$ are substituted into the turbulence equations (5.36) to (5.38), and as discussed in Section 5.3, solved for the relevant pipe geometry. A Fortran 77 computer program was written for this purpose, and the results—which took about a minute on an IBM compatible PC with a Pentium processor—are shown on Figure 8-17.

Figure 8-17 admits an interesting result: turbulent flow predictions are sensitive for higher volume fractions of activated sludge, though not for higher volume fractions of digested sludge. Although the straight line fit of $b$ with $\Phi$ is poor for these values, it nonetheless transpires that this does not matter too much for digested sludge. This is not the case for the thicker activated sludges where much unexplained variation prevails.

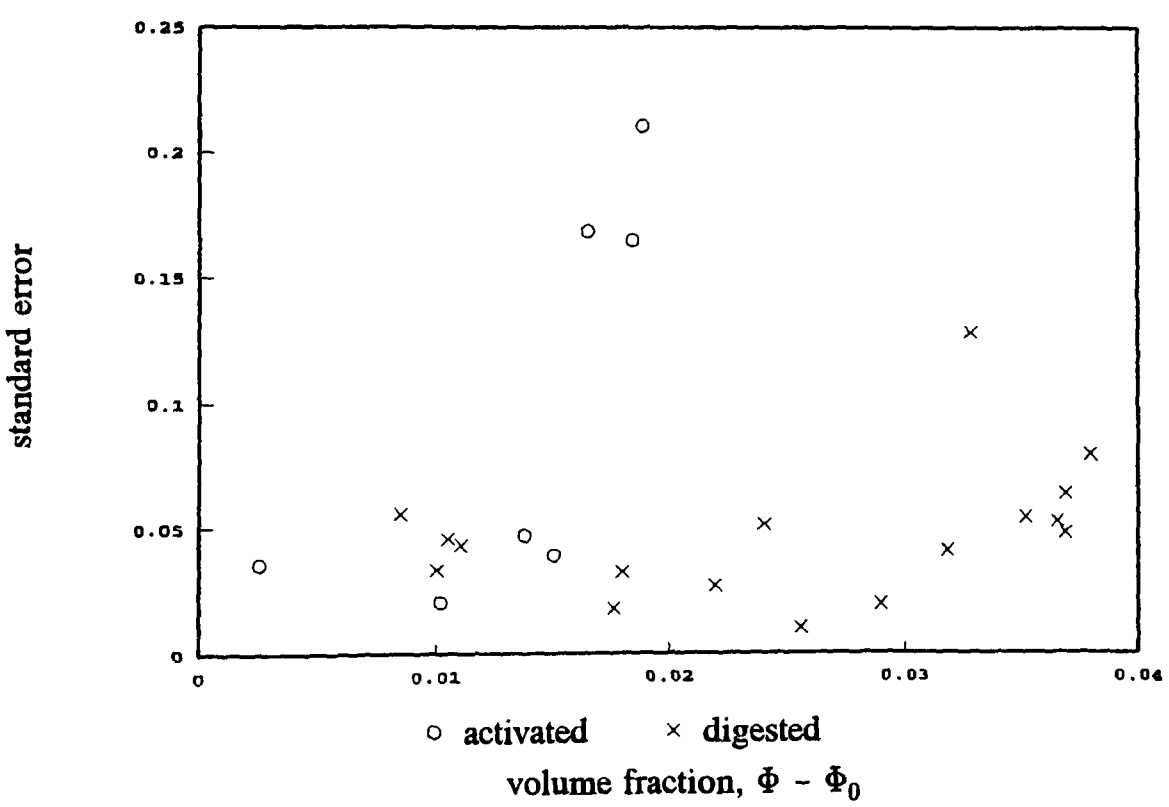


**Figure 8-17** The standard errors of the approximate generalised turbulence models.

## 8.2.2 Generalised Model

So far, the turbulence parameter $b$ has been estimated for various sludges at various solids concentrations, and an empirical relationship between $b$ and the volume fraction of solids, $\Phi$ has been obtained. There is clearly something crude in the way that a model-of-a-model approach has been taken. To obtain a generalised turbulent flow model as a function of $\Phi$,

it can realistically be assumed that the relationship between $b$ and $\Phi$ is of the form

$$b = \beta(\Phi - \Phi_0) + 22. \tag{8.19}$$

For each individual sludge sample, the error sum of squares was given by Equation (6.29), but for all $N$ turbulent flow sludge samples, the error sum of squares (Section 6.3) is now given by

$$E = \sum_{i=1}^{N} \sum_{j=1}^{M_i} (q_{ij} - \hat{q})^2, \tag{8.20}$$

where the hat denotes a prediction. The objectives are therefore to minimise $E$ with respect to the parameter $\beta$. The algorithm for estimating $\beta$ for $N$ sludge samples is little different than that for estimating $b$ for one sludge sample: quadratic interpolation is used as a bracketing method to obtain the minimum of $E$ with respect to $\beta$. A Fortran 77 program was written to estimate the parameter $\beta$ based on the turbulent pipe flow data, but for the model to be valid, the resulting standard errors have to be evenly distributed about the independent axis. On the evidence of Figure 8-17, this seems unlikely, so the four sludges with a standard error greater than 0.1 were therefore taken as outliers and excluded from the calculation. Using a relative convergence check of $5 \times 10^{-4}$, the calculation took about three minutes on an IBM compatible PC with a Pentium processor (about half an hour on a 386/387).

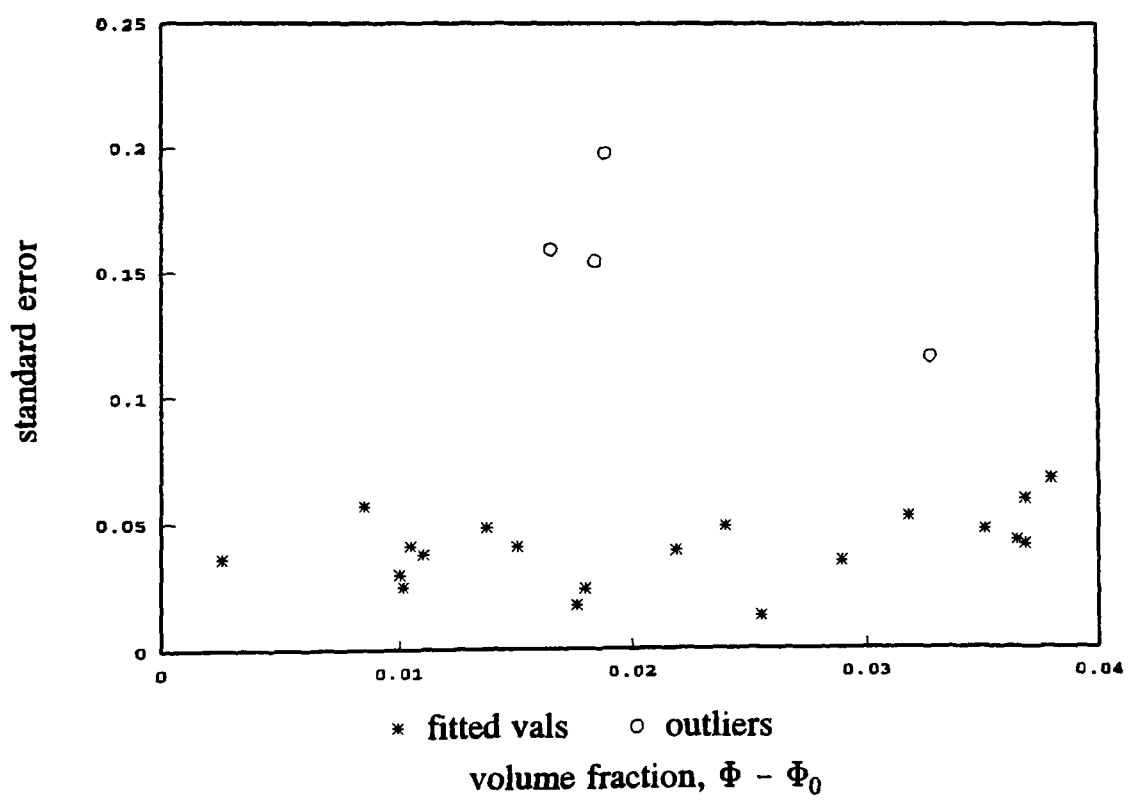


**Figure 8-18** The standard errors of the optimal generalised turbulence models.

The value of $\beta$ that minimises the error is 974, so the final relationship of $b$ with volume fraction is therefore

$$b = 974(\Phi - \Phi_0) + 22. \tag{8.21}$$

Along with Equations (8.18), (4.57) and (4.66), this defines a generalised turbulent flow model. The standard errors of this model for each sludge sample are shown on Figure 8-18. They are, as anticipated, better than those of Figure 8-17, though not considerably so.

## 8.2.3 Error Analysis

Analogous to the laminar flow case, it is convenient to partition the error into the error *within* each sludge sample and the error *between* samples. This is given as an error sum of squares (Section 6.3) relation

$$E_T = E_B + E_W. \tag{8.22}$$

The distribution of standard errors within the sludge samples was shown by Figure 7-31, and from this figure, the global standard errors were estimated to be 0.04 for activated sludge and 0.03 for digested sludge. Now, Figure 8-18 shows the distribution of total standard errors for the sludge samples. It is remarkable to note that, outliers apart, the standard errors are scarcely greater those within the sludge samples, and shows that the generalised model accounts for much error between the sludge samples. The global standard error is estimated from Figure 8-18 to be around 0.04. Since the total standard errors and the standard errors within the sludge samples are similar, it is clear that the error between samples must be very small, though larger for the outliers. The outlying values come as no surprise as these are thicker sludges that exhibit some erratic turbulent flow behaviour (as discussed in Subsection 8.2.1). For these thicker sludges, fully-developed turbulent flow probably occurs at higher shear rates, so much of these data are therefore either extended laminar flow or simply irregular flow. However, it is true to say that a turbulent flow prediction consistently gives a conservative estimate of any transitional flow data, and in spite of the larger error associated with the thicker sludges, this seems to be the best solution to the problem.

In summary, for both the sludge specific model and the generalised model, the standard error is about 0.04. Considering the success of the generalised model, there is obviously no point in measuring $b$ unless the volume fraction, $\Phi$, is large. From Figure 8-15 (neglecting $\Phi_0$) the volume fraction ranges are given in Table 8-6.

**Table 8-6** Volume fraction ranges and standard errors

| Sludge type | Volume fraction range | Standard error, $E$ |
|---|---|---|
| Digested | 0.015 - 0.047 | 0.04 |
| Activated | 0.010 - 0.025 | 0.04 |

Beyond these volume fractions, the standard error of the generalised model may be several times higher than normal. For these sludges, either the generalised model can be used to give conservative estimates of turbulent flow, or the end-user must estimate $b$ from their own data.

# 9 Conclusions

## 9.1 The Algorithms

Algorithms were developed to model the viscous flow of time-independent, non-Newtonian fluids through a straight, smooth pipe. The algorithms are not limited to the choice of relation between shear stress and rate of shearing strain, so any appropriate function of the explicit form $\tau = g(\dot{\gamma})$, or of the implicit form $G(\dot{\gamma}, \tau) = 0$ may be specified by the end-user. The algorithms can be used to make laminar, critical and turbulent flow predictions of pressure gradient, mean cross-sectional velocity, and the velocity distribution. The laminar flow algorithms are based on the Mooney-Rabinowitsch equation[52, 53], the critical flow algorithms are based on the Ryan and Johnson stability parameter[54], and the turbulent flow algorithms are based on an equation by Hanks[26]. Wall slippage modelling, as proposed by Jastrzebski[78], has also been included. The algorithms have been implemented in Fortran 77 on an IBM compatible PC.

### 9.1.1 Scope of Use

The limitations of an algorithm are difficult to define since many of the variables and parameters are interdependent. The algorithms were mainly tested using the general Bingham shear flow function[6], given as

$$\tau = \tau_y + K\dot{\gamma}^n. \tag{9.1}$$

This is an empirical relation, and since it is a good model of any time-independent, non-Newtonian, viscous fluid, the tests are equally valid for other shear flow relations of a different functional form.

A general guide to the valid ranges of parameters for the algorithms is given in Table 9-1. For laminar and critical flow, these ranges meet the required tolerance for all but the most unlikely combinations of these parameters. For turbulent flow, it would be fair to say that

**Table 9-1** Applicable ranges of the parameters for the algorithms

| Parameter | Laminar flow | Critical flow | Turbulent flow |
|---|---|---|---|
| Mean velocity, $U$/m s$^{-1}$ | $10^{-3}$ - $10^{3}$ | - | $10^{-3}$ - $10^{3}$ |
| Pressure gradient, $(\Delta P/L)$/Pa m$^{-1}$ | $10^{-3}$ - $10^{9}$ | - | $10^{-3}$ - $10^{9}$ |
| Pipe diameter, $D$/m | $10^{-3}$ - $10^{3}$ | $10^{-3}$ - $10^{3}$ | $10^{-2}$ - 10 |
| Yield stress, $\tau_y$/Pa | 0 - $10^{6}$ | 0 - $10^{3}$ | 0 - 100 |
| Consistency coeff, $K$ | $10^{-6}$ - $10^{6}$ | $10^{-6}$ - $10^{3}$ | $10^{-6}$ - $10^{6}$ |
| Consistency index, $n$ | 0.1 - 2.0 | 0.1 - 1.0 | 0.3 - 1.0 |

the required tolerance is generally met, though if not, a reasonably accurate answer is almost always given.

Although the laminar flow algorithms are valid well beyond any practical range, this was considered desirable for the extensive parameter estimation of the data where robust pipe-to-shear transformations were required. The valid range of parameters for the critical flow algorithms also proved extensive, though critical flow conditions are not always possible for a dilatant fluid (where $n > 1$) as shear thickening may develop faster than flow instability. For turbulent flow, the algorithms are more limited in their flexibility as Table 9-1 shows.

### 9.1.2 Efficiency

A measure of the efficiency of an algorithm was reasonably taken to be the total number of shear flow function evaluations made by the algorithm; other measures, such as timings would not have been suitable as they would have been machine and implementation dependent. For any of the algorithms, it was consoling to find that the number of evaluations did not vary considerably between any of the problems. Table 9-2 gives the order of magnitude of number of evaluations for each algorithm.

**Table 9-2** The number of the shear flow function evaluations in orders of magnitude made by each algorithm. Efficiencies of explicit and implicit shear flow functions are treated separately, except for turbulent flow where there is no difference.

| Estimate | Laminar/ explicit | Laminar/ implicit | Critical/ explicit | Critical/ implicit | Turbulent |
|---|---|---|---|---|---|
| Mean velocity/m $s^{-1}$ | 10 - $10^2$ | $10^2$ | $10^2$ | 10 - $10^2$ | $10^2$ - $10^3$ |
| Pressure grad/Pa $m^{-1}$ | 10 - $10^2$ | $10^2$ | $10^2$ | 10 - $10^2$ | $10^3$ - $10^4$ |
| Velocity dist'n/m $s^{-1}$ | $10^2$ | $10^2$ | — | — | $10^2$ - $10^3$ |

## 9.2 Data Analysis

A large body of data was analysed, which is comprised of the flow measurements of concentrated sewage sludge through straight pipes. Laminar and turbulent shear flow functions were developed for each sludge type as a function of volume fraction of solids. A qualitative assessment of the data revealed that sewage flow is time-dependent, but the data were not extensive enough to fully quantify these effects. The data also revealed evidence of wall-slip (a finite velocity of fluid at the pipe wall); the data were also inadequate to account for this effect. The final models were derived from the thicker, undisturbed sludges to give upper-bound estimates of the time-dependent effects.

### 9.2.1 Laminar Flow Analysis

For laminar flow, the general Bingham function (9.1) was chosen to model the data since it is widely recognised as a good empirical model of any time-independent, non-Newtonian, viscous fluid. A straight fit of the function to the data was found to yield non-constant standard errors, so the following log version of the function was fitted:

$$\log_{10}(\tau - \tau_y) = \log_{10}K + n\log_{10}\dot{\gamma}. \tag{9.2}$$

For activated and digested sludges, all three parameters, $\tau_y$, $K$ and $n$ of the model were tested to be significant, but for primary sludge, the yield stress parameter $\tau_y$ was tested to be superfluous, reducing the model to a power law model.

For each of the three sludge types, Table 9-3 gives the selected model, the applicable volume fraction range, and the applicable shear rate range. The ranges are only applicable to the laminar flow regime. For volume fraction, the lower value of each range is the critical value, $\Phi_0$ (which have nothing to do with critical flow). A critical volume fraction defines the Newtonian/non-Newtonian boundary where a thinner sludge is Newtonian and a thicker sludge is non-Newtonian. The critical volume fractions of Table 9-3 are quoted from the Water Research Centre [91].

**Table 9-3** For each sludge type, the choice of model, and the applicable ranges of volume fraction and shear rate.

| Sludge type | Selected model | Volume fraction range, $\Phi_0$ - $\Phi_{max}$ | Shear rate range $\dot{\gamma}_{min}$ /s$^{-1}$ - $\dot{\gamma}_{max}$ /s$^{-1}$ |
|---|---|---|---|
| Digested | General Bingham | 0.015 - 0.104 | 1.9 - 2 400 |
| Activated | General Bingham | 0.010 - 0.036 | 6.3 - 1 600 |
| Primary | Power law | 0.020 - 0.072 | 7.8 - 1 100 |

Empirical relations were examined between each parameter and the volume fraction of solids $\Phi$, and were found to be of the form

$$\tau_y = \alpha_1(\Phi - \Phi_0)^{\alpha_2}, \tag{9.3}$$

$$K = \alpha_3(\Phi - \Phi_0)^{\alpha_4}, \tag{9.4}$$

$$n = \frac{1}{1 + \alpha_5(\Phi - \Phi_0)^{\alpha_6}}, \tag{9.5}$$

where $\alpha_j$, $j = 1,\ldots,6$ are themselves parameters. It was considered excessive to collectively

estimate all six parameters from the immense data, so the indices, $\alpha_2$, $\alpha_4$ and $\alpha_6$ were first estimated and rounded individually for these functions, and the remaining three parameters were then fitted collectively to all of the relevant data. The results are given in Table 9-4 and the standard errors are given in Table 9-5.

**Table 9-4** Parameter estimates of Equations (9.3) to (9.5)

| Sludge Type | Parameter estimate | | | | | |
|---|---|---|---|---|---|---|
| | $\alpha_1$ | $\alpha_2$ | $\alpha_3$ | $\alpha_4$ | $\alpha_5$ | $\alpha_6$ |
| Digested | $1.519 \times 10^4$ | 2.5 | $4.335 \times 10^3$ | 2.5 | 3.842 | 0.5 |
| Activated | $5.759 \times 10^6$ | 3.5 | $2.525 \times 10^6$ | 3.5 | 11.345 | 0.5 |
| Primary | — | — | 97.25 | 1.5 | 4.061 | 0.5 |

For an improved standard error to the model, the end-user may fit one or two parameters to their own data. $\alpha_3$ and $\alpha_5$ were respectively regarded as the most suitable parameters to do this where the remaining parameters are left unchanged. These one- and two-parameter models were refitted to our data, and the reduced standard errors are given in Table 9-5.

**Table 9-5** Standard errors of the generalised models

| Sludge Type | Number of user fitting parameters | | |
|---|---|---|---|
| | 0 | 1 | 2 |
| Digested | 0.2940 | $5.901 \times 10^{-2}$ | $1.932 \times 10^{-2}$ |
| Activated | 0.5420 | 0.2012 | $8.106 \times 10^{-2}$ |
| Primary | 0.2491 | $5.323 \times 10^{-2}$ | $2.125 \times 10^{-2}$ |

## 9.2.2 Critical Flow Assessment

Critical flow is the upper bound of laminar flow. The Ryan and Jonson stability parameter [54] was used on the data to predict the critical flow conditions, and the results were qualitatively assessed. It was found that the stability parameter succeeded in predicting critical flow for activated and digested sludges, but failed on primary sludge. Due to the dependence of critical flow on turbulence, it was decided to exclude the modelling of turbulent flow for primary sludge.

### 9.2.3 Turbulent Flow Analysis

For turbulent flow, the function proposed by Hanks[26] was used, and is the following sum of laminar and turbulent flow stresses:

$$\tau = \tau_y + K\dot{\gamma}^n + \rho l^2 \dot{\gamma}^2. \tag{9.6}$$

$l$ is a mixing length that includes a fluid-dependent parameter $b$. To be consistent with the laminar flow method, a log version of the model was fitted to the data:

$$\log_{10}(\tau - \tau_y) = \log_{10}(K\dot{\gamma}^n + \rho l^2 \dot{\gamma}^2). \tag{9.7}$$

An empirical relation between $b$ and the volume fraction of solids was examined, and found to be of the linear form

$$b = \beta(\Phi - \Phi_0) + 22. \tag{9.8}$$

For each of the two sludge types, Table 9-6 gives the applicable volume fraction range, the standard error, and the applicable shear rate range. The ranges are only applicable to the transitional and turbulent flow regime.

**Table 9-6** For each sludge type, the applicable range of volume fraction, the standard error, and the applicable range of shear rates.

| Sludge type | Volume fraction range, $\Phi_0$ - $\Phi_{max}$ | Standard error, $E$ | Shear rate range $\dot{\gamma}_{min}/s^{-1}$ - $\dot{\gamma}_{max}/s^{-1}$ |
|---|---|---|---|
| Digested | 0.015 - 0.047 | 0.04 | 190 - 33 000 |
| Activated | 0.010 - 0.025 | 0.04 | 44 - 57 000 |

Using all of the relevant turbulent flow data, $\beta$ was estimated to be 974 for both activated and digested sludges with an overall standard error of 0.04. However, for volume fractions higher than those of Table 9-6, this estimate of $\beta$ gives conservative turbulent flow predictions with an associated standard error several times higher. In the latter case, either a poorer standard error is accepted, or the end-user must estimate $b$ from their own data. The standard error of the turbulent flow model is very low compared to any of the one-parameter laminar flow models. This suggests that some of the unpredictable effects of sewage flow diminish under high shear. The problem with any of the volume fraction models is that they are based on sludge samples from a limited number of sewage works, so there may be a greater regional variation than the results suggest.

## 9.3 Epilogue

All of the objectives of the research have been met. Methods have been presented in this thesis for predicting the laminar and turbulent flow of yield pseudoplastic fluids through straight pipes. These methods are of particular interest to the sewage industry and many other industries concerned with the flow of a complex fluid mixtures through straight pipes. These methods were then used to analyse a large body of data of the laminar and turbulent flow of sewage sludge through straight pipes. Laminar and turbulent shear flow relations have been constructed as a function of solids concentration to be ultimately used for modelling the viscous flow of sewage in complex geometries. The sewage industry has since commissioned the sewage stirring tank to be modelled[17] using this approach. It has also been recognised that modelling the flow of sewage through pipe fittings such as bends, valves and constrictions would be of great value, so this research would provide a good platform on which to start.

# 10 References


1. Michelbach, S., 'Origin, resuspension and settling characteristics of solids transported in combined sewage', *Water, Science and Technology*, **31** (7), pp. 69-76 (1995).

2. Babbitt, H.E. and Caldwell, D.H., 'Laminar flow of sludge in pipes with special reference to sewage sludge', *University of Illinois, Urbana, Engineering Experiment Station*, Bulletin 319 (1939).

3. Mulbarger, M.C., Copas, S.R., Kordic, J.R. and Cash, F.M., 'Pipeline friction losses for wastewater sludges', *Journal WPCF*, **53** (8), pp. 1303-1313 (1981).

4. Carthew, G.A., Goehring, C.A. and van Teylingen, J.E., 'Development of dynamic head loss criteria for raw sludge pumping', *Journal WPCF*, **55** (5), pp. 472-483 (1983).

5. Walski, T.M., 'Transport of dewatered sludge', *Journal of Environmental Engineering—ASCE*, **119** (2), PP. 212-213 (1993).

6. Herschel, W.H. and Bulkley, R., 'Measurements of consistency as applied to rubber-benzene solutions', *A.S.T.M. Proc.*, **26**, pp. 621-633 (1926).

7. Cheng, D.C.-H., 'A design procedure for pipeline flow of non-Newtonian dispersal systems', *In Hydrotransport 1 Proc.*, Paper J5, pp. 77-95 (1970).

8. Frost, R.C., *Prediction of Friction Losses for the Flow of Sewage Sludges in Straight Pipes*, WRC Process Engineering Technical Report TR175 (1982).

9. Heywood, N.I., 'Pipeline design for non-Newtonian fluids', *Proc. Interflow 80*, IChemE Symposium Series No. 60, pp. 33-55 (1980).

10. Johnson, M., Harwood, N. and Frost, R.C., *First Report on WRC Sewage Sludge Pumping Project*, **App. A**, Water Research Centre (1982).

11. Binnie and partners (consulting engineers, London) 'Appendices to report on sludge pipeline scheme', Prepared for the sludge disposal consortium of South Lancashire and North Cheshire, England (1991).

12. Hayes, J., Flaxman, E.W. and Scvier, J.B., 'A comprehensive scheme for sewage sludge disposal in north-west England', *Proc Inst Civ Engrs, Part 2: Res and Theory*, **55**, paper 7604, pp. 1-21 (1973).

13. Cham Ltd, Wimbledon, London.

14. Spalding, D.B., 'Mathematical modelling of fluid-mechanics, heat transfer and chemical reaction processes', A Lecture Course, CFDU Report HTS/80/1, Imperial College, London (1980).

15. Patankar, S.V. and Spalding D.B., 'A calculation procedure for heat, mass and momentum transfer in three-dimensional parabolic flows, *Int. J. Heat Mass Transfer*, **15**, pp. 1787-1806 (1972).

16. Bird, R.B., Stewart, W.E. and Lightfoot, E.N., *Transport Phenomena*, Wiley Int. (1960).

17. Kostamis, P. and Patel, M.K., 'Numerical modelling of ploughs in sewage sludge tanks for increased efficiency', Thames Polytechnic, (1990).

18. Pericleous, K.A. and Patel, M.K., 'Industrial and environmental modelling of non-Newtonian fluid flows', *FED*, **145**, p. 133 (1992).

19. Caswell, B., 'Report on the IXth international workshop on numerical methods in non-Newtonian flows', *Journal of Non-Newtonian Fluid Mechanics*, **62**, pp. 99-110 (1996).

20. Metzner, A.B. and Reed, J.C., 'Flow of non-Newtonian fluids—correction of the laminar, transitional, and turbulent flow regions', *AIChE Jnl.*, **1**, pp. 434-440 (1955).

21. Dodge, D.W. and Metzner, A.B., 'Turbulent flow of non-Newtonian systems', *AIChE Jnl.*, **5**, pp. 189-204 (1959).

22. Frost, R.C., *How to Design Sewage Sludge Pumping Systems*, WRC Process Engineering Technical Report TR185 (1983).

23. Shook, C.A. and Bartosik, A.S., 'Particle wall stress in vertical slurry flows', *Powder Technology*, **81** (2), pp. 117-124 (1994).

24. Grovier, G.W. and Aziz, K., *The Flow of Complex Mixtures in Pipes*, Van Nostrand-Reinhold, p. 24 (1972).

25. Prandtl, L., *Z. angew. Math. u. Mech.*, **5**, p. 136 (1925).

26. Hanks, R.W., 'Low Reynolds number turbulent pipeline flow of pseudohomogeneous slurries', *BHRA proc. 5th Int. Conf. on Hydraulic Transport of Solids in Pipes*, paper C2, pp. 23-33 (1978).

27. Torrance, B, McK., 'Friction factors for turbulent non-Newtonian fluid flow in circular pipes', *South African Mechanical Engineer*, pp. 89-91 (1963).

28. Tsuji, Y., Tanaka, T. and Ishida T., 'Lagrangian numerical simulation of plug flow of cohesionless particles in a horizontal pipe', *Powder Technology*, **71**, pp. 239-250 (1992).

29. Elansary, A.S., Silva, W. and Chaudhry, M.H., 'Numerical and experimental investigation of transient pipe flow', *Journal of Hydraulic Research*, **32** (5) pp. 689-706 (1994).

30. Eggels, J.G.M, Westerweel J. and Nieuwstadt, F.T.M., 'Direct numerical simulation of turbulent pipe flow', *Applied Scientific Research*, **51**, pp. 319-324 (1993).

31. Eggels, J.G.M, Unger, F., Weiss, M.H., Westerweel J., Adrian, R.J., Fredrich, R. and Nieuwstadt, F.T.M., 'Fully developed turbulent pipe flow: a comparison between direct numerical simulation and experiment', *J. Fluid Mech.*, **268**, pp. 175-209 (1994).

32. Khan, A.R. and Richardson, J.F., 'Fluid particle interactions and flow characteristics of fluidized beds and settling suspensions of spherical particles', *Chem. Eng. Commun.*, **78**, pp. 111-130 (1989).

33. Chhabra, R.P., Unnikrishnan, A. and Nair V.R.U., 'Hindered settling in non-Newtonian power law liquids', *Canadian Journal of Chemical Engineering*, **70** (4), pp.716-720 (1992).

34. Walton, I.C., 'Eddy Diffusivity of solid particles in a turbulent liquid flow in a horizontal pipe', *AIChE*, **41** (7), pp. 1815-1820 (1995).

35. Binder, J.L. and Hanratty, T.J., 'Use of lagrangian statistics to describe slurry transport', *AIChE Jnl*, **39** (10), pp. 1581-1591 (1993).

36. Bouzaïene, R. and Hassani, F.P., 'A selection of pressure loss predictions based of slurry/backfill characterization and flow conditions', *CIM Bulletin*, **84** (959), pp. 63-68 (1992).

37. Einstein, A., *Ann. Physik*, **17**, p. 459 (1905); **19**, p. 289 (1906); **34**, p. 591 (1911).

38. Thomas, D.G., 'Transport characteristics of suspensions: part VIII. A note on the viscosity of Newtonian suspensions of uniform spherical particles', *Jnl. Colloid Sci.*, **20**, p. 267 (1965).

39. Thomas, D.G., *AIChE Journal*, **7**, p. 431 (1961).

40. Dick, R.I. and Ewing, B.B., *Jnl. WPCF*, **39**, p. 543 (1967).

41. Eyring, H.J., 'Viscosity, plasticity, and diffusion as examples of absolute reaction rates', *Jnl. Chem. Phys.*, **4**, pp. 283-291 (1936).

42. Prandtl, L., *Z. Angew. Math. Mech.*, **8**, p. 85 (1928).

43. Carreau, P.J., 'Rheological equations from molecular network theories', *Trans. Soc. Rheo.'*, **16**, pp. 99-127 (1972).

44. Meter, D.M., Ph.D. thesis, University of Wisconsin, Madison, Wisconsin (1963).

45. Silvester, R.S., 'Mixing of non-Newtonian media', **12**, *BHRA Fluid Engineering* (1985).

46. Van Driest, E.R., 'On turbulent flow near a wall', *Jnl. Aeronaut. Sci.*, **23**, pp. 1007-1011 (1956).

47. Gill, W.N. and Scher, M., 'A modification of momentum transport hypothesis', *AIChE Jnl.*, **7**, pp. 61-63 (1961).

48. Cheremisinoff, N.P., *Encyclopedia of Fluid Mechanics*, **1**, p. 320, Gulf (1986).

49. Buckingham, E., 'Model experiments and the form of empirical equations', *Trans. ASME*, **37**, pp. 263-269 (1915).

50. Hedström, B.O.A., 'Flow of plastic materials in pipes', *Ind. Eng. Chem.*, **44**, pp. 651-656 (March, 1952).

51. Buckingham, E., 'On plastic flow through capillary tubes', *ASTM proc*, **21**, pp. 1154-1161 (1921).

52. Mooney, M., 'Explicit formulas for slip and fluidity', *Jnl. Rheo.*, **2**, pp. 210-222 (1931).

53. Rabinowitsch, B., *Z. Phisik. Chem., Ser. A*, **145**, p. 1 (1929).

54. Ryan, N.W. and Johnson, M.M., 'Transition from laminar to turbulent flow in pipes', *AIChE Jnl.*, **5**, pp. 433-435 (1959).

55. Hanks, R.W. and Pratt, D.R., 'On the flow of Bingham plastic slurries in pipes and between parallel plates', *Soc. Petroleum Engrs. Jnl.*, **7**, pp. 342-346 (1967).

56. Hanks, R.W. and Christiansen, E.B., 'The laminar-turbulent transition in nonisothermal flow of pseudoplastic fluids in tubes', *AIChE Journal*, **8** (4), pp. 467-471 (1962).

57. Hanks, R.W., 'The laminar-turbulent transition for fluids with a yield stress', *AIChE Jnl.*, **9**, pp. 306-309 (1963).

58. Thomas, D.G., 'Non-Newtonian suspensions', *Part I, Ind. Eng. Chem.*, **55**, pp. 18-29 (1963).

59. Hanks, R.W. and Ricks, B.L., 'Laminar-turbulent transition in flow of pseudoplastic fluids with yield stresses', *Jnl. Hydronautics*, **8**, pp. 163-166 (1974).

60. Slatter, P.T. and Lazarus, J.H., 'Critical flow in slurry pipelines', *12th Int. Conf. on Slurry Handling and Pipeline Transport*, Hydrotransport 12, BHR Group, p. 639 (1993).

61. Slatter, P.T., 'The laminar/turbulent transition of non-Newtonian slurries in pipes', *14th World Dredging Congress*, Amsterdam, pp. 31-47 (1995).

62. Blasius, H., *Mitt. Forschungsarb*, No. 131, (1913).

63. von Kármán, T., *Nachr. Ges. Wiss. Göttingen, Math.-physik, Klasse*, (1930).

64. Nikuradse, J., 'Gesetzmässigkeiten der turbulenten Strömung in glatten Rohren', *Forschungsheft Ver Deut Ing*, **356**, Verlag, Berlin, 36pp (1932).

65. Clapp, R.M., 'Turbulent heat transfer in pseudoplastic non-Newtonian fluids', *ASME Part III*, Section A, p. 652 (1961).

66. Slatter, P.T., 'The turbulent flow of non-Newtonian slurries in pipes', *8th Int. Conf. on Transport and Sedimentation of Particles*, paper A3, pp. 1-12 (1995).

67. Park, J.T., Mannheimer, R.J., Grimley, T.A. and Morrow, T.B., 'Pipe flow measurements of a transparent non-Newtonian slurry', *Journal of Fluids Engineering*, **111**, pp. 331-336 (1989).

68. Xu, J., Gillies, R., Small, M. and Shook, C.A., 'Laminar and turbulent flow of kaolin slurries', *Int. Conf. on Slurry Handling and Pipeline Transport*, Hydro-transport 12, BRH Group, p. 595 (1993).

69. Hanks, R.W., 'On the theoretical calculation of friction factors for laminar, transitional, and turbulent flow of Newtonian fluids in pipes', *AIChE Jnl.*, **14**, pp. 691-695 (1968).

70. Hanks, R.W. and Dadia, B.H., 'Theoretical analysis of the turbulent flow of non-Newtonian slurries in pipes', *AIChE Jnl.*, **17**, pp. 554-557 (1971).

71. Hanks, R.W. and Ricks, B.L., 'Transitional and turbulent pipe flow of pseudoplastic fluids', *Jnl. Hydronautics*, **9**, pp. 39-44 (1975).

72. Tam, K.C. and Tiu C., 'A general correlation for purely viscous non-Newtonian fluids flowing in ducts of arbitrary cross-section', *Canadian Journal of Chemical Engineering*, **66**, pp. 542-549 (1988).

73. Coulson, J.M. and Richardson, J.F., *Chemical Engineering (5th Ed.)*, Vol. 1, Pergamon Press (1997).

74. Dziubiński, M., 'A simple method of determination of friction factor for turbulent flow of non-Newtonian liquids in pipes', *Inżynieria Chemiczna I Procesowa*, **15** (4), pp. 491-502 (1994).

75. Moody, L.F., 'Friction factors for pipe flow', *Trans ASME*, **66**, p. 671 (1944).

76. Cheng, D.C.-H. and Heywood, N.I., *Pipeline Design for Sewage Sludge from Bench-Scale Viscometric Tests: Report No. 2.* Report from Warren Spring Laboratory of the Department of Industry to WRC, p. 207 (1980).

77. Cheng, D.C.-H. and Parker, B.R., 'The determination of wall-slip velocity in the coaxial cylinder viscometer', *Proc. 7th International Cong. Rheol.*, Gothenberg, Sweden, pp. 518-519 (1976).

78. Jastrzebski, Z.D., 'Entrance effects and wall effects in an extrusion rheometer during the flow of concentrated suspensions', *Industrial and Engineering Chemistry, Fundamentals*, **6** (3), pp. 445-454 (1967).

79. Sommerville, I., *Software Engineering (5th Ed.)*, Addison Wesley (1996).

80. Gill, P.E. and Murray, W., *Numerical Methods for Constrained Optimization*, Academic Press (1974).

81. Jeffrey, A., *Mathematics for Engineers and Scientists (5th Ed.)*, Nelson (1996).

82. Montgomery, D.C., *Design and Analysis of Experiments (4th Ed.)*, Wiley (1997).

83. Kleinbaum, D.G., Kupper, L.L., Muller, K.E. and Nizan, A., *Applied Regression Analysis and Multivariable Methods (3rd Ed.)*, Duxbury (1988).

84. Rousseeuw, P.J. and Leroy, A.M., *Robust Regression and Outlier Detection*, John Wiley and Sons (1987).

85. Wasp, E.J., Kenny, J.P. and Gandhi, R.L., *Solid-Liquid Flow—Slurry Pipeline Transportation*, Trans Tech (1977).

86. Thomas, G., Ph.D. thesis, University College of Swansea, UK (1960).

87. Shaver, R.G. and Merill, E.W., 'Turbulent flow of pseudoplastic polymer solutions in straight cylindrical pipes', *AIChE Jnl*, **5**, pp. 181-188 (1959).

88. Tomita, Y., 'A study on non-Newtonian flow in pipes', *Bull. JSME*, **2** (5), pp. 10-16 (1959).

89. Kemblowski, Z. and Kolodziejski, J., 'Flow resistances of non-Newtonian fluids in transitional and turbulent flow', *Int Chem Eng*, **13** (2), pp. 265-279 (1973).

90. Heywood, N.I. and Cheng, D.C.-H., 'Comparison of methods for predicting head loss in turbulent pipe flow of non-Newtonian fluids', *Trans Ins M C*, **6** (1), pp. 33-45 (1984)

91. Hoyland, G., verbal communication, Water Research Centre (1990).

92. Davis, P.J. and Rabinowitz, P., *Methods of Numerical Integration*, Academic Press (1975).

93. Marquardt, D.W., *Jnl. Soc. Ind. Appl. Math.*, **11**, pp. 431-441 (1963).

94. Phillips, G.M. and Taylor, P.J., *Theory and Applications of Numerical Analysis (2nd Ed.)*, Academic Press (1996).

95. Muller, D.E., 'A method for solving algebraic equations using an automatic computer', *Math. Tables Aids Comput.*, **10**, pp. 208-215 (1956).

96. Stoer, J. and Bulirsch, R., *Introduction to Numerical Analysis*, Springer-Verlag (1980).

97. Lambert, J.D., *Numerical Methods for Ordinary Differential Systems*, John Wiley and Sons (1991).

98. Fehlberg, E., 'Classical fifth, sixth, seventh and eighth order Runge-Kutta formulas with stepsize control', *NASA* TR R-287 (1968).

99. Fehlberg, E., 'Low order classical Runge-Kutta formulas with stepsize control and their application to some heat transfer problems', *NASA* TR R-315 (1969).

100. Press, W.H., Teukolsky, S.A., Vetterling, W.T. and Flannery, B.P., *Numerical Recipes in Fortran (2nd Ed.)*, Cambridge (1992).

# 11 Nomenclature

| | |
|---|---|
| $a$ | Parameter of the Meter model (2.13) |
| $a$ | Required area under the $t$ distribution |
| $a$ | Turbulence parameter equal to 60. |
| $A$ | Area |
| $A$ | Constant |
| $b$ | Turbulence parameter |
| $\hat{b}$ | Estimate of $b$ |
| $B$ | Constant |
| $B$ | $\mathrm{Re}\sqrt{f}$ |
| $B_B$ | $\mathrm{Re}_B\sqrt{f}$ |
| $(B_B)_c$ | $(\mathrm{Re}_B)_c\sqrt{f_c}$ |
| $B_c$ | $\mathrm{Re}_c\sqrt{f_c}$ |
| $B_{GB}$ | $\mathrm{Re}_{GB}\sqrt{f}$ |
| $(B_{GB})_c$ | $(\mathrm{Re}_{GB})_c\sqrt{f_c}$ |
| $B_P$ | $\mathrm{Re}_P\sqrt{f}$ |
| $(B_P)_c$ | $(\mathrm{Re}_P)_c\sqrt{f_c}$ |
| $C_w$ | Percentage solids concentration by mass |
| $\mathrm{d}P/\mathrm{d}z$ | Axial direction pressure gradient |
| $\mathrm{d}u/\mathrm{d}r$ | Rate of shear at radial distance $r$ |
| $\mathrm{d}u/\mathrm{d}y$ | Rate of shearing strain (strain rate) |
| $\mathrm{d}x/\mathrm{d}y$ | Shear strain |
| $d_x$ | Representative particle diameter |
| $D$ | Pipe diameter |
| $D_y$ | Plug core diameter |
| e | Constant = 2.71828 |
| $e$ | Residual of a fitted shear flow function |
| $E$ | Error sum of squares |
| $E_B$ | Error sum of squares between samples |
| $E_T$ | Total error sum of squares |
| $E_W$ | Error sum of squares within a sample |
| $f$ | Fanning friction factor |
| **f** | Critical flow equation pair |
| $f_c$ | Fanning friction factor at critical flow |
| $F$ | Force |
| $F$ | $F$ statistic |
| $g$ | Acceleration due to gravity |
| $g$ | Laminar shear flow function—explicit |
| $G$ | Laminar shear flow function—implicit |
| $h$ | Elastic shear stress function |

| | |
|---|---|
| $H$ | Turbulent shear flow function |
| He | Hedström number |
| He* | Numerical estimate of Hedström number |
| $\mathrm{He}_{GB}$ | General Bingham Hedström number |
| HLR | Sludge-to-water head loss ratio |
| $i$ | Hydraulic gradient |
| $i$ | $i$th sludge sample |
| $I$ | An integral value |
| $j$ | $j$th measurement of a sludge sample |
| $J$ | The Jacobian matrix |
| $k$ | $k$th parameter |
| $k_1$ | Constant |
| $k_2$ | Constant |
| $K$ | Consistency coefficient |
| $\hat{K}$ | Consistency coefficient estimate |
| $K'$ | $K\left(\frac{3n + 1}{4n}\right)^n$ |
| $l$ | Mixing length |
| $L$ | Pipe length |
| $m$ | $m$th iteration |
| $m$ | Rate of change of viscosity with shear rate |
| $M$ | Number of viscometric measurements of a sludge sample |
| $n$ | Consistency index |
| $\hat{n}$ | Consistency index estimate |
| $n'$ | $\mathrm{d}\ln\tau_R/\mathrm{d}\ln\Gamma$ |
| $n''$ | $\mathrm{d}\ln\tau_R/\mathrm{d}\ln(\Gamma - \Gamma_s)$ |
| $N$ | Number of sludge samples |
| $O$ | To the order of |
| $p$ | Independent variable of log shear flow function |
| $P$ | Pressure |
| $q$ | Dependent variable of log shear flow function |
| $Q$ | Number of parameters |
| $\hat{q}$ | Predicted value of $q$ |
| $r$ | Radial distance from pipe axis |
| $r_c$ | Radial point of unsteady flow at critical flow |
| $r_s$ | Radial distance at point $s$ |
| $r_y$ | Plug core radius |
| $R$ | Pipe radius |
| Re | Reynolds number |
| Re* | Numerical estimate of Reynolds number |
| Re* | Frictional Reynolds number |

$Re^{**}$ Modified Reynolds number
$Re_B$ Bingham Reynolds number
$(Re_B)_c$ Bingham Reynolds number at critical flow
$Re_c$ Reynolds number at critical flow
$Re_c^{\star}$ Numerical estimate of $Re_c$
$Re_{GB}$ General Bingham Reynolds number
$(Re_{GB})_c$ General Bingham Reynolds number at critical flow
$Re_{MR}$ Metzner-Reed Reynolds number
$Re_P$ Power law Reynolds number
$(Re_P)_c$ Power law Reynolds number at critical flow
$Re_r$ Particle roughness Reynolds number
$Re_S$ Slatter Reynolds number
$Re_{SL}$ Slatter and Lazarus Reynolds number
$Re_T$ Torrance Reynolds number
$s$ $s$th discrete value
$S$ Standard Error
$t$ $t$ statistic
$T$ Number of velocity distribution points of annular region
$u$ Axial direction velocity distribution
$u^{\star}$ Numerical estimate of $u$
$\bar{u}$ Mean $x$-directional velocity
$u'$ $x$-directional velocity fluctuation
$U$ Mean cross-sectional velocity
$U^{\star}$ Numerical estimate of $U$
$U^*$ Friction velocity
$U_{ann}$ Mean cross-sectional velocity of annular flow
$U_c$ Mean cross-sectional velocity at critical flow
$U_s$ Slip velocity
$v'$ $y$-directional velocity fluctuation
$W$ Number of discrete values of a distribution
$x$ Cartesian coordinate in the direction of flow
$x$ Dependent variable
$y$ Cartesian coordinate perpendicular to the direction of flow
$y$ Distance from wall
$y$ Independent variable
$\hat{y}$ Overall estimate of the independent variable
$Y$ Maximum value of $y$—the wall distance
$z$ Axial distance of pipe
$Z$ Maximum value of $\zeta$
$Z_c$ $Z$ at critical flow
$\alpha$ Constant

| | |
|---|---|
| $\alpha$ | Laminar shear flow function parameters |
| $\hat{\alpha}$ | Parameter estimates |
| $\beta$ | Constant |
| $\beta$ | Parameter of the generalised turbulent shear flow function |
| $\gamma$ | Shear strain |
| $\dot{\gamma}$ | Rate of shearing strain (strain rate) |
| $\dot{\boldsymbol{\gamma}}$ | $[\dot{\gamma}, \dot{\gamma}_R]^T$ |
| $\dot{\gamma}_c$ | Rate of shear at critical flow |
| $\overline{\dot{\gamma}^n}$ | Mean value of $\dot{\gamma}^n$ |
| $\dot{\gamma}_R$ | Wall rate of shear |
| $\dot{\gamma}_s$ | Rate of shear at point $s$ |
| $(\dot{\gamma}_R)_0$ | Starting value of $\dot{\gamma}_R$ for numerical scheme |
| $(\dot{\gamma}_R)_c$ | Wall rate of shear at critical flow |
| $\Gamma$ | A pseudo-shear rate, $8U/D$ |
| $\Gamma^\star$ | Numerical estimate of $\Gamma$ |
| $\Gamma_0$ | Starting value of $\Gamma$ for numerical scheme |
| $\Gamma_c$ | A pseudo-shear rate at critical flow |
| $\Gamma_s$ | Wall slip pseudo-shear rate |
| $\Delta P$ | Pressure drop |
| $\Delta u$ | $x$-direction velocity difference |
| $\Delta y$ | $y$-direction displacement |
| $\Delta\dot{\gamma}$ | Rate of shear difference |
| $\Delta\dot{\gamma}_R$ | Wall rate of shear difference |
| $\Delta\tau$ | Shear stress difference |
| $\Delta\tau_R$ | Wall shear stress difference |
| $\epsilon$ | Relative tolerance check |
| $\epsilon$ | Residual of a fitted log shear flow function |
| $\zeta$ | Stability parameter |
| $\eta$ | Coefficient of rigidity |
| $\theta$ | Angle |
| $\kappa$ | Universal turbulence constant, usually 0.36 |
| $\lambda$ | Characteristic time |
| $\lambda$ | Leverage |
| $\mu$ | Absolute viscosity |
| $\mu_0$ | Viscosity at initial shear |
| $\mu_\infty$ | Viscosity at infinite shear |
| $\mu_a$ | Apparent viscosity, $\tau/\dot{\gamma}$ |
| $\mu_e$ | Effective viscosity, $\tau_R/\Gamma$ |
| $\mu_l$ | Viscosity of liquid |
| $\mu_m$ | Viscosity of mixture |
| $\xi$ | $\tau_y/\tau_R$ |

| | |
|---|---|
| $\xi_c$ | $\tau_y/(\tau_R)_c$ |
| $\rho$ | Density |
| $\rho_l$ | Density of liquid medium |
| $\rho_m$ | Density of sludge mixture |
| $\varsigma$ | Right-hand side of Eq. (5.8) |
| $\tau$ | Shear stress |
| $\overline{\tau}$ | Mean shear stress |
| $\tau_L$ | Laminar or viscous stress |
| $\tau_m$ | Shear stress for which the viscosity is $\frac{1}{2}(\mu_0 + \mu_\infty)$. |
| $\tau_R$ | Pipe wall shear stress |
| $\tau_R^\star$ | Numerical estimate of $\tau_R$ |
| $\hat{\tau}_R$ | Wall stress estimate |
| $(\tau_R)_c$ | Wall shear stress at critical flow |
| $(\tau_R)_c^\star$ | Numerical estimate of $(\tau_R)_c$ |
| $\tau_T$ | Turbulent or Reynolds stress |
| $\tau_w$ | Wall shear stress |
| $\tau_y$ | Yield stress |
| $\hat{\tau}_y$ | Yield stress estimate |
| $\upsilon$ | Right-hand side of Eq. (5.7) |
| $\phi$ | Mixing length parameter |
| $\phi_B$ | Bingham mixing length parameter |
| $\phi_{GB}$ | General Bingham mixing length parameter |
| $\phi_P$ | Power law mixing length parameter |
| $\Phi$ | Volume fraction of solids |
| $\Phi_0$ | Newtonian/non-Newtonian critical volume fraction of solids |
| $\varphi$ | Loss coefficient |
| $\psi$ | Laminar pseudo-shear flow function |
| $\omega$ | Turbulent pseudo-shear flow function |

# Appendix A The Methods

## A.1 Integration Methods—Adaptive

Consider the area $A$ of a function $f(x)$ over the interval $[a, b]$,

$$A = \int_a^b f(x)\mathrm{d}x.$$

Estimates of this area can be given by the following integration rules[92]:

Trapezium rule

$$A \approx \frac{h}{2}[f(a) + f(b)], \qquad h = (b - a);$$

Simpson's rule

$$A \approx \frac{h}{3}[f(a) + 4f(a + h) + f(b)], \qquad h = \frac{(b - a)}{2};$$

Boole's rule

$$A \approx \frac{2h}{45}[7f(a) + 32f(a + h) + 12f(a + 2h) + 32f(a + 3h) + 7f(b)],$$

$$h = \frac{(b - a)}{4}.$$

These are two-, three- and five-point Newton-Cotes estimates respectively.

### Adaptive Quadrature

Let $A_w$ denote an estimate of $A$ over the whole interval $[a, b]$, and let $A_l$ and $A_r$ denote the left and right area estimates of the bisected intervals of $[a, b]$ respectively (see Figure A-1). The area difference between the full and half interval approximates is

$$\Delta A = A_w - (A_l + A_r).$$

For a given tolerance $\epsilon$, this can be used to define the relative convergence criterion

$$\left|\frac{\Delta A}{A}\right| < \epsilon.$$

Each half interval is repeatedly bisected until convergence is met on a local basis. Since the number of half intervals for a particular level is between one and two times the number for the previous level, $\epsilon$ must be reduced by a suitable factor. The factor $\sqrt{2}$ is considered suitable [92].

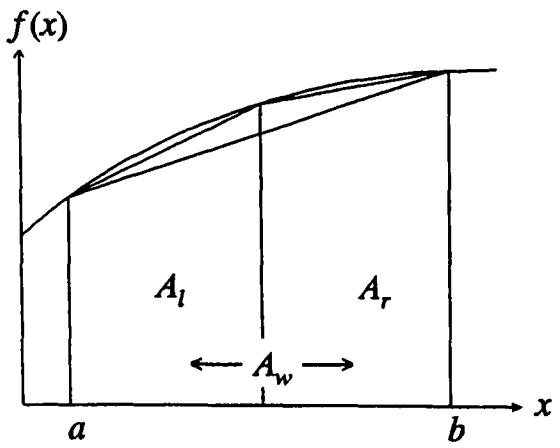


**Figure A-1** Graphical representation of the Trapezium rule applied to a function $f(x)$ for the whole and bisected intervals

A safeguard is used against unnecessary computation for relatively small intervals. For adaptive Simpson, for instance, there is an initial comparison between a Simpson's estimate and two Trapezium estimates. If this fails the convergence test, Simpson's method is continued adaptively. For adaptive Boole, there is an initial comparison between estimates of Simpson and Trapezium; if this fails the convergence test, there is a further comparison between estimates of Boole and Simpson.

## A.2 Levenberg-Marquardt's Method

Levenberg-Marquardt's method [93] can be used to fit a function of the form

$$y = f(x;\ \alpha),$$

where $\alpha_k$, $k = 1,2,...,Q$ are the fitting parameters, to a set of data coordinates $(x_j, y_j)$, $j = 1,2,...,M$. The error sum of squares between the data and the function is

$$E(\alpha) = \sum_{j=1}^{M} [y_j - f(x_j;\ \alpha)]^2.$$

The gradient of $E$ with respect to the parameters $\alpha$ is given by

$$\frac{\partial E}{\partial \alpha_k}, \qquad k = 1,2,...,Q,$$

and the Hessian matrix is defined as

$$\frac{\partial^2 E}{\partial \alpha_k \partial \alpha_l}.$$

Levenberg Marquardt's method transforms continuously between the steepest descent method [80] and the inverse Hessian method [80]. The steepest descent method is used far from

the minimum and depends on the gradient of $E$, and the inverse Hessian method is used as the minimum is approached on a relatively flat surface.

## A.3 Minimisation using Quadratic Interpolation

Consider the minimum of a unimodal function $f(x)$ within the interval $[a, c]$. Quadratic interpolation[94] can be used to reduce the interval to convergence. Let $b$ be some point within the interval $[a, c]$. A Lagrangian interpolation of the three points at $a$, $b$ and $c$ is given as

$$P_2(x) = \frac{(x - b)(x - c)}{(a - b)(a - c)} f(a) + \frac{(x - a)(x - c)}{(b - a)(b - c)} f(b) + \frac{(x - a)(x - b)}{(c - a)(c - b)} f(c).$$

Let the minimum of the quadratic lie at $d$. By basic turning point techniques,

$$d = \frac{(b + c)(b - c)f(a) + (c + a)(c - a)f(b) + (a + b)(a - b)f(c)}{2\{(b - c)f(a) + (c - a)f(b) + (a - b)f(c)\}}.$$

For $d < b$: if $f(d) < f(b)$ the new interval becomes $[a, b]$; if $f(d) > f(b)$ the new interval becomes $[d, c]$ (see Figure A-2). Similar reasoning follows for $d > b$.

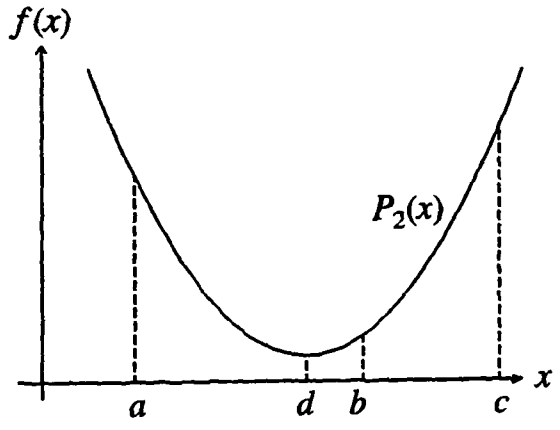


**Figure A-2** Quadratic interpolation through the points at $a$, $b$ and $c$, with estimate of minimum at $d$.

## A.4 Muller's Method

For a function $f(x)$ that has a single root contained within an interval $[a, c]$, Muller's method[95] is a bracketing method that successively reduces the interval to convergence. Let $b$ be some point within the interval $[a, c]$. A lagrangian interpolation[94] of the three points at $a$, $b$ and $c$ is given as

$$P_2(x) = \frac{(x - b)(x - c)}{(a - b)(a - c)} f(a) + \frac{(x - a)(x - c)}{(b - a)(b - c)} f(b) + \frac{(x - a)(x - b)}{(c - a)(c - b)} f(c).$$

The convenient rearrangement $(a - b)(b - c)(c - a)P_2(x)$ is a quadratic in $x$ with the

following coefficients:

$$x^2: \quad -(b - c)f(a) - (c - a)f(b) - (a - b)f(c),$$

$$x: \quad (b + c)(b - c)f(a) + (c + a)(c - a)f(b) + (a + b)(a - b)f(c),$$

$$1: \quad -bc(b - c)f(a) - ca(c - a)f(b) - ab(a - b)f(c).$$

Let $d$ be the root of the quadratic. If $f(b)f(c) < 0$, then $a$ is discarded to make the new triple $b$, $d$ and $c$ (See Figure A-3). Conversely, if $f(a)f(b) < 0$, then $c$ is discarded to make $a$, $d$ and $b$ the new triple.

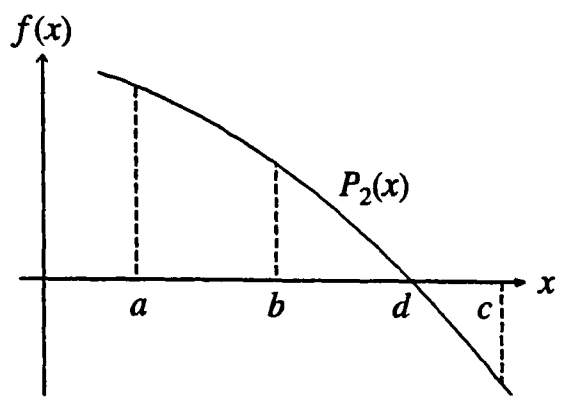


**Figure A-3** Quadratic interpolation through the points at $a$, $b$ and $c$, with an estimate of the root at $d$.

## A.5 Newton's Method for Two-Variable Functions

Consider the equation pair

$$\mathbf{f}(\mathbf{x}) = \mathbf{0},$$

where $\mathbf{f} = [f_1, f_2]^T$ and $\mathbf{x} = [x_1, x_2]^T$. Newton's method [96] for a function of two variables is given as

$$\mathbf{x}^{[m+1]} = \mathbf{x}^{[m]} - J^{-1}(\mathbf{x}^{[m]})\,\mathbf{f}(\mathbf{x}^{[m]}),$$

where $J$—the *Jacobian* of $\mathbf{f}$—is given as

$$J = \begin{bmatrix} \dfrac{\partial f_1}{\partial x_1} & \dfrac{\partial f_1}{\partial x_2} \\ \dfrac{\partial f_2}{\partial x_1} & \dfrac{\partial f_2}{\partial x_2} \end{bmatrix},$$

and $J^{-1}(\mathbf{x}^{[m]})$ is the inverse of $J$ evaluated at $\mathbf{x}^{[m]}$.

## A.6 Runge-Kutta Fehlberg's Method

Consider the initial value problem

$$y' = f(x, y), \qquad y(a) = b.$$

Let $y_i$ be the numerical solution of $y$ at $x_i$. The general $R$-stage, $R$ - 1th order Runge-Kutta method [97] is defined as

$$y_{n+1} = y_n + h\sum_{i=1}^{R} c_i k_i,$$

$$k_i = f\left(x_n + hb_i,\ y_n + h\sum_{j=1}^{R} a_{ij}k_j\right), \qquad i = 1,2,...,R,$$

$$b_i = \sum_{j=1}^{R} a_{ij}.$$

The Butcher matrix [97]—a convenient way of presenting the constants—is

$$\begin{array}{c|c} A & \mathbf{b} \\ \hline \mathbf{c} & \end{array}$$

where $A$ is comprised of $a_{ij}$, $\mathbf{b} = [b_1,...,b_R]^T$, and $\mathbf{c} = [c_1,...,c_R]^T$. Fehlberg's embedded method [98, 99] is variable step, and uses the following fourth and fifth order methods:

$$\begin{array}{ccccc|c}
0 & 0 & 0 & 0 & 0 & 0 \\
\frac{1}{4} & 0 & 0 & 0 & 0 & \frac{1}{4} \\
\frac{3}{32} & \frac{9}{32} & 0 & 0 & 0 & \frac{3}{8} \\
\frac{1932}{2197} & -\frac{7200}{2197} & \frac{7296}{2197} & 0 & 0 & \frac{12}{13} \\
\frac{439}{216} & -8 & \frac{3680}{513} & -\frac{845}{4104} & 0 & 1 \\
\hline
\frac{25}{216} & 0 & \frac{1408}{2565} & \frac{2197}{4104} & -\frac{1}{5} &
\end{array}$$

$$\begin{array}{cccccc|c}
0 & 0 & 0 & 0 & 0 & 0 & 0 \\
\frac{1}{4} & 0 & 0 & 0 & 0 & 0 & \frac{1}{4} \\
\frac{3}{32} & \frac{9}{32} & 0 & 0 & 0 & 0 & \frac{3}{8} \\
\frac{1932}{2197} & -\frac{7200}{2197} & \frac{7296}{2197} & 0 & 0 & 0 & \frac{12}{13} \\
\frac{439}{216} & -8 & \frac{3680}{513} & -\frac{845}{4104} & 0 & 0 & 1 \\
-\frac{8}{27} & 2 & -\frac{3544}{2565} & \frac{1859}{4104} & -\frac{11}{40} & 0 & \frac{1}{2} \\
\hline
\frac{16}{135} & 0 & \frac{6656}{12825} & \frac{28561}{56430} & -\frac{9}{50} & \frac{2}{55} &
\end{array}$$

For computational efficiency, the fourth order methods is embedded within the fifth order method. If $y_{n+1}$ is the fourth order estimate and $y^*_{n+1}$ is the fifth order estimate, the repeated or next step of integration is given by

$$h' = 0.8\,h\left[\frac{\epsilon\,|y^*_{n+1}|}{|y^*_{n+1} - y_{n+1}|}\right]^{\frac{1}{5}},$$

where $\epsilon$ is the required relative tolerance.

# Appendix B The Software

## B.1 Introduction

This appendix lists the key Fortran 77 (Ryan-McFarland, Version 2) routines developed and used for the research. Details are given of each routine's purpose, parameters, and auxiliary routines. Each routine is self-contained and general enough to be relevant for other applications. The routines are grouped into four main sections: the pipe flow routines of Chapter 5; the data reduction routines Chapters 6 and 7; the volume fraction routines of Chapter 8; and routines of the general methods discussed in Appendix A. For simplicity, the routine names of Chapters 5 to 8 have codes such that each letter of a name represents the function given in the following table:

| Flow regime | Prediction | Flow function |
|---|---|---|
| C Critical<br>L Laminar<br>T Turbulent | D Velocity distribution<br>L Log model<br>M Mixing length<br>P Pressure gradient<br>U Mean velocity<br>S Standard model<br>V Volume fraction model<br>W Wall stress | B Bingham<br>E Explicit†<br>G General Bingham<br>I Implicit†<br>N Newtonian<br>P Power law |

† user-defined

Chapter 5 routines are

| | | | | | | |
|---|---|---|---|---|---|---|
| CUE | LDE | LPE | LUE | TDE | TPE | TUE |
| CUI | LDI | LPI | LUI | TDI | TPI | TUI |

Chapters 6 and 7,

| | | | | | | |
|---|---|---|---|---|---|---|
| CUB | LLB | LSB | LWB | | | |
| CUG | LLG | LSG | LWG | TLG | TMG | TWG |
| CUN | LLN | LSN | LWN | | | |
| CUP | LLP | LSP | LWP | | | |

Chapter 8,

| | |
|---|---|
| LVG | TVG |
| LVP | |

The routines of the general methods discussed in Appendix A are summarised in the following table:

| Routine | Purpose |
|---|---|
| BOOLE | Adaptive, non-recursive quadrature using Boole's method. |
| INVERT | Inversion estimate of a single valued function using Muller's method. |
| LEVEN | Fit a non-linear function to a set of values using Levenberg-Marquardt's method (based on the Numerical Recipes [100] routine MRQMIN). |
| LINREG | Simple linear regression. |
| MINIM | Estimate the minimum of a single-valued function using quadratic interpolation. |
| RKFEHL | Numerical approximation of a first order differential equation using Runge-Kutta Fehlberg's method. |
| ROOT | Estimate the root of a single-valued function using Muller's method. |
| SIMP | Adaptive, non-recursive quadrature using Simpson's method. |
| TRAP | Adaptive, non-recursive quadrature using the Trapezium method. |

# B.2 Pipe Flow Routines

## CUE

1. Purpose

The critical flow of a time-independent non-Newtonian viscous fluid through a straight pipe. The predictions are of critical mean cross-sectional velocity and critical pressure gradient. The shear flow relation is a user-definable function of the explicit form

STRESS = FUNONE (RATE).

2. Specification

```
SUBROUTINE  CUE (UCRIT, PGCRIT, DENS, D, TOL)
DOUBLE  PRECISION  UCRIT, PGCRIT, DENS, D, TOL
```

UCRIT - On exit, a prediction of the critical mean cross-sectional velocity [m/s].
PGCRIT - On exit, a prediction of the critical pressure gradient [Pa/m].
DENS - On entry, the density of the fluid [kg/m3].
D - On entry, the diameter of the pipe [m].
TOL - On entry, a relative tolerance check.

3. User-defined function

```
DOUBLE  PRECISION  FUNCTION  FUNONE (RATE)
DOUBLE  PRECISION  RATE
```

RATE - On entry, the rate of shearing strain [1/s].

4. Auxiliary routines

Routines required: INVERT, SIMP.

## CUI

1. Purpose

The critical flow of a time-independent non-Newtonian viscous fluid through a straight pipe. The predictions are of critical mean cross-sectional velocity and critical pressure gradient. The shear flow relation is user-definable function of the implicit form

FUNTWO (RATE, STRESS) = 0.

2. Specification

```
SUBROUTINE CUI (UCRIT, PGCRIT, DENS, D, TOL)
DOUBLE PRECISION UCRIT, PGCRIT, DENS, D, TOL
```

UCRIT - On exit, a prediction of the critical mean cross-sectional velocity [m/s].
PGCRIT - On exit, a prediction of the critical pressure gradient [Pa/m].
DENS - On entry, the density of the fluid [kg/m3].
D - On entry, the diameter of the pipe [m].
TOL - On entry, a relative tolerance check.

3. User-defined function

```
DOUBLE PRECISION FUNCTION FUNTWO (RATE, STRESS)
DOUBLE PRECISION RATE, STRESS
```

RATE - On entry, the rate of shearing strain [1/s].
STRESS - On entry, the shear stress [Pa].

4. Auxiliary routines

Routines required: INVERT, ROOT, SIMP.

## LDE

1. Purpose

The laminar flow of a time-independent non-Newtonian viscous fluid through a straight pipe. The prediction is the velocity distribution; the shear flow relation is a user-definable function of the explicit form

STRESS = FUNONE (RATE).

2. Specification

```
SUBROUTINE LDE (R, U, RPLUG, NPTS, PGRAD, D, TOL)
INTEGER NPTS
DOUBLE PRECISION R (NPTS), U (NPTS), RPLUG, PGRAD, D, TOL
```

R - On exit, a set of equally spaced, radial points of ascending order [m].
U - On exit, an axial-direction velocity prediction at each radial point [m/s].
RPLUG - On exit, a prediction of the radius of the plug core [m].
NPTS - On entry, the number of velocity distribution points.
PGRAD - On entry, pressure gradient—pressure drop per unit pipe length [Pa/m].
D - On entry, the diameter of the pipe [m].
TOL - On entry, a relative tolerance check.

3. User-defined function

```
DOUBLE PRECISION FUNCTION FUNONE (RATE)
DOUBLE PRECISION RATE
```

RATE - On entry, the rate of shearing strain [1/s].

4. Auxiliary routines

Routines required: BOOLE, INVERT.

## LDI

1. Purpose

The laminar flow of a time-independent non-Newtonian viscous fluid through a straight pipe. The prediction is the velocity distribution; the shear flow relation is user-definable function of the implicit form

FUNTWO (RATE, STRESS) = 0.

2. Specification

```
SUBROUTINE LDI (R, U, RPLUG, NPTS, PGRAD, D, TOL)
INTEGER NPTS
DOUBLE PRECISION R (NPTS), U (NPTS), RPLUG, PGRAD, D, TOL
```

R - On exit, a set of equally spaced, radial points of ascending order [m].
U - On exit, an axial-direction velocity prediction at each radial point [m/s].

RPLUG - On exit, a prediction of the radius of the plug core [m].
NPTS - On entry, the number of velocity distribution points.
PGRAD - On entry, pressure gradient—pressure drop per unit pipe length [Pa/m].
D - On entry, the diameter of the pipe [m].
TOL - On entry, a relative tolerance check.

3. User-defined function

```
DOUBLE PRECISION FUNCTION FUNTWO (RATE, STRESS)
DOUBLE PRECISION RATE, STRESS
```

RATE - On entry, the rate of shearing strain [1/s].
STRESS - On entry, the shear stress [Pa].

4. Auxiliary routines

Routines required: BOOLE, ROOT.

## LPE

1. Purpose

The laminar flow of a time-independent non-Newtonian viscous fluid through a straight pipe. The prediction is of pressure gradient; the shear flow relation is a user-definable function of the explicit form

STRESS = FUNONE (RATE).

2. Specification

```
SUBROUTINE LPE (PGRAD, UMEAN, D, TOL)
DOUBLE PRECISION PGRAD, UMEAN, D, TOL
```

PGRAD - On exit, a prediction of pressure drop per unit pipe length [Pa/m].
UMEAN - On entry, the mean cross-sectional velocity of the flow [m/s].
D - On entry, the diameter of the pipe [m].
TOL - On entry, a relative tolerance check.

3. User-defined function

```
DOUBLE PRECISION FUNCTION FUNONE (RATE)
DOUBLE PRECISION RATE
```

RATE - On entry, the rate of shearing strain [1/s].

4. Auxiliary routines

Routines required: RKFEHL, SIMP.

## LPI

1. Purpose

The laminar flow of a time-independent non-Newtonian viscous fluid through a straight pipe. The prediction is of pressure gradient; the shear flow relation is user-definable function of the implicit form

FUNTWO (RATE, STRESS) = Ø.

2. Specification

```
SUBROUTINE LPI (PGRAD, UMEAN, D, TOL)
DOUBLE PRECISION PGRAD, UMEAN, D, TOL
```

PGRAD - On exit, a prediction of pressure drop per unit pipe length [Pa/m].
UMEAN - On entry, the mean cross-sectional velocity of the flow [m/s].
D - On entry, the diameter of the pipe [m].
TOL - On entry, a relative tolerance check.

3. User-defined function

```
DOUBLE PRECISION FUNCTION FUNTWO (RATE, STRESS)
DOUBLE PRECISION RATE, STRESS
```

RATE - On entry, the rate of shearing strain [1/s].
STRESS - On entry, the shear stress [Pa].

4. Auxiliary routines

Routines required: RKFEHL, ROOT, SIMP.

## LUE

1. Purpose

The laminar flow of a time-independent non-Newtonian viscous fluid through a straight pipe. The prediction is of mean cross-sectional velocity; the shear flow relation is a user-definable function of the explicit form

STRESS = FUNONE (RATE).

2. Specification

```
SUBROUTINE  LUE (UMEAN, PGRAD, D, TOL)
DOUBLE  PRECISION  UMEAN, PGRAD, D, TOL
```

UMEAN - On exit, a prediction of the mean cross-sectional velocity [m/s].
PGRAD - On entry, pressure gradient—pressure drop per unit pipe length [Pa/m].
D - On entry, the diameter of the pipe [m].
TOL - On entry, a relative tolerance check.

3. User-defined function

```
DOUBLE  PRECISION  FUNCTION  FUNONE (RATE)
DOUBLE  PRECISION  RATE
```

RATE - On entry, the rate of shearing strain [1/s].

4. Auxiliary routines

Routines required: INVERT, SIMP.

## LUI

1. Purpose

The laminar flow of a time-independent non-Newtonian viscous fluid through a straight pipe. The prediction is of mean cross-sectional velocity; the shear flow relation is user-definable function of the implicit form

FUNTWO (RATE, STRESS) = Ø.

2. Specification

```
SUBROUTINE  LUI (UMEAN, PGRAD, D, TOL)
DOUBLE  PRECISION  UMEAN, PGRAD, D, TOL
```

UMEAN - On exit, a prediction of the mean cross-sectional velocity [m/s].
PGRAD - On entry, pressure gradient—pressure drop per unit pipe length [Pa/m].
D - On entry, the diameter of the pipe [m].
TOL - On entry, a relative tolerance check.

3. User-defined function

```
DOUBLE  PRECISION  FUNCTION  FUNTWO (RATE, STRESS)
DOUBLE  PRECISION  RATE, STRESS
```

RATE - On entry, the rate of shearing strain [1/s].
STRESS - On entry, the shear stress [Pa].

4. Auxiliary routines

Routines required: ROOT, SIMP.

## TDE

1. Purpose

The turbulent flow of a time-independent non-Newtonian viscous fluid through a straight pipe. The prediction is the velocity distribution; the laminar shear flow relation is a user-definable function of the explicit form

STRESS = FUNONE (RATE).

2. Specification

```
SUBROUTINE  TDE (R, U, RPLUG, NPTS, PGRAD, WCRIT, DENS, D, TOL)
INTEGER  NPTS
DOUBLE  PRECISION  R (NPTS), U (NPTS),
+          RPLUG, PGRAD, WCRIT, DENS, D, TOL
```

R - On exit, a set of equally spaced, radial points of ascending order [m].
U - On exit, an axial-direction velocity prediction at each radial point [m/s].
RPLUG - On exit, a prediction of the radius of the plug core [m].
NPTS - On entry, the number of velocity distribution points.
PGRAD - On entry, pressure gradient—pressure drop per unit pipe length [Pa/m].
WCRIT - On entry, the critical shear stress at the pipe wall [Pa].
DENS - On entry, the density of the fluid [kg/m3].

D - On entry, the diameter of the pipe [m].
TOL - On entry, a relative tolerance check.

3. User-defined function

```
DOUBLE PRECISION FUNCTION FUNONE (RATE)
DOUBLE PRECISION RATE
```

RATE - On entry, the rate of shearing strain [1/s].

4. Auxiliary routines

Routines required: BOOLE, ROOT, TMG.

## TDI

1. Purpose

The turbulent flow of a time-independent non-Newtonian viscous fluid through a straight pipe. The prediction is the velocity distribution; the laminar shear flow relation is user-definable function of the implicit form

FUNTWO (RATE, STRESS) = Ø.

2. Specification

```
SUBROUTINE TDI (R, U, RPLUG, NPTS,
+          PGRAD, WCRIT, DENS, D, TOL)
INTEGER NPTS
DOUBLE PRECISION R (NPTS), U (NPTS), RPLUG,
+          PGRAD, WCRIT, DENS, D, TOL
```

R - On exit, a set of equally spaced, radial points of ascending order [m].
U - On exit, an axial-direction velocity prediction at each radial point [m/s].
RPLUG - On exit, a prediction of the radius of the plug core [m].
NPTS - On entry, the number of velocity distribution points.
PGRAD - On entry, pressure gradient—pressure drop per unit pipe length [Pa/m].
WCRIT - On entry, the critical shear stress at the pipe wall [Pa].
DENS - On entry, the density of the fluid [kg/m3].
D - On entry, the diameter of the pipe [m].
TOL - On entry, a relative tolerance check.

3. User-defined function

```
DOUBLE PRECISION FUNCTION FUNTWO (RATE, STRESS)
DOUBLE PRECISION RATE, STRESS
```

RATE - On entry, the rate of shearing strain [1/s].
STRESS - On entry, the shear stress [Pa].

4. Auxiliary routines

Routines required: BOOLE, ROOT, TMG.

## TPE

1. Purpose

The turbulent flow of a time-independent non-Newtonian viscous fluid through a straight pipe. The prediction is of pressure gradient; the laminar shear flow relation is a user-definable function of the explicit form

STRESS = FUNONE (RATE).

2. Specification

```
SUBROUTINE TPE (PGRAD, UMEAN, WCRIT, DENS, D, TOL)
DOUBLE PRECISION PGRAD, UMEAN, WCRIT, DENS, D, TOL
```

PGRAD - On exit, a prediction of pressure drop per unit pipe length [Pa/m].
UMEAN - On entry, the mean cross-sectional velocity of the flow [m/s].
WCRIT - On entry, the critical shear stress at the pipe wall [Pa].
DENS - On entry, the density of the fluid [kg/m3].
D - On entry, the diameter of the pipe [m].
TOL - On entry, a relative tolerance check.

3. User-defined function

```
DOUBLE PRECISION FUNCTION FUNONE (RATE)
DOUBLE PRECISION RATE
```

RATE - On entry, the rate of shearing strain [1/s].

4. Auxiliary routines

Routines required: BOOLE, INVERT, ROOT, TMG.

## TPI

1. Purpose

The turbulent flow of a time-independent non-Newtonian viscous fluid through a straight pipe. The prediction is of pressure gradient; the laminar shear flow relation is user-definable function of the implicit form

FUNTWO (RATE, STRESS) = Ø.

2. Specification

```
SUBROUTINE  TPI (PGRAD, UMEAN, WCRIT, DENS, D, TOL)
DOUBLE  PRECISION  PGRAD, UMEAN, WCRIT, DENS, D, TOL
```

PGRAD - On exit, a prediction of pressure drop per unit pipe length [Pa/m].
UMEAN - On entry, the mean cross-sectional velocity of the flow [m/s].
WCRIT - On entry, the critical shear stress at the pipe wall [Pa].
DENS - On entry, the density of the fluid [kg/m3].
D - On entry, the diameter of the pipe [m].
TOL - On entry, a relative tolerance check.

3. User-defined function

```
DOUBLE  PRECISION  FUNCTION  FUNTWO (RATE, STRESS)
DOUBLE  PRECISION  RATE, STRESS
```

RATE - On entry, the rate of shearing strain [1/s].
STRESS - On entry, the shear stress [Pa].

4. Auxiliary routines

Routines required: BOOLE, INVERT, ROOT, TMG.

## TUE

1. Purpose

The turbulent flow of a time-independent non-Newtonian viscous fluid through a straight pipe. The prediction is of mean cross-sect velocity; the laminar shear flow relation is a user-definable function of the explicit form

STRESS = FUNONE (RATE).

2. Specification

```
SUBROUTINE  TUE (UMEAN, PGRAD, WCRIT, DENS, D, TOL)
DOUBLE  PRECISION  UMEAN, PGRAD, WCRIT, DENS, D, TOL
```

UMEAN - On exit, a prediction of the mean cross-sectional velocity [m/s].
PGRAD - On entry, pressure gradient—pressure drop per unit pipe length [Pa/m].
WCRIT - On entry, the critical shear stress at the pipe wall [Pa].
DENS - On entry, the density of the fluid [kg/m3].
D - On entry, the diameter of the pipe [m].
TOL - On entry, a relative tolerance check.

3. User-defined function

```
DOUBLE  PRECISION  FUNCTION  FUNONE (RATE)
DOUBLE  PRECISION  RATE
```

RATE - On entry, the rate of shearing strain [1/s].

4. Auxiliary routines

Routines required: INVERT, ROOT, SIMP, TMG.

## TUI

1. Purpose

The turbulent flow of a time-independent non-Newtonian viscous fluid through a straight pipe. The prediction is of mean cross-sect velocity; the laminar shear flow relation is user-definable function of the implicit form

FUNTWO (RATE, STRESS) = Ø.

2. Specification

```
SUBROUTINE  TUI (UMEAN, PGRAD, WCRIT, DENS, D, TOL)
DOUBLE  PRECISION  UMEAN, PGRAD, WCRIT, DENS, D, TOL
```

UMEAN - On exit, a prediction of the mean cross-sectional velocity [m/s].

PGRAD - On entry, pressure gradient—pressure drop per unit pipe length [Pa/m].
WCRIT - On entry, the critical shear stress at the pipe wall [Pa].
DENS - On entry, the density of the fluid [kg/m3].
D - On entry, the diameter of the pipe [m].
TOL - On entry, a relative tolerance check.

3. User-defined function

```
DOUBLE PRECISION FUNCTION FUNTWO (RATE, STRESS)
DOUBLE PRECISION RATE, STRESS
```

RATE - On entry, the rate of shearing strain [1/s].
STRESS - On entry, the shear stress [Pa].

4. Auxiliary routines

Routines required: ROOT, SIMP, TMG.

# B.3 Data Reduction Routines

## CUB

1. Purpose

The critical flow of a Bingham fluid through a straight pipe. The predictions are of critical mean cross-sectional velocity and critical pipe wall stress. The shear flow relation is the Bingham function

```
STRESS = Y + ETA * RATE.
```

2. Specification

```
SUBROUTINE CUB (UCRIT, WCRIT, Y, ETA, DENS, D, TOL)
DOUBLE PRECISION UCRIT, WCRIT, Y, ETA, DENS, D, TOL
```

UCRIT - On exit, a prediction of the critical mean cross-sectional velocity [m/s].
WCRIT - On exit, a prediction of the critical shear stress at the pipe wall [Pa].
Y - On entry, the yield stress of the fluid [Pa].
ETA - On entry, the coefficient of rigidity of the fluid [Pa s].
DENS - On entry, the density of the fluid [kg/m3].
D - On entry, the diameter of the pipe [m].
TOL - On entry, a relative tolerance check.

## CUG

1. Purpose

The critical flow of a general Bingham fluid through a straight pipe. The predictions are of critical mean cross-sectional velocity and critical pipe wall stress. The shear flow relation is the general Bingham function

```
STRESS = Y + GK * RATE ** GN.
```

2. Specification

```
SUBROUTINE CUG (UCRIT, WCRIT, Y, GK, GN, DENS, D, TOL)
DOUBLE PRECISION UCRIT, WCRIT, Y, GK, GN, DENS, D, TOL
```

UCRIT - On exit, a prediction of the critical mean cross-sectional velocity [m/s].
WCRIT - On exit, a prediction of the critical shear stress at the pipe wall [Pa].
Y - On entry, the yield stress of the fluid [Pa].
GK - On entry, the general Bingham consistency coefficient of the fluid.
GN - On entry, the general Bingham consistency index of the fluid.
DENS - On entry, the density of the fluid [kg/m3].
D - On entry, the diameter of the pipe [m].
TOL - On entry, a relative tolerance check.

3. Auxiliary routines

Routines required: INVERT.

## CUN

1. Purpose

The critical flow of a Newtonian viscous fluid through a straight pipe. The predictions are of critical mean cross-sectional velocity and critical pipe wall stress. The shear flow relation is the Newtonian function

```
STRESS = VISC * RATE.
```

2. Specification

```
SUBROUTINE  CUN (UCRIT, WCRIT, VISC, DENS, D)
DOUBLE  PRECISION  UCRIT, WCRIT, VISC, DENS, D
```

UCRIT - On exit, a prediction of the critical mean cross-sectional velocity [m/s].
WCRIT - On exit, a prediction of the critical shear stress at the pipe wall [Pa].
VISC - On entry, the dynamic viscosity of the fluid [Pa s].
DENS - On entry, the density of the fluid [kg/m3].
D - On entry, the diameter of the pipe [m].

## CUP

1. Purpose

The critical flow of a power law fluid through a straight pipe. The predictions are of critical mean cross-sectional velocity and critical pipe wall stress. The shear flow relation is the power law function

STRESS = PK * RATE ** PN.

2. Specification

```
SUBROUTINE  CUP (UCRIT, WCRIT, PK, PN, DENS, D)
DOUBLE  PRECISION  UCRIT, WCRIT, PK, PN, DENS, D
```

UCRIT - On exit, a prediction of the critical mean cross-sectional velocity [m/s].
WCRIT - On exit, a prediction of the critical shear stress at the pipe wall [Pa].
PK - On entry, the power law consistency coefficient of the fluid.
PN - On entry, the power law consistency index of the fluid.
DENS - On entry, the density of the fluid [kg/m3].
D - On entry, the diameter of the pipe [m].

## LLB

1. Purpose

The laminar flow of a Bingham fluid through a straight pipe. For a given data set, estimate the parameters of the log Bingham model

LOG10 (STRESS - Y) = LOG10 (ETA) + LOG10 (RATE).

2. Specification

```
      SUBROUTINE  LLB (Y, ETA, RESID, SSERR, SERR,
     +          PSRATE, WALL, NVALS, TOL)
      INTEGER  NVALS
      DOUBLE  PRECISION  Y, ETA, RESID (NVALS), SSERR, SERR,
     +          PSRATE (NVALS), WALL (NVALS), TOL
```

Y - On exit, an estimate of the yield stress of the fluid [Pa].
ETA - On exit, an estimate of the coefficient of rigidity of the fluid [Pa s].
RESID - On exit, the residuals—observed minus predicted values—of the model.
SSERR - On exit, the error sum of squares of the model.
SERR - On exit, the standard error of the model.
PSRATE - On entry, the pseudo-shear rate values, 8*UMEAN/D [1/s].
WALL - On entry, the wall shear stress values corresponding to PSRATE [Pa].
NVALS - On entry, the number of data values.
TOL - On entry, a relative tolerance check.

3. Working storage parameters

```
PARAMETER (MAXV=20)
```

in the main routine LLB itself.

MAXV - The maximum possible number of data values.

4. Auxiliary routines

Routines required: LWB.

## LLG

1. Purpose

The laminar flow of a general Bingham fluid through a straight pipe. For a given data set, estimate the parameters of the log general Bingham model

LOG10 (STRESS - Y) = LOG10 (GK) + GN * LOG10 (RATE).

2. Specification

```
      SUBROUTINE  LLG (Y, GK, GN, RESID, SSERR, SERR,
     +          PSRATE, WALL, NVALS, TOL)
      INTEGER  NVALS
      DOUBLE  PRECISION  Y, GK, GN, RESID (NVALS), SSERR, SERR,
     +          PSRATE (NVALS), WALL (NVALS), TOL
```

Y - On exit, an estimate of the yield stress of the fluid [Pa].
GK - On exit, an estimate of the consistency coefficient of the fluid.
GN - On exit, an estimate of the consistency index of the fluid.
RESID - On exit, the residuals—observed minus predicted values—of the model.
SSERR - On exit, the error sum of squares of the model.
SERR - On exit, the standard error of the model.
PSRATE - On entry, the pseudo-shear rate values, 8*UMEAN/D [1/s].
WALL - On entry, the wall shear stress values corresponding to PSRATE [Pa].
NVALS - On entry, the number of data values.
TOL - On entry, a relative tolerance check.

3. Working storage parameters

PARAMETER (MAXV=2Ø)
in the main routine LLG itself.

MAXV - The maximum possible number of data values.

4. Auxiliary routines

Routines required: LWG.

## LLN

1. Purpose

The laminar flow of a Newtonian viscous fluid through a straight pipe. For a given data set, estimate the parameter of the log Newtonian model

LOG1Ø (STRESS) = LOG1Ø (VISC) + LOG1Ø (RATE).

2. Specification

```
      SUBROUTINE  LLN (VISC, RESID, SSERR, SERR, PSRATE, WALL, NVALS)
      INTEGER  NVALS
      DOUBLE  PRECISION  VISC, RESID (NVALS), SSERR, SERR,
     +          PSRATE (NVALS), WALL (NVALS)
```

VISC - On exit, an estimate of the dynamic viscosity of the fluid [Pa s].
RESID - On exit, the residuals—observed minus predicted values—of the model.
SSERR - On exit, the error sum of squares of the model.
SERR - On exit, the standard error of the model.
PSRATE - On entry, the pseudo-shear rate values, 8*UMEAN/D [1/s].
WALL - On entry, the wall shear stress values corresponding to PSRATE [Pa].
NVALS - On entry, the number of data values.

## LLP

1. Purpose

The laminar flow of a power law fluid through a straight pipe. For a given data set, estimate the parameters of the log power law model

LOG1Ø (STRESS) = LOG1Ø (PK) + PN * LOG1Ø (RATE).

2. Specification

```
      SUBROUTINE  LLP (PK, PN, RESID, SSERR, SERR, PSRATE, WALL, NVALS)
      INTEGER  NVALS
      DOUBLE  PRECISION  PK, PN, RESID (NVALS), SSERR, SERR,
     +          PSRATE (NVALS), WALL (NVALS)
```

PK - On exit, an estimate of the consistency coefficient of the fluid.
PN - On exit, an estimate of the consistency index of the fluid.
RESID - On exit, the residuals—observed minus predicted values—of the model.
SSERR - On exit, the error sum of squares of the model.
SERR - On exit, the standard error of the model.
PSRATE - On entry, the pseudo-shear rate values, 8*UMEAN/D [1/s].
WALL - On entry, the wall shear stress values corresponding to PSRATE [Pa].
NVALS - On entry, the number of data values.

3. Working storage parameters

PARAMETER (MAXV=20)
in the main routine LLP itself.

MAXV - The maximum possible number of data values.

4. Auxiliary routines

Routines required: LINREG.

## LSB

1. Purpose

The laminar flow of a Bingham fluid through a straight pipe. For a given data set, estimate the parameters of the standard Bingham model

STRESS = Y + ETA * RATE.

2. Specification

```
      SUBROUTINE  LSB (Y, ETA, RESID, SSERR, SERR,
     +          PSRATE, WALL, NVALS, TOL)
      INTEGER  NVALS
      DOUBLE  PRECISION  Y, ETA, RESID (NVALS), SSERR, SERR,
     +          PSRATE (NVALS), WALL (NVALS), TOL
```

Y - On exit, an estimate of the yield stress of the fluid [Pa].
ETA - On exit, an estimate of the coefficient of rigidity of the fluid [Pa s].
RESID - On exit, the residuals—observed minus predicted values—of model [Pa].
SSERR - On exit, the error sum of squares of the model [Pa2].
SERR - On exit, the standard error of the model [Pa].
PSRATE - On entry, the pseudo-shear rate values, 8*UMEAN/D [1/s].
WALL - On entry, the wall shear stress values corresponding to PSRATE [Pa].
NVALS - On entry, the number of data values.
TOL - On entry, a relative tolerance check.

3. Auxiliary routines

Routines required: LEVEN, LWB.

## LSG

1. Purpose

The laminar flow of a general Bingham fluid through a straight pipe. For a given data set, estimate the parameters of the standard general Bingham model

STRESS = Y + GK * RATE ** GN.

2. Specification

```
      SUBROUTINE  LSG (Y, GK, GN, RESID, SSERR, SERR,
     +          PSRATE, WALL, NVALS, TOL)
      INTEGER  NVALS
      DOUBLE  PRECISION  Y, GK, GN, RESID (NVALS), SSERR, SERR,
     +          PSRATE (NVALS), WALL (NVALS), TOL
```

Y - On exit, an estimate of the yield stress of the fluid [Pa].
GK - On exit, an estimate of the consistency coefficient of the fluid.
GN - On exit, an estimate of the consistency index of the fluid.
RESID - On exit, the residuals—observed minus predicted values—of model [Pa].
SSERR - On exit, the error sum of squares of the model [Pa2].
SERR - On exit, the standard error of the model [Pa].
PSRATE - On entry, the pseudo-shear rate values, 8*UMEAN/D [1/s].
WALL - On entry, the wall shear stress values corresponding to PSRATE [Pa].
NVALS - On entry, the number of data values.
TOL - On entry, a relative tolerance check.

3. Auxiliary routines

Routines required: LEVEN, LWG.

## LSN

1. Purpose

The laminar flow of a Newtonian viscous fluid through a straight pipe. For a given data set, estimate the parameter of the standard Newtonian model

STRESS = VISC * RATE.

2. Specification

```
SUBROUTINE  LSN (VISC, RESID, SSERR, SERR, PSRATE, WALL, NVALS)
INTEGER  NVALS
DOUBLE  PRECISION  VISC, RESID (NVALS), SSERR, SERR,
+          PSRATE (NVALS), WALL (NVALS)
```

VISC - On exit, an estimate of the dynamic viscosity of the fluid [Pa s].
RESID - On exit, the residuals—observed minus predicted values—of model [Pa].
SSERR - On exit, the error sum of squares of the model [Pa2].
SERR - On exit, the standard error of the model [Pa].
PSRATE - On entry, the pseudo-shear rate values, 8*UMEAN/D [1/s].
WALL - On entry, the wall shear stress values corresponding to PSRATE [Pa].
NVALS - On entry, the number of data values.

## LSP

1. Purpose

The laminar flow of a power law fluid through a straight pipe. For a given data set, estimate the parameters of the standard power law model

STRESS = PK * RATE ** PN.

2. Specification

```
SUBROUTINE  LSP (PK, PN, RESID, SSERR, SERR,
+          PSRATE, WALL, NVALS, TOL)
INTEGER  NVALS
DOUBLE  PRECISION  PK, PN, RESID (NVALS), SSERR, SERR,
+          PSRATE (NVALS), WALL (NVALS), TOL
```

PK - On exit, an estimate of the consistency coefficient of the fluid.
PN - On exit, an estimate of the consistency index of the fluid.
RESID - On exit, the residuals—observed minus predicted values—of model [Pa].
SSERR - On exit, the error sum of squares of the model [Pa2].
SERR - On exit, the standard error of the model [Pa].
PSRATE - On entry, the pseudo-shear rate values, 8*UMEAN/D [1/s].
WALL - On entry, the wall shear stress values corresponding to PSRATE [Pa].
NVALS - On entry, the number of data values.
TOL - On entry, a relative tolerance check.

## LWB

1. Purpose

The laminar flow of a Bingham fluid through a straight pipe. The prediction is of wall shear stress; the shear flow relation is the Bingham function

STRESS = Y + ETA * RATE.

2. Specification

```
SUBROUTINE  LWB (WALL, PSRATE, Y, ETA, TOL)
DOUBLE  PRECISION  WALL, PSRATE, Y, ETA, TOL
```

WALL - On exit, a prediction of shear stress at the pipe wall [Pa].
PSRATE - On entry, the pseudo-shear rate, 8*UMEAN/D [1/s].
Y - On entry, the yield stress of the fluid [Pa].
ETA - On entry, the coefficient of rigidity of the fluid [Pa s].
TOL - On entry, a relative tolerance check.

## LWG

1. Purpose

The laminar flow of a general Bingham fluid through a straight pipe. The prediction is of wall shear stress; the shear flow relation is the general Bingham function

STRESS = Y + GK * RATE ** GN.

2. Specification

```
SUBROUTINE LWG (WALL, PSRATE, Y, GK, GN, TOL)
DOUBLE PRECISION WALL, PSRATE, Y, GK, GN, TOL
```

WALL - On exit, a prediction of shear stress at the pipe wall [Pa].
PSRATE - On entry, the pseudo-shear rate, 8*UMEAN/D [1/s].
Y - On entry, the yield stress of the fluid [Pa].
GK - On entry, the general Bingham consistency coefficient of the fluid.
GN - On entry, the general Bingham consistency index of the fluid.
TOL - On entry, a relative tolerance check.

## LWN

1. Purpose

The laminar flow of a Newtonian viscous fluid through a straight pipe. The prediction is of wall shear stress; the shear flow relation is the Newtonian function

```
STRESS = VISC * RATE.
```

2. Specification

```
SUBROUTINE LWN (WALL, PSRATE, VISC)
DOUBLE PRECISION WALL, PSRATE, VISC
```

WALL - On exit, a prediction of shear stress at the pipe wall [Pa].
PSRATE - On entry, the pseudo-shear rate, 8*UMEAN/D [1/s].
VISC - On entry, the dynamic viscosity of the fluid [Pa s].

## LWP

1. Purpose

The laminar flow of a power law fluid through a straight pipe. The prediction is of wall shear stress; the shear flow relation is the power law function

```
STRESS = PK * RATE ** PN.
```

2. Specification

```
SUBROUTINE LWP (WALL, PSRATE, PK, PN)
DOUBLE PRECISION WALL, PSRATE, PK, PN
```

WALL - On exit, a prediction of shear stress at the pipe wall [Pa].
PSRATE - On entry, the pseudo-shear rate, 8*UMEAN/D [1/s].
PK - On entry, the power law consistency coefficient of the fluid.
PN - On entry, the power law consistency index of the fluid.

## TLG

1. Purpose

The turbulent flow of a general Bingham fluid through a straight pipe. For a given data set, estimate the parameter of the log turbulent flow model

```
LOG1Ø (STRESS - Y) + LOG1Ø (GK * RATE ** GN +
DENS * TMG (STRESS, GK, GN, B, WALL,...)**2 * RATE**2).
```

2. Specification

```
SUBROUTINE TLG (B, RESID, SSERR, SERR,
+          PSRATE, WALL, NVALS, Y, GK, GN, WCRIT, DENS, D, TOL)
INTEGER NVALS
DOUBLE PRECISION B, RESID (NVALS), SSERR, SERR,
+          PSRATE (NVALS), WALL (NVALS), Y, GK, GN, WCRIT, DENS, D, TOL
```

B - On exit, an estimate of the turbulence parameter of the fluid.
RESID - On exit, the residuals—observed minus predicted values—of the model.
SSERR - On exit, the error sum of squares of the model.
SERR - On exit, the standard error of the model.
PSRATE - On entry, the pseudo-shear rate values, 8*UMEAN/D [1/s].
WALL - On entry, the wall shear stress values corresponding to PSRATE [Pa].
NVALS - On entry, the number of data values.
Y - On entry, an estimate of the yield stress of the fluid [Pa].
GK - On entry, an estimate of the consistency coefficient of the fluid.
GN - On entry, an estimate of the consistency index of the fluid.
WCRIT - On entry, the critical shear stress at the pipe wall [Pa].
DENS - On entry, the density of the fluid [kg/m3].
D - On entry, the diameter of the pipe [m].
TOL - On entry, a relative tolerance check.

3. Working storage parameters

PARAMETER (MAXV=20)
in both the main routine TLG and in the subroutine TLG1 of the same file.

MAXV - The maximum possible number of data values.

4. Auxiliary routines

Routines required: BOOLE, INVERT, MINIM, ROOT, TMG.

## TMG

1. Purpose

The turbulent flow of a general Bingham fluid through a straight pipe. The prediction is of the mixing length.

2. Specification

```
      DOUBLE PRECISION FUNCTION TMG
     +          (STRESS, GK, GN, B, WALL, WCRIT, DENS, D)
      DOUBLE PRECISION STRESS, GK, GN, B, WALL, WCRIT, DENS, D
```

STRESS - On entry, the shear stress [Pa].
GK - On entry, the general Bingham consistency coefficient of the fluid.
GN - On entry, the general Bingham consistency index of the fluid.
B - On entry, the turbulence parameter of the fluid.
WALL - On entry, the shear stress at the pipe wall [Pa].
WCRIT - On entry, the critical shear stress at the pipe wall [Pa].
DENS - On entry, the density of the fluid [kg/m3].
D - On entry, the diameter of the pipe [m].

## TWG

1. Purpose

The turbulent flow of a general Bingham fluid through a straight pipe. The prediction is of wall shear stress; the shear flow relation is the following sum of the laminar flow general Bingham function and the turbulent flow function.

```
STRESS = Y + GK * RATE ** GN +
DENS * TMG (STRESS, GK, GN, B, WALL,...)**2 * RATE**2.
```

2. Specification

```
      SUBROUTINE TWG (WALL, PSRATE, Y, GK, GN, B, WCRIT, DENS, D, TOL)
      DOUBLE PRECISION WALL, PSRATE, Y, GK, GN, B, WCRIT, DENS, D, TOL
```

WALL - On exit, a prediction of shear stress at the pipe wall [Pa].
PSRATE - On entry, the pseudo-shear rate, 8*UMEAN/D [1/s].
Y - On entry, the yield stress of the fluid [Pa].
GK - On entry, the general Bingham consistency coefficient of the fluid.
GN - On entry, the general Bingham consistency index of the fluid.
B - On entry, the turbulence parameter of the fluid.
WCRIT - On entry, the critical shear stress at the pipe wall [Pa].
DENS - On entry, the density of the fluid [kg/m3].
D - On entry, the diameter of the pipe [m].
TOL - On entry, a relative tolerance check.

3. Auxiliary routines

Routines required: BOOLE, INVERT, ROOT, TMG.

# B.4 Volume Fraction Routines

## LVG

1. Purpose

The laminar flow of a general Bingham fluid through a straight pipe. For a specific sludge type and for I = 1,...,N sludge samples, estimate parameters of the volume fraction model

```
LOG10 (STRESS - A1 * (VF (I) - VFC) ** A4) =
LOG10 (A3) + A4 * (VF (I) - VFC) +
LOG10 (RATE) / (1 + A5 * (VF (I) - VFC) ** A6).
```

2. Specification

```
      SUBROUTINE  LVG (A4, A6, A1, A3, A5, RESID, SSERR, SERR,
     +          PSRATE, WALL, VF, VFC, NVALS, MAXV, NSETS, TOL)
      INTEGER  NVALS (NSETS), MAXV, NSETS
      DOUBLE  PRECISION  A4, A6, A1, A3, A5, RESID (MAXV, NSETS),
     +          SSERR, SERR, PSRATE (MAXV, NSETS), WALL (MAXV, NSETS),
     +          VF (NSETS), VFC, TOL
```

A4, A6 - On entry, the fixed parameters.
A1, A3, A5 - On exit, estimates of the parameters.
RESID - On exit, the residuals—observed minus predicted values—of the model.
SSERR - On exit, the total error sum of squares of the model.
SERR - On exit, the total standard error of the model.
PSRATE - On entry, the pseudo-shear rate values, 8*UMEAN/D [1/s].
WALL - On entry, the wall shear stress values corresponding to PSRATE [Pa].
VF - On entry, the volume fraction of solids for each data set.
VFC - On entry, the Newtonian/non-Newtonian critical volume fraction of solids.
NVALS - On entry, the number of data values for each data set.
MAXV - On entry, the maximum number of possible data values for any data set.
NSETS - On entry, the number of data sets.
TOL - On entry, a relative tolerance check.

3. Working storage parameters

```
PARAMETER (MAXDAT=600, MAXS=100)
```
in main routine LVG, and
```
PARAMETER (MAXS=100)
```
in subroutine LVG1 of the same file.

MAXDAT - The total maximum number of data values possible.
MAXS - The maximum number of data sets possible.

4. Auxiliary routines

Routines required: LEVEN, LWG.

## LVP

1. Purpose

The laminar flow of a power law fluid through a straight pipe. For a specific sludge type and for I = 1,...,N sludge samples, estimate parameters of the volume fraction model

```
LOG10 (STRESS) = LOG10 (A3) + A4 * (VF (I) - VFC) +
LOG10 (RATE) / (1 + A5 * (VF (I) - VFC) ** A6).
```

2. Specification

```
      SUBROUTINE  LVP (A4, A6, A3, A5, RESID, SSERR, SERR,
     +          PSRATE, WALL, VF, VFC, NVALS, MAXV, NSETS, TOL)
      INTEGER  NVALS (NSETS), MAXV, NSETS
      DOUBLE  PRECISION  A4, A6, A3, A5, RESID (MAXV, NSETS),
     +          SSERR, SERR, PSRATE (MAXV, NSETS), WALL (MAXV, NSETS),
     +          VF (NSETS), VFC, TOL
```

A4, A6 - On entry, the fixed parameters.
A3, A5 - On exit, estimates of the parameters.
RESID - On exit, the residuals—observed minus predicted values—of the model.
SSERR - On exit, the total error sum of squares of the model.
SERR - On exit, the total standard error of the model.
PSRATE - On entry, the pseudo-shear rate values, 8*UMEAN/D [1/s].
WALL - On entry, the wall shear stress values corresponding to PSRATE [Pa].
VF - On entry, the volume fraction of solids for each data set.
VFC - On entry, the Newtonian/non-Newtonian critical volume fraction of solids.
NVALS - On entry, the number of data values for each data set.
MAXV - On entry, the maximum number of possible data values for any data set.
NSETS - On entry, the number of data sets.
TOL - On entry, a relative tolerance check.

3. Working storage parameters

```
PARAMETER (MAXDAT=600, MAXS=100)
```
in main routine LVP, and
```
PARAMETER (MAXS=100)
```
in subroutine LVP1 of the same file.

MAXDAT - The total maximum number of data values possible.
MAXS - The maximum number of data sets possible.

4. Auxiliary routines

Routines required: LEVEN, LWP.

## TVG

1. Purpose

The turbulent flow of a general Bingham fluid through a straight pipe. For a specific sludge type and for I = 1,...,N sludge samples, estimate the parameter BETA of the volume fraction model with the turbulence parameter

$$B = BETA * (VF(I) - VFC) + 22.$$

2. Specification

```
      SUBROUTINE  TVG (BETA, RESID, SSERR, SERR,
     +          PSRATE, WALL, Y, GK, GN, WCRIT, DENS, D, VF, VFC,
     +          NVALS, MAXV, NSETS, TOL)
      INTEGER  NVALS (NSETS), MAXV, NSETS
      DOUBLE PRECISION  BETA, RESID (MAXV, NSETS), SSERR, SERR,
     +          PSRATE (MAXV, NSETS), WALL (MAXV, NSETS),
     +          Y (NSETS), GK (NSETS), GN (NSETS), WCRIT (NSETS),
     +          DENS (NSETS), D (NSETS), VF (NSETS), VFC, TOL
```

BETA - On exit, an estimate of the parameter.
RESID - On exit, the residuals—observed minus predicted values—of the model.
SSERR - On exit, the total error sum of squares of the model.
SERR - On exit, the total standard error of the model.
PSRATE - On entry, the pseudo-shear rate values, 8*UMEAN/D [1/s].
WALL - On entry, the wall shear stress values corresponding to PSRATE [Pa].
Y - On entry, the yield stress for each data set [Pa].
GK - On entry, the general Bingham consistency coefficient for each data set.
GN - On entry, the general Bingham consistency index for each data set.
WCRIT - On entry, the critical shear stress at the pipe wall for each data set [Pa].
DENS - On entry, the density of the fluid for each data set [kg/m3].
D - On entry, the diameter of the pipe for each data set [m].
VF - On entry, the volume fraction of solids for each data set.
VFC - On entry, the Newtonian/non-Newtonian critical volume fraction of solids.
NVALS - On entry, the number of data values for each data set.
MAXV - On entry, the maximum number of possible data values for any data set.
NSETS - On entry, the number of data sets.
TOL - On entry, a relative tolerance check.

3. Working storage parameters

PARAMETER (MAXDAT=600, MAXS=100)
in main routine TVG, and
PARAMETER (MAXS=100)
in subroutine TVG1 of the same file.

MAXDAT - The total maximum number of data values possible.
MAXS - The maximum number of data sets possible.

4. Auxiliary routines

Routines required: BOOLE, INVERT, MINIM, ROOT, TMG.

# B.5 General Method Routines

## BOOLE

1. Purpose

Estimate the area under a curve for a single valued function. This uses Boole's five-point method adaptively, but non-recursively. A feature of this routine is that the area estimate on exit will be the sum of the value on entry with the new area estimate. To safeguard against a relatively small new area compared to the entry value, there is an initial comparison between estimates of Simpson and Trapezium, and then if necessary, a further comparison between estimates of Boole and Simpson. The tolerance check will always apply to the total area.

2. Specification

```
      SUBROUTINE  BOOLE (AREA, A, B, TOL, FUN)
      DOUBLE  PRECISION  AREA, A, B, TOL, FUN
```

AREA - On exit, the sum of AREA on entry with the new area estimate.

A - On entry, the lower limit of integration.
B - On entry, the upper limit of integration.
TOL - On entry, a relative tolerance check for the total area.
FUN - The integrand as an external function.

3. External function

```
DOUBLE PRECISION FUNCTION FUN (X)
DOUBLE PRECISION X
```

X - On entry, the value at which the function is to be evaluated.

## INVERT

1. Purpose

For an equation Y = FUN (X) where FUN is a smooth, well-behaved function, estimate positive X for a given Y using Muller's method.

2. Specification

```
SUBROUTINE INVERT (X, Y, XØ, XN, TOL, FUN)
DOUBLE PRECISION X, Y, XØ, XN, TOL, FUN
```

X - On exit, an estimate of the inverted function at Y.
Y - On entry, the value of Y for estimate X.
XØ - On entry, a low estimate of X.
XN - On entry, a high estimate of X.
TOL - On entry, a relative tolerance check.
FUN - An externally defined function for which the inversion is required.

3. External function

```
DOUBLE PRECISION FUNCTION FUN (X)
DOUBLE PRECISION X
```

X - On entry, the value at which the function is to be evaluated.

## LEVEN

(This routine is based on the publicly available Numerical Recipes routine MRQMIN.)

1. Purpose

Fit a non-linear function to a data set using Levenberg-Marquardt's method.

2. Specification

```
      SUBROUTINE LEVEN (A, COVAR, CURVE, CHISQ, MA,
     + X, Y, NDATA, ALAMDA, TOL, FUN)
      INTEGER NDATA, MA
      DOUBLE PRECISION A (MA), COVAR (MA,MA), CURVE (MA,MA), CHISQ,
     + X (NDATA), Y (NDATA), ALAMDA, TOL, FUN
```

A - On entry, initial guesses of the parameters.
On exit, the estimates of the parameters.
COVAR - On exit, the estimated covariance (inverse curvature) matrix.
CURVE - On exit, the estimated curvature (one-half times the Hessian) matrix.
CHISQ - On exit, the chi squared value of the fitted curve.
MA - On entry, the number of parameters.
X - On entry, the independent data values.
Y - On entry, the dependent data values.
NDATA - On entry, the number of data values.
ALAMDA - On entry, usually set small, say Ø.ØØ1.
(small—inverse Hessian, large—steepest descent.)
TOL - On entry, a relative tolerance check.
FUN - An externally defined (non-linear) function.

3. External function

```
DOUBLE PRECISION FUNCTION FUN (X, Y, A, DYDA, NDATA, MA)
INTEGER NDATA, MA
DIMENSION X(NDATA), Y(NDATA), A(MA), DYDA (NDATA, MA)
```

X - On entry, the independent data values.
Y - On exit, the fitted values at X and A.
A - On entry, the values of the parameters.
DYDA - On exit, the derivatives of Y (with respect to A) at X and A.
NDATA - On entry, the number of data values.
MA - On entry, the number of parameters.

4. Working storage parameters

PARAMETER (MAXDAT=1ØØØ, MAXA=5)
in routines LEVEN and COEFF, and
PARAMETER (MAXA=5)
in routine GAUSSJ all of the same file.

MAXDAT - The maximum number of data values possible.
MAXA - The maximum number of parameters possible.

## LINREG

1. Purpose

Simple linear regression of the model Y = A + B * X.

2. Specification

```
SUBROUTINE  LINREG (A, B, SSE, X, Y, NVALS)
INTEGER NVALS
DOUBLE  PRECISION  A, B, SSE, X, Y
```

A - On exit, the intercept of the fitted line.
B - On exit, the slope of the fitted line.
SSE - On exit, the error sum of squares of the fitted line.
X - On entry, the independent data values.
Y - On entry, the dependent data values.
NVALS - On entry, the number of data values.

## MINIM

1. Purpose

For an equation Y = FUN (X) where FUN is a smooth, unimodal function, find the minimum using quadratic interpolation.

2. Specification

```
SUBROUTINE  MINIM (X, Y, XØ, XN, TOL, FUN)
DOUBLE  PRECISION  X, Y, XØ, XN, TOL, FUN
```

X - On exit, an estimate of the location of the minimum.
Y - On exit, an estimate of the minimum value of the function.
XØ - On entry, a low estimate of X.
XN - On entry, a high estimate of X.
TOL - On entry, a relative tolerance check.
FUN - The externally defined function for which the minimum is required.

3. External function

```
DOUBLE PRECISION FUNCTION FUN (X)
DOUBLE PRECISION X
```

X - On entry, the value at which the function is to be evaluated.

## RKFEHL

1. Purpose

Estimate Y for a given X of a differential equation dY/dX = FUN (X, Y) using Runge-Kutta Fehlberg's embedded pair method.

2. Specification

```
SUBROUTINE  RKFEHL (XØ, YØ, XN, YN, HØ, TOL, FUN)
DOUBLE  PRECISION  XØ, YØ, XN, YN, HØ, TOL, FUN
```

XØ - On entry, the initial value of X.
YØ - On entry, the initial value of Y.
XN - On entry, the value of X for estimate Y.
YN - On exit, an estimate of Y at XN.
HØ - On entry, the initial step length.
TOL - On entry, a relative tolerance check.
FUN - An externally defined function to be integrated.

3. External function

```
DOUBLE PRECISION FUNCTION FUN (X, Y)
DOUBLE PRECISION X, Y
```

X, Y - On entry, the two values at which the function is to be evaluated.

## ROOT

1. Purpose

For an equation FUN (X, Y) = Ø, where FUN is a smooth, well-behaved function, estimate positive X for a given Y using Muller's method.

2. Specification

```
SUBROUTINE  ROOT (X, Y, XØ, XN, TOL, FUN)
DOUBLE  PRECISION  X, Y, XØ, XN, TOL, FUN
```

X - On exit, an estimate of the location of the root at Y.
Y - On entry, the value of Y for estimate X.
XØ - On entry, a low estimate of X.
XN - On entry, a high estimate of X.
TOL - On entry, a relative tolerance check.
FUN - The externally defined function for which the root is required.

3. External function

```
DOUBLE  PRECISION  FUNCTION  FUN (X)
DOUBLE  PRECISION  X, Y
```

X, Y - On entry, the two values at which the function is to be evaluated.

## SIMP

1. Purpose

Estimate the area under a curve for a single valued function. This uses Simpson's three-point method adaptively, but non-recursively. A feature of this routine is that the area estimate on exit will be the sum of the value on entry with the new area estimate. To safeguard against a relatively small new area compared to the entry value, there is an initial comparison between estimates of Simpson and Trapezium. The tolerance check will always apply to the total area.

2. Specification

```
SUBROUTINE  SIMP (AREA, A, B, TOL, FUN)
DOUBLE  PRECISION  AREA, A, B, TOL, FUN
```

AREA - On exit, the sum of AREA on entry with the new area estimate.
A - On entry, the lower limit of integration.
B - On entry, the upper limit of integration.
TOL - On entry, a relative tolerance check for the total area.
FUN - The integrand as an external function.

3. External function

```
DOUBLE  PRECISION  FUNCTION  FUN (X)
DOUBLE  PRECISION  X
```

X - On entry, the value at which the function is to be evaluated.

## TRAP

1. Purpose

Estimate the area under a curve for a single valued function. This uses the trapezium two-point method adaptively, but non-recursively. A feature of this routine is that the area estimate on exit will be the sum of the value on entry with the new area estimate. The tolerance check will always apply to the total area.

2. Specification

```
SUBROUTINE  TRAP (AREA, A, B, TOL, FUN)
DOUBLE  PRECISION  AREA, A, B, TOL, FUN
```

AREA - On exit, the sum of AREA on entry with the new area estimate.
A - On entry, the lower limit of integration.
B - On entry, the upper limit of integration.
TOL - On entry, a relative tolerance check for the total area.
FUN - The integrand as an external function.

3. External function

```
DOUBLE  PRECISION  FUNCTION  FUN (X)
DOUBLE  PRECISION  X
```

X - On entry, the value at which the function is to be evaluated.